

ENERGY LOSSES AND PRESSURE HEAD  
CHANGES AT STORM DRAIN  
JUNCTIONS

C. M. HARE

Submitted in fulfilment of the requirements for the  
Master of Engineering Degree at The New South Wales  
Institute of Technology.

November, 1980.



(ii)

STATEMENT

I hereby declare that the content of this thesis does not comprise in the main any work or material which I have previously submitted for a degree or other similar award from any other Institute of Technology or University.

Production Note:

- Signature removed prior to publication.

ACKNOWLEDGEMENTS

I wish to acknowledge, with gratitude, the following people and organizations, who gave me valuable assistance in the course of this project.

In the first instance, I would like to express my appreciation to Dr. Allan Pattison, thesis supervisor and previously Dean of Engineering, The New South Wales Institute of Technology, for his guidance throughout the research programme and his assistance in the preparation of this thesis.

I would also like to convey my special thanks to the staff of the School of Civil Engineering, The New South Wales Institute of Technology, especially Dr. Brian Cornish and Dr. Geoffrey O'Loughlin, for the interest and encouragement that they have given to this work.

In addition, I am grateful for the efforts of Mr. Ron Moore, Director of Industrial Liaison, Faculty of Engineering, The New South Wales Institute of Technology, who helped make this project possible. In this respect, I am also thankful to Mr. D. Bonouvrie of Vinidex Tubemakers Aust. Pty. Ltd., Mr. A. Ambler of Tubemakers Aust. Pty. Ltd., and Mr. H. Greenup of Cadillac Plastics Pty. Ltd., for their material contributions.

I would also like to express my gratitude to Mr. B. Ireland, Mr. G. Cooper and other practitioners who have shown so much interest in this work.

Finally, many thanks to Mrs. G. O'Neale, who was responsible for the excellent typing of the manuscript over which many hours were laboured.

Thank you.

CONTENTS

ACKNOWLEDGEMENTS	(iii)
CONTENTS	(iv)
LIST OF ILLUSTRATIONS	(vi)
LIST OF TABLES	(ix)
ABSTRACT	(x)
NOMENCLATURE	(xi)
<u>CHAPTER 1</u> Introduction	1
<u>CHAPTER 2</u> Pipe Junction Hydraulics	6
2.1 Introduction	7
2.2 Assumptions	7
2.3 Development of a General Theory	13
2.4 A Check of Theory Against Experimental Data	17
2.5 Hydraulic Performance of Commercially Available Pipe Junctions	17
2.6 Effect of the Reynold's Number	36
2.7 Summary : Pipe Junction Hydraulics	37
<u>CHAPTER 3</u> Junction Pit Hydraulics	38
3.1 Introduction	39
3.2 Literature Review	39
3.3 Flow Across Pit Junction Structures	46
3.4 Effect of Pit Size and Shape	50
3.5 Combining Flow at Three-Pipe Junctions	55
3.6 Effect of Froude Number and Submergence on Pressure Head Change Coefficients	55
3.7 Summary : Pit Junction Hydraulics	57
<u>CHAPTER 4</u> Hydraulic Models of Junction Pits	59
4.1 Use of Hydraulic Models	60
4.2 Model Construction and Apparatus	60

	4.2.1	Scope of the Investigation	60
	4.2.2	Water Supply System	64
	4.2.3	Model System and Pipelines	64
	4.2.4	Model Geometries	81
	4.2.5	Experimental Procedures	88
	4.2.6	Error Analysis	94
.	<u>CHAPTER 5</u>	Experimental Results	98
	5.1	Introduction	99
	5.2	Flow Straight-Through Junction Pits.	102
	5.3	22½° Bends at Pits	104
	5.4	45° Bends at Pits	106
	5.5	67½° Bends at Pits	109
	5.6	90° Bends at Pits	110
.	<u>CHAPTER 6</u>	Conclusions	147
.	<u>CHAPTER 7</u>	Selected Bibliography	154
.	<u>APPENDIX</u>	Test Data	A-1

LIST OF ILLUSTRATIONS

1.1	Effect of Selection of Water Surface Elevation Coefficient, $k_w$ , on Pipe Diameter.	3
2.1	Theoretical Analysis for Pipe Junctions.	8
2.2	Fluid Pressures Acting at a Sudden Expansion.	11
2.3	Commercially Available Pipe Junctions.	16
2.4	Comparison between Equation 2.25 and Experimental Evidence for Sudden Expansions.	19
2.5	Energy Losses and Pressure Head Changes at Sudden Expansions.	20
2.6	Energy Losses and Pressure Head Changes for Reducers (Sudden Contractions)	22
2.7	Comparison between Equation 2.33 and Experimental Evidence for Mitre Bend Pipe Junctions	24
2.8	Performance of Mitre Bends.	25
2.9	Performance of Compound $90^\circ$ Mitre Bends.	26
2.10	Recommended Equation for Pressure Head Change Coefficients at Intake Junctions.	28
2.11	Pressure Head Change Coefficients in Main Conduit at a $45^\circ$ Slope Junction.	32
2.12	Pressure Head Change Coefficients in Lateral Conduit at a $45^\circ$ Slope Junction	33
2.13	Recommended Equations for Pressure Head Change Coefficients at Slope Junctions.	34
3.1	Junction Configurations Tested by Sangster <i>et al</i> (1958)	41
3.2	Junction Configurations Tested by Archer <i>et al</i> (1978)	44
3.3	Positive and Negative Pressure Head Changes.	46
3.4	Typical Junction Pit Operation.	48
3.5	Effect of Box Size and Shape with all Flow Straight Through.	51

3.6	Effect of Pit Size on Pressure Head Change Coefficients at 90° Junctions.	53
3.7	Effect of Pit Size on Water Surface Elevation Coefficients at 90° Junctions.	54
3.8	Pressure Line Elevations at 0° and 90° Bends.	56
4.1	Schematic Layout for Junction Pit Experiments.	63
4.2	Headtank.	65
4.3	Manometers.	66
4.4	Model Setup for Straight Through Flow.	66
4.5	Flow Through a 45° Pit Junction.	67
4.6	Flow Through a 45° Pit Junction	67
4.7	Typical Inlet Pit.	69
4.8	Tailwater Tank.	71
4.9	70 mm Diameter Model Pipeline.	74
4.10	94 mm Diameter Model Pipeline.	75
4.11	127 mm Diameter Model Pipeline.	76
4.12	Angle Adaptors	78
4.13 - 4.18	Model Geometries Tested.	82-87
4.19	Data and Calculation Sheet	89
4.20	Typical Data Plot (Pressure Head Change Coefficients).	92
4.21	Typical Data Plot (Water Surface Elevation Coefficients).	93
4.22	Friction Slope vs Discharge for 70 mm Diameter Pipe.	96
5.1	Comparison of Experimental Results with those of Investigators and with the Theoretical Analysis for Straight Through Flow	112
5.2	Coefficients for Straight Through Flow ( $S/D_0 = 2.5$ ).	113

5.3	Comparison of Theoretical Analysis with Experimental Results for $\theta = 22\frac{1}{2}^{\circ}$ .	114
5.4 - 5.8	Coefficients for $22\frac{1}{2}^{\circ}$ Bends at Pit Junctions.	115-119
5.9	Comparison of Theoretical Analysis with Experimental Results for $\theta = 45^{\circ}$ .	120
5.10 - 5.19	Coefficients for $45^{\circ}$ Bends at Pit Junctions.	121-130
5.20	Comparison of Theoretical Analysis with Experimental Results for $\theta = 67\frac{1}{2}^{\circ}$ .	131
5.21 - 5.28	Coefficients for $67\frac{1}{2}^{\circ}$ Bends at Pit Junctions.	132-138
5.29	Hydraulic Improvement of $90^{\circ}$ Bends at Pit Junctions.	139
5.30 - 5.31	Comparison of Experimental Results with those of Other Investigators and with the Theoretical Analysis for $\theta = 90^{\circ}$ .	141-142
5.32 - 5.35	- Coefficients for $90^{\circ}$ Bends at Junction.	143-146
A.1 - A.60	Data Plot.	A3-A62



LIST OF TABLES

2.1	Total Energy Loss Coefficients for Compound Mitre Bends	27
2.2	Comparison of Energy Loss Equations for Sharp-Edged Slope Junctions	31
3.1	Typical Values of $k_u$ for Pit Junctions Tested by Sangster <i>et al</i> (1958)	42
3.2	Magnitude of $k_u$ ( $=C_u$ ) as Determined by Archer <i>et al</i> (1978)	43
3.3	Percentage Conversion of Kinetic to Potential Head Derived from Archer's Experimental Data	50
4.1	Constructed Inlet Pit Size Ratios	68
4.2	Diameter and Area Ratios Used in Model Programme	72
4.3	Pipe Lengths Used in Model Programme	77
4.4	Angle Adaptors	80
5.1	Quick Reference Guide to Geometries Tested	101
5.2	Modification Table for Values of $S/D_o$ Other than 2.5	103
6.1	Typical Values of $k_u$ and $k_w$ (branch point located on downstream face of pit)	149
6.2	Typical Values of $k_u$ and $k_w$ (branch point not located on downstream face of pit)	152

ABSTRACT

...  
An investigation has been made of the magnitude of hydraulic losses produced by storm drain junction structures which connect pipes operating under flow-full conditions.

The study comprised three parts:

- (a) a literature review;
- (b) a study of losses associated with commercially available 'closed' pipe junctions;
- (c) an experimental study, using hydraulic models, to investigate the magnitude of losses at 'open' pit structures.

A theoretical analysis was developed for closed pipe junctions. The theory was found to be adequate when checked against available experimental data. For pit junction structures, the experimental programme comprised thirty models covering an extensive range of geometric and hydraulic variables. The model studies indicated that maximum hydraulic efficiency is attained when the junction branch point is located on the downstream face of the pit. Data have been plotted for bend deflections angles of between  $0^{\circ}$  and  $90^{\circ}$ , and for upstream to downstream pipe diameter ratios within the range 0.55 to 1.00. Grate inlet flow and submergence have been identified as parameters affecting losses. Semi-empirical equations have been developed to account for junction losses when the branch point is located on the downstream face of the pit.

Nomenclature

The symbols used in this thesis are listed hereunder. Alphabetical subscripts have been used which conform to a standard format. The subscript 'u' refers to the primary upstream pipe. If more than one upstream pipe converges at a junction, the second such pipe is characterized by the subscript 'b' (branch or lateral pipe). The outfall pipe is identified by the subscript 'o'.

Notation

- a spacer length for compound mitre bend junction.  
 $A_b$  mean cross sectional area of the lateral pipe.  
 $A_m$  mean cross section area of the model pipeline.  
 $A_o$  mean cross sectional area of the outfall pipe.  
 $A_p$  mean cross sectional area of the prototype pipeline.  
 $A_r$  model-prototype area ratio.  
 $A_u$  mean cross sectional area of the upstream pipe.  
B pit dimension (square in plan).  
 $C_b$  dimensionless total energy loss coefficient as defined by the difference between the lateral total energy line elevation and the downstream total energy line elevation when extrapolated linearly to the branch point of the junction, divided by the average downstream velocity head.  
 $C_u$  dimensionless total energy loss coefficient as defined by the difference between the upstream total energy line elevation and the downstream total energy line elevation when extrapolated linearly to the branch point of the junction, divided by the average downstream velocity head.  
 $D_b$  mean diameter of the lateral pipe.  
 $D_m$  mean diameter of the model pipeline.  
 $D_o$  mean diameter of the outfall pipe.  
 $D_p$  mean diameter of the prototype pipeline.  
 $D_r$  model-prototype diameter ratio.  
 $F_o$  Froude number in the outfall pipe.  
g acceleration due to gravity ( $9.81 \text{ m/s}^2$ ).

HGL	Hydraulic Grade Line (or pressure line or piezometric head line).
$k_b$	dimensionless pressure head change coefficient as defined by the difference between the lateral and downstream pressure line elevations when extrapolated linearly to the branch point of the junction, divided by the average downstream velocity head.
$k_u$	dimensionless pressure head change coefficient as defined by the difference between the upstream and downstream pressure line elevations when extrapolated linearly to the branch point of the junction, divided by the average downstream velocity head.
$k_w$	dimensionless pressure head change coefficient as defined by the difference between the water surface elevation in a pit junction and the elevation of the downstream pressure line when extrapolated linearly to the branch point of the junction, divided by the average downstream velocity head.
$L_m$	characteristic length in a model.
$L_p$	characteristic length in a prototype.
$L_r$	scalar ratio of the model equal to the characteristic length of the model divided by the characteristic length of the prototype.
$p_b$	static pressure in the lateral conduit.
$p_o$	static pressure in the main conduit.
$p_u$	static pressure in the upstream conduit.
$Q_b$	mean discharge in the lateral pipe.
$Q_g$	mean grate flow discharge through the pit grate inlet
$Q_m$	mean discharge in the model pipeline.
$Q_o$	mean discharge in the outfall pipe.
$Q_p$	mean discharge in the prototype pipeline.
$Q_r$	model-prototype discharge ratio.
$Q_u$	mean discharge in the upstream pipe.
$R_x$	resultant force component acting at the junction used in the impulse-momentum equation.
S	depth of water in a pit junction measured from pit invert elevation to water surface elevation (submergence).
TEL	Total Energy Line.

$V_b$	mean velocity in the lateral pipe.
$V_m$	mean velocity in the model pipeline.
$V_o$	mean velocity in the outfall pipe.
$V_p$	mean velocity in the prototype pipeline.
$V_r$	characteristic model-prototype velocity ratio.
$V_u$	mean velocity in the upstream pipe.
WSE	pressure head change defining the difference between the water surface elevation in a junction pit and the elevation of the downstream pressure line when extrapolated linearly to the branch point of the junction.
$\gamma$	specific weight of a fluid.
$\Delta H$	available head.
$\Delta H_b$	total energy loss across a junction as defined by the difference between the lateral total energy line elevation and the downstream total energy line elevation when extrapolated linearly to the branch point of the junction.
$\Delta H_u$	total energy loss across a junction as defined by the difference between the upstream total energy line elevation and the downstream total energy line elevation when extrapolated linearly to the branch point of the junction.
$\Delta k_p$	incremental pressure head change coefficient due to presence of a pit structure, over and above a theoretical solution
$\Delta k_s$	incremental pressure head change coefficient due to submergence effects, over and above a theoretical solution
$\frac{\Delta P}{\gamma}$	change in pressure head as defined by the difference between an upstream pressure line elevation and the downstream pressure line elevation when extrapolated linearly to the branch point of the junction.
$\rho$	density of water ( $\approx 1000 \text{ kg/m}^3$ ).
$\theta_b$	angle of lateral pipe deflection.
$\theta_u$	angle of upstream pipe deflection.

1.

CHAPTER 1

INTRODUCTION

## INTRODUCTION

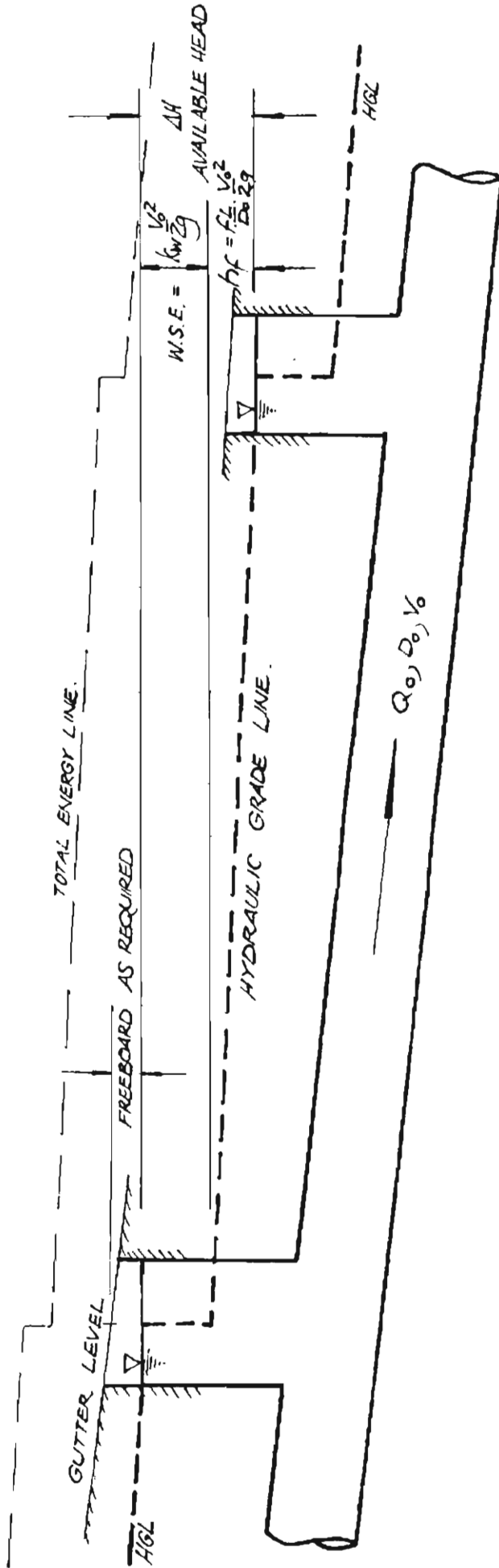
The hydraulic design of piped drainage systems involves an analysis of pipe friction losses and energy losses at junction structures. Methods for determining friction losses in individual pipe reaches are well documented and an accurate assessment of such losses can be made with a high degree of confidence if appropriate assumptions are made about condition of pipe wall surfaces and pipe joints. This is not so, however, for energy losses at junction structures. "This problem is so complicated that only a few simple and specific cases have been studied. The conclusions of such studies indicate that generalization of the problem is not possible or even desirable." (Chow, 1959) p. 512).

Little information is available with regard to the magnitude of energy losses and pressure head changes occurring at pit junction structures. Jens and McPherson state: "There are virtually no data on which estimates of such losses can be based, other than those from the recent University of Missouri experiments." (Chow, 1954) p. 20-31). The use of closed pipe junctions, where expensive pit structures can be avoided, is likewise prohibited by the lack of design information that has had widespread publication. Consequently, methods used for the design of piped drainage systems may or may not lead to efficient designs.

The level to which water will rise in a pit junction structure is equal to or slightly greater than the elevation of the upstream pipe pressure line. The water surface elevation in the pit is, therefore, determined by the magnitude of the pressure head change (W.S.E.) attributable to the junction structure (see Figure 1.1). Without definitive data concerning the magnitude of such pressure head changes, it is not possible to accurately determine the minimum pipe sizes required to prevent flooding or to make an accurate assessment of the discharge capacity of the pipe system. There is, therefore, a need to develop a design method which simulates flow through surcharged pipes and which

FIGURE 1.1

EFFECT OF SELECTION OF WATER SURFACE ELEVATION COEFFICIENT,  $k_w$ , ON PIPE DIAMETER.



3.

EXAMPLE: FOR A PIPE LENGTH OF 50M, AN AVAILABLE HEAD OF 1M AND A DISCHARGE OF  $1 \text{ m}^3/\text{s}$ :

$k_w$	* REQUIRED DIA., $D_o$ : ( $\epsilon = 0.0008 \text{ M}$ )
~1.5	525 mm.
0.2	600 mm.
1.5	675 mm.
2.0	750 mm.

\* CALCULATED USING EQUATION 1.1. TO NEAREST COMMERCIAL PIPE SIZE.



accurately accounts for pit junction losses.

Figure 1.1 illustrates a design method for piped drainage systems using hydraulic grade line computation. Although total energy line concepts are conventionally employed in hydraulic design, it is more convenient to use hydraulic grade line computations in storm drain design since such methods yield direct solutions to pit water surface elevations without the unnecessary inclusion of velocity heads. The design procedure is iterative: a pipe diameter is assumed, from which both friction loss and pressure head change are calculated. The pipe size is hydraulically adequate when the change in hydraulic grade line ( $\Delta HGL$ ) is sufficiently small to avoid surface flooding at the upstream structure, i.e., the required head is less than or equal to the available head.

Utilizing the Darcy-Weisbach Equation:

$$\Delta H > \left[ \frac{fL}{D_o} + k_w \right] \cdot \frac{V_o^2}{2g} \quad \dots \text{Eq. 1.1}$$

where  $\Delta H$  is the available head difference between pits (equal to the difference between the gutter invert elevation at the upstream pit and the pressure line elevation at the downstream pit minus the required freeboard) (m),  
 $f$  is the Darcy-Weisbach friction factor,  
 $L$  is the length of pipe (m),  
 $D_o$  is the pipe diameter (m),  
 $V_o$  is the mean velocity of flow (m/s),  
 $g$  is the acceleration due to gravity ( $m/s^2$ ),  
 and  $k_w$  is the water surface elevation coefficient for the upstream junction.

The left and right hand sides of Equation 1.1 represent available head and required head respectively.

The magnitude of  $k_w$  was found by Sangster (1958) to vary within the range  $-4 < k_w < 2.5$  for most practical applications,

depending on the junction geometry. A similar range of values was found to occur for the range of junction pit geometries covered in the research reported on in this thesis. Such variations in  $k_w$  create either large variations in head requirements for a pipe of given diameter or large variations in required pipe diameters when the available head is fixed. An example is illustrated in Figure 1.1. The selection of  $k_w$  can be seen to be of critical importance in the selection of required pipe sizes and, therefore, on overall construction economics.

An extensive literature search relating to losses at junction structures revealed few prior experimental investigations. These publications are reviewed in Chapter 3 and, in summary, provide data on a limited range of pit and pipe geometries. The work contained in subsequent chapters herein provides a state-of-the-art report on data for both closed pipe junctions and open pit structures, reports on original work which expands current knowledge, and presents design recommendations and constructional improvements which will produce more efficient and economic drainage systems. With such data, a surcharged pipe design method can be more successfully utilized - such designs yielding a more satisfactory correlation between the desirable frequency of surface flooding and the design storm recurrence interval.

CHAPTER 2

PIPE JUNCTION HYDRAULICS

- 2.1 Introduction
- 2.2 Assumptions
- 2.3 Development of a General Theory
- 2.4 A Check of Theory Against Experimental Data.
- 2.5 Hydraulic Performance of Commercially Available Pipe Junctions
  - 2.5.1 Sudden Expansions
  - 2.5.2 Sudden Contractions
  - 2.5.3 Mitre Bends
  - 2.5.4 Compound Mitre Bends
  - 2.5.5 Intake Junctions
  - 2.5.6 Slope Junctions
  - 2.5.7 Vertical Entry Junctions
- 2.6 Effect of the Reynold's Number .
- 2.7 Summary : Pipe Junction Hydraulics

## PIPE JUNCTION HYDRAULICS

### 2.1 Introduction

This chapter is concerned with the development of a theoretical approach to the determination of energy losses and pressure head changes occurring at converging pipe junctions, to compare the derived equations with known experimental data, and to provide design data for the range of commercially available pipe junctions.

When water flows in a number of conduits converging to a common junction point, the resultant energy losses and pressure head changes may be determined theoretically using the principles of flow continuity, impulse-momentum and energy. A number of assumptions need to be made before such a theoretical analysis can be developed.

### 2.2 Assumptions

The initial assumption adopted in this analysis is that all pipes entering the junction are flowing full, and are under pressure. Uniform velocity distributions are also assumed for all connecting conduits and the flow both upstream and downstream of the junction is assumed to be fully established and representative of steady flow conditions. Experimental evidence has shown that correction factors for non-uniform velocity distributions are not warranted on the grounds that the differences between the observed values and the corrected theoretical equations are several times greater than the correction obtained. (Blaisdell and Manson, 1963, p. 10). The hydraulic grade line and the total energy line for each of the conduits is assumed to extend linearly to the point of intersection, in plan, of the centrelines of the connecting pipes. This point is referred to as the *branch point* of the junction (see Figure 2.1). Where the centrelines of connecting pipes are not coincident, added complexities of multiple branch points affect the development of an adequate theory. The linear extension of the energy lines to the branch point of the junction means that the analysis ignores the acceleration

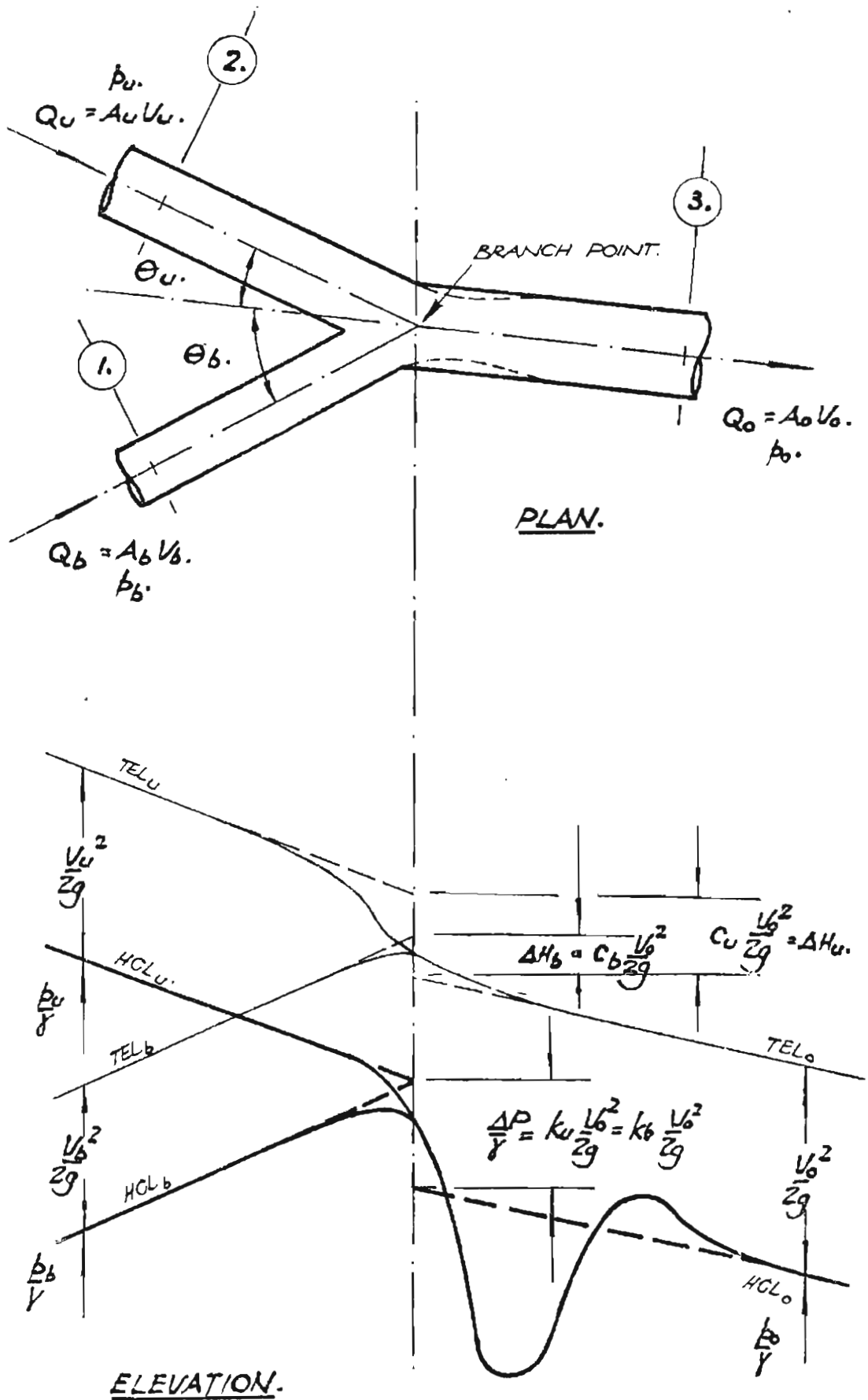


FIGURE 2.1: THEORETICAL ANALYSIS FOR PIPE JUNCTIONS.

and deceleration of fluid particles in the region of the junction, particularly just downstream of the junction where a *vena contracta* is likely to occur.

All junctions are assumed to be sharp-edged. The theoretical analysis does not take into account the effects of curvature at pipe entrances and exits.

The energy losses and pressure head changes derived are those due to fluid impact eddying, turbulence and separation (form losses). Losses due to frictional resistance across a junction are accounted for by the linear extension of the energy lines to the branch point of the junction.

To simplify the theoretical analysis, certain assumptions have been made concerning the impulse-momentum equation. For a three-pipe junction (as shown in Figure 2.1), Equation 2.1 applies. The left-hand side represents the impulse per unit time due to all forces acting at the junction in the downstream flow direction (x), and the right-hand side is the rate of change of flow momentum, also in the downstream flow direction:

$$\Delta F_x = \rho [Q_o V_o - Q_u V_u \cos \theta_u - Q_b V_b \cos \theta_b] \quad \dots \text{Eq. 2.1}$$

Thus, for two upstream conduits, Equation 2.2 holds:

$$\begin{aligned} p_u A_u \cos \theta_u + p_b A_b \cos \theta_b - p_o A_o - R_x \\ = \rho [Q_o V_o - Q_u V_u \cos \theta_u - Q_b V_b \cos \theta_b] \quad \dots \text{Eq. 2.2} \end{aligned}$$

The impulse-momentum relationship states that the pressure plus the momentum forces upstream of the junction must equal the pressure plus the momentum forces downstream of the junction (friction forces being neglected). This equality is maintained by a reaction force, R, exerted on the fluid by the junction structure. Evidence derived from experiments by various investigators indicates that this

force can either assist or oppose the flow across a junction depending upon junction geometry and the flow characteristics.

In the case of more than one upstream pipe converging at a junction (such as in Figure 2.1), the elevation of the pressure lines for all upstream branches must be the same at the junction. Thus for 'n' upstream pipes:

$$P_{u/\gamma} = P_{b_1/\gamma} = P_{b_2/\gamma} = \dots = P_{b_{n-1}/\gamma} \quad \dots \text{Eq. 2.3}$$

Favre (1937) argues that, if this were not the case, "the gradient of the pressure will be enormous in that zone (where two flows combine, and) one would have there in any practical case a pressure discontinuity".

Favre's theory is not, however, altogether supported by experimental evidence. Blaisdell and Manson (1963) and Gardel (1957) suggest that some variation exists between any two upstream hydraulic grade line elevations when these lines are extended linearly to the branch point of the junction. The difference becomes evident when the energy loss equations developed by each of these investigators are converted into pressure head change equations. (Compare, for example, Figure 2.11 and Figure 2.12 which present pressure head change coefficients for main and lateral pipes respectively at a 45° slope junction.) For the theory being developed here, however, coincident pressure line elevations are assumed to occur as shown in Figure 2.1. Upstream total energy line elevations will be located one velocity head above the corresponding hydraulic grade line elevations. Therefore, unless the upstream velocity heads are equal in magnitude, the upstream total energy line elevations will not be coincident at the junction branch point.

On the left hand side of the impulse-momentum relationship (Equation 2.2), two further assumptions must be made. First, it must be assumed that the upstream pressures ( $p_u, p_b, \dots$ ) each act uniformly over the downstream area  $A_o$ . Taking the upstream lateral as an example, it is thus reasonable to assume that the pressure on the area ( $A_o - A_b$ ) is the same as that in the lateral pipe, namely  $p_b$ . The assumption can be illustrated using the simple case of a sudden expansion as shown in Figure 2.2.

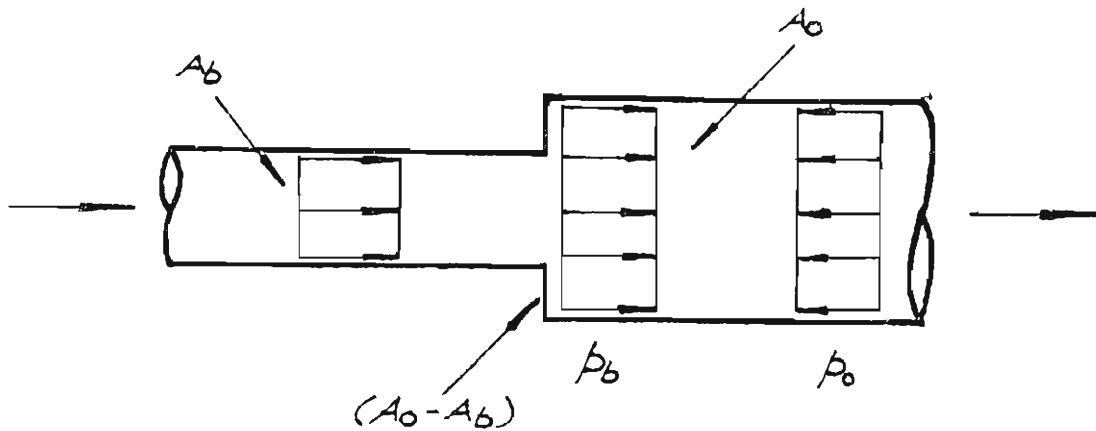


FIGURE 2.2 : FLUID PRESSURES ACTING AT A SUDDEN EXPANSION.

The pressure acting on the face of the downstream pipe at the section of enlargement is the same as the pressure in the approach flow ( $p_b$ ). For a three-pipe junction, this situation is assumed to exist for each upstream conduit. This line of argument is supported by Karaki (1971) p.142, Webber (1971) p. 106, Vennard (1961) p. 180, and has been used previously in the establishment of the Borda-Carnot formula for the energy loss attributable to a sudden enlargement. Favre (1937) justifies the use of such an assumption on the basis that, "it is known that the Borda-Carnot formula is remarkably well confirmed in practice and it is at the Munich Laboratory that the best series



of experiments for the verification of this formula have been performed". Favre is referring to the work of Vogel (1926, 1928), Kinne (1931) and Petermann (1929). Other experimental work such as that performed by Blaisdell and Manson (1963) and by Gardel (1957) add weight to Favre's justification.

Second, it has been assumed that the flow across the junction operates under a pressure distribution such that the pressure on a horizontal plane is equal in magnitude in all directions. Such an assumption effectively eliminates the need to introduce  $\theta_u$  and  $\theta_b$  into the left-hand side of the impulse-momentum equation (Equation 2.2), and the pressure components of the approach flows ( $p_u A_u \cos \theta_u$ ,  $p_b A_b \cos \theta_b$ , ..... ) may be assumed simply as  $p_u A_u$ ,  $p_b A_b$  .... etc. Blaisdell and Manson (1963) have used such an assumption in the theoretical analysis they provide for total energy loss coefficients at sloped pipe junctions. Stevens (1926) used the same assumption stating that the change in momentum across the junction is simply equal to the pressure at the junction minus the average pressure in the main below the junction, multiplied by the area of the downstream main. Use of Stevens' terminology leads to Equation 2.4.

$$(J - P) A = \Delta M \quad \dots \text{Eq. 2.4}$$

where J is the pressure at the junction,  
 P is the maximum average pressure in the downstream main,  
 A is the downstream pipe area, and  
 $\Delta M$  is the change in momentum.

The impulse-momentum equation stated previously (Equation 2.2) may now be rewritten as Equation 2.5.

$$(p_u + p_b - p_o) A_o - R_x = \rho [ Q_o V_o - Q_u V_u \cos \theta_u - Q_b V_b \cos \theta_b ] \quad \dots \text{Eq. 2.5}$$

This equation is the modified form of the impulse-momentum equation used in the development of a general theory for flow through a pipe junction system.

### 2.3 Development of a General Theory

Consider the control volume for a pipe junction defined within Sections 1, 2 and 3 as shown in Figure 2.1. The sections are assumed to be located so that the fluid motion is not influenced by the convergence of the two branch flows.

The distance  $(\Delta P/\gamma)$  represents the change in pressure head across the junction, whilst  $\Delta H_u$  and  $\Delta H_b$  represent the loss of total energy that occurs in the upstream main and lateral conduits respectively.

The Bernoulli Equation may be written for each of the upstream conduits as Equations 2.6 and 2.7.

$$\frac{p_o}{\gamma} + \frac{V_o^2}{2g} + C_u \frac{V_o^2}{2g} = \frac{p_u}{\gamma} + \frac{V_u^2}{2g} \quad \dots \text{Eq. 2.6}$$

$$\frac{p_o}{\gamma} + \frac{V_o^2}{2g} + C_b \frac{V_o^2}{2g} = \frac{p_b}{\gamma} + \frac{V_b^2}{2g} \quad \dots \text{Eq. 2.7}$$

Utilizing the continuity equation ( $V = Q/A$ ) and rearranging the above expressions, the total energy loss coefficients,  $C_u$  and  $C_b$  may be stated as shown in Equations 2.8 and 2.9 respectively.

$$C_u = -1 + \frac{2g}{\gamma} (p_u - p_o) \frac{A_o^2}{Q_o^2} + \frac{A_o^2}{Q_o^2} \cdot \frac{Q_u^2}{A_u^2} \quad \dots \text{Eq. 2.8}$$

$$C_b = -1 + \frac{2g}{\gamma} (p_b - p_o) \frac{A_o^2}{Q_o^2} + \frac{A_o^2}{Q_o^2} \cdot \frac{Q_b^2}{A_b^2} \quad \dots \text{Eq. 2.9}$$

The modified impulse momentum equation (Equation 2.5) may be used to eliminate the absolute pressures  $p_o$ ,  $p_u$  and  $p_b$  from the above equations. Restating Equation 2.5 for both the main and the lateral leads respectively to Equations 2.10 and 2.11.

$$(p_u - p_o)A_o - R_x = \rho [Q_o V_o - Q_u V_u \cos \theta_u - Q_b V_b \cos \theta_b] - p_b A_o \quad \dots \text{Eq. 2.10}$$

$$(p_b - p_o)A_o - R_x = \rho [ Q_o V_o - Q_u V_u \cos \theta_u - Q_b V_b \cos \theta_b ] - p_u A_o \quad \dots \text{Eq. 2.11}$$

Dividing Equations 2.10 and 2.11 by  $A_o$ , recognizing that  $\gamma = \rho g$ , and substituting into Equations 2.8 and 2.9, Equations 2.12 and 2.13 may be derived:

$$C_u = 1 - \left( 2 \frac{A_o}{A_b} \cos \theta_b \right) + \left( 4 \frac{A_o}{A_b} \cos \theta_b \right) \left( \frac{Q_u}{Q} \right) - 2A_o \left( \frac{\cos \theta_u}{A_u} + \frac{\cos \theta_b}{A_b} - \frac{A_o}{2A_u^2} \right) \left( \frac{Q_u}{Q_o} \right)^2 - \frac{2p_b A_o}{\rho Q_o V_o} + \frac{2R_x}{\rho Q_o V_o} \quad \dots \text{Eq. 2.12}$$

and, for the lateral,

$$C_b = \left( 1 - 2 \frac{A_o}{A_u} \cos \theta_u \right) + \left( 4 \frac{A_o}{A_u} \cos \theta_u \right) \left( \frac{Q_b}{Q} \right) - 2A_o \left( \frac{\cos \theta_u}{A_u} + \frac{\cos \theta_b}{A_b} - \frac{A_o}{2A_b^2} \right) \left( \frac{Q_b}{Q_o} \right)^2 - \frac{2p_u A_o}{\rho Q_o V_o} + \frac{2R_x}{\rho Q_o V_o} \quad \dots \text{Eq. 2.13}$$

From Figure 2.1, Equations 2.14 and 2.15 may be derived.

$$\frac{V_b^2}{2g} - C_b \frac{V_o^2}{2g} - \frac{V_o^2}{2g} + k_b \frac{V_o^2}{2g} = 0 \quad \dots \text{Eq. 2.14}$$

$$\text{and } \frac{V_u^2}{2g} - C_u \frac{V_o^2}{2g} - \frac{V_o^2}{2g} + k_u \frac{V_o^2}{2g} = 0 \quad \dots \text{Eq. 2.15}$$

Simplifying these equations and solving for  $k_u$  and  $k_b$  leads to Equations 2.16, 2.17 and 2.18.

$$k_b = 1 + C_b - \left( \frac{Q_b}{Q_o} \right)^2 \cdot \left( \frac{A_o}{A_b} \right)^2 \quad \dots \text{Eq. 2.16}$$

$$k_u = 1 + C_u - \left(\frac{Q_u}{Q_o}\right)^2 \cdot \left(\frac{A_o}{A_u}\right)^2 \quad \dots \text{Eq. 2.17}$$

$$= C_u + 2 \left(\frac{Q_b}{Q_o}\right) - \left(\frac{Q_b}{Q_o}\right)^2 \quad \dots \text{Eq. 2.18}$$

Since  $p_u/\gamma$  has been assumed to equal  $p_b/\gamma$ , then  $k_u$  must equal  $k_b$ . It is necessary, therefore, to derive only one equation for the pressure head change coefficient. Substituting Equation 2.13 into Equation 2.16, the final expression for the pressure head change coefficient may be stated as:

$$k_u = k_b = 2 - 2 \left(\frac{A_o}{A_u}\right) \cos \theta_u + 4 \left(\frac{Q_b}{Q_o}\right) \left(\frac{A_o}{A_u}\right) \cos \theta_u - 2A_o \left(\frac{\cos \theta_b}{A_b} + \frac{\cos \theta_u}{A_u}\right) \left(\frac{Q_b}{Q_o}\right)^2 - \frac{2p_u A_o}{\rho Q_o V_o} + \frac{2R_x}{\rho Q_o V_o} \quad \dots \text{Eq. 2.19}$$

The pressure head change may now be determined

$$\frac{\Delta P}{\gamma} = k_u \cdot \frac{V_o^2}{2g} = k_b \cdot \frac{V_o^2}{2g} \quad \dots \text{Eq. 2.20}$$

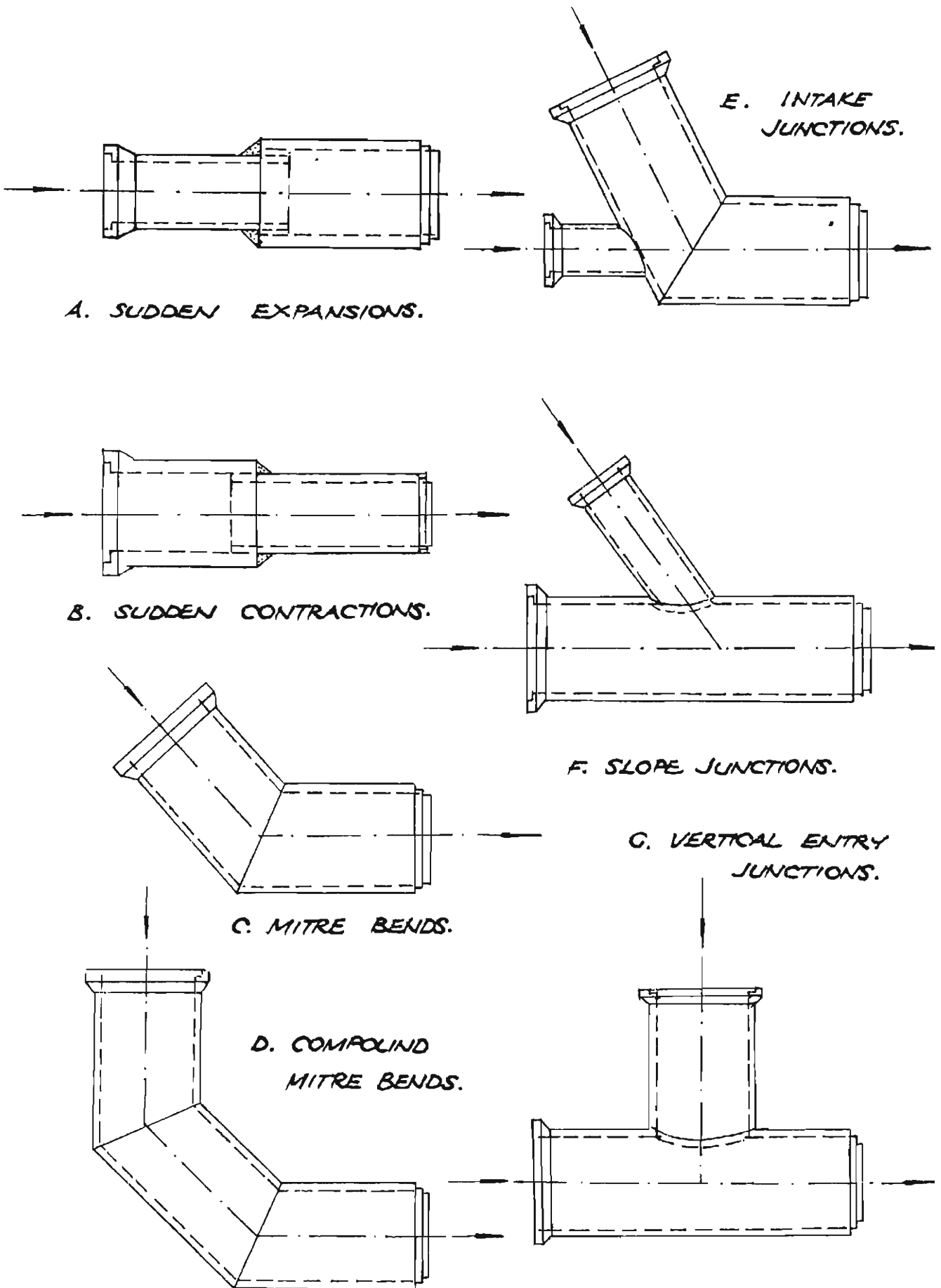
Similarly, total energy losses may be calculated using Equations 2.21 and 2.22 which have been derived using Equations 2.12 and 2.13 and substituting

$$\Delta H_u = C_u \cdot \frac{V_o^2}{2g} \quad \dots \text{Eq. 2.21}$$

$$\Delta H_b = C_b \cdot \frac{V_o^2}{2g} \quad \dots \text{Eq. 2.22}$$

Commercially available pipe junctions are shown in Figure 2.3. With the exception of compound mitre bends (which have no theoretical base and depend on experimentally derived data for the evaluation of losses) Equations 2.12, 2.13 and 2.19 may be simplified to provide theoretical solutions for each of the junction geometries shown.

FIGURE 2.3: COMMERCIALLY AVAILABLE PIPE JUNCTIONS.



## 2.4 A Check of Theory Against Experimental Data

It has been shown that equations for total energy loss and pressure head change coefficients can be derived provided that terms are included "for the corresponding unbalanced force component acting on the wall of the lateral" (McNown (1954) p. 1105), and for the absolute upstream pressure acting at the branch point of the junction. Both terms are introduced in the impulse-momentum equation (Equation 2.5) and are carried through, as unknowns, to Equation 2.19, which is the equation for the pressure head change coefficients  $k_u$  and  $k_b$ . The theoretical equations obtained contain three unknowns. The application of Equations 2.12, 2.13 and 2.19 is not possible without first assuming the magnitudes of the reaction force and the upstream pressure.

In previous theoretical analyses (Favre 1937) and Stevens (1928) ), the reaction force component,  $R_x$ , and the upstream pressure component were assumed equal to zero. With these assumptions, a comparison can be made between simplified theoretical and experimentally derived energy loss and pressure head change coefficients. Differences between the theoretical and experimental coefficients may be attributed to the resultant force and pressure having non-zero magnitudes, errors introduced by the assumptions made in the development of the theory and from experimental error. In the following section, the hydraulic performance of various pipe junctions is evaluated and a comparison is made wherever possible between the experimental evidence and the simplified theoretical equations.

## 2.5 Hydraulic Performance of Commercially Available Pipe Junctions.

### 2.5.1 Sudden Expansions

For a sudden expansion of a pipeline (Figure 2.3(A) ), the theoretical equation for the pressure head change coefficient (Equation 2.19) reduces to Equation 2.23.

$$k_u = 2 \left(1 - \frac{A_o}{A_u}\right) - \frac{2p_u A_o}{\rho Q_o V_o} + \frac{2R_x}{\rho Q_o V_o} \quad \dots \text{Eq. 2.23}$$

Setting  $R_x$  and  $p_u$  equal to zero:

$$k_u = 2 \left(1 - \frac{A_o}{A_u}\right) \quad \dots \text{Eq. 2.24}$$

Similarly, from Equation 2.12:

$$C_u = \left(1 - \frac{A_o}{A_u}\right)^2 \quad \dots \text{Eq. 2.25}$$

Using continuity and the Bernoulli Equation, it can be shown that:

$$\Delta H_u = \left(1 - \frac{A_o}{A_u}\right)^2 \cdot \frac{V_o^2}{2g} \quad \dots \text{Eq. 2.26}$$

$$= \frac{(V_u - V_o)^2}{2g} \quad \dots \text{Eq. 2.27}$$

Equation 2.27 is known as the Borda-Carnot Formula and is plotted in Figure 2.4. Experimental work on the performance of sudden enlargements has been investigated by Archer (1913), who developed Equations 2.28 and 2.29:

$$\Delta H_u = \frac{1.098 (V_u - V_o)^{1.919}}{2g} \quad \dots \text{Eq. 2.28}$$

$$= 0.01705 (V_u - V_o)^{1.919} \quad \dots \text{Eq. 2.29}$$

where  $g$  is measured in imperial units (32.17 ft/s).

In metric units ( $g = 9.81 \text{ m/s}$ ), Archer's Equation becomes:

$$\Delta H_u = 0.05081 (V_u - V_o)^{1.919} \quad \dots \text{Eq. 2.30}$$

For the limiting case where  $V_o$  equals zero, experiments at the University of Michigan indicate that Archer's Formula

FIGURE 2.4

COMPARISON BETWEEN EQUATION 2.25 AND  
EXPERIMENTAL EVIDENCE FOR SUDDEN EXPANSIONS.

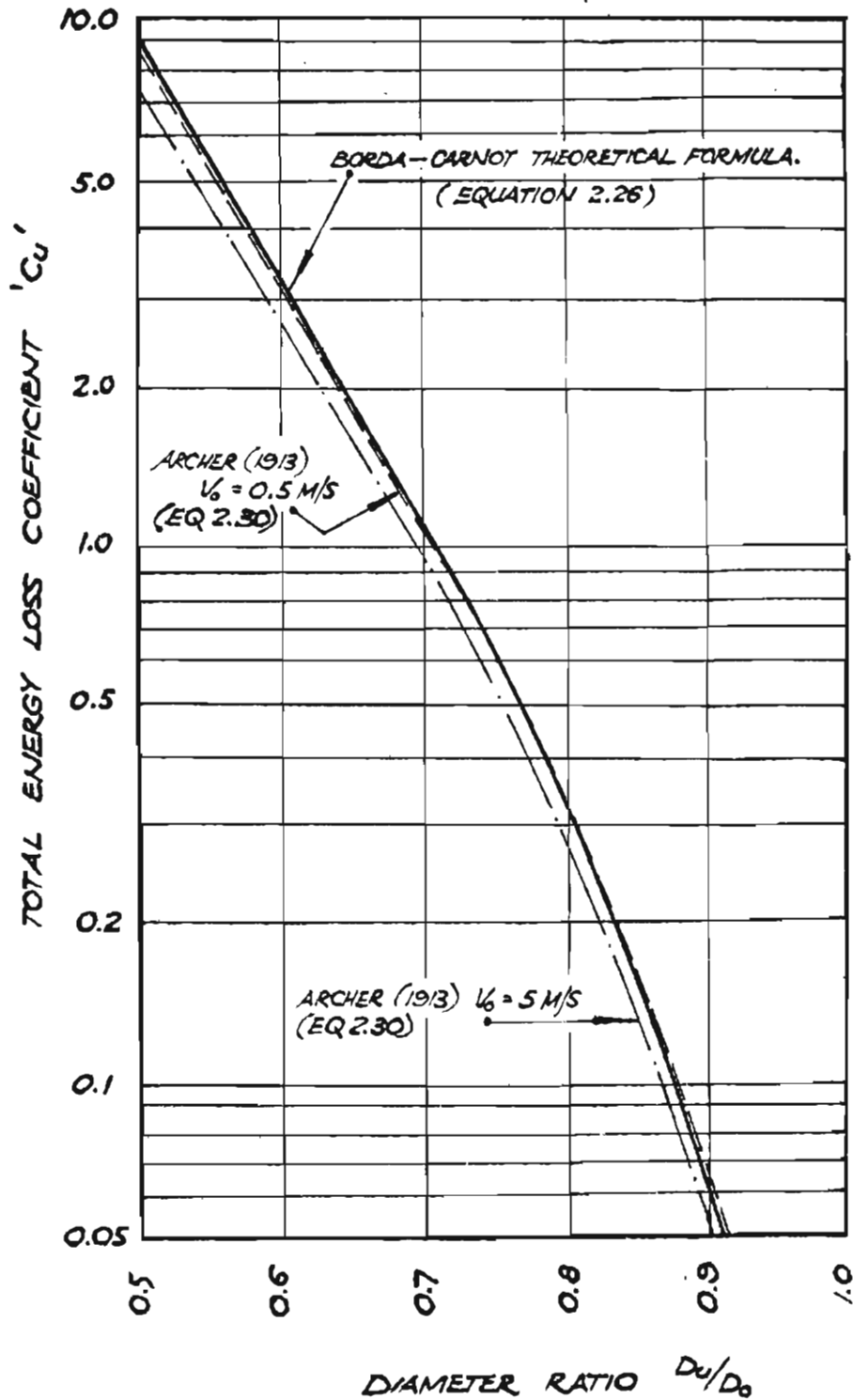
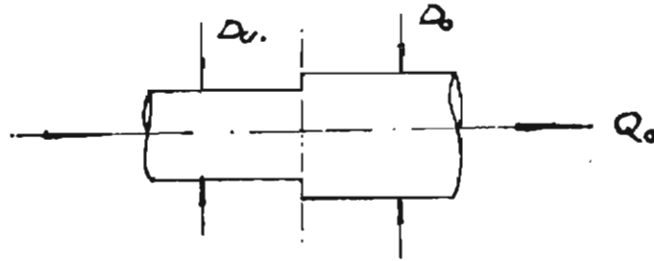
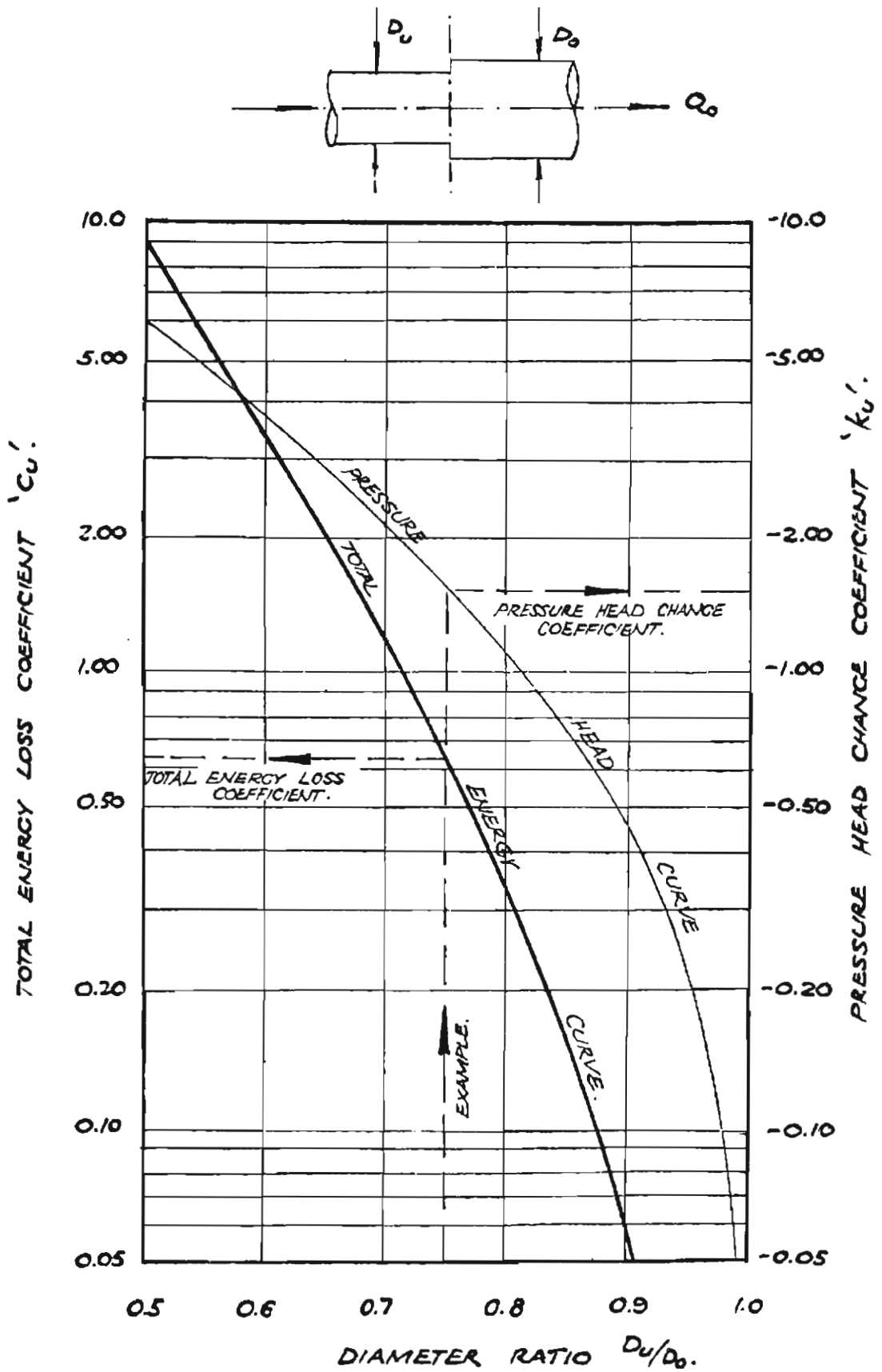




FIGURE 2.5: ENERGY LOSSES AND PRESSURE HEAD CHANGES AT SUDDEN EXPANSIONS.



$$C_u = \left[ \left( \frac{D_o}{D_u} \right)^2 - 1 \right]^2 \quad \text{AND} \quad k_u = 2 \left( 1 - \left( \frac{D_o}{D_u} \right)^2 \right)$$

is quite satisfactory. Equation 2.30 has been plotted on Figure 2.4 for  $V_o = 0.5$  m/s and  $V_o = 5$  m/s. From the figure, Equation 2.25 may be considered to give a good approximation of energy losses when the diameter ratio  $D_u/D_o$  approaches 1.00, and may be considered conservative for lower values of  $D_u/D_o$ .

Figure 2.5 presents total energy loss and pressure head change coefficients based on Equations 2.25 and 2.24 respectively.

### 2.5.2 Sudden Contractions

For sudden contractions, a reduction of Equation 2.19 setting  $R_x$  and  $p_u$  equal to zero, will yield Equation 2.24. However, "Expansions and contractions ..... cannot be treated in the same fashion due to the unknown distribution of piezometric head over the contraction face in the latter case" (Sangster, 1958, p. 22). Various authors present design data relating to the losses across reducers. Few, however, cite the source of experimental evidence. Energy loss and pressure head change coefficients from various source are presented in Figure 2.6. King (1963) accredits Merriman (1916) with the universally recognized formula of Equation 2.31.

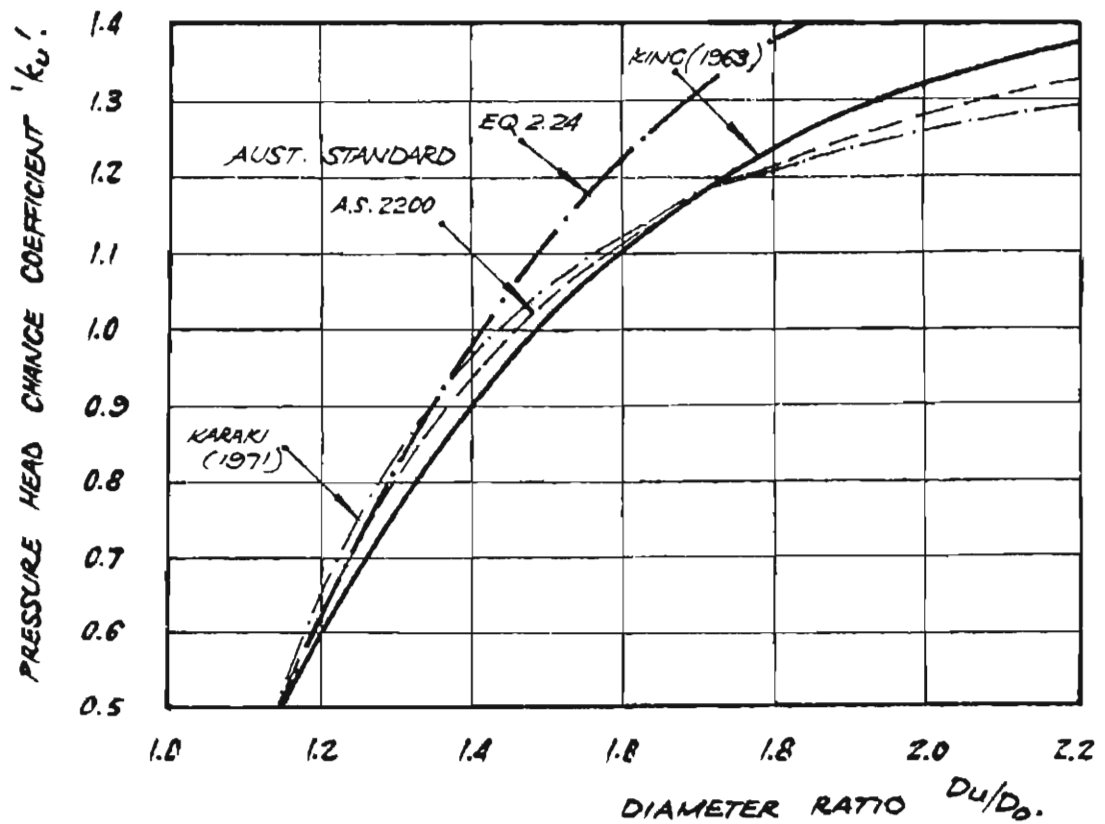
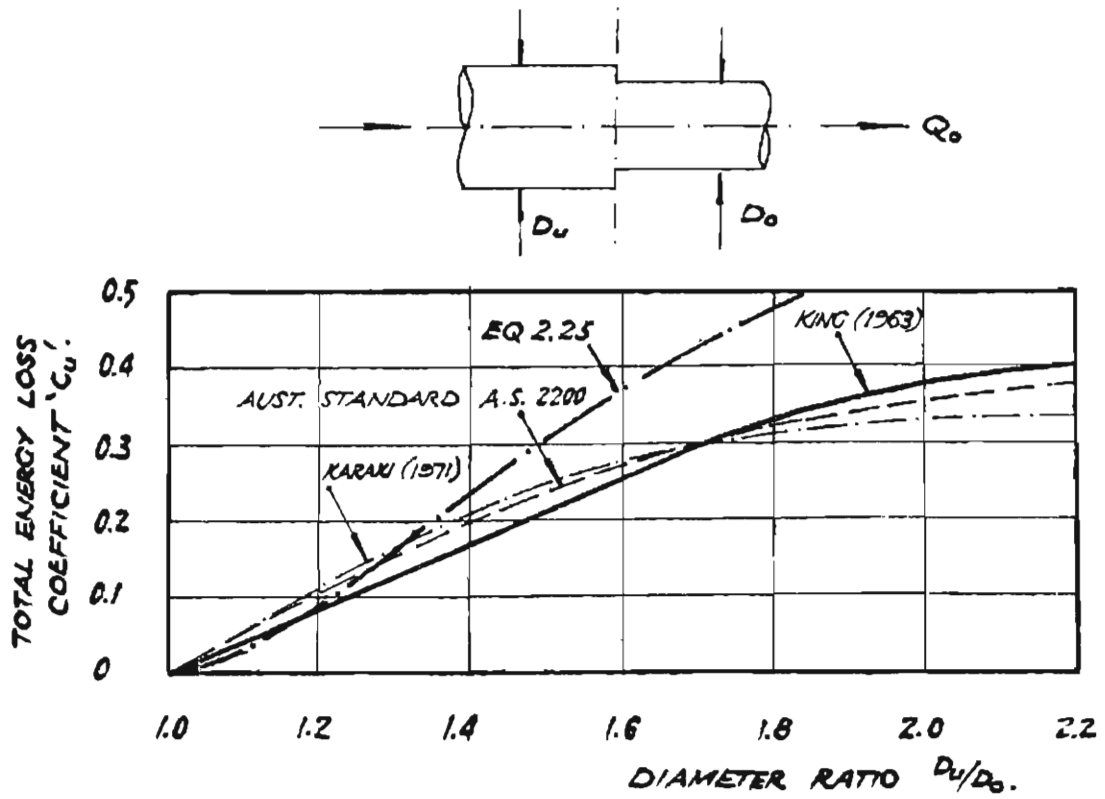
$$\Delta H_u = \left( \frac{1}{C_c} - 1 \right)^2 \frac{V_o^2}{2g} \quad \dots \text{Eq. 2.31}$$

where  $C_c$  is the contraction co-efficient defined by Equation 2.32.

$$C_c = 0.582 - \frac{0.0418}{1.10 - (D_o/D_u)} \quad \dots \text{Eq. 2.32}$$

The formula has been found to be accurate when the head loss exceeds 0.3m but is somewhat conservative for smaller head losses. Data by Karaki (1971) and data from Australian Standard A.S.2200 have been included in Figure 2.6 for comparative purposes.

FIGURE 2.6: ENERGY LOSSES AND PRESSURE HEAD CHANGES FOR REDUCERS  
(SUDDEN CONTRACTIONS).



### 2.5.3 Mitre Bends

Simplifying Equation 2.19 for the geometry of a mitre bend and setting  $R_x$  and  $p_u$  equal to zero, Equation 2.33 may be developed.

$$k_u = 2 (1 - \cos\theta_u) \quad \dots \text{Eq. 2.33}$$

The distribution of piezometric head at the vena contracta in the downstream pipe is unknown. A logarithmic plot of total energy loss and pressure head change coefficients against angle of deflection ( $\theta_u$ ) for Equation 2.33 is shown in Figure 2.7. Ambrose (1953) has presented an alternative theoretical analysis using a "free streamline" approach, by consideration of separation at the vena contracta immediately downstream of the bend. Where the theoretical analysis set out in Section 2.3 overestimates the magnitude of losses when  $R_x$  and  $p_u$  are set equal to zero, the free streamline theory underestimates these losses. This comes about because the theory does not take into account secondary flow patterns and the resulting secondary flow losses.

Experimental work by Kirchbach (1929) and Schubart (1929) are shown to plot between the two theoretical approaches. Equation 2.33 is shown to be conservative for large deflection angles; the reaction force in these cases being more significant. Figure 2.8 shows curves fitted visually to Kirchbach and Schubart's experimental data.

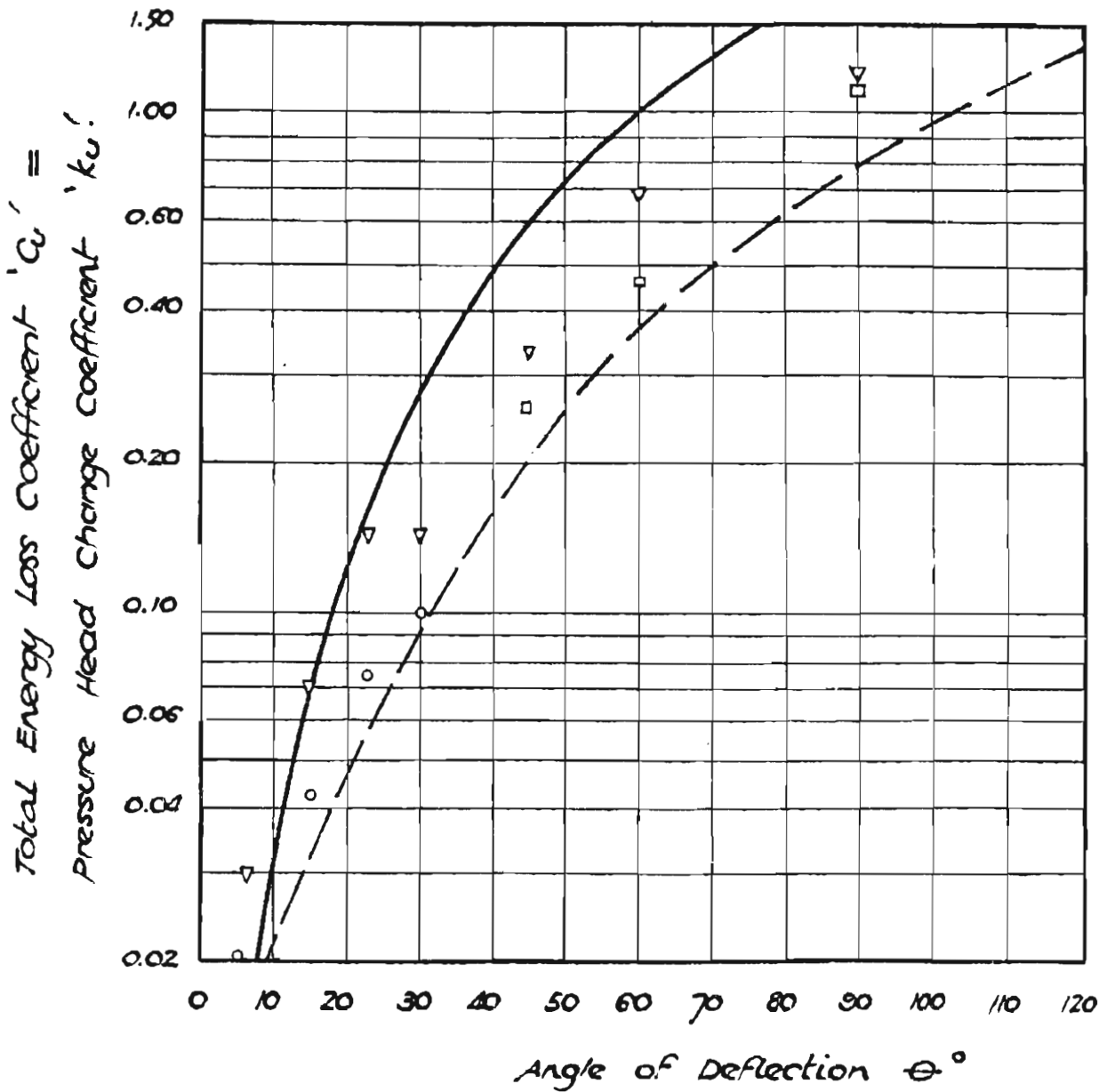
### 2.5.4 Compound Mitre Bends

Miller (1971) has presented performance curves for compound 90° mitre bends (Figure 2.9). With such bends, an adequate length must be provided between adjacent bends in order to minimize the overall bend loss. This length should be approximately 1.5 pipe diameters for optimal design. Data is not presented by Miller for bends having a total deflection angle less than 90° (for example, 2 x 30° mitre bends making a 60° compound junction) and such junctions do not lend themselves to theoretical solutions.

FIGURE 2.7

COMPARISON BETWEEN EQUATION 2.33 AND EXPERIMENTAL EVIDENCE FOR SINGLE MITRE BEND PIPE JUNCTIONS.

- LEGEND : □ KIRCHBACH (1929) SMOOTH PIPES  
 ○ SCHUBART (1929) SMOOTH PIPES  
 ▽ SCHUBART (1929) ROUGH PIPES.  
 — EQUATION 2.33  
 - - - FREE STREAMLINE THEORY (AMBROSE, 1953).



**FIGURE 2.8: PERFORMANCE OF MITRE BENDS.**

(NOTE : CURVES HAVE BEEN FITTED VISUALLY TO EXPERIMENTAL DATA AS PER FIGURE 2.7.)

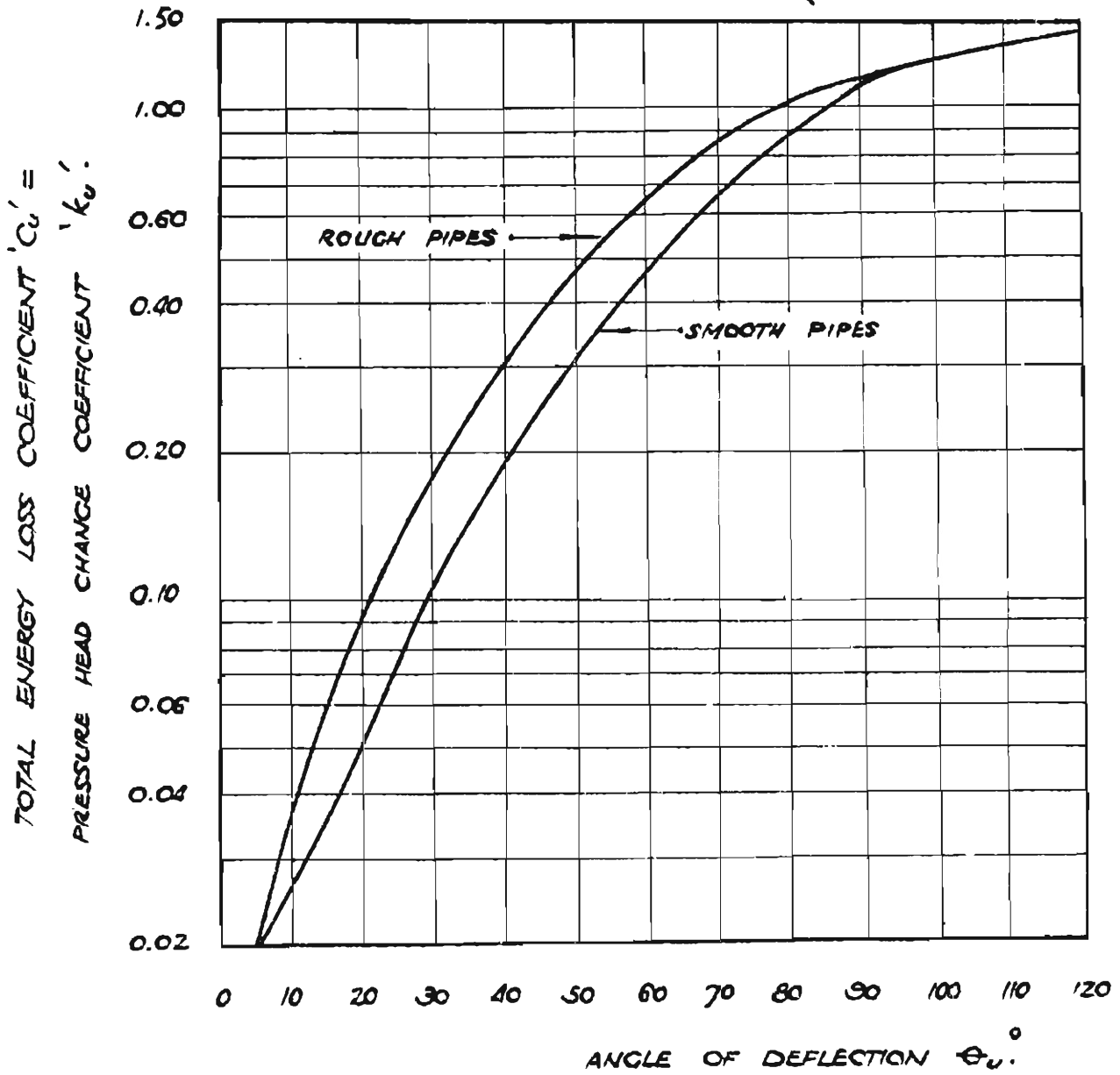
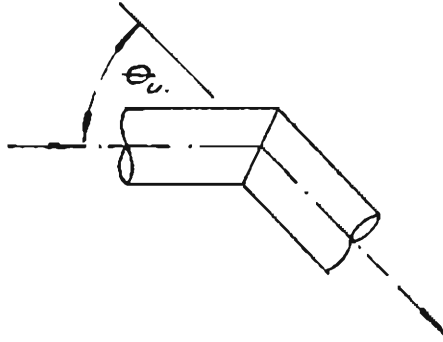
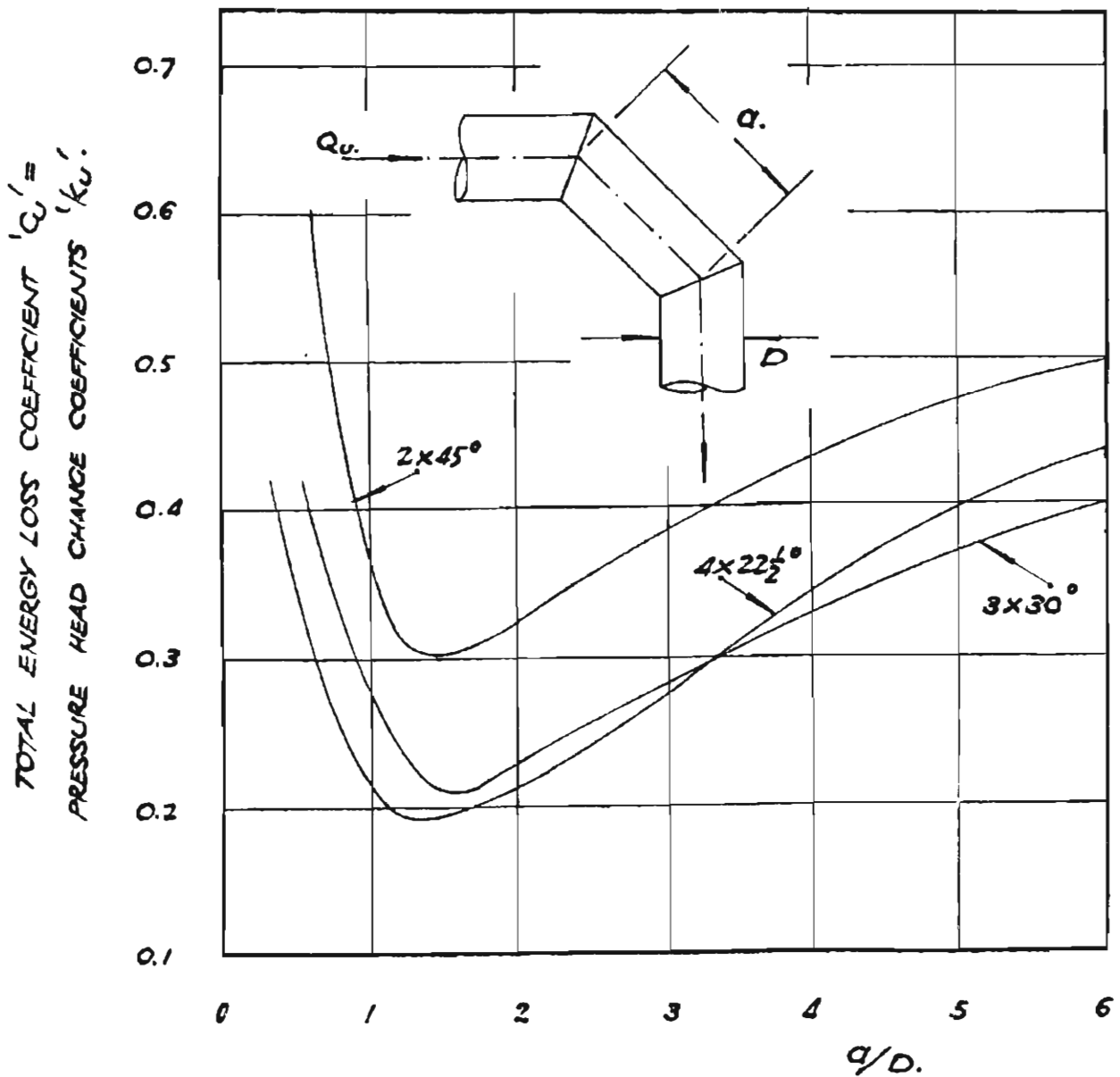


FIGURE 2.9PERFORMANCE OF COMPOUND 90° MITRE BENDS.(SOURCE: MILLER (1971)).

FOR COMPOUND BENDS OF LESS THAN 90° DEFLECTION,  
USE TABLE 2.1.



Based on the hydraulic performance of single mitre bends (Figure 2.7), and compound  $90^\circ$  junctions (Figure 2.8), the values of loss coefficients as set out in Table 2.1 have been obtained by interpolation for a spacer length (a/D in Figure 2.9) of 1.5 pipe diameters. The values thus represent minimum design values.

TABLE 2.1

TOTAL ENERGY LOSS COEFFICIENTS FOR COMPOUND MITRE BENDS

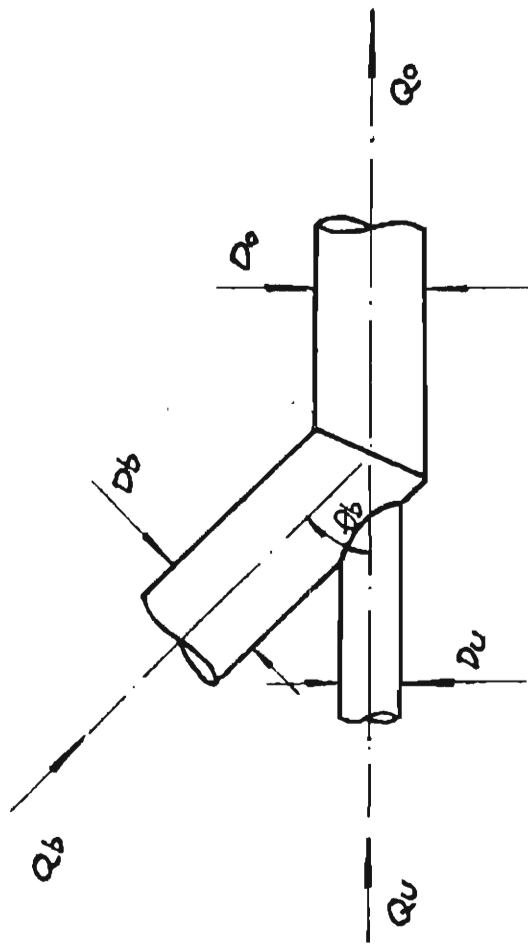
Geometric Configuration	Total Energy Loss Coefficient	
	Smooth Pipes	Rough Pipes
2 x $22\frac{1}{2}^\circ$	0.10	0.14
3 x $22\frac{1}{2}^\circ$	0.14	0.17
2 x $30^\circ$	0.16	0.20
2 x $37\frac{1}{2}^\circ$	0.24	0.27

(Note: Total Energy Loss and Pressure Head Change Coefficients are equal)

For other spacer length dimensions, larger coefficient values should be expected. While no experimental evidence is known to be available to support Table 2.1, interpolation between Figures 2.8 and 2.9 yields values accurate to approximately 0.03.

Little advantage appears to be gained from use of "lobster-back" bends when more than three individual mitre bends are used compositely. By comparison with available data, the curve representing 4 x  $22\frac{1}{2}^\circ$  bends in Figure 2.9 approximates the curve attributable to a circular arc for values of a/D greater than 1.5 (Miller (1971) pp. 194-195).





FOR BOTH MAIN AND LATERAL CONDUITS :

$$k_u = k_b = 2 \left( 1 - \frac{A_b}{A_u} \right) + 4 \left( \frac{Q_b}{Q_o} \right) \left( \frac{A_b}{A_u} \right) - 2 \left( \frac{A_b}{A_u} + \frac{A_b}{A_b} \cos \theta_b \right) \left( \frac{Q_b}{Q_o} \right)^2 .$$

———— EQUATION 2.34

**FIGURE 2.10**  
**RECOMMENDED EQUATION FOR PRESSURE HEAD CHANGE COEFFICIENTS**  
**AT INTAKE JUNCTIONS.**

### 2.5.5 Intake Junctions

The provision of a simple upstream inlet pipe attached to a mitre bend junction (as shown in Figure 2.3(E) ) is easily achieved in pipe junction manufacture. Unfortunately, experimental evidence regarding the hydraulic efficiency of such junctions does not appear to be available and a theoretical solution is necessary. Such solutions should yield conservative values of loss coefficients for most geometric configurations.

Equation 2.34 is presented as a theoretical solution for intake junctions.

$$k_u = k_b = 2 \left( 1 - \frac{A_o}{A_u} \right) + 4 \left( \frac{Q_b}{Q_o} \right) \left( \frac{A_o}{A_u} \right) - 2 \left( \frac{A_o}{A_u} + \frac{A_o}{A_b} \cos \theta_b \right) \left( \frac{Q_b}{Q_o} \right)^2$$

... Eq. 2.34

Equation 2.34 is a simplification of Equation 2.19 with  $R_x$  and  $p_u$  set equal to zero.

### 2.5.6 Slope Junctions

For slope junctions (Figure 2.3(F) ), Equation 2.19 may be reduced to Equation 2.35.

$$k_u = k_b = 4 \left( \frac{Q_b}{Q_o} \right) - 2 \left( 1 + \frac{A_o}{A_b} \cdot \cos \theta_b \right) \left( \frac{Q_b}{Q_o} \right)^2$$

... Eq. 2.35

Total Energy Loss Equations 2.12 and 2.13 similarly reduce to Equations 2.36 and 2.37 respectively.

$$C_u = 2 \left( \frac{Q_b}{Q_o} \right) - \left( 1 + 2 \frac{A_o}{A_b} \cos \theta_b \right) \left( \frac{Q_b}{Q_o} \right)^2$$

... Eq. 2.36

$$C_b = -1 + 4 \left( \frac{Q_b}{Q_o} \right) - \left[ 2 + 2 \frac{A_o}{A_b} \cos \theta_b - \left( \frac{A_o}{A_b} \right)^2 \right] \left( \frac{Q_b}{Q_o} \right)^2$$

... Eq. 2.37

Equations 2.36 and 2.37 were derived by Favre (1937). Blaisdell and Manson (1963) performed a comprehensive series of experiments to check derived theory for total energy loss coefficients at slope junctions. They reported that:

"In general, the theoretical junction loss coefficients are greater than the observed loss coefficients. Use of the theoretical coefficients in place of the observed coefficients would thus err on the side of conservatism." (ibid p. 46)

"Graphical analysis of the general equations for determining the junction energy loss coefficients in the main (pipe) shows that the theoretical equations generally give predictions as good as or better than the least squares developed equations. For the lateral the situation is reversed with the least squares equations giving predictions of the junction energy loss coefficients that are in better agreement with the observed values than are the theoretical coefficients. Statistical tests ... show that the theoretical equations well represent the observed data even though the least squares equations are more representative".

(ibid p.58)

Gardel (1957) makes no comparative analysis between the theoretical equations and his experimental results; he does briefly state, however, that:

"One finds several differences, especially when the loss of head is small ... " (p. 6).

Theoretical and experimentally derived equations for total energy loss coefficients,  $C_u$  and  $C_b$ , are compared in Table 2.2, and need to be modified using Equations 2.16 and 2.18 to determine the pressure head change coefficients,  $k_u$  and  $k_b$ . Figures 2.11 and 2.12 illustrate for a  $45^\circ$  slope junction the equations set out in Table 2.2, after modification to pressure head change coefficients.

Figure 2.11 represents the pressure head change coefficients ( $k_u$ ) for the main conduit whilst those for the lateral ( $k_b$ ) are represented in Figure 2.12. Comparison of the two figures reveals some variation between  $k_u$  and  $k_b$  for experimentally derived curves. The variation becomes more pronounced as  $\theta_b$  approaches  $90^\circ$ . Also of

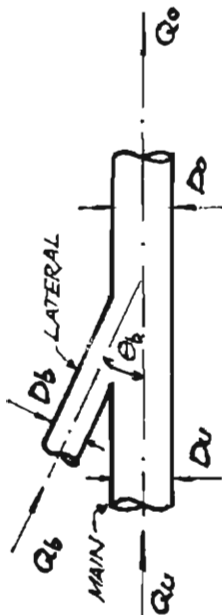


TABLE 2.2.

COMPARISON OF ENERGY LOSS EQUATIONS FOR SHARP-EDGED SLOPE JUNCTIONS.		(SOURCE: BLAISDELL & MANSON (1967)).	
MAIN:			
GARDEL (1957)	$C_v = 0.03 \left(1 - \frac{D_6}{D_0}\right)^2 + \left(2 - \frac{A_6}{A_0}\right) \left(\frac{D_6}{D_0}\right) - [1.00$	$+ 1.62 \frac{A_0}{A_6} \cos \theta_6 - 0.62 \frac{A_6}{A_0}$	$]\left(\frac{D_6}{D_0}\right)^2$
BLAISDELL & MANSON (1963) - GRAPHICAL.	$C_v = 0$	$+ 1.50 \left(\frac{D_6}{D_0}\right) - [0.75$	$+ 1.90 \frac{A_0}{A_6} \cos \theta_6$
BLAISDELL & MANSON (1963) - LEAST SQUARES	$C_v = 0$	$+ 2.78 \left(\frac{D_6}{D_0}\right) - [2.15$	$+ 1.91 \frac{A_0}{A_6} \cos \theta_6$
THEORETICAL	$C_v = 0$	$+ 2 \left(\frac{D_6}{D_0}\right) - [1$	$+ 2 \frac{A_0}{A_6} \cos \theta_6$
LATERAL:			
GARDEL (1957)	$C_b = -0.92 \left(1 - \frac{D_6}{D_0}\right)^2 + \left(2 - \frac{A_6}{A_0}\right) \left(\frac{D_6}{D_0}\right) - [1.60$	$+ 0.20 \frac{A_0}{A_6} \cos \theta_6 - \frac{A_6}{A_0} - 0.8 \left(\frac{A_0}{A_6}\right)^2 + \cos \theta_6$	$]\left(\frac{D_6}{D_0}\right)^2$
BLAISDELL & MANSON (1963) - GRAPHICAL	$C_b = -0.95$	$+ 3.70 \left(\frac{D_6}{D_0}\right) - [1.20$	$+ \frac{A_0}{A_6} - \left(\frac{A_0}{A_6}\right)^2$
BLAISDELL & MANSON (1963) - LEAST SQUARES	$C_b = -0.76$	$+ 2.16 \left(\frac{D_6}{D_0}\right) - [1.61$	$+ 0.56 \frac{A_0}{A_6} \cos \theta_6 - 0.87 \left(\frac{A_0}{A_6}\right)^2$
THEORETICAL	$C_b = -1$	$+ 4 \left(\frac{D_6}{D_0}\right) - [2$	$+ 2 \frac{A_0}{A_6} \cos \theta_6 - \left(\frac{A_0}{A_6}\right)^2$

N.B. TO CONVERT TO PRESSURE HEAD CHANGE COEFFICIENTS USE EQUATIONS 2.16 AND 2.18 .

FIGURE 2.11

45° SLOPE JUNCTION.

PRESSURE HEAD CHANGE COEFFICIENT IN MAIN CONDUIT VS. DISCHARGE RATIO.

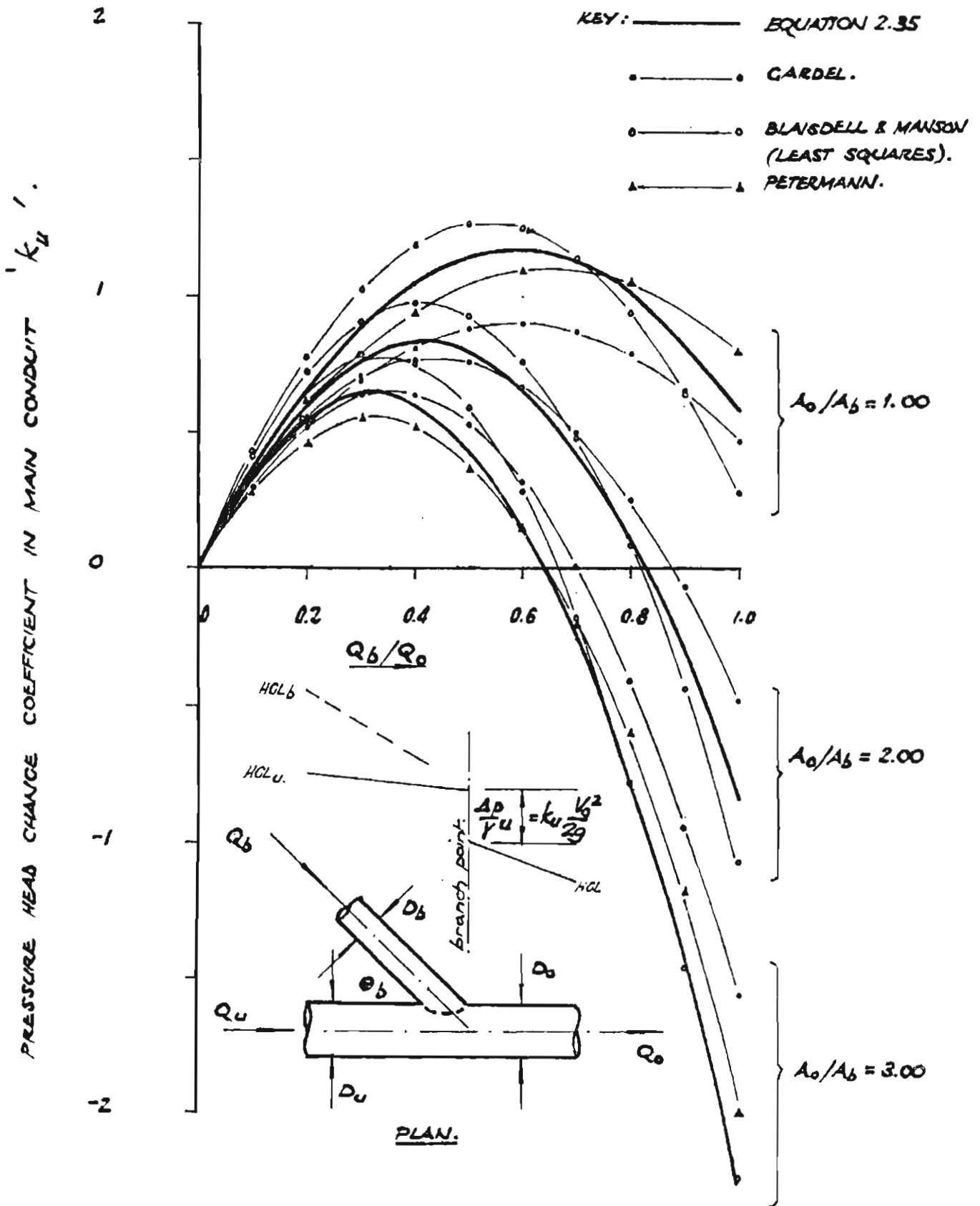
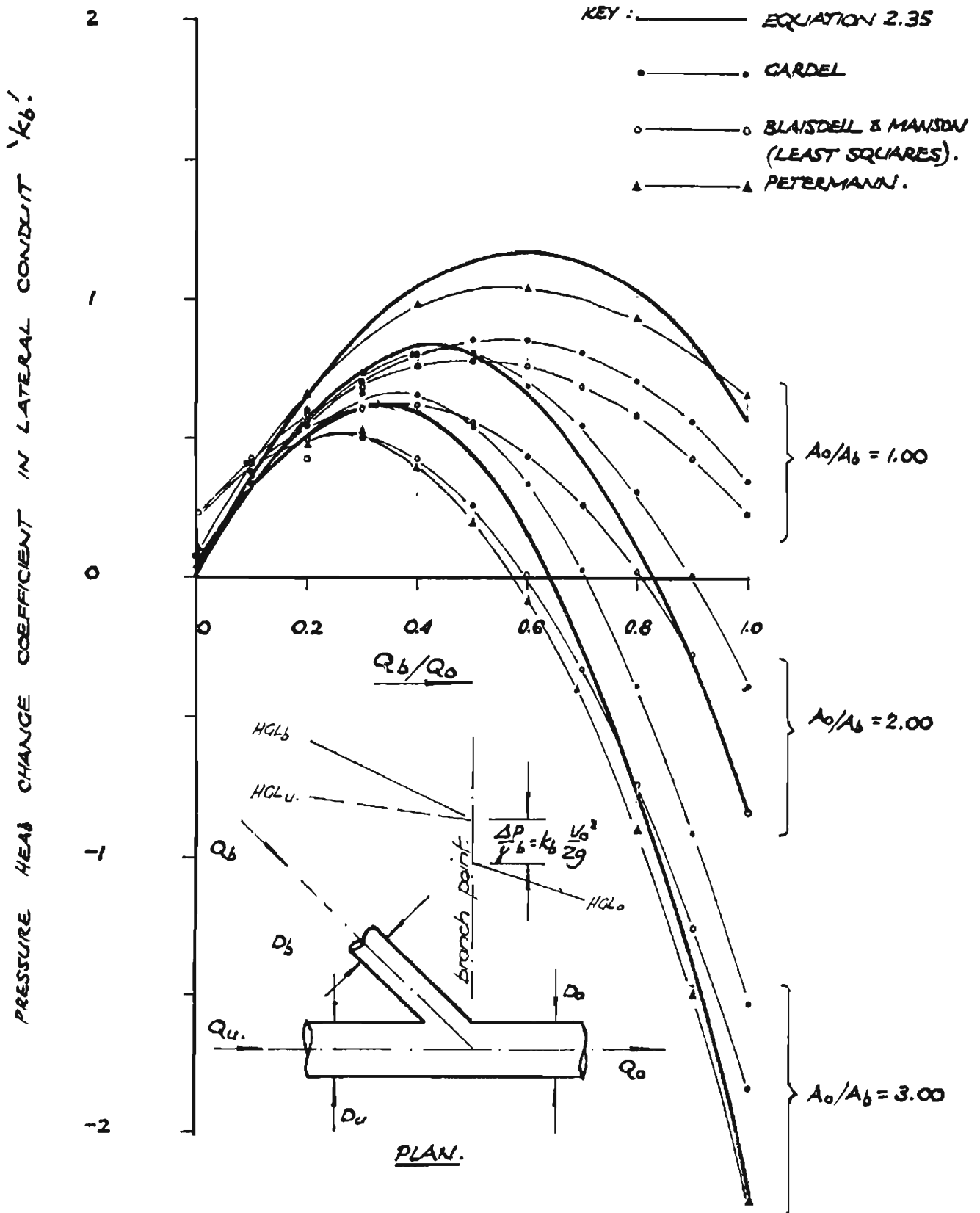


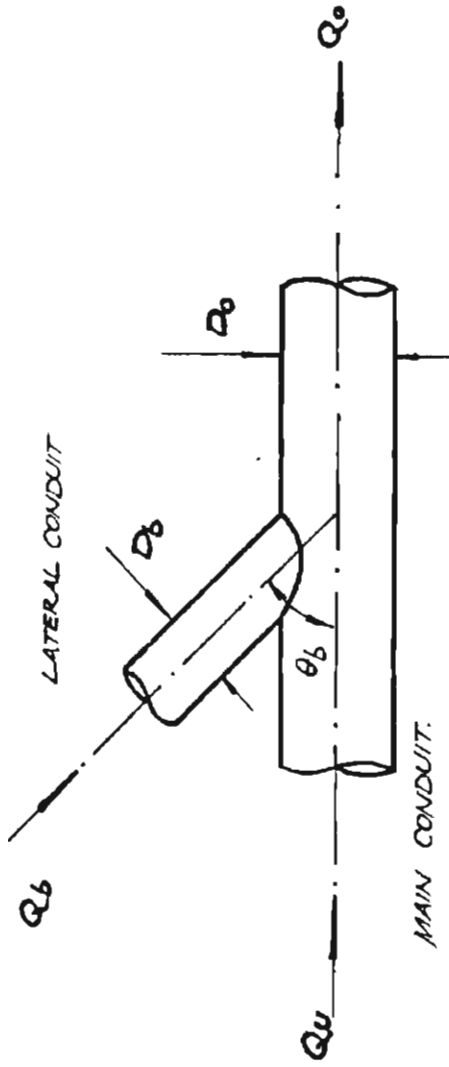
FIGURE 2.12

45° SLOPE JUNCTION.

PRESSURE HEAD CHANGE COEFFICIENT IN LATERAL CONDUIT VS.

DISCHARGE RATIO.





FOR THE MAIN CONDUIT:

$$k_u = 4 \left( \frac{Q_b}{Q_0} \right) - 2 \left( 1 + \frac{A_b}{A_0} \cdot \cos \theta_b \right) \left( \frac{Q_b}{Q_0} \right)^2 \quad \text{--- EQUATION 2.35}$$

FOR THE LATERAL CONDUIT:

$$k_b = 0.24 + 2.16 \left( \frac{Q_b}{Q_0} \right) - \left[ 1.61 + 0.56 \frac{A_b}{A_0} \cos \theta_b - 1.84 \left( \frac{A_b}{A_0} \right)^2 \right] \left( \frac{Q_b}{Q_0} \right)^2.$$

--- EQUATION 2.44

FIGURE 2.13

RECOMMENDED EQUATIONS FOR PRESSURE HEAD CHANGE COEFFICIENTS  
AT SLOPE JUNCTIONS.

interest in these figures is the ability to obtain negative values for the pressure head change coefficients given suitable geometric and flow configurations. Such values occur as a result of flow deceleration across the junction.

A comparison of total energy loss coefficients determined by various investigators was developed by Blaisdell and Manson (1963). Equations 2.36 and 2.37 have been shown to produce conservative results for most junction geometries and flow divisions. Use of the theoretical equations generally yields higher coefficient values than experimental data support.

In conclusion, Figure 2.13 presents the Equations recommended by Blaisdell and Manson (1963) for both main and lateral conduit pressure head change coefficients for slope junctions. (Equation 2.44 is the pressure head change equation corresponding to the least squares total energy loss equation developed by Blaisdell and Manson for the lateral conduit (shown as Equation 2.43 in Table 2.2).

#### 2.5.7 Vertical Entry Junctions

For vertical entry junctions (Figure 2.3(G) ), Equation 2.19 reduces to Equation 2.45.

$$k_u = 4 \left( \frac{Q_b}{Q_o} \right) - 2 \left( \frac{Q_b}{Q_o} \right)^2 \quad \dots \text{Eq. 2.45}$$

where  $Q_b$  is the discharge through the vertical entry.

Using the relationship  $Q_o = Q_u + Q_b$ , Equation 2.45 may be rewritten as Equation 2.46.

$$k_u = 2 \left( 1 - \frac{Q_u}{Q_o} \right)^2 \quad \dots \text{Eq. 2.46}$$

This equation has been checked against data for pit junctions where additional flow enters through a grate-inlet (the pit being larger than the connecting pipes). The



reader is referred to Chapter 5 for details. It should be noted, however, that when  $Q_u/Q_o$  is equal to 0.50, the pressure head change coefficient has been found experimentally to equal 1.5 for pit junctions when  $D_u/D_o$  is equal to 1.00. Similar values for pipe junctions will result using Equation 2.46. The corresponding total energy loss equation for vertical entry junctions may be determined from Equation 2.47.

$$C_u = 1 - \left(\frac{Q_u}{Q_o}\right)^2 \quad \dots \text{Eq. 2.47}$$

## 2.6 Effect of the Reynold's Number

Blaisdell and Manson (1963) state that viscosity effects, as measured by the Reynold's Number, are known to affect the magnitudes of the various resistance coefficients. This relationship is reflected in the derived theoretical equations (Equations 2.12, 2.13 and 2.19) by the inclusion of the pressure component  $(-2p_u A_o / \rho Q_o V_o)$ . For a fixed geometry, the static upstream pressure can only rise with an increase in discharge (i.e., Reynold's Number).

Anderson and Straub (1948) point out that, "in the turbulent range, the bend coefficient decreases with increasing Reynold's Number until ..... a point is reached where it becomes independent of the Reynold's Number, and remains constant".

Miller (1971) suggests that the Reynold's Number correction factor remains constant (equal to 1.00) for Reynold's Numbers greater than 200,000. Similarly, Blaisdell and Manson (1967) conclude that, "the energy loss coefficient will decrease slightly as the Reynold's Number increases for Reynold's Numbers somewhat below about 150,000".

In urban drainage design, Reynold's Numbers below 200,000 are rarely present due to minimum pipe diameter and minimum flow velocity specifications. It may therefore be concluded that viscosity effects are not significant in such applications.

## 2.7 Summary : Pit Junction Hydraulics

A theoretical solution has been developed to evaluate the hydraulic performance of flow through pipe junctions for the general case of three converging pipes. Certain assumptions have been applied to the theory to provide a simplified approach which can be checked against experimental data. Where such data is not available, the simplified theoretical solution will yield conservative but adequate values. For commercially available junctions which do not lend themselves to theoretical analysis (such as compound bends), experimental data have been reviewed to allow the determination of loss coefficients for such geometries.

Estimates of hydraulic performance have thus been provided for most commercially available pipe junctions.

CHAPTER 3

JUNCTION PIT HYDRAULICS

- 3.1 Introduction
- 3.2 Literature Review
- 3.3 Flow Across Pit Junction Structures
- 3.4 Effect of Pit Size and Shape
- 3.5 Combining Flow at Three Pipe Junction
- 3.6 Effect of Froude Number and Submergence  
on Pressure Head Change Coefficients
- 3.7 Summary : Pit Junction Hydraulics

## JUNCTION PIT HYDRAULICS

### 3.1 Introduction

When water flows through a piped drainage system, energy is lost due to frictional resistance along each pipe length. In addition, other energy losses occur wherever the flow undergoes a change in momentum, such as at a change in flow direction or with the introduction of additional flow at a junction structure. In some circumstances, particularly where pipe lengths are short or where pipes are laid on hydraulically steep grades, losses attributable to such structures may be relatively large. For a design example given by Sangster *et al* (1958), Jens and McPherson calculated losses at inlets and manholes to comprise 37% of the overall pipe friction loss and conclude that such losses are much greater than estimates made by ordinary design criteria. (Chow (1964) p. 20-31).

### 3.2 Literature Review

A comprehensive literature search, using both manual techniques and a computerized reference system, revealed relatively little past research into storm drain junction hydraulics. Two of the three research programmes that were uncovered were concerned with the nature of flow across pit junctions for which all connecting pipes were flowing full and under pressure (Sangster *et al* (1958) and Archer *et al* (1978) ). A third study, Prins (1976) dealt with energy losses under part-full flow conditions and was aimed at establishing the optimum channel invert shape across the junction. These investigations, however, are limited in their application to design since only specific geometric configurations have been tested to satisfy localized design problems. Other references were found to present fragmented material or, in some cases, to simply present a repeat of Sangster's work. Only the three references above gave an adequate appreciation of junction hydraulics. These references are reviewed below.

### 3.2.1 Sangster, Wood, Smerdon, and Bossy (1958)

In 1953, a research programme to establish the effects of open pit junctions on the magnitude of pressure head changes in storm drain systems flowing full was initiated by Sangster, Wood, Smerdon and Bossy at the Civil Engineering Department of the University of Missouri. The project took five years to complete. The majority of tests performed by these investigators involved grate drop inlet junctions of rectangular shape. The junctions investigated were in common use by the Missouri State Highway Department. The extent of the work may be summarized as follows:

"Rectangular boxes serving as inlets for surface flow alone, and as combination inlets and pipe junctions, were studied. Square and round manholes were also investigated. Several measures were evolved to reduce pressure losses for junction types otherwise characterized by especially large losses. The report covers the laboratory investigation and presents an analysis of the hydraulic characteristics of most of the structures investigated. Methods for converting the test results into design methods are discussed. A concluding section includes methods for the design of inlets and junctions in storm drain systems flowing full, together with illustrative examples." (*ibid*, p.iii)

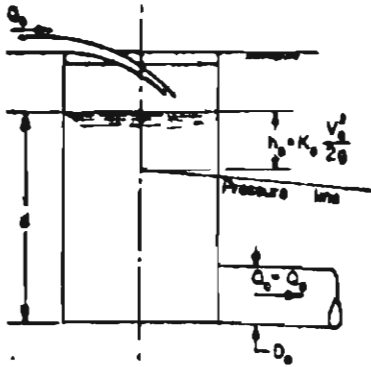
The geometries tested by Sangster *et al* are shown in Figure 3.1. Each geometry tested comprised either a  $0^{\circ}$  or  $90^{\circ}$  bend structure. The study of junctions with angles other than those tested was recommended by the authors as a topic worthy of further investigation (*ibid*, p. 81).

The work of Sangster *et al* at the University of Missouri provided data and methods which may be used in the hydraulic design of stormwater drainage structures. "Designs based on the data can be made with assurance so long as the basic limitations of the data are not exceeded" (*ibid*, p. 81). The main difficulty in the use of their data is the limited range of manhole geometries considered. The hydraulic

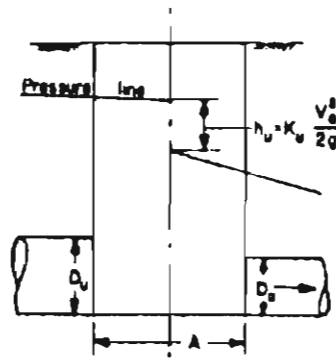
FIGURE 3.1

JUNCTION CONFIGURATIONS TESTED BY SANGSTER ET AL.

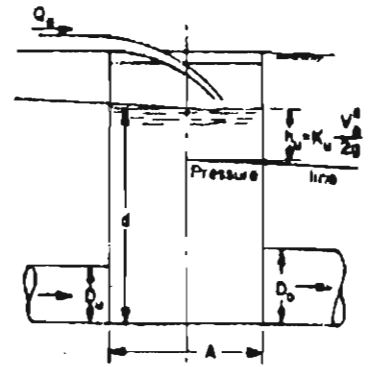
(source : Queensland Dept of Main Roads Road Manual).



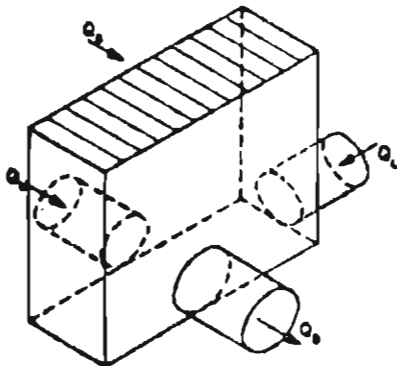
B. Rectangular inlet with grate flow only.



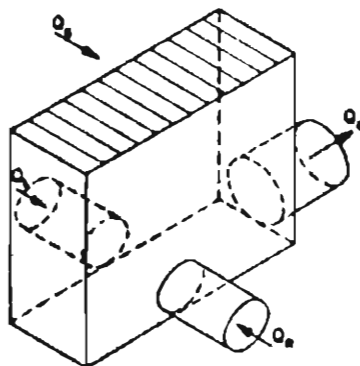
C. Flow straight through any junction



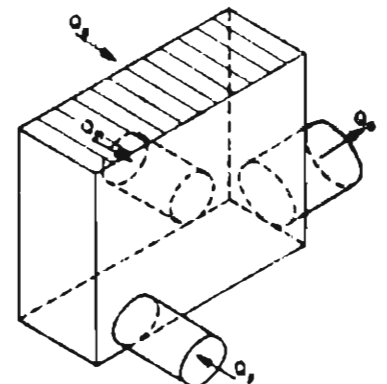
D. Rectangular inlet with through pipeline and grate flow.



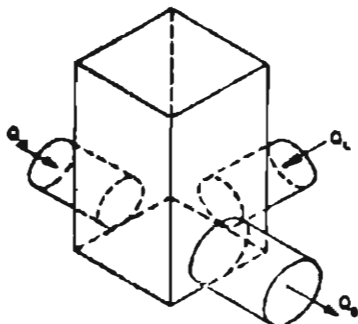
E. Rectangular inlet with in-line up-stream main and 90° lateral pipe (with or without grate flow)



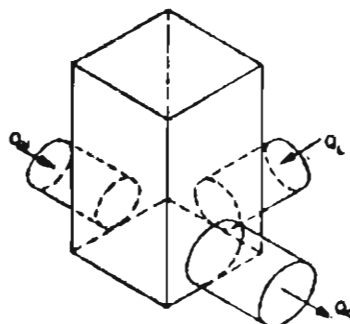
F. Rectangular inlet with in-line opposed lateral pipes each at 90° to outfall (with or without grate flow)



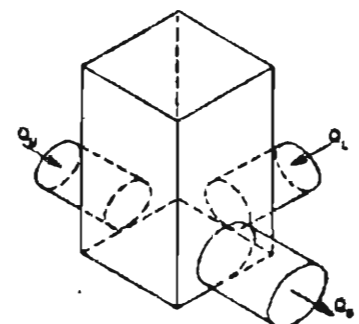
G. Rectangular inlet with offset opposed lateral pipes each at 90° to outfall (with or without grate flow)



H. Lateral coefficient



J. In-line pipe coefficient



K. Lateral or in-line pipe coefficient.

Square or round manholes at 90° deflection or on through pipeline at junction of a 90° pipe.

performance of geometries of angles other than  $0^\circ$  and  $90^\circ$  cannot be determined using interpolation or modification procedures, since junctions invariably produce significant discontinuities in flow patterns with changing angles of deflection. Typical results obtained by Sangster *et al* are summarized in Table 3.1:

TABLE 3.1  
TYPICAL VALUES OF  $k_u$  FOR PIT JUNCTIONS TESTED BY SANGSTER  
*et al*, (1958)

Junction Geometry	Typical $k_u$
1. Straight through manhole without lateral or change in pipe size.	0.1 - 0.2
2. Straight through manhole with change in pipe size.	- 0.5
3. Upstream pipe in line with outlet with 20% grate flow.	0.6
4. Upstream pipe in line with outlet pipe and $90^\circ$ lateral. Flow from lateral 20% of total flow.	0.5
5. Two opposed laterals, one-third the flow from the lateral with the higher velocity.	0.7
6. Two offset opposed laterals, two-third of the flow from the lateral nearest the outlet pipe.	1.5 - 1.9
7. $90^\circ$ angle, without change in size. No lateral.	1.6
8. Upstream pipe in line with outlet, plus $90^\circ$ lateral. Flow equally divided between the upstream pipes	1.2

### 3.2.2 Archer, Bettess and Colyer (1978)

Work on junction pit losses has also been performed at the Hydraulic Research Station, Wallingford, England, by Archer *et al*. The test programme involved the use of

rectangular and circular structures, to determine the magnitude of energy losses occurring at surcharged sewer manholes:

"The manholes were designed to represent typical configurations used in current sewerage practice".

(*ibid*, p.3)

The tests were limited to deflection angles of  $0^\circ$ ,  $30^\circ$  and  $60^\circ$ , with no secondary inflow through a top grate and with a constant diameter ratio,  $D_u/D_o$ , of unity. The configurations used are shown in Figure 3.2.

The authors concluded that the magnitude of the loss coefficient was independent of the discharge, the degree of submergence (i.e, pressure) and the extent of the air entrainment. The change in alignment and the manhole shape were the main factors influencing the loss of head. Results applicable to the cases tested are given in Table 3.2. The benching shown in Figure 3.2 has, in each case, a slope of 1 : 12 towards the channel.

TABLE 3.2

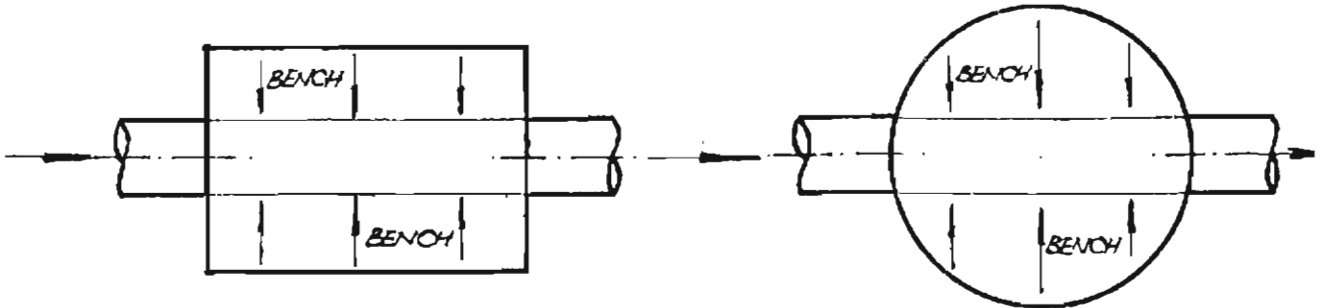
MAGNITUDE OF  $k_u$  (=  $C_u$ ) AS DETERMINED BY ARCHER *et al*

Type of Manhole	$0^\circ$ deflection	$30^\circ$ deflection	$60^\circ$ deflection
Rectangular	0.1	0.4	0.85
Circular	0.15	0.5	0.95

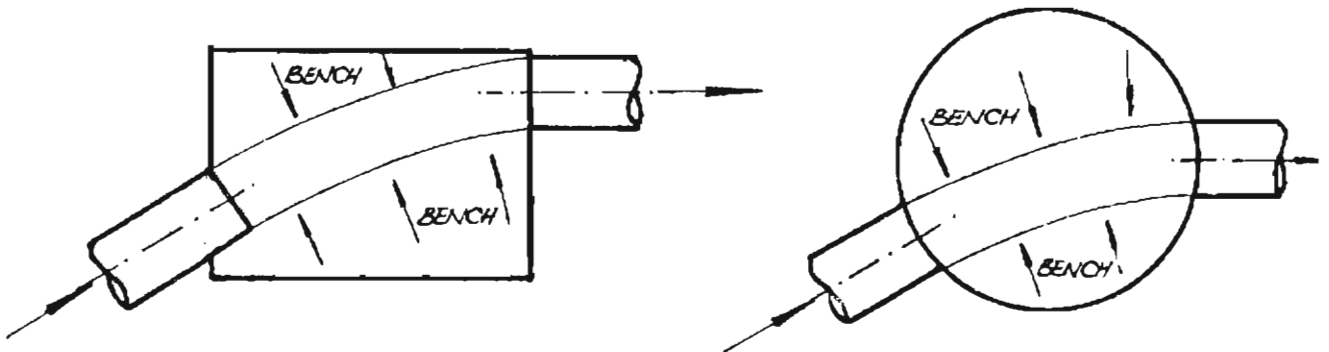


FIGURE 3.2JUNCTION CONFIGURATIONS TESTED BY ARCHER ET AL (1978).

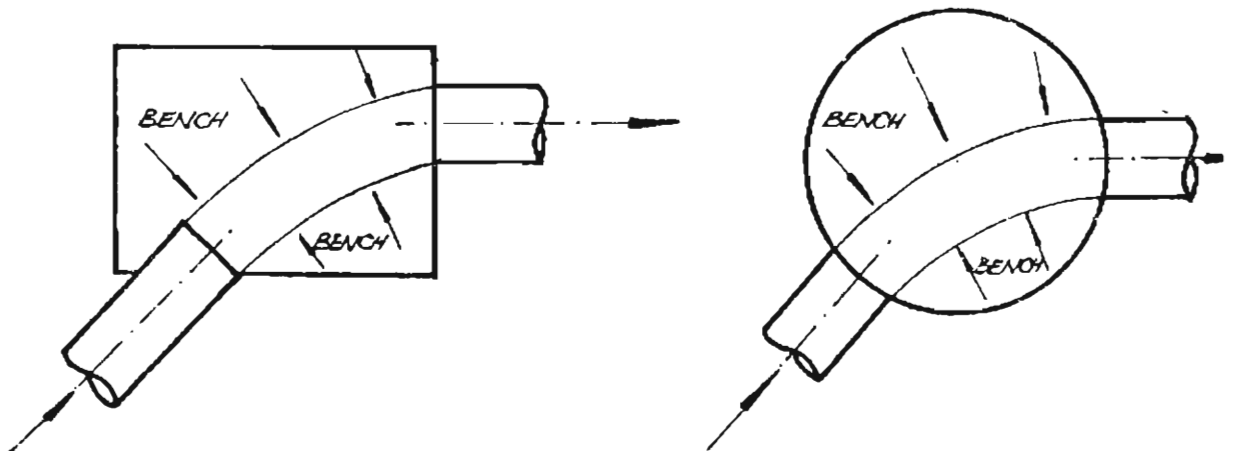
(ARROWS IN PITS INDICATE BENCHING HAS A 1:12 SLOPE TOWARDS CHANNEL).



0° DEFLECTION.



30° DEFLECTION.



60° DEFLECTION.

### 3.2.3 Prins (1976)

A research programme undertaken by Prins (1976) at the University of Ottawa was concerned primarily with variations in pit invert geometry and the magnitude of related energy losses. Prins studies the effects of such variations for pipes flowing under part-full conditions. For junctions having a 152 mm in-line main and a 102 mm lateral connecting to a junction box at either a 45° or 90° angle, Prins arrived at the following conclusions:

1. A U-shaped cross-section resulted in minimum energy loss.
2. An open junction box (with no furnishings) resulted in the highest energy loss.
3. An abrupt or smooth drop provided across a junction between pipe inverts was effective in reducing the energy loss.
4. Pit dimensions should be kept as small as possible.
5. Deflectors tested were not helpful for the 45° junction but were of benefit for 90° lateral configurations.

Prins' experimental results apply exclusively to junctions for which all connecting pipes are operating under part-full flow conditions. The conclusions drawn, however, serve as indicators for possible field improvements in existing storm drain systems which fail to perform satisfactorily.

### 3.3 Flow Across Pit Junction Structures

As water flows through a junction pit, a loss of total energy occurs due to turbulence, eddying, impact and structural vibration. This loss of total energy ( $\Delta H$ ) is converted to heat and sound energy and represents an additional energy that is required to the drain system due to the presence of the junction structure. The total energy loss is usually defined as a function of the downstream velocity head (Equations 2.21 and 2.22), where the coefficients  $C_u$  and  $C_b$  are always positive (i.e. a loss of energy occurs). A redistribution of total energy components (pressure head and velocity head) also occurs as the flow proceeds across the junction. The change in pressure head across the junction may be expressed as a function of the downstream velocity head (Equation 2.20). In this equation,  $k_u$  and  $k_b$ , the pressure head change coefficients for each upstream conduit may be either positive or negative depending upon the specific geometric and flow characteristics of the junction (i.e. either a drop or a rise in the hydraulic grade line occurs across the structure).

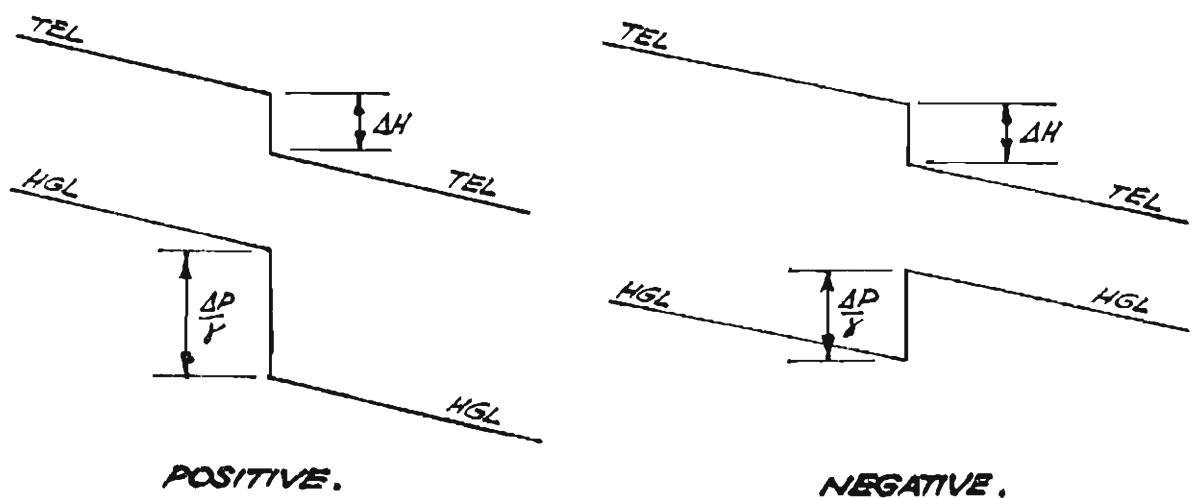


FIGURE 3.3 : POSITIVE AND NEGATIVE PRESSURE HEAD CHANGES.

Negative pressure head changes are confined to junction structures where the downstream pipe diameter is larger than the upstream pipe diameter and, based on experiment observations, where the angle of deflection across the junction is generally less than  $45^\circ$ .

If the upstream and downstream velocity heads are equal in magnitude (i.e.  $Q_u$  equals  $Q_o$  and  $D_u$  equals  $D_o$ ), the change in the pressure head across the junction will be equal to the loss in total energy. If, however, the flow configuration at the junction is complicated by either the provision of a secondary inflow (such as inlet grate flow), or by a change in pipe diameters across the junction, the upstream and downstream velocity heads cannot be equal. In these circumstances, the magnitude of the pressure head change will not correspond to the magnitude of the total energy loss across the junction. It has been shown in Chapter 2 that a relationship exists between the total energy loss and the pressure head change. Equations 2.16, 2.17 and 2.18, which were developed for pipe junctions, also apply to pit junction structures.

The energy lines shown in Figure 3.4 represent the magnitude of the total energy components (pressure head, velocity head and potential head) at the pipe centreline elevations. For example, the point 'e' represents the point of intersection of the total energy line for the upstream pipe with the centre of the junction pit. The water surface elevation in the pit will rise (or fall) to a level at least equal to the elevation of the upstream hydraulic grade line at the junction branch point (point b). The water surface elevation in the pit does not represent the total energy of the flow, but is an indication of the upstream pressure head plus some kinetic energy contributed by the upstream flow which has been lost by conversion to an additional pressure head as the flow proceeds across the junction (bc in Figure 3.4). The dimension of ec represents the upstream kinetic energy which has not undergone

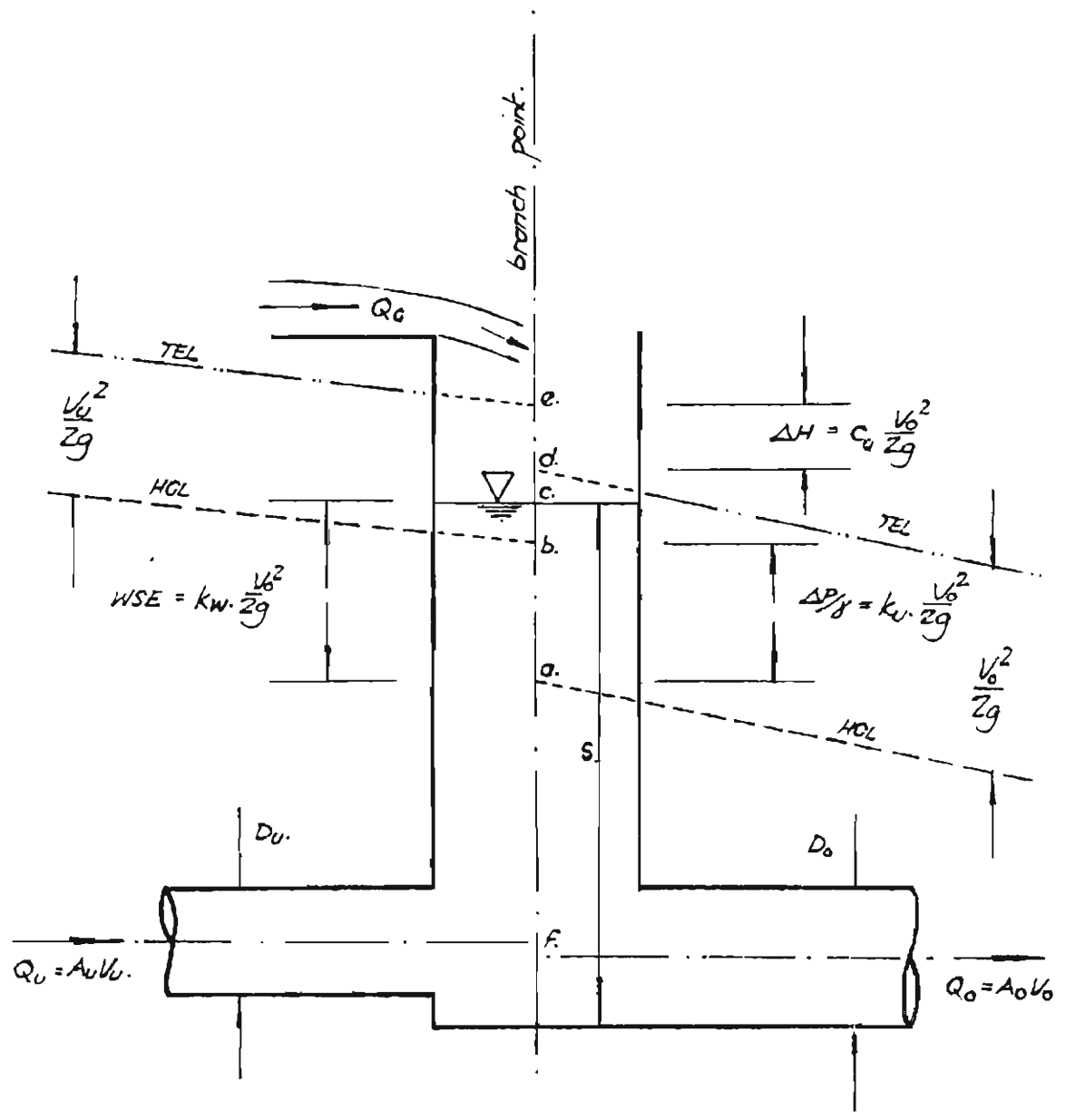


FIG. 3.4: TYPICAL JUNCTION PIT OPERATION.

conversion to potential head. The conversion of kinetic energy will vary with pit geometry being approximately 5 per cent for straight through flow and up to 30 per cent at a 90° junction structure. Thus, in Figure 3.4, Equation 3.1 applies:

$$0.05 \frac{V^2}{2g} \leq \left( \text{WSE} - \frac{\Delta P}{\gamma} \right) \leq 0.3 \frac{V^2}{2g} \quad \dots \text{Eq.3.1}$$

These figures have been determined experimentally by Sangster *et al* (1958) for three-pipe tee junctions and by the author (see Chapter 5) for two-pipe bend structures for pit sizes of twice the downstream diameter ( $B/D_o = 2.0$ ). Larger pit sizes can be expected to increase the percentage conversion, but increasing the proportion of total flow contributed by grate flow\* decreases the percentage conversion. For low submergence depths ( $S$ ), conversion to potential head increases. Research work by Archer *et al* (1978) indicates that, for the junction geometries shown in Figure 3.2, percentage conversion of upstream velocity head to potential head may, in some circumstances, be higher than indicated by Equation 3.1:

"It will be observed that there is better than 80% conversion of velocity energy to potential energy in some instances when the surcharge heads are very low .... but as the surcharge over the exit pipe increases, the proportion of the velocity energy converted to potential energy decreases. " (ibid p.6)

The larger conversion figures obtained by Archer may be partly attributable to the channel benching across the junction, causing the flow to be diverted in an upstream direction. In addition, the use of circular manholes was found to produce "a strong vortex in the pool of water in the manhole" (*ibid*, p. 6), which may also contribute to an increased energy conversion.

---

\* Secondary flow entering the junction through a top grate inlet.

For medium to high submergence heads ( $V_0 > 1\text{m/s}$ ) the figures shown in Table 3.3 have been derived from Archer's results for rectangular manholes.

TABLE 3.3

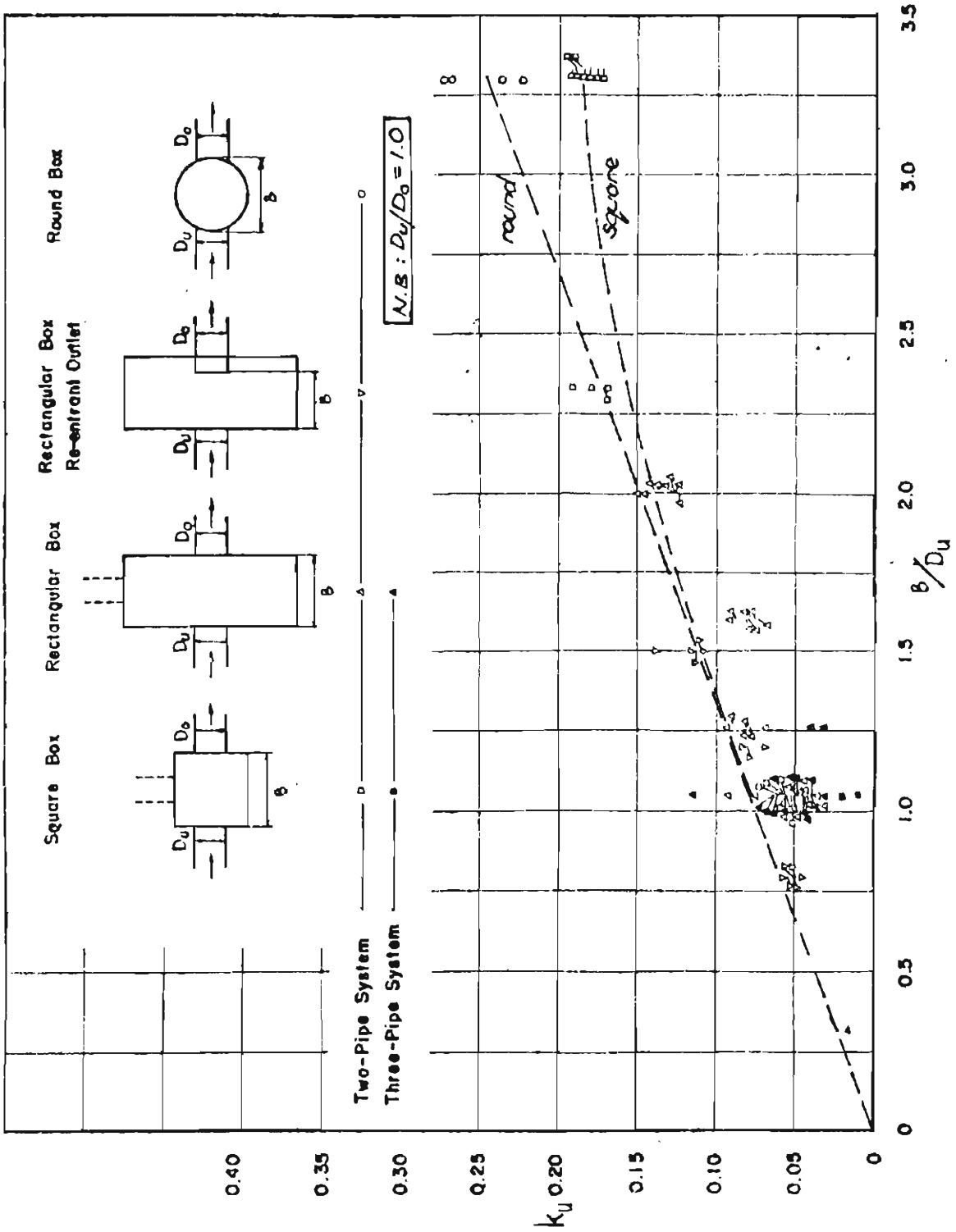
PERCENTAGE CONVERSION OF KINETIC TO POTENTIAL HEAD :  
DERIVED FROM ARCHER'S EXPERIMENTAL DATA

Angle of Deflection	Mean % Conversion of Velocity Head
0°	10
30°	25
60°	24

The foregoing discussion reveals that it is necessary to differentiate between two pressure head change coefficients, namely,  $k_u$  which determines the elevation of the upstream hydraulic grade line, and  $k_w$ , which determines the water surface elevation in the pit. The role of each coefficient is shown in Figure 3.4

#### 3.4 Effect of Pit Size and Shape

The effects of inlet pit size and shape variations have been studied by Sangster *et al* (1958) and by Archer *et al* (1978). Archer's study is confined to the effect of pit shape (rectangular or circular) and examines large pit structures of constant size. Sangster's work includes an analysis of both junction size and shape effects, and shows these to vary with junction geometry. Two cases are considered by Sangster: 0° and 90° deflection.



**FIGURE 3.5**  
**EFFECT OF BOX SIZE AND SHAPE WITH ALL FLOW STRAIGHT THROUGH**

SOURCE : SANGSTER ET AL (1958) (ADAPTED WITH MINOR CHANGES TO NOMENCLATURE).



### 3.4.1 Straight Through Flow

Figure 3.5 (Sangster, 1958) illustrates the variation in the pressure head change coefficient,  $k_u$ , corresponding to a change in pit size and shape for  $0^\circ$  deflection. Because of the relatively small variations in pressure head change coefficients ( $0.01 \leq k_u \leq 0.28$ ), changes in pit size and shape produce insignificant changes to the hydraulic efficiency of such structures. With manhole access and minimum pipe size restrictions, maximum values for B/D likely to be encountered for urban drainage systems would be approximately 2.4. It may be concluded, therefore, that pit shape also produces insignificant changes within the usual design limitations.

### 3.4.2 Flow Through a $90^\circ$ Bend

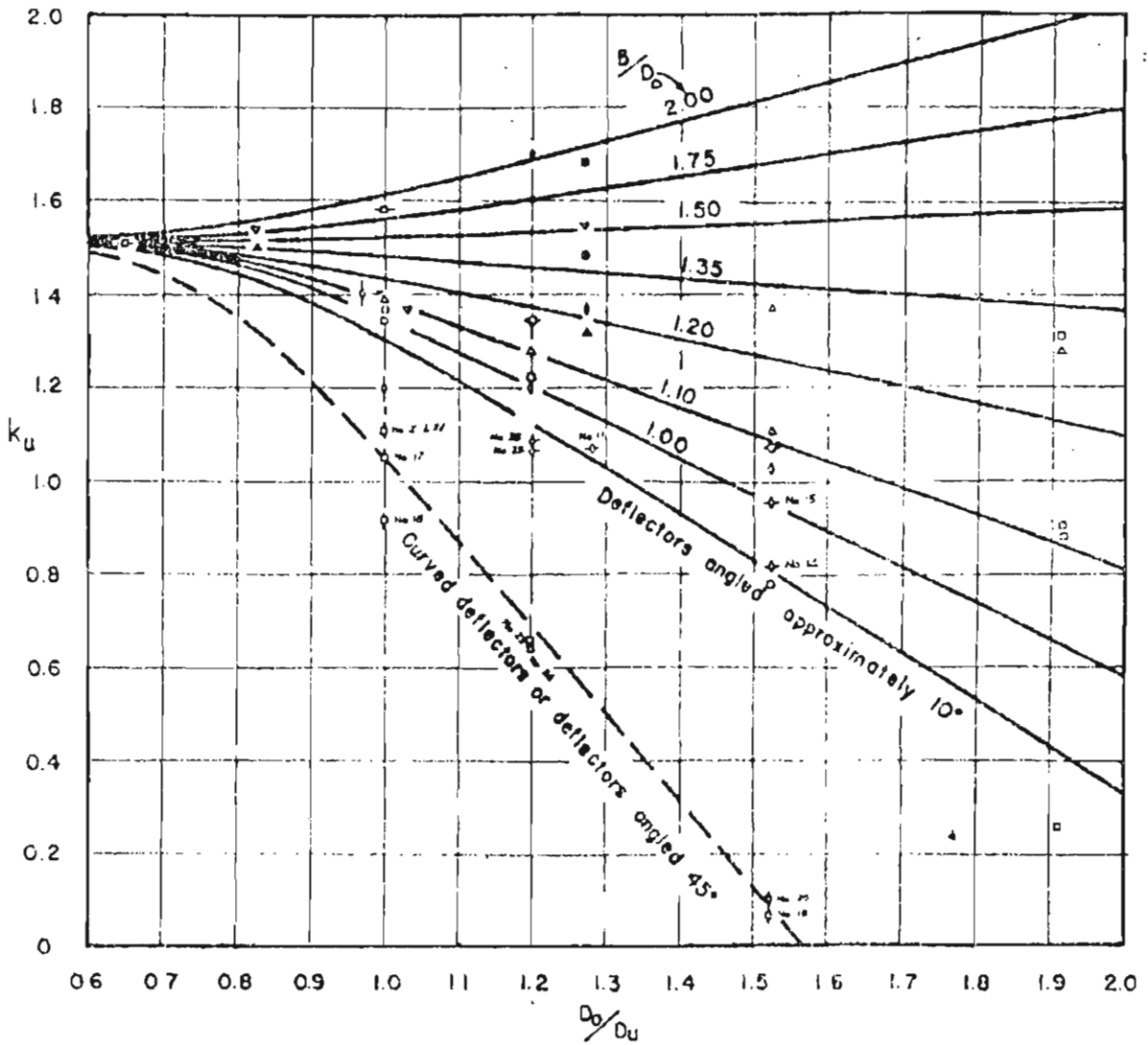
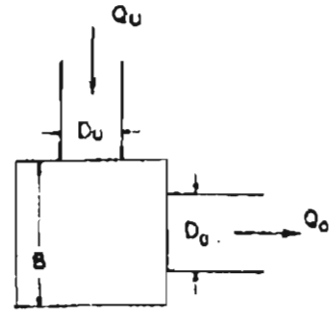
Figures 3.6 and 3.7 (Sangster, 1958) present experimental results for flow through a  $90^\circ$  bend. The figures represent pressure head change ( $k_u$ ) and water surface elevation ( $k_w$ ) coefficients respectively. The figures illustrate, for the usual design range ( $1.0 < D_o/D_u < 1.25$ ), that the coefficients decrease by up to 0.4 as B/D<sub>o</sub> is reduced from 2.0 to 1.0. For a downstream velocity of 3 m/s, a variation in water surface elevation of 180 mm may be anticipated by such a change in pit size.

Small pit sizes result in a significant reduction of pressure head changes because the wall opposing the lateral is nearly flush with the rim of the outfall pipe resulting in a less turbulent flow across the junction. The use of deflectors is encouraged by Sangster "in moderately large manholes", and "straight walls placed flush with the side of the outfall pipe and opposite the lateral exit, effecting a reduction in manhole width, exhibited significantly beneficial effects" (*ibid*, p. 63). The hydraulic effectiveness of deflectors is illustrated in Figure 3.5.

For  $90^\circ$  bend structures, Sangster recommends that, "the data on square manholes generally by used unchanged for

**Legend**

$B/D_0$	Symbol	Symbol
1.00	Square	Manhole
1.05	•	•
1.09	•	•
1.22	•	•
1.32	•	•
1.47	•	•
1.75	•	•
1.87	•	•
2.10	•	•
Deflectors Angled 10°		+
Deflectors Curved or Angled 45°		◊
1.20	Round	Manhole
1.73	•	•
2.08	•	•

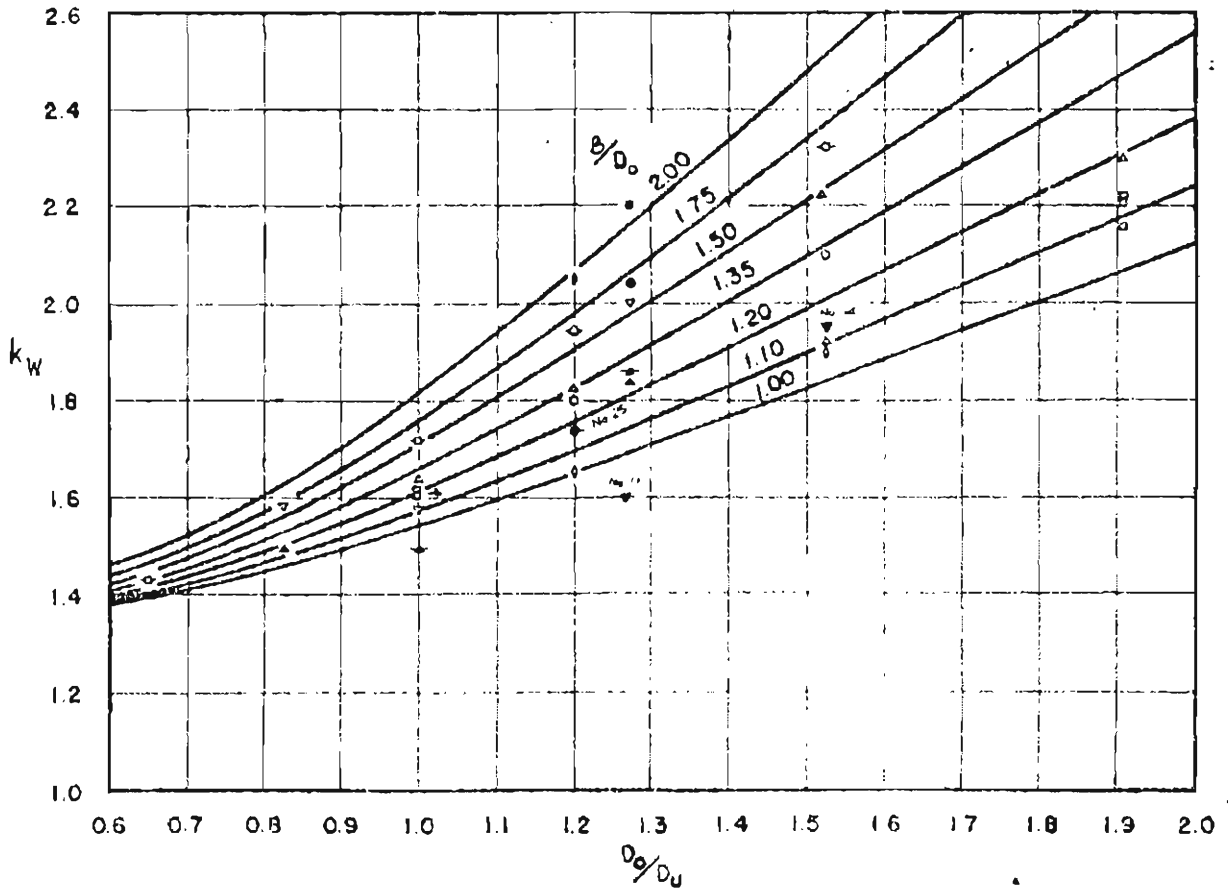
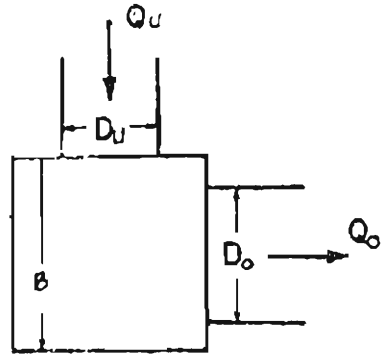


**FIGURE 3.6 : EFFECT OF PIT SIZE ON PRESSURE HEAD CHANGE COEFFICIENTS AT 90° JUNCTIONS.**

*SOURCE : SANGSTER ET AL (1958). (ADAPTED WITH MINOR CHANGES TO NOMENCLATURE).*

**Legend**

$B/D_o$	Manhole	Symbol
1.00	Square Manhole	—
1.05	"	○
1.09	"	◐
1.22	"	△
1.32	"	▽
1.47	"	◊
1.75	"	◑
1.87	"	◒
2.10	"	◓
Devices	"	•
1.20	Round Manhole	○
1.73	"	◐
2.08	"	◑
Devices	"	•



**FIGURE 3.7 : EFFECT OF PIT SIZE ON WATER SURFACE ELEVATION COEFFICIENTS AT 90° JUNCTIONS.**

SOURCE : *SANGSTER ET AL (1958) (ADAPTED WITH MINOR CHANGES TO NOMENCLATURE).*

for round manholes" (*ibid*, p. 63). This statement seems to conflict with experimental results provided by Archer (see Table 3.1). Application of the data for square pits to circular manholes might slightly underestimate the pressure head changes.

### 3.5 Combining Flow at Three-Pipe Junctions

In Section 3.3, it was shown that, for two-pipe junctions with deflection angles up to  $90^\circ$ , there are two pressure head change coefficients,  $k_u$  and  $k_w$ , defining the upstream hydraulic grade line and the water surface elevations respectively. The water surface elevation is located at approximately 0.3 upstream velocity heads above the upstream hydraulic grade line when the angle of deflection is  $90^\circ$ . If consideration is now given to the inclusion of an upstream in-line pipe, the configuration becomes a  $90^\circ$  Tee junction and the hydraulics become more complicated; such a junction is illustrated in Figure 3.8. The hydraulic grade line of the upstream in-line pipe adopts the water surface elevation as its elevation (Figure 3.8a). As the lateral flow is reduced and the in-line flow is increased, the conversion of kinetic to potential energy will also be reduced until, for the limiting case, all flow occurs in the in-line main and the two pressure head change coefficients are approximately equal (Figure 3.8b). The water surface and the upstream in-line hydraulic grade line elevations are always coincident. The lateral hydraulic grade line is located up to 0.3 lateral velocity heads below this elevation, depending upon the ratio  $Q_b/Q_o$ . Tables for calculating the various coefficients at such junctions are presented by Sangster *et al* (1958).

### 3.6 Effect of Froude Number and Submergence on Pressure Head Change Coefficients

By dimensional analysis and the application of the Buckingham  $\Pi$  Theorem, Sangster (1958) found that a functional relationship may exist between the pressure head change

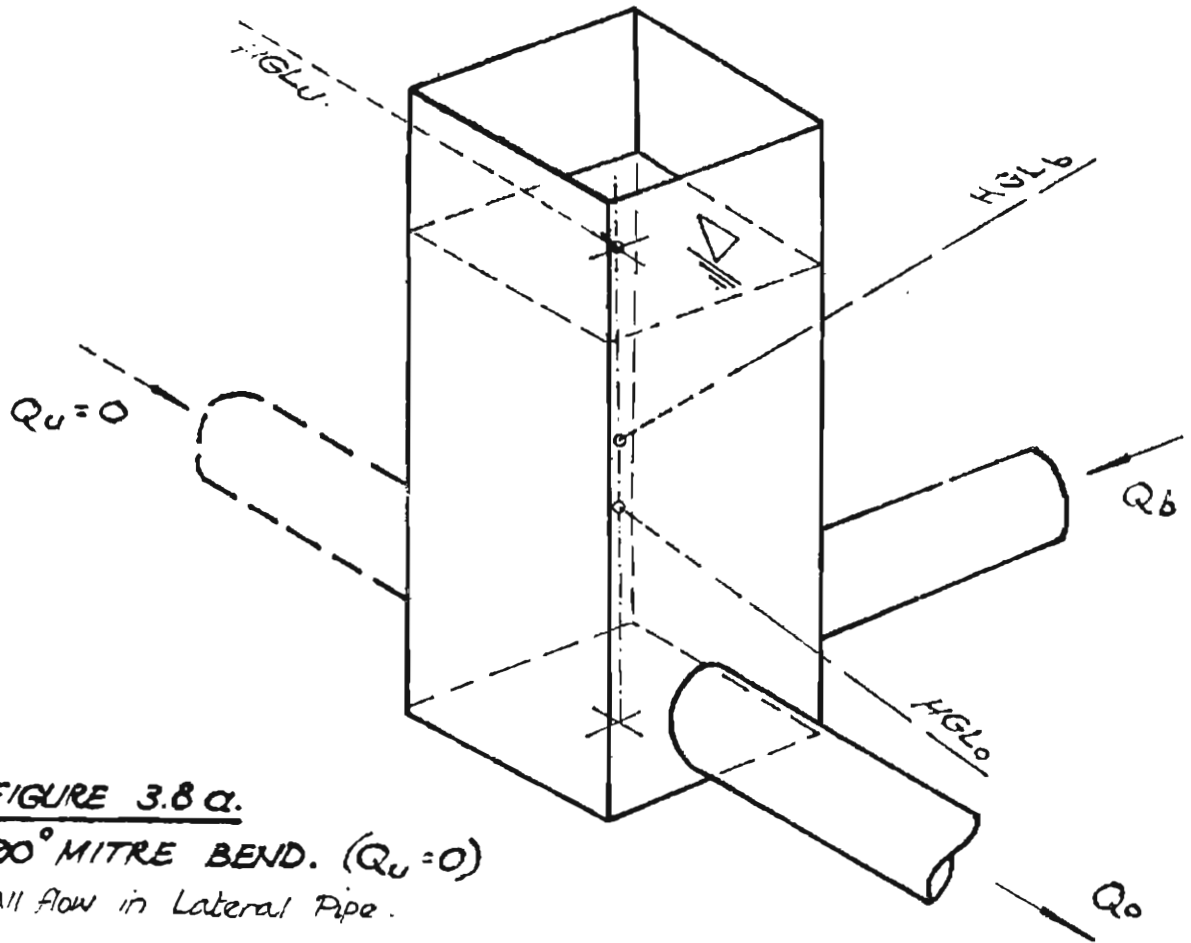


FIGURE 3.8 a.

90° MITRE BEND. ( $Q_u = 0$ )

*All flow in Lateral Pipe.*

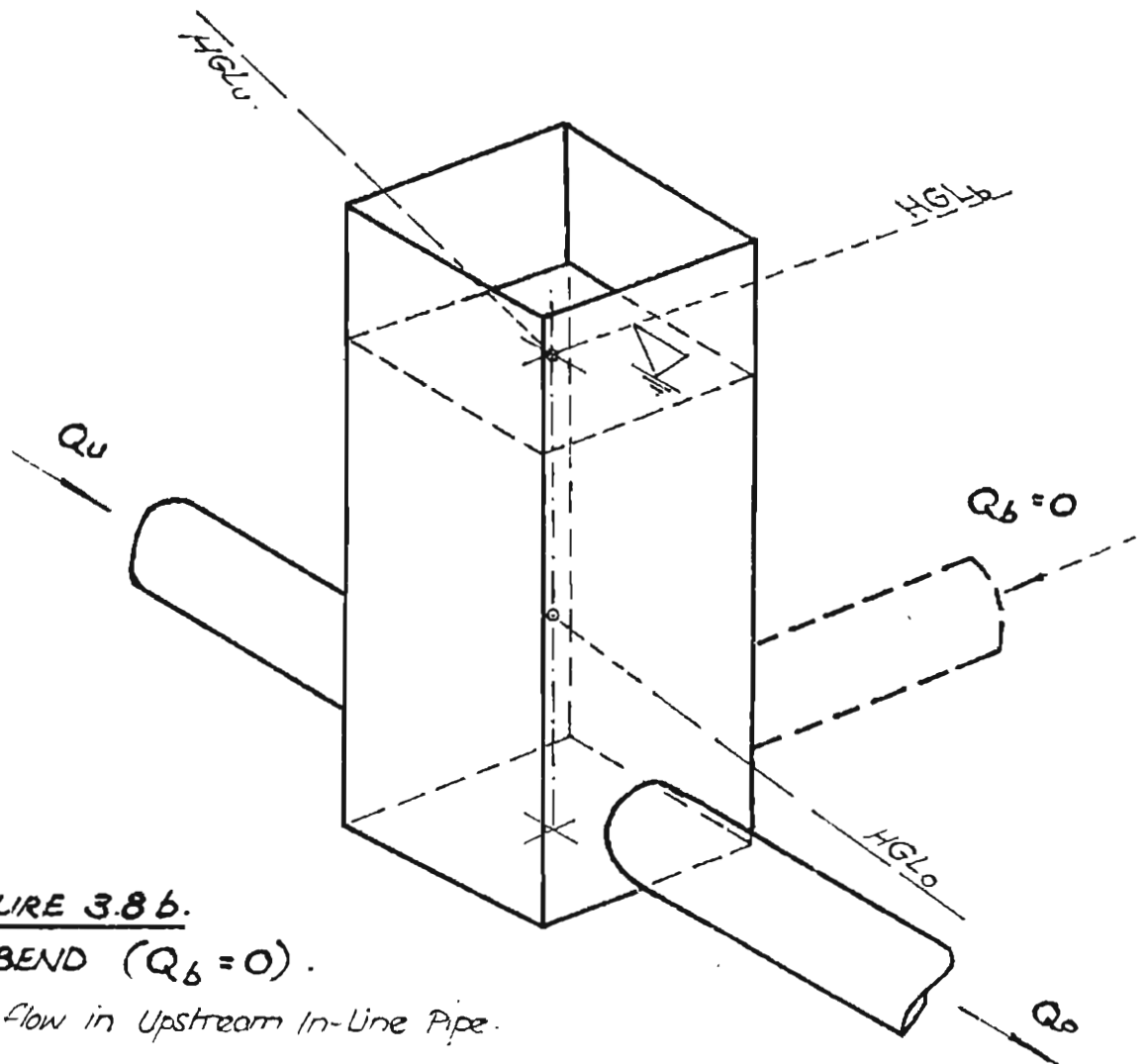


FIGURE 3.8 b.

0° BEND ( $Q_b = 0$ ).

*All flow in Upstream In-Line Pipe.*

coefficients and the downstream Froude Number,  $F_o$  (*ibid* p. 14). For a given geometry, the Froude Number may be varied only by varying the rate of flow.

For straight through flow, Sangster tested eight different geometries and plotted graphs of  $k_u$  versus  $F_o$ . From this information, Sangster concluded that it, "appears inescapable that the coefficient for a given geometry is independent of the Froude Number . . . . . In as much as  $k_u$  does not depend on the Froude Number, it follows that neither does it depend on the rate of flow, but rather is constant for a given geometry" (*ibid* p. 24).

However, under the geometric and flow configuration that Sangster selected to test for a functional relationship between  $k_u$  and  $F_o$ , the pressure head change coefficient,  $k_u$ , is independent of the degree of surcharge (*ibid* p. D-15). For other geometric or flow configurations (see Chapter 5)  $k_u$  is not independent of submergence,  $s$ , and, since submergence is, for a fixed geometry, partially a function of discharge, then  $k_u$  must be a function of the Froude Number. It is unfortunate that the inter-relationship between  $k_u$ ,  $Q_o$ ,  $F_o$  and  $s$  was developed by Sangster, resulting in a conclusion being drawn which is applicable only to a limited range of geometric and flow configurations.

### 3.7 Summary : Pit Junction Hydraulics

The discharge capacity of a single pipe reach is determined by the friction loss within the conduit and by the pressure head change that occurs at the pit junction immediately upstream. For the majority of pit configurations this pressure head change is an unknown quantity. Some configurations have been tested and appropriate design data have been established. In general, however, the lack of data inhibits the use of accurate design methods which incorporate hydraulic grade line or energy line computations.

The nature of flow across pit structures has been described in Sections 3.3 to 3.6. Information on loss coefficients

and junction geometry efficiency is limited to that applying to a limited number of cases. The available data have been obtained from the use of hydraulic models.

In view of the paucity of suitable data which could be used in the design of junction pits with the wide range of geometries found in practice, an experimental programme, using hydraulic models, was initiated to produce appropriate design data. Details of the programme are set out in the following chapters.

CHAPTER 4

HYDRAULIC MODELS OF JUNCTION PITS

- 4.1 Use of Hydraulic Models
- 4.2 Model Construction and Apparatus
  - 4.2.1 Scope of the Investigation
  - 4.2.2 Water Supply System
  - 4.2.3 Model System and Pipelines
  - 4.2.4 Model Geometries
  - 4.2.5 Experimental Procedures
  - 4.2.6 Error Analysis



#### 4.1 The Use of Hydraulic Models

The magnitude of energy losses and pressure head changes at stormwater junction pits must invariably be determined using hydraulic modelling techniques. Such models must conform with geometric and dynamic laws of similarity. Simultaneous compliance in every respect, however, is not always possible and losses in similarity lead to scale effect errors when model results are extrapolated to a prototype. These errors can, however, be minimized if the models are made sufficiently large. Hydraulic models of stormwater junction pits have been used by Sangster *et al* (1958) and by Archer *et al* (1978). These investigators concentrated on junction geometries which have specific local applications in each case. Sangster, for example, tested geometries which are in common use by the Missouri State Highway Department. Archer considered systems where pipes are small, pits are relatively large and sharp bends are avoided. The design data available from these tests have limitations and need to be expanded before an accurate estimate of flow through surcharged pipe systems can be made. An experimental programme involving the use of hydraulic models was established by the author and aimed at reducing these limitations. Details of the programme are reported in the following sections.

#### 4.2 Model Construction and Apparatus for Pit Junction Experimental Programme

##### 4.2.1 Scope of the Investigation

In view of the limitations of the existing pit junction hydraulic data, an experimental programme was initiated to determine the magnitude of pressure head changes at junction pits with two connecting pipes. The investigation was undertaken for a variety of pipe sizes, pipe configurations, pit geometries and flow conditions. The following constraints were applied to the programme:

1. All pipes were to flow full and under pressure.
2. The range of deflection angles ( $\theta$ ) to be tested was to be within the range commonly found in practice, i.e.,  $0^\circ \leq \theta \leq 90^\circ$ .

3. Pipe area ratios were to cover the range  $1.00 \leq A_o/A_u \leq 2.50$ . (Commercially available pipes for the models extended this range to  $1.00 \leq A_o/A_u \leq 3.29$ ).
4. All pits were to be constructed square in plan and of a size so that the ratio of the pit width divided by the downstream pipe diameter was equal to 2 (i.e.,  $B/D_o = 2$ ). Because of the infinite number of junction configurations possible with respect to pit size and shape, the experimental programme was limited to geometric configurations typically found in prototypes and, where this was not possible, to configurations which would allow the use of appropriate adjustments to the test data during the prototype design. In arriving at the pit size ratio used in the model tests, consideration was given to the following:
  - (a) standard Department of Main Roads (N.S.W.) gully pit design practice;
  - (b) the previous experimental investigation of Sangster *et al* (1958);
  - (c) minimum prototype pit size requirements for access and maintenance;
  - (d) the reductions in pit size ratios that will necessarily occur as a result of increased downstream pipe sizes;
  - (e) current design practice regarding minimum pipe diameters to prevent blockage by debris: ("It is common practice not to use pipes smaller than 450 mm diameter" (Institution of Engineers, Australia (1977) p.146), but some designers may use pipes as small as 375 mm).
5. Grate flows were to be tested for ratios of  $Q_u/Q_o \leq 0.50$ . During the experimental programme, however, grate flows were sometimes taken beyond this limit to check trends in data. A limit of  $Q_u/Q_o \leq 0.50$  allows design criteria to be formulated for all pit junctions up to the second downstream pit in a drainage system.
6. Model discharges of up to 10 l/s were to be used during the experiments. This maximum model discharge was adopted by consideration of a maximum velocity in a prototype system of 6 m/s. Where  $D_u/D_o < 1.00$ , the maximum velocity will occur in the upstream pipe when the grate flow is small. The relevant calculations are

set out below. Due to the possible free surface effects at the junction structure, a Froude model is used:

$$V_m(\text{max}) = V_p(\text{max}) \times (L_R)^{-\frac{1}{2}} \quad \dots \text{Eq. 4.1}$$

where

$V_m(\text{max})$  is the maximum average velocity in the model pipeline;

$V_p(\text{max})$  is the maximum average velocity in the prototype pipeline;

$L_R$  is the scalar model to prototype length ratio

The smallest prototype pipe diameter used in Australia is 375 mm nominal (381 mm actual). For a model pipe diameter of 70 mm (the smallest model diameter used), the length ratio,  $L_R$ , would equal:

$$L_R = 381/70 = 5.44$$

$$\therefore V_m(\text{max}) = 6 \times (5.44)^{-\frac{1}{2}} = 2.57 \text{ m/s}$$

$$\begin{aligned} Q_m(\text{max}) &= V_m(\text{max}) \times A_m \\ &= 2.57 \times (0.07^2 \times \pi) / 4 \\ &= 0.0099 \text{ m}^3/\text{s} \\ &= (\text{say}) 10 \text{ l/s} \end{aligned}$$

7. The practical limits for submergence ratio (i.e. depth of water in pit expressed as a number of outlet pipe diameters,  $S/D_o$ ) were considered to fall within the range  $1.00 < S/D_o < 4.0$ . (Submergence ratios greater than 4.0 were sometimes tested to examine trends in data, but were considered unlikely to occur in prototype conditions).
8. All pipe entrances were to be sharp-edged. It was not feasible to study the effects of rounding the pipe entrance.
9. All pits were to be flat bottomed with no benching or deflection devices. Pipe obverts were to be aligned in accordance with construction techniques practised in Sydney.

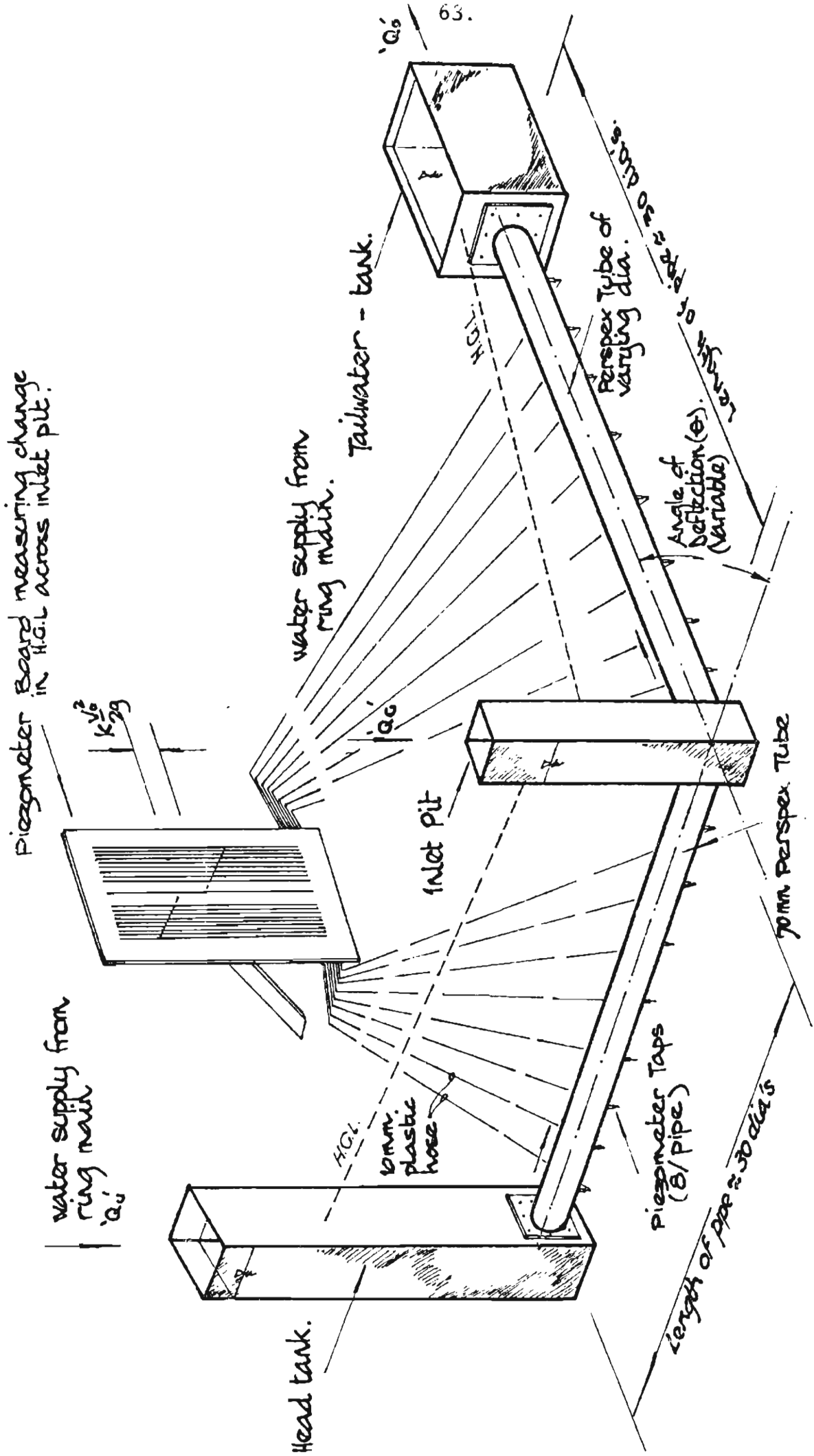


FIGURE 4.1 : SCHEMATIC LAYOUT FOR PIT JUNCTION EXPERIMENTS.

#### 4.2.2 Water Supply System

The hydraulic models were supplied with water by pump from a reservoir through a 150 mm diameter overhead ringmain. The pressure in the ringmain was held constant through a constant-head tank located approximately 20 m above the floor of the laboratory. The ringmain is permanently suspended from the ceiling of the laboratory and is fitted with flanged outlet connections. Two such connecting flanges were utilized in the model tests. One supplied water to the headtank and the other supplied water to the inlet pit to simulate grate flow in the prototype. Each of the two supply lines was constructed with a p.v.c. flange bolted to a ringmain outlet flange, connecting an 80 mm diameter p.v.c. conduit to the headtank and to the inlet pit respectively.

Each supply line was provided with a gate valve to regulate the flow and an orifice meter to measure the rate of flow. The orifice plates were calibrated using a weighing tank. Pressure differences across the orifice plates were observed using mercury manometers for high flowrates and water manometers for low flowrates (Figure 4.3). The pressure differences were converted to flowrates using equations derived during the meter calibrations. Velocity heads and grate flow discharge ratios were calculated using the flowrates determined by the orifice meters.

#### 4.2.3 Model System and Pipelines

##### Headtank:

The headtank at the upstream end of the model pipeline (Figures 4.1 and 4.2) was constructed with a height sufficient to provide flows of up to 10 l/s through the models when the tailwater tank downstream was fully closed. A headtank with a height of 1500 mm was found to be adequate. Horizontal stiffeners were provided around the headtank at 300 mm centres for structural strength. A transparent

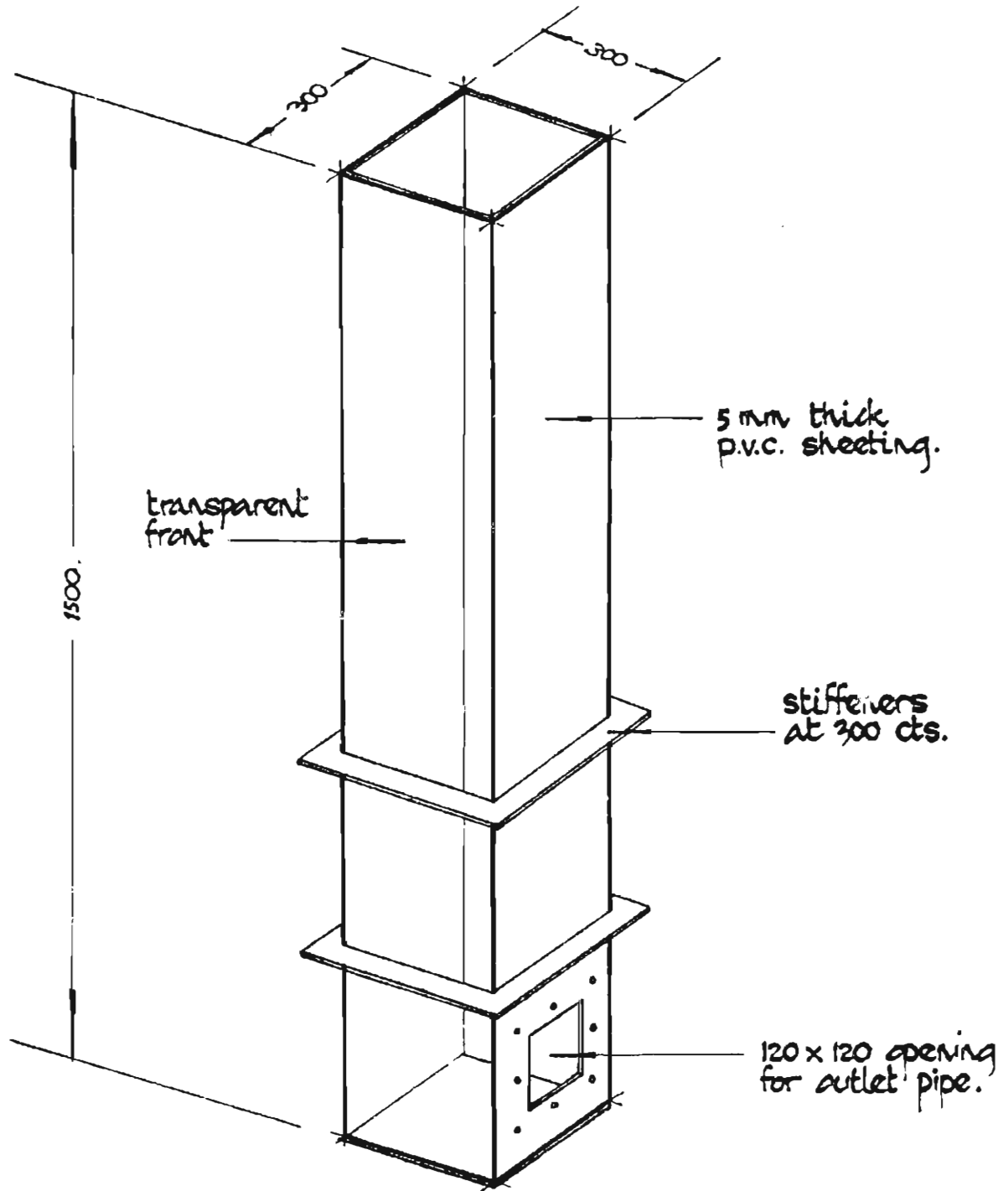


FIGURE 4.2 : HEADTANK.

FIGURE 4.3 : MANOMETERS.

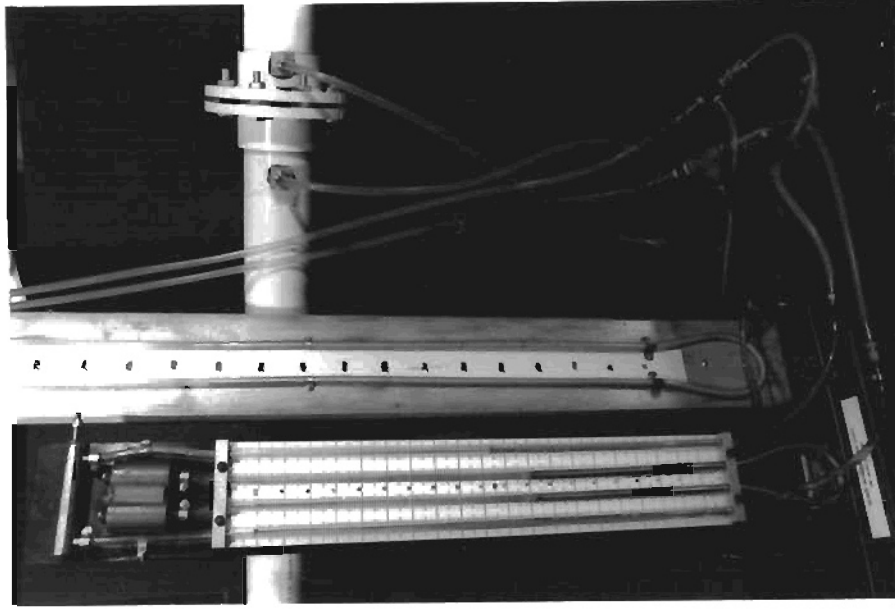
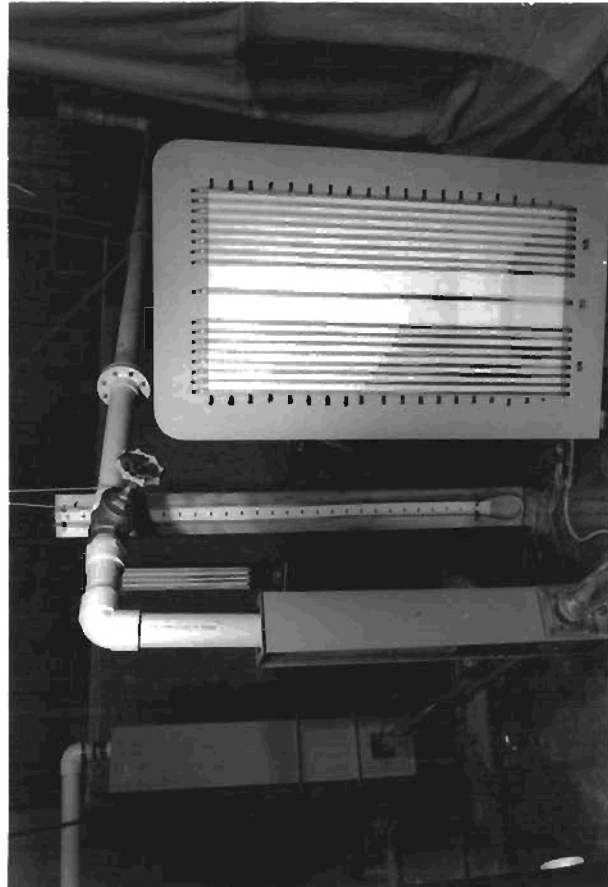


FIGURE 4.4 : MODEL SETUP FOR STRAIGHT THROUGH FLOW.



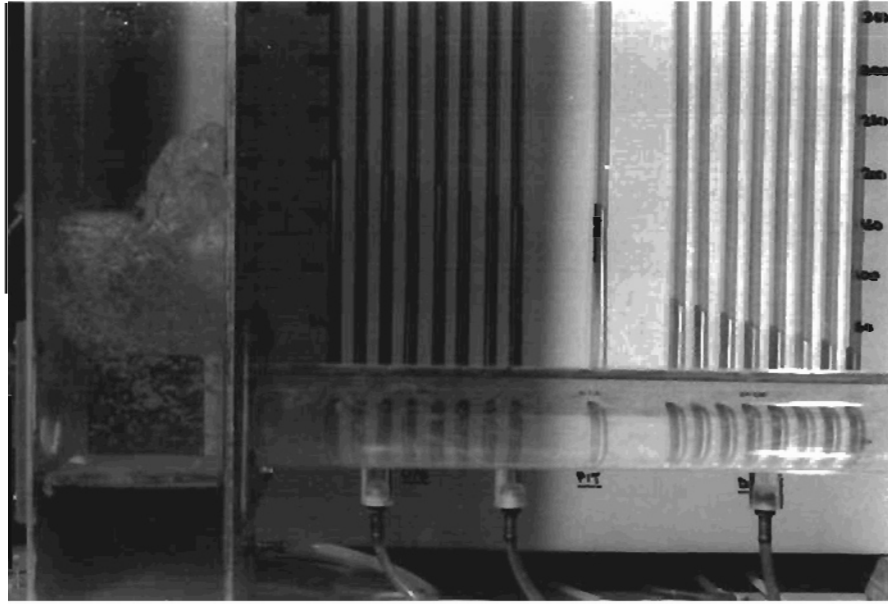


FIGURE 4.5: FLOW THROUGH A 45° JUNCTION.



FIGURE 4.6: FLOW THROUGH A 45° JUNCTION.



p.v.c. face was provided for the front of the tank to view water surface elevations.

Inlet Pits:

Three model inlet pits were constructed for the experiment programme, each pit being used in conjunction with each of three downstream pipe sizes, thus providing a near constant ratio of pit size to downstream diameter.

TABLE 4.1

CONSTRUCTED INLET PIT SIZE RATIOS

Pit No.	Size (mm) (B x B)	Outlet Pipe Dia. (mm) (D <sub>o</sub> )	(B/D <sub>o</sub> )
1	140 x 140	70	2.00
2	190 x 190	94	2.02
3	240 x 240	127	1.89

Pits were standardized as square in plan and of size such that  $B/D_o \approx 2.0$  (see Section 4.2.1). For pit number 3,  $B/D_o$  was equal to 1.89. This departure resulted from a changeover to metric pipe sizes in the course of the experiment programme.

The differences in the  $B/D_o$  ratios, however, do not yield significant errors in the experimental work and all three inlet pipes have been dimensioned as having  $B/D_o$  ratios equal to 2.0.

The inlet pits were constructed so as to allow the testing of various geometric configurations. Each inlet pit could be used to test ten different model geometries (models 1 to 30 are illustrated in Figures 4.13 through 4.18).

A floor was built in the inlet pit to provide a stilling basin, from which an average pit water surface elevation could be read on the accompanying piezometer board. A

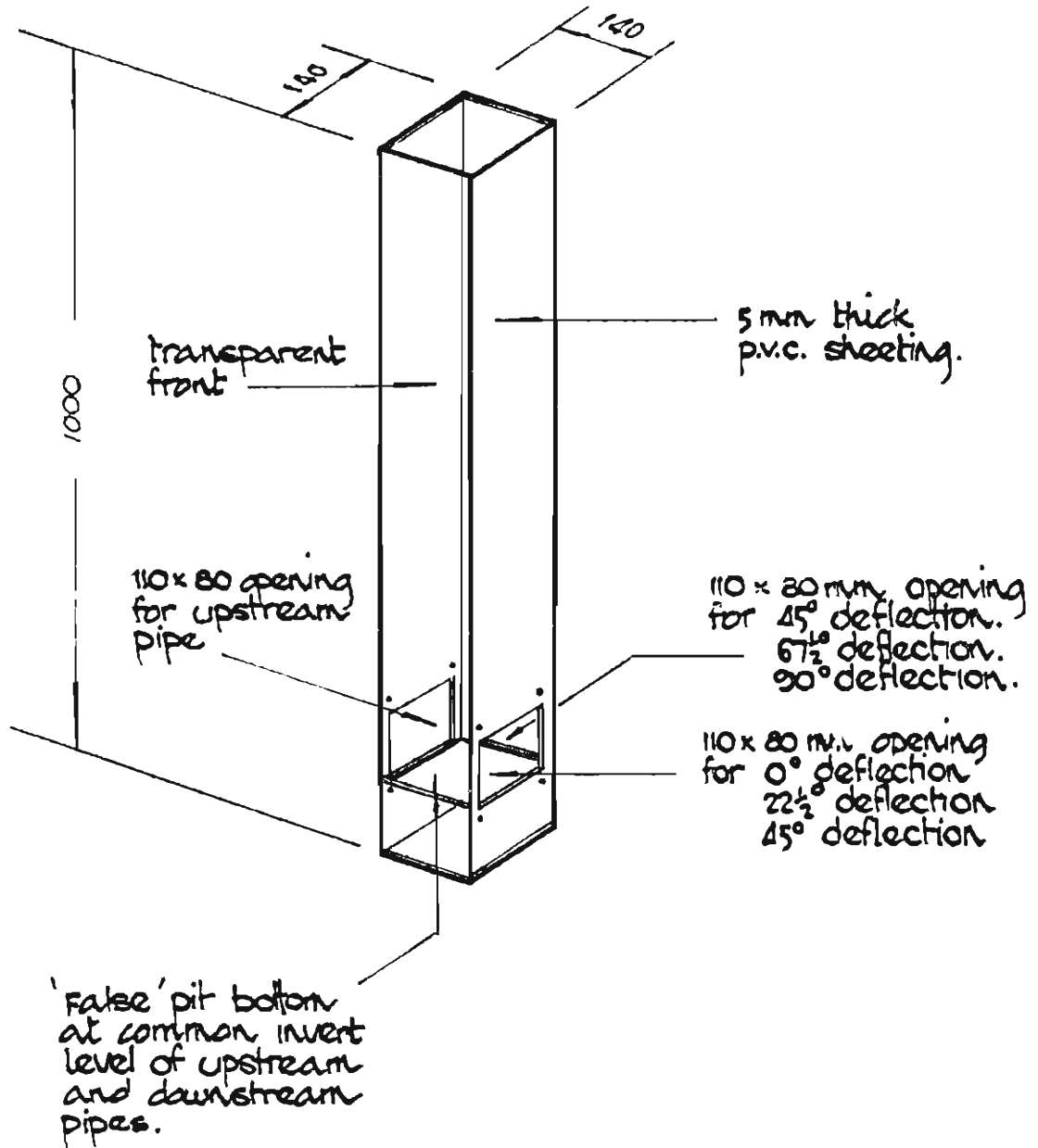


FIGURE 4.7 : TYPICAL INLET PIT.

piezometer tapping was located below the floor to measure the mean hydrostatic head within the pit. To eliminate errors due to the possible inclusion of a hydrodynamic head attributable to turbulence under the floor, the pit bottom was sealed at invert level leaving the four corners of the pit floor unsealed to measure an average static head. In addition, checks were made during testing to ensure that the static head on the piezometer board was representative of the water surface elevation in the pit. Each pit was constructed to a height of 1000 mm above floor level, providing for submergence ratios ( $S/D_0$ ) in excess of those that could be expected in

Grate flow was discharged into each pit at a constant height above the pit invert equal to five outfall pipe diameters for each of the models. (Tests performed by Sangster *et al* (1958) indicate that the height of fall of grate flow relative to the degree of submergence is not a significant factor in the determination of the pressure head change (*ibid* p. 53)). It would be reasonable to expect that the fall-to-submergence ratio would be most significant at low submergences. However, Sangster found that, even for submergence depths of approximately 1.5 outfall pipe diameters, the scatter of the experimental data was reduced to acceptable limits using a single submergence parameter ( $S/D_0$ ).

#### Tailwater Tank

A tailwater tank was constructed as shown in Figure 4.6. An important feature was the provision of an adjustable tail-gate structure that could be used to vary the submergence depths in the upstream inlet pit without having to change either the upstream or grate flow discharge.

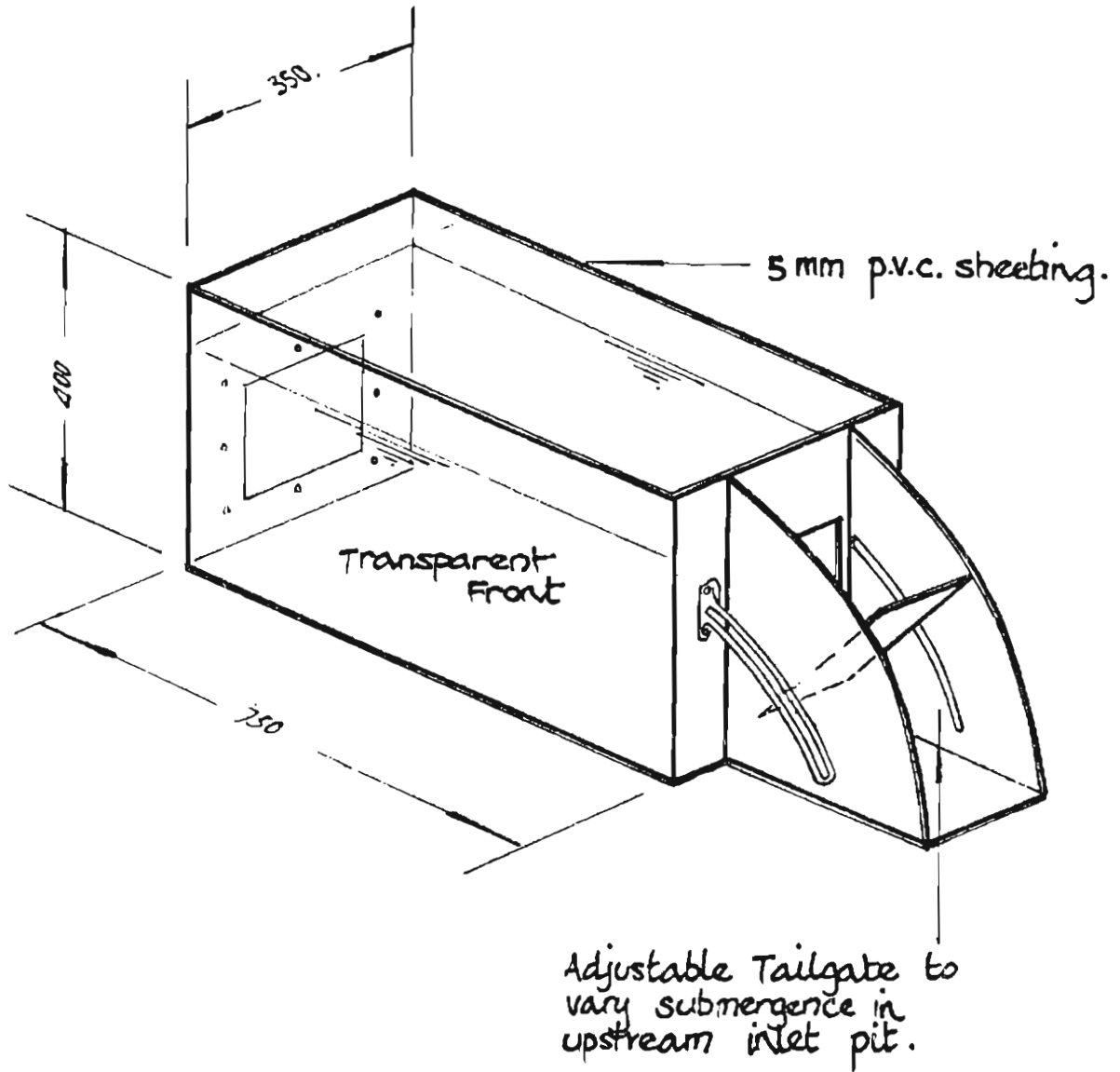


FIGURE 4.8 : TAILWATER TANK.

### Model Pipelines

Model pipelines were constructed with transparent perspex tubing so that hydraulic behaviour could be observed.

Three nominal pipe diameters were used, viz: 70 mm, 94 mm and 127 mm. Actual pipe diameters were carefully measured. The most significant percentage error occurred in the smallest pipe size of 70 mm, resulting in errors of 0.2 per cent in nominal cross-sectional area. These errors were considered as being of only minor importance.

The use of pipes smaller than 70 mm diameter was avoided to minimize undesirable scale effects. Pipes larger than 127 mm diameter presented difficulties in handling and maintenance of pipe-full conditions.

Only the 70 mm diameter pipe was used upstream from the inlet pit; all three pipe sizes were used as downstream outlet pipes. Such an arrangement yielded the diameter and area ratios shown in Table 4.2.

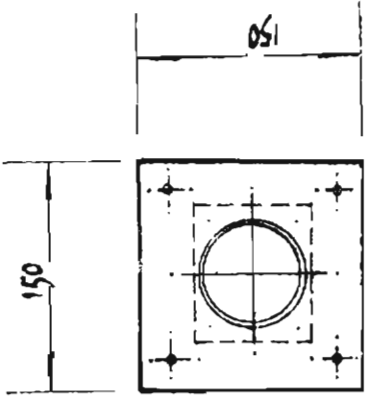
TABLE 4.2

DIAMETER AND AREA RATIOS USED IN MODEL PROGRAMME

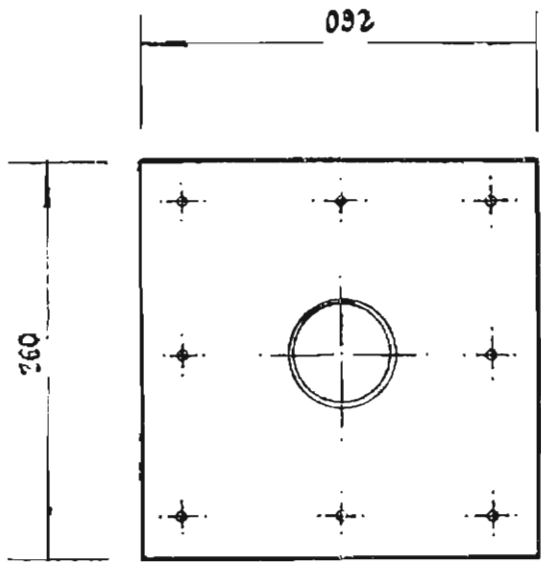
Pipe Diameter	Ratio of Diameter $\frac{D_o}{D_u}$	Ratio of Areas $\frac{A_o}{A_u}$
70 mm I.D. downstream	1.00	1.00
94 mm I.D. downstream	1.343	1.803
127 mm I.D. downstream	1.814	3.292

The range of pipe diameter ratios ( $D_o/D_u$ ) tested is considered to represent most practical applications. Pipe diameter ratios less than unity were not tested. Ratios less than unity were tested by Sangster *et al* (1958) for pipe deflection angles of  $0^\circ$  to  $90^\circ$ .

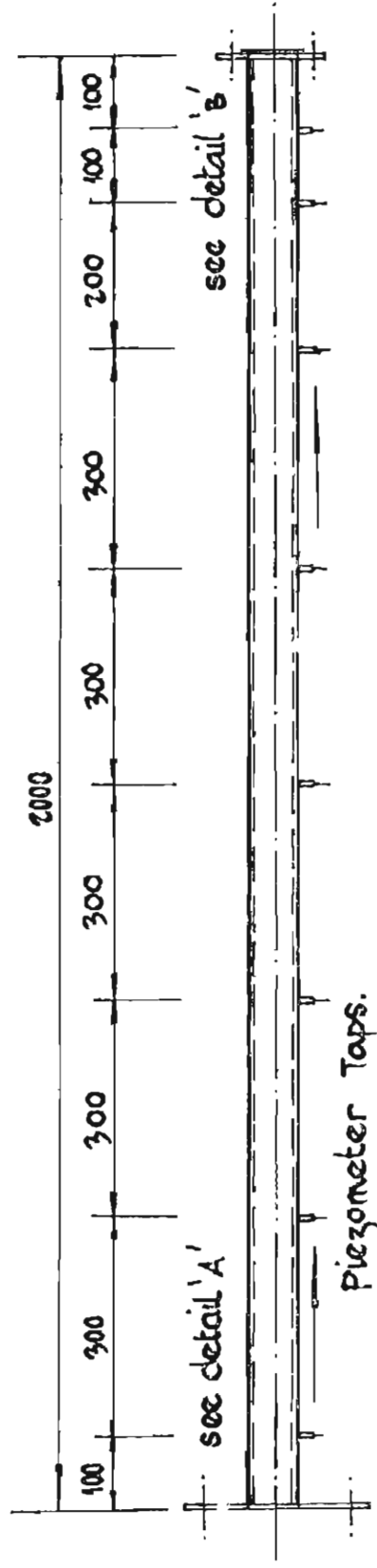
The length required for a pipeline to develop fully established flow has been stated by Rouse (1950) and by others to be in excess of 25 - 40 pipe diameters. Such a specification defines the length of pipe which is required before piezometer readings can yield a linear hydraulic gradient. The pipe lengths required are thus significant, and limitations in laboratory space and difficulties in handling pipes required consideration. Also, technical limitations had to be considered. For example, for the 70 mm diameter conduit, a pipe length greater than approximately 30 diameters would yield high friction losses making it impossible to produce low submergence ratios except for low rates of flow (less than 1.5 l/s). Small discharges consequently increase the experimental errors because the dimensionless pressure head change coefficients are derived by the division of the pressure head change by the downstream velocity head, both of these variables being small and susceptible to larger errors for small discharges. To minimize such errors, pipe lengths were kept to a minimum. Approximate linear friction gradients were found to occur when piezometer tappings were located at a distance greater than ten pipe diameters downstream from the headtank and the inlet pit. Under these conditions, for discharges greater than 2 l/s, the coefficient of determination for linear regression ( $r^2$ ) was, in most cases, greater than 0.99, despite the fact that the flow was not fully developed. Photographs shown in Figure 4.4 and 4.5 show linear friction gradients for pipe lengths much less than those expected for the establishment of the flow. It was decided, therefore, that for the purposes of reading the common piezometer board to an accuracy of 0.5 mm of water, linear friction gradients could be obtained in much shorter development lengths than is commonly assumed. The pipe lengths used in the course of the experiment programme are shown in Table 4.3.



DETAIL 'B'  
 Flange plate bolts to inlet pit (0°, 90° deflection) or to adaptor (22½°, 45°, & 60° deflection).



DETAIL 'A'  
 Flange plate bolts to Head Tank for upstream pipe and to Tailwater Tank for downstream pipe.

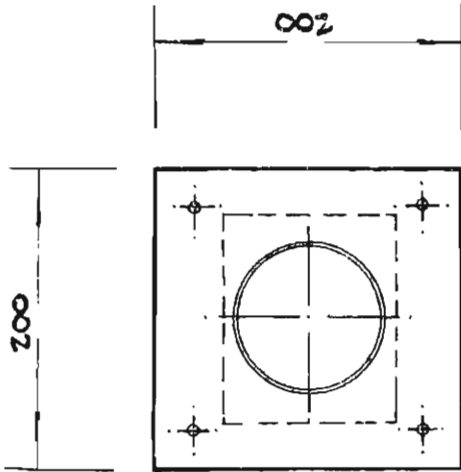


see detail 'B'

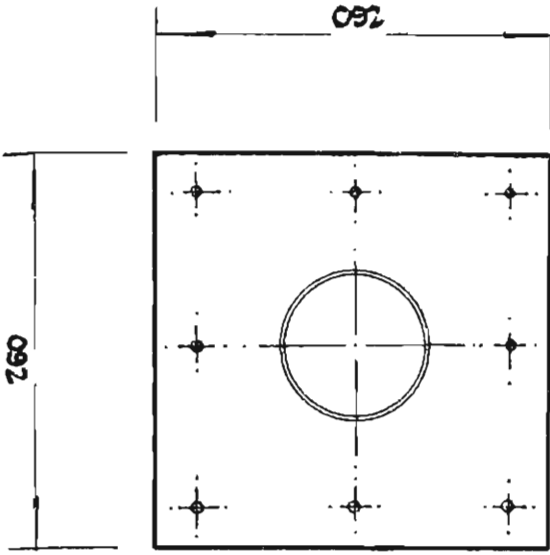
see detail 'A'

Piezometer Taps.

FIGURE 4.9: 70 MM I.D. PIPE (U/S AND D/S).



DETAIL 'C'  
 Flange plate bolts to  
 inlet pit (0°, 90° deflection)  
 or to adaptor (22½°, 45°,  
 & 60° deflection).



DETAIL 'D'  
 Flange plate bolts to Tail-  
 water tank.

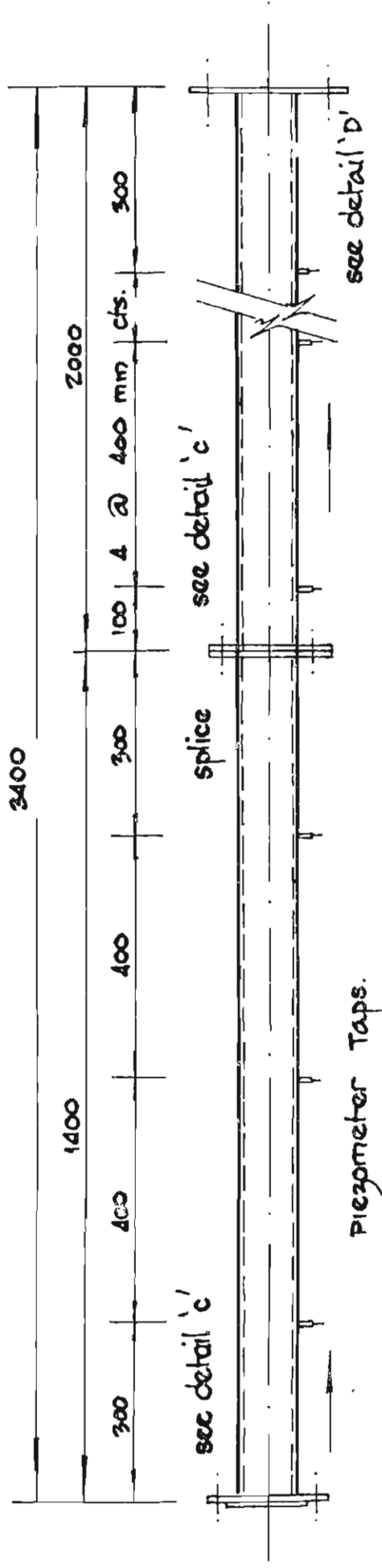
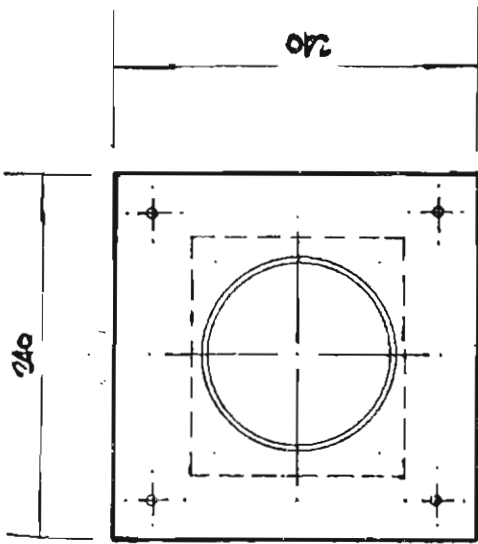


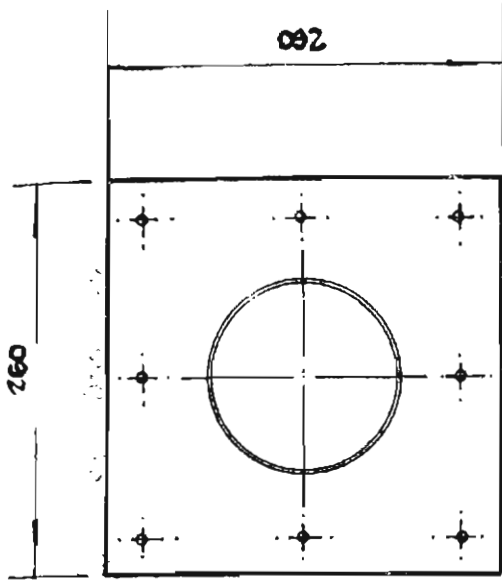
FIGURE 4.10: 94 MM I.D. PIPE. (D/S ONLY).





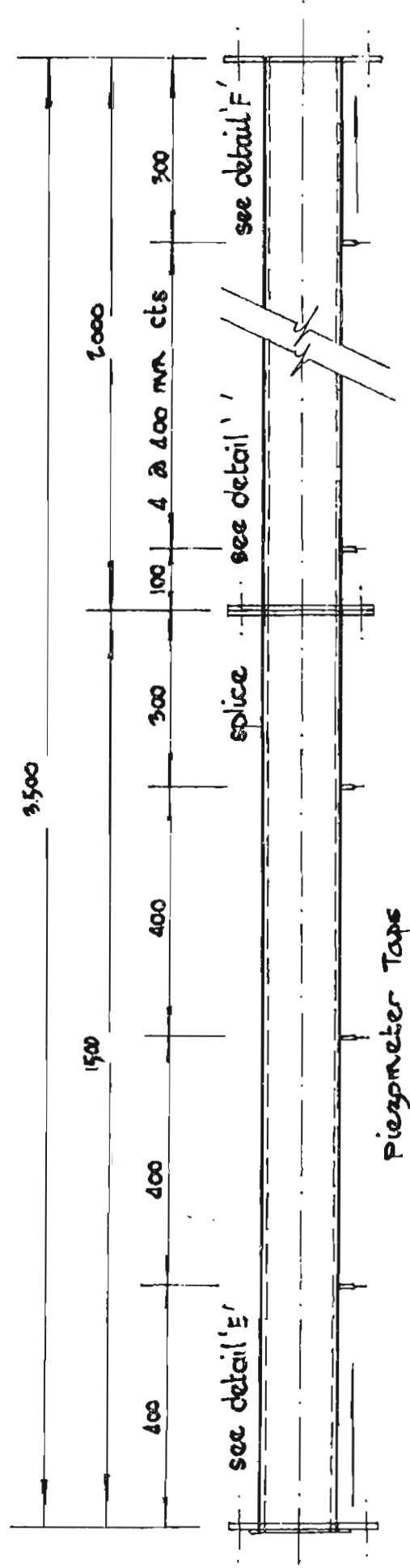
DETAIL 'E'

Flange plate bolts to inlet pit (0°, 30° deflection) or to adaptor (22½°, 45°, & 67½° deflection).



DETAIL 'F'

Flange plate bolts to tail-water tank.



Piezometer Taps

FIGURE 4.11 27 MM I.D. PIPE (D/S ONLY).

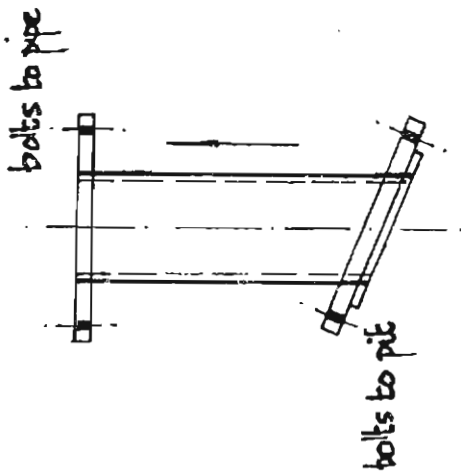
TABLE 4.3

PIPE LENGTHS USED IN MODEL PROGRAMME

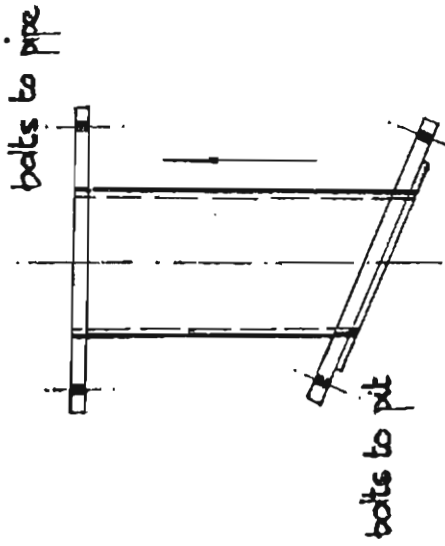
Pipe	Length		No. of Tappings in Pipe Length Exceeding 10 dias.
	(mm)	(diameter)	
70 mm I.D. upstream	2000	28.57	6
70 mm I.D. downstream	2000	28.57	6
94 mm I.D. downstream	3400	36.17	6
127 mm I.D. downstream	3500	27.56	5

Metric sized pipes were supplied in 2m lengths. Consequently, the 94 mm and 127 mm diameter pipes were spliced. Details of flange splices are shown in Figures 4.10 and 4.11. The square flange plates were bored to the exact outside diameter of the pipe using a specially made trepanning tool. For each splice, both flanges were clamped and drilled simultaneously to ensure accurate alignment when the acrylic pipes were glued to the flanges, and the flanges were bolted together. A grease gasket was found to be adequate to prevent leakage from the splice. Similar splices were required to attach specially made angle adaptors (see Figure 4.12) between the junction pit and a connecting pipe. The length of each adaptor was 200 mm. Two adaptors were cut for each pipe diameter, the six adaptors being used for the junction configurations and deflection angles described in Table 4.4. The table shows that each angle adaptor was constructed so as to be used for two or more different angles or junction configurations. For example, adaptor No. 1 was used for a downstream pipe diameter of 70 mm as a  $22\frac{1}{2}^{\circ}$  bend when fitted to the opposing face of the pit or as a  $67\frac{1}{2}^{\circ}$  bend when fitted upside down to the adjacent face of the pit. The adaptor could also be connected to the upstream pipe as a  $22\frac{1}{2}^{\circ}$  or a  $67\frac{1}{2}^{\circ}$  bend. The use of the adaptors provided an economical means of testing bend structures.

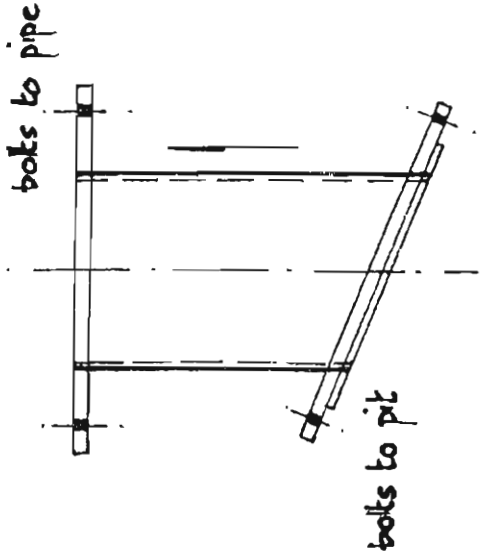
FIGURE 4.12 : ANGLE ADAPTORS.



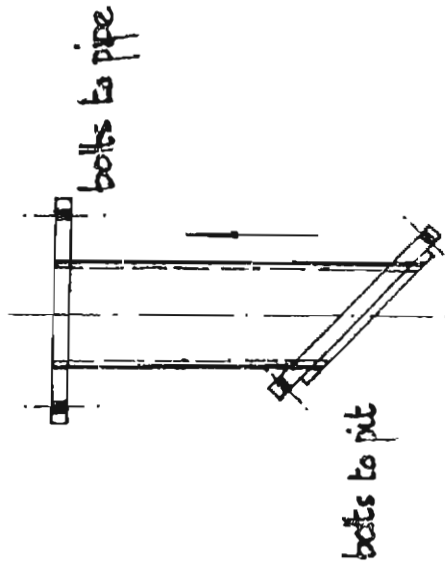
70 mm I.D. pipe :  $22\frac{1}{2}^\circ$  /  $67\frac{1}{2}^\circ$



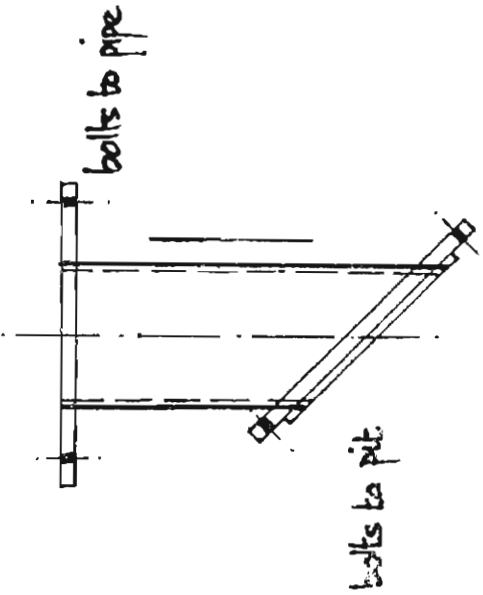
94 mm I.D. pipe :  $22\frac{1}{2}^\circ$  /  $67\frac{1}{2}^\circ$



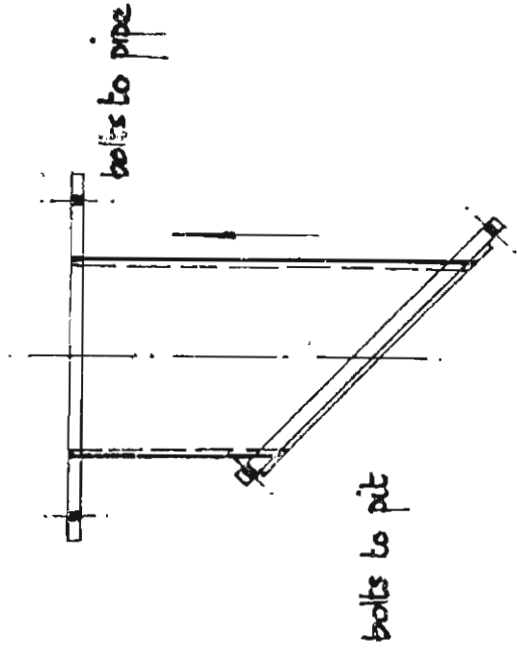
127 mm I.D. pipe :  $22\frac{1}{2}^\circ$  /  $67\frac{1}{2}^\circ$



70 mm I.D. pipe :  $45^\circ$



94 mm I.D. pipe :  $45^\circ$



127 mm I.D. pipe :  $45^\circ$

The angle flange of each adaptor was accurately bored to form the required ellipse created by the angle of deflection. The centre of the ellipse was located coincident with the centreline of the appropriate pit face. A flushing plate was provided to each adaptor so that, when the adaptor was bolted to the pit, the pipe entrance (or exit) was flush with the inside of the pit wall. This provided sharp-edged entrances and exits. Similar removable flushing plates were provided to the upstream end of the downstream pipe and the downstream end of the upstream pipe so that sharp-edged conditions could be maintained for deflection angles of  $0^\circ$  and  $90^\circ$ .

Eight peizometer tappings were provided to each pipe reach. The spacing and location of tappings were detailed as shown in Figures 4.9 to 4.11. The tappings were made from 25 mm diameter acrylic rod which was cut to size, tapped and fitted with 6 mm brass airline fittings. Each tapping was then glued to the pipe at the desired location. Holes of 3 mm diameter were then carefully drilled through the conduit taking care to avoid chipping or burring the inside of the tubing. Typical peizometer tappings are shown in Figure 4.5. Six millimetre diameter hose was used to connect the piezometer tappings to the piezometer board. Wherever possible, tappings were placed upstream from splices in the conduits.

In addition to the pressure tappings in the pipes, an additional tapping was provided in each junction pit. This tapping was located under the false floor of the pit and a check was made for each model to ensure that the pressure tapping did not measure additional hydrodynamic head on the piezometer board due to potential turbulence under the false floor.

#### Connecting Pipes to Pits

Each pipe was bolted either directly to the pit so that the pipe was perpendicular to a pit face, or was bolted to the appropriate angle adaptor which was then bolted to the pit

TABLE 4.4 : ANGLE ADAPTORS

Adaptor No.	I.D.	Angle and location of Adaptor
1	70 mm	22½° attached to d/s pipe on opposing face of pit (model no. 2)
	70 mm	22½° attached to u/s pipe on opposing face of pit (model nos. 19, 23 & 27)
	70 mm	67½° attached to d/s pipe on adjacent face of pit (model no. 5)
	70 mm	67½° attached to u/s pipe on adjacent face of pit (model nos. 22, 24 & 30)
2	70 mm	45° attached to d/s pipe on opposing face of pit (model no. 3)
	70 mm	45° attached to d/s pipe on adjacent face of pit (model no. 4)
	70 mm	45° attached to u/s pipe on opposing face of pit (model nos. 20, 24 & 28)
	70 mm	45° attached to u/s pipe on adjacent face of pit (model nos. 21, 25 & 29)
3	94 mm	22½° attached to d/s pipe on opposing face of pit (model no. 8)
	94 mm	67½° attached to d/s pipe on adjacent face of pit (model no. 11)
4	94 mm	45° attached to d/s pipe on opposing face of pit (model no. 9)
	94 mm	45° attached to d/s pipe on adjacent face of pit (model no. 10)
5	127 mm	22½° attached to d/s pipe on opposing face of pit (model no. 14)
	127 mm	67½° attached to d/s pipe on adjacent face of pit (model no. 17)
6	127 mm	45° attached to d/s pipe on opposing face of pit (model no. 15)
	127 mm	45° attached to d/s pipe on adjacent face of pit (model no. 16)

face. An initial test programme (models 1 to 18) contained geometries such that the upstream pipe was always perpendicular to the upstream face of the pit, and the angle adaptors were always located on the downstream pipe. With the completion of this initial programme, further investigation revealed major hydraulic variations when the angle adaptors were attached to the upstream face of the pit and the downstream pipe bolted directly to the downstream pit face. Consequently, the initial test programme was extended to include geometries characterised by reverse orientations (models 19 to 30).

For each model, the pipes were aligned so that the pipe obverts were at the same elevation. This is in accordance with the alignment procedures adopted throughout Sydney. (Sangster's tests (1958) were performed with the alignment of pipe inverts). In all cases, the invert of the downstream connecting pipe was located at the elevation of the pit floor. The pit floor was constructed horizontal. No tests were conducted to investigate the hydraulic effects of shaping the pit bottom, such as those conducted by Prins (1976).

#### 4.2.4 Model Geometries

Figures 4.13 to 4.18 show details of model junction geometries tested.

Models 1 to 18 comprise the initial test programme and incorporate six angles of deflection ( $\theta$ ) and three downstream pipe sizes ( $D_o$ ). Each downstream pipe diameter is associated with a corresponding increase in pit size such that the ratio  $B/D_o$  is approximately constant and equal to 2.

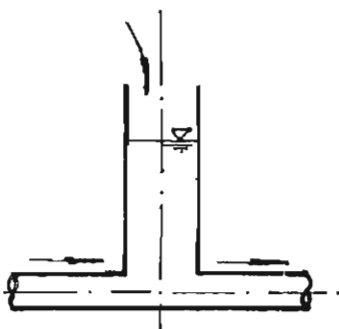
The remaining models (19 - 30) were tested with geometries identical to corresponding models in the original test

FIGURE 4.13 : HYDRAULIC MODELS 1 TO 6

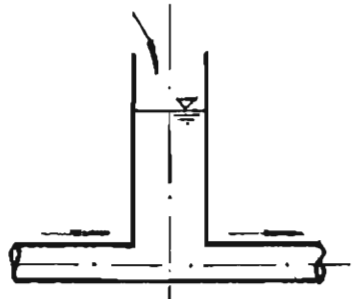
PIT SIZE : 140 MM X 140 MM.

UPSTREAM PIPE DIAMETER : 70 MM

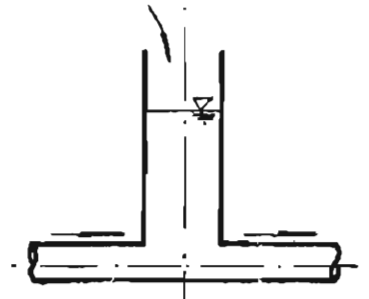
DOWNSTREAM PIPE DIAMETER : 70 MM.

MODEL NO. 1.

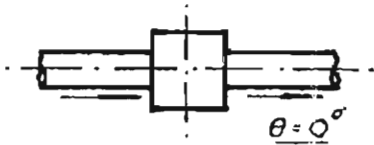
ELEVATION.

MODEL NO. 2.

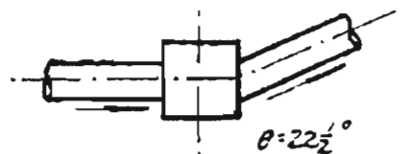
ELEVATION.

MODEL NO. 3

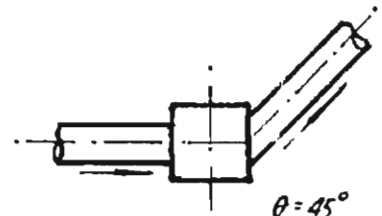
ELEVATION.



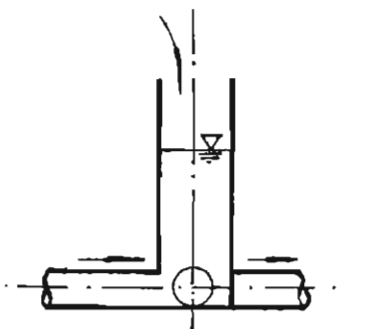
PLAN.



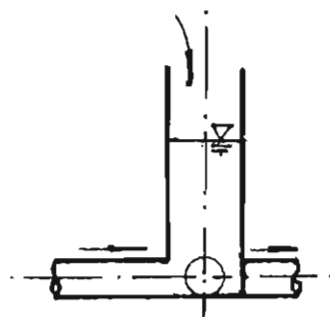
PLAN.



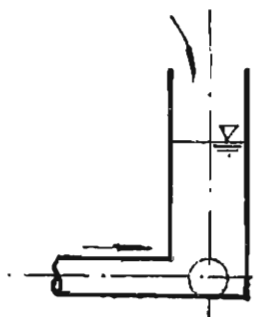
PLAN.

MODEL NO. 4

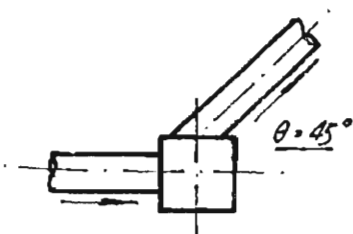
ELEVATION.

MODEL NO. 5

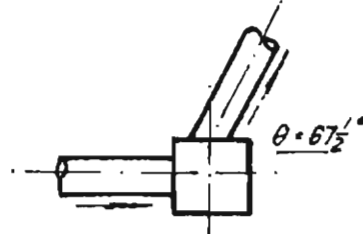
ELEVATION.

MODEL NO. 6

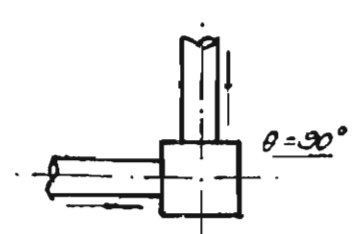
ELEVATION.



PLAN.



PLAN.



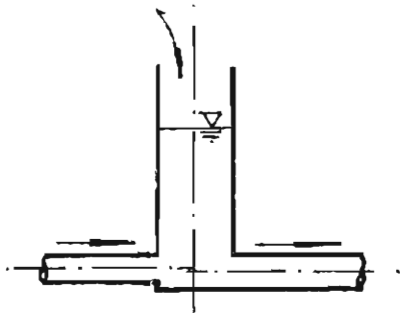
PLAN.

FIGURE 4.14 : HYDRAULIC MODELS 7-12.

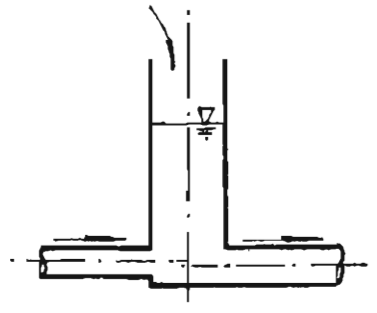
PIT SIZE : 190 MM x 190 MM.

UPSTREAM PIPE DIAMETER : 70 MM.

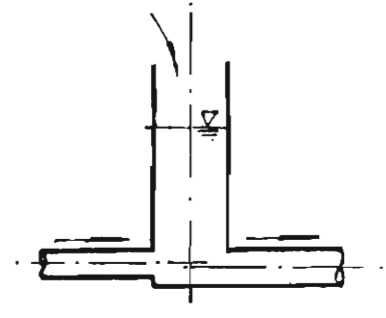
DOWNSTREAM PIPE DIAMETER : 94 MM.

MODEL NO. 7.

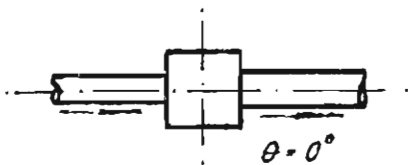
ELEVATION.

MODEL NO. 8

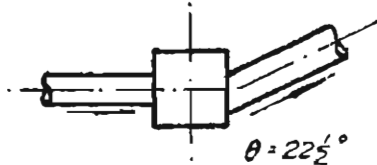
ELEVATION.

MODEL NO. 9.

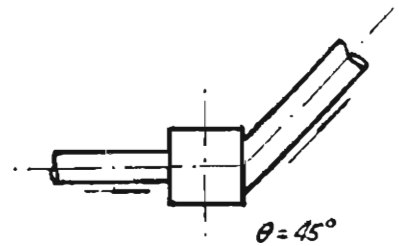
ELEVATION



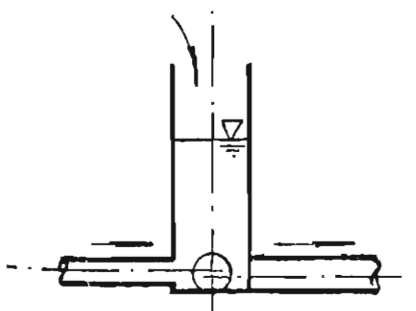
PLAN.



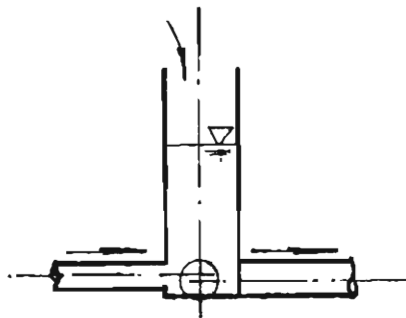
PLAN.



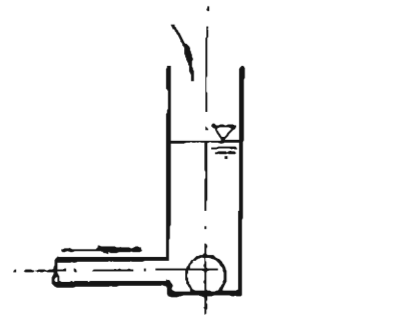
PLAN

MODEL NO. 10

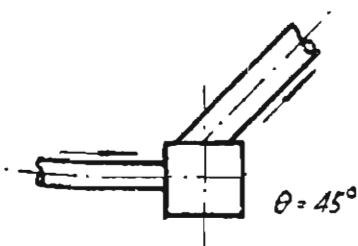
ELEVATION.

MODEL NO. 11

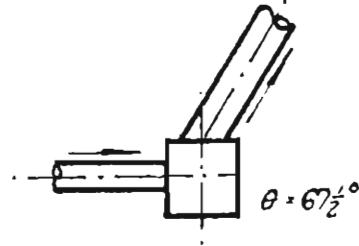
ELEVATION.

MODEL NO. 12

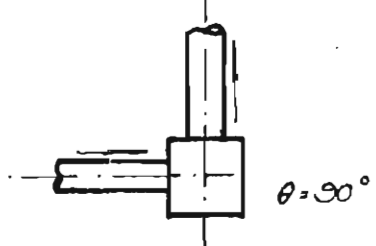
ELEVATION.



PLAN.



PLAN.



PLAN.



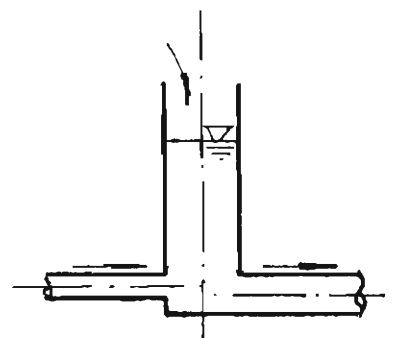
FIGURE 4.15 : HYDRAULIC MODELS 13 TO 18

PIT SIZE : 240MMX 240MM

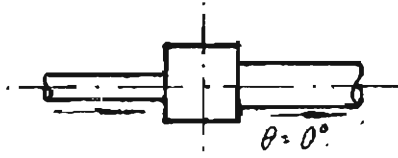
UPSTREAM PIPE DIAMETER : 70 MM.

DOWNSTREAM PIPE DIAMETER : 127 MM.

MODEL NO. 13.

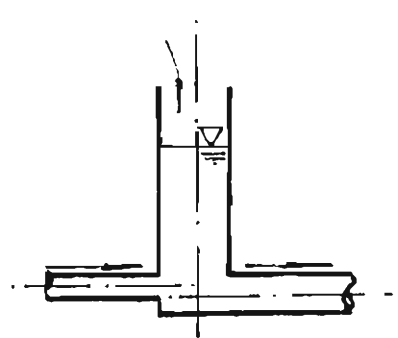


ELEVATION.

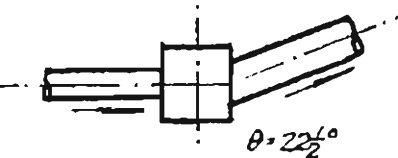


PLAN.

MODEL NO. 14.

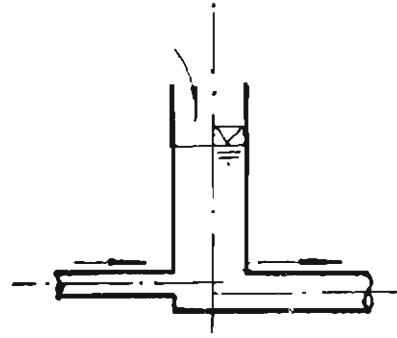


ELEVATION

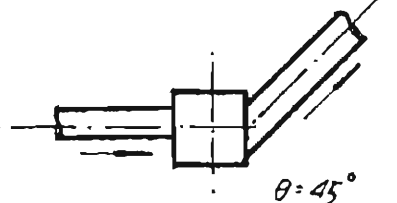


PLAN.

MODEL NO. 15

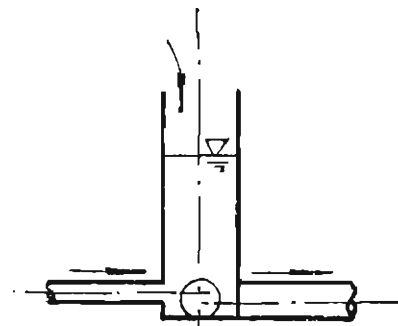


ELEVATION

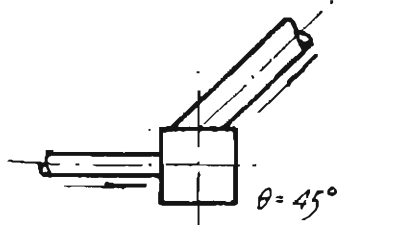


PLAN.

MODEL NO. 16

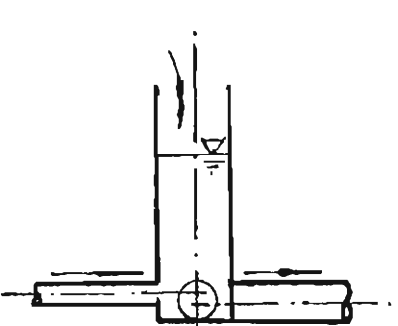


ELEVATION

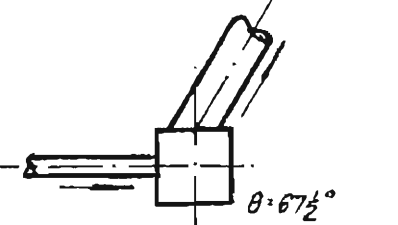


PLAN.

MODEL NO. 17

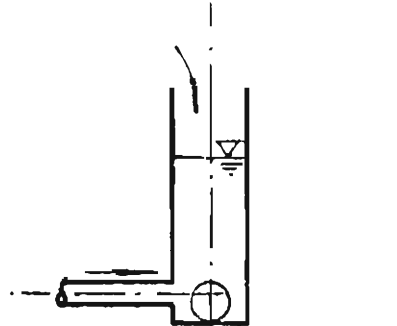


ELEVATION.

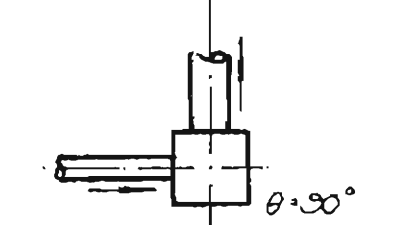


PLAN.

MODEL NO. 18.



ELEVATION.



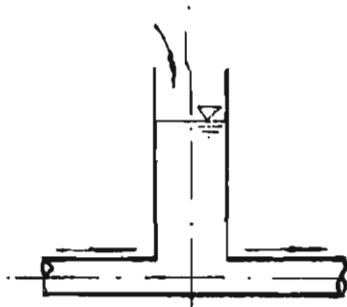
PLAN.

FIGURE 4.16 : HYDRAULIC MODELS 19-TO 23.

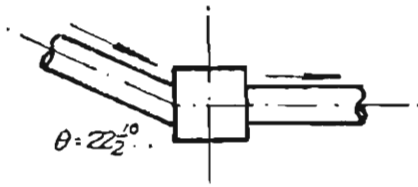
PIT SIZE : 140 MM x 140 MM

UPSTREAM PIPE DIAMETER : 70 MM

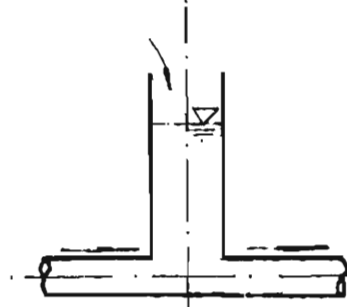
DOWNSTREAM PIPE DIAMETER : 70 MM.

MODEL N° 19.

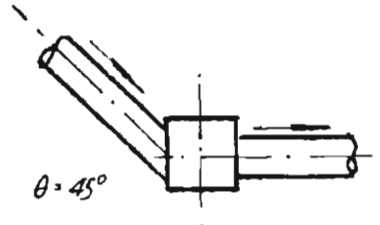
ELEVATION



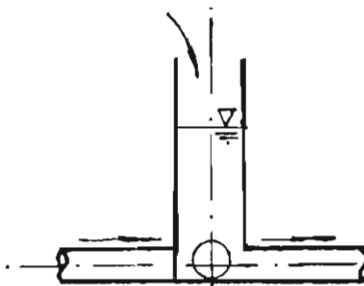
PLAN.

MODEL N° 20.

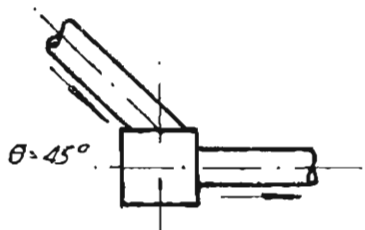
ELEVATION



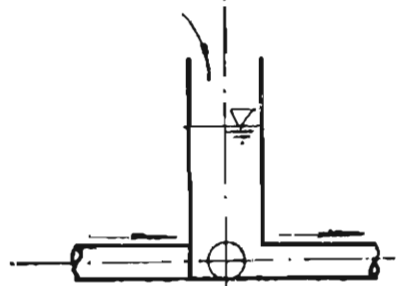
PLAN

MODEL N° 21.

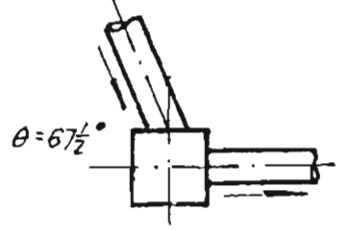
ELEVATION.



PLAN

MODEL N° 22.

ELEVATION



PLAN

FIGURE 4.17 : HYDRAULIC MODELS 23 TO 25.

PIT SIZE : 190 MM X 190 MM

UPSTREAM PIPE DIAMETER : 70 MM.

DOWNSTREAM PIPE DIAMETER : 94 MM.

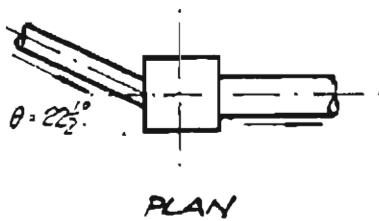
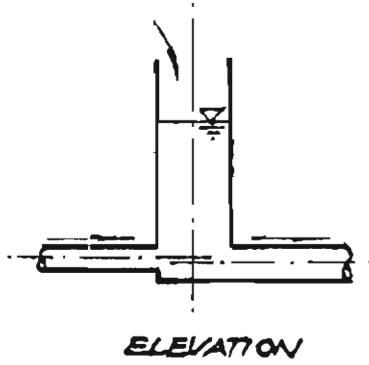
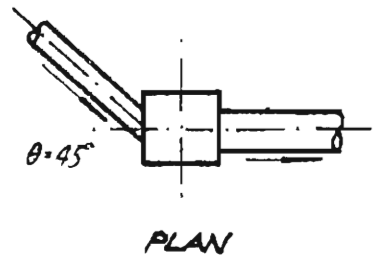
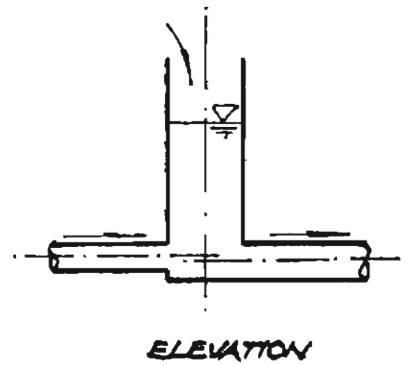
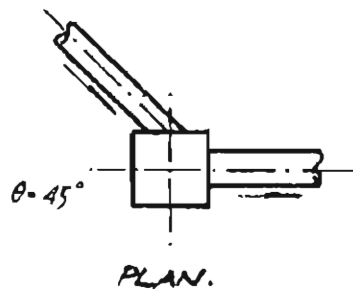
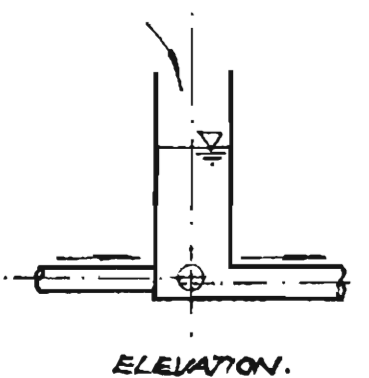
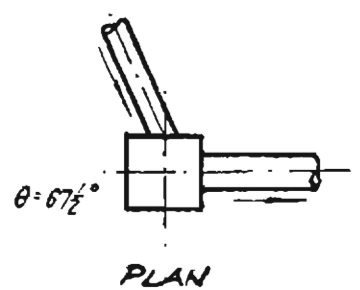
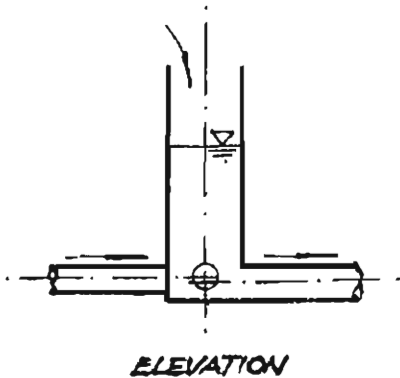
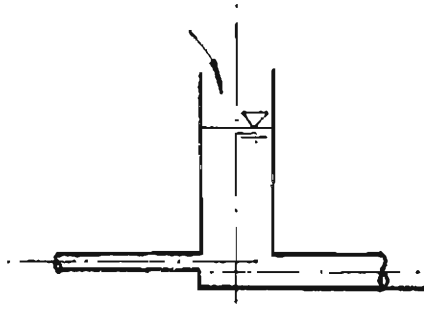
MODEL NO. 23.MODEL NO. 24MODEL NO. 25MODEL NO. 26

FIGURE 4.18 : HYDRAULIC MODELS 27-30

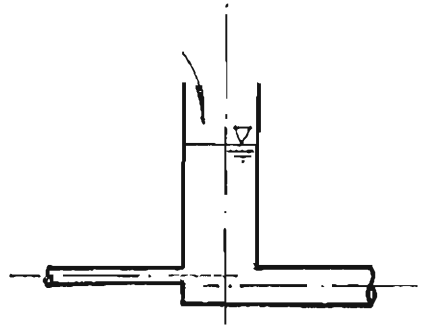
PIT SIZE : 240 MM x 240 MM

UPSTREAM PIPE DIAMETER : 70 MM

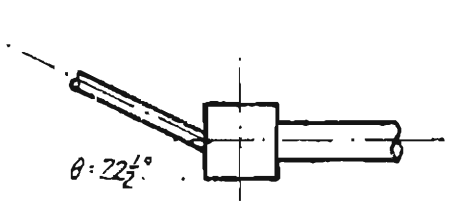
DOWNSTREAM PIPE DIAMETER : 127 MM.

MODEL NO. 27

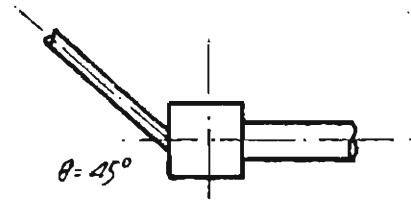
ELEVATION.

MODEL NO. 28.

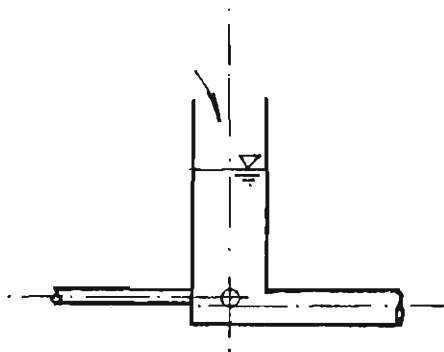
ELEVATION.



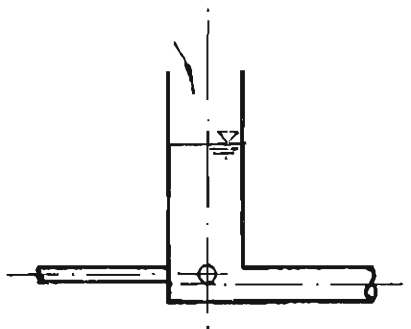
PLAN.



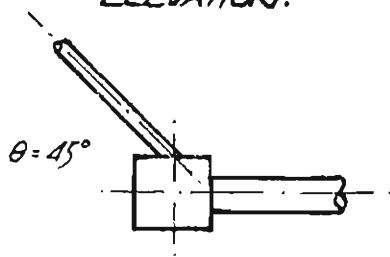
PLAN

MODEL NO. 29.

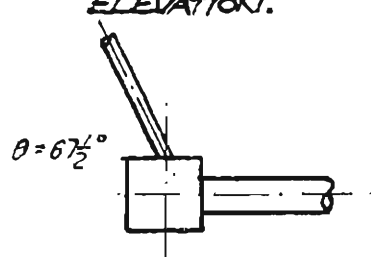
ELEVATION.

MODEL NO. 30.

ELEVATION.



PLAN.



PLAN.

programme except that the bend angle adaptor was fitted to the upstream pipe. In these cases, the flow entered the junction pit at an angle inclined to the upstream face of the pit. Thus, for the same basic bend geometry (defined by  $\theta$  and  $D_u/D_o$ ), there may occur a number of orientations of the pit relative to the connecting pipe (four such orientations may be compared in models 3, 4, 20 and 21). Significant differences in hydraulic behaviour were observed for each orientation.

Each model was tested for the effects of the following flow conditions:

- (i) variation in discharge,  $Q_o$
- (ii) variation in submergence,  $S$
- (iii) variation in grate flow ratio,  $Q_g/Q_o$

For reasons discussed in Section 3.6, variations in prototype discharge and submergence are inter-related in the prototype. In the models, however, it was possible, using the adjustable tailgate, to independently regulate discharge and submergence so that the effect of each parameter could be considered separately.

#### 4.2.5 Experimental Procedures

To determine the upstream and grate flow discharges ( $Q_u$  and  $Q_g$ ), both water and mercury manometers were used for each supply line (see Figure 4.3). The mercury manometers were used for discharges greater than 2 l/s. For low discharges, water manometers were used to measure flow rates. Low discharge tests were found to be necessary for the smallest (70 mm) outfall pipe size, because, in these models, the friction losses in the downstream pipe were relatively large and resulted in high submergence depths for the pit. To test these models with low submergence ratios ( $S/D_o$ ), the discharges were reduced to less than 2 l/s. This procedure produces large experimental errors.

FIGURE 4.19 DATA AND CALCULATION SHEET.

DATA AND CALCULATION SHEET												MODEL NO:		TEST NO:									
GEOMETRY.				FLOW.				VELOCITY.				Equation of HGL: (r <sup>2</sup> = )		Equation of HGL: (r <sup>2</sup> = )									
D <sub>0</sub>	D <sub>u</sub>	D <sub>0</sub> /D <sub>u</sub>	A <sub>0</sub> /A <sub>u</sub>	B	B/D <sub>0</sub>	θ	Q <sub>0</sub>	Q <sub>u</sub>	Q <sub>u</sub> /Q <sub>0</sub>	V <sub>0</sub>	V <sub>u</sub>	V <sub>u</sub> <sup>2</sup> /2g	Elev. of HGL in pit:	mm. Elev of HGL in pit:	mm.	mm.							
mm	mm	.	.	mm	.	°	l/s	l/s	.	mm/s	mm/s	mm	Elev of TEL in pit:	mm. Elev of TEL in pit:	mm.	mm.							
CONCLUSIONS:				MR: mmHg				MR: mmHg				ΔHGL across pit: (ΔP/γ)		mm. ΔTEL across pit:		mm. k <sub>u</sub> =							
												Water surface in pit:		mm. k <sub>u</sub> =		k <sub>u</sub> γ							
PIEZOMETERS.				SUBMERGENCE RATIO S/D <sub>0</sub> =				SKETCH:															
1	2	3	4	5	6	7	8	9	10	11	12					13	14	15	16	17	Submergence ratio S/D <sub>0</sub>	H.C.L. ELEV (mm)	LOCATION (mm)

Initially, tests were run with arbitrarily selected manometer settings. The calculation of discharge, velocity and velocity head then followed. As the work proceeded, discharges of integer values up to 10 l/s were used directly with known velocities and velocity heads. This procedure minimized the necessary calculations.

Geometric and flow data were recorded on data-computation sheets as shown in Figure 4.19. Piezometer tapping chainages measured to the branch point of the junction were also recorded.

Prior to reading the piezometer board, a number of important checks were made:

- (i) The piezometer board was levelled.
- (ii) The water surface elevation in the pit was checked against the piezometer reading for the pit tapping.
- (iii) Each of the manometer and piezometer hoses were carefully checked for the inclusion of air.
- (iv) For low flowrates, it was found that the model system took some time to reach hydraulic stability.

For high discharges, each hose on the piezometer board was generally read to an accuracy of one millimetre. For low discharges, where pressure differences between adjacent tappings were less than 1 millimetre, the board was generally read to the nearest millimetre.

Readings which were not consistent with the general trend of other readings were not included in the calculations. The first and second piezometers downstream of a junction structure were usually disregarded in this respect. In models where the upstream and downstream pipes were placed on adjacent faces of the pit (such as a  $90^\circ$  bend), and where the continuity of the jet discharge across the junction was disturbed by the pit, the

pressure fluctuations were extensive and the piezometer lines were difficult to read. Due to the general turbulence created at sharply angled junctions, the pressure variations to a distance of approximately half the downstream pipe length were extensive and readings were taken as the mean value of the upper and lower readings. Large pressure variations at such junctions led to errors which are reflected in the scatter of the experimental data for these models. Despite such difficulties, however, linear equations for the hydraulic grade lines were usually developed with a coefficient of determination ( $r^2$ ) greater than 0.95.

For each of the 2000 test runs, seventeen piezometer tappings were read, eight of which were located in each connecting pipe and one at the junction pit. Only the piezometer tappings located more than 10 pipe diameters downstream of a pipe inlet, however, were used in calculations. From the piezometer readings and the respective distances away from the branch point of the junction, two linear regression equations for the hydraulic grade lines could be developed for each test run, using a least-squares fit. These equations were used to calculate the ordinate at the junction branch point and the slope of the friction line. The equations were recorded on each data-computation sheet (Figure 4.19) as "Equation U/S HGL" and "Equation D/S HGL". The equation ordinates thus represent the elevations of the upstream and downstream hydraulic grade lines when extrapolated linearly to the branch point of the junction, and their subtraction yielded the absolute pressure head change ( $\Delta p/\gamma$  in Figure 3.4) occurring across the structure. Similarly, the subtraction of the pit piezometer reading from the downstream equation ordinate yielded the pressure head change plus the degree of conversion of upstream kinetic energy (WSE in Figure 3.4). From the values of  $\Delta p/\gamma$  and WSE, obtained in this way, division by the downstream velocity head yielded the dimensionless coefficients,  $k_u$  and  $k_w$ .



FIGURE 4.20: DATA PLOT FOR MODEL NO. 2.

PRESSURE HEAD CHANGE COEFFICIENT VS. DISCHARGE  $Q_0$ .

$\theta = 22\frac{1}{2}^\circ$ ,  $D_0 = 70$  MM,  $D_u = 70$  MM,  $A_0/A_u = 1.00$

(FIGURES INDICATE SUBMERGENCE RATIOS.)

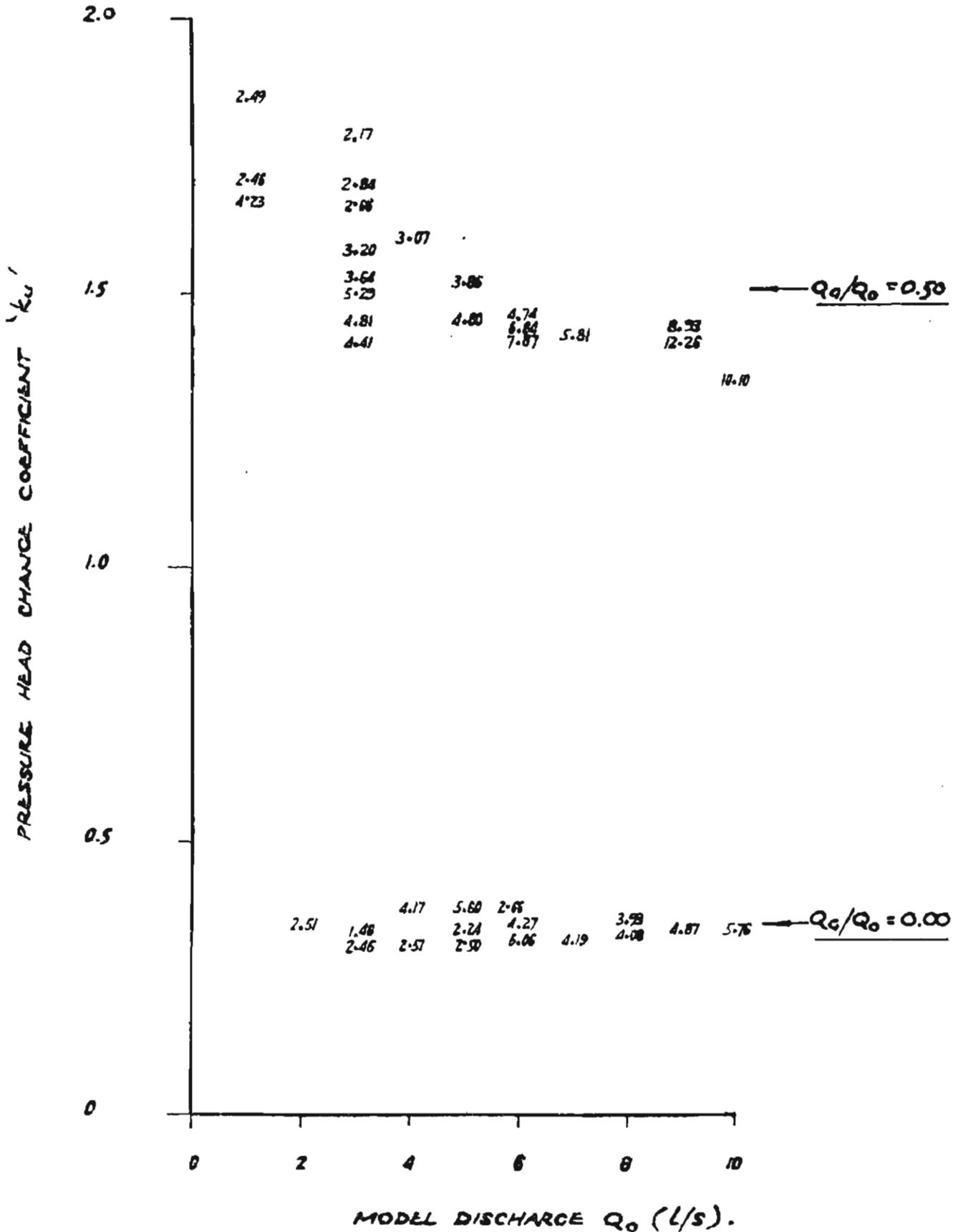
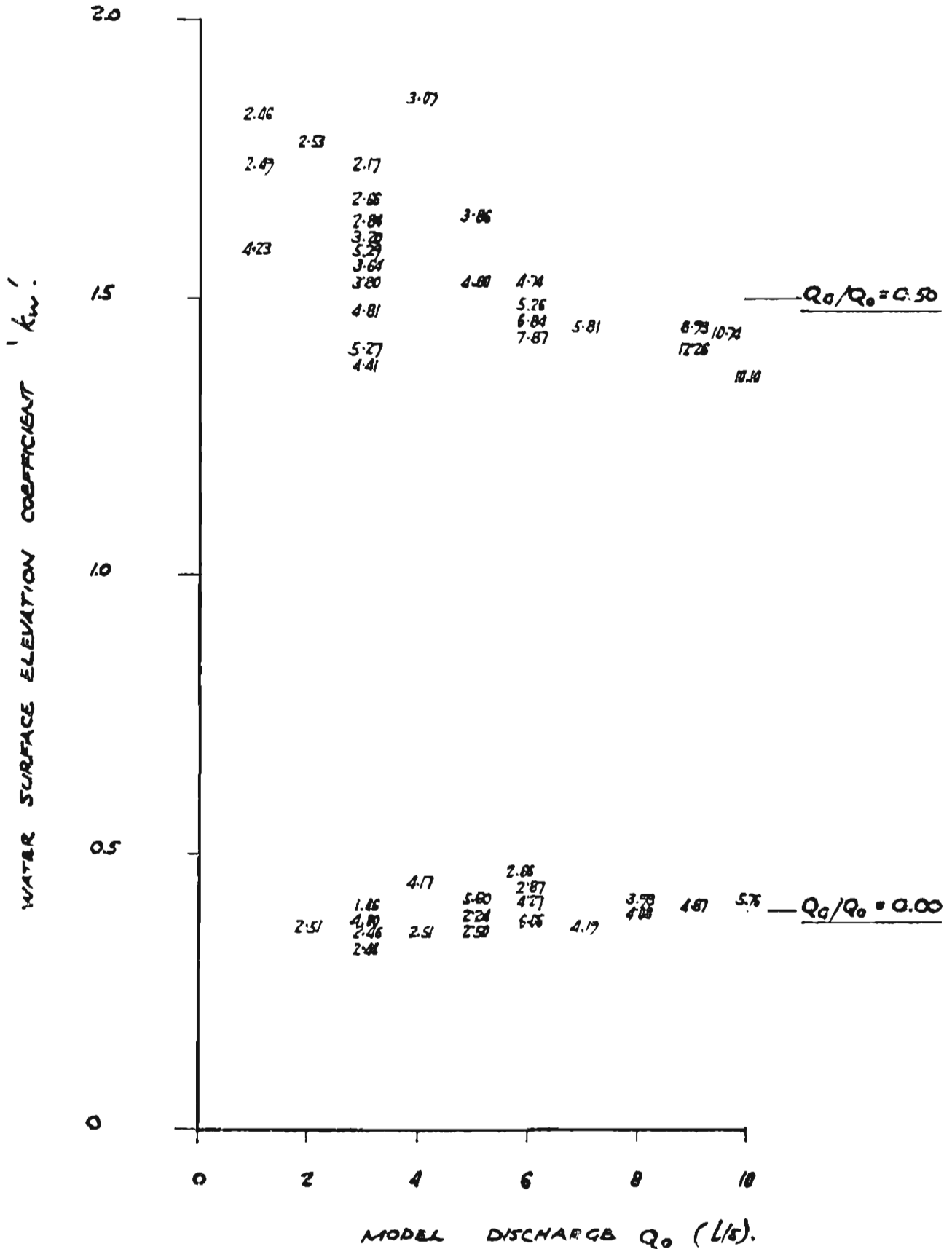


FIGURE 4.21: DATA PLOT FOR MODEL NO. 2.

— WATER SURFACE ELEVATION COEFFICIENT VS DISCHARGE  $Q_0$ .

$\theta = 22\frac{1}{2}^\circ$ ,  $D_0 = 70$  MM,  $D_u = 70$  MM,  $A_0/A_u = 1.00$ .

(FIGURES INDICATE SUBMERGENCE RATIOS.)



Having determined these coefficients, the values were plotted for each test run against the downstream discharge  $Q_o$ , with grate flow and submergence ratios as secondary parameters. Typical data plots are shown in Figures 4.20 and 4.21. Such plots served two purposes:

1. to check the consistency of data; and
2. to enable the visual interpolation of pressure head change coefficients,  $k_u$  and  $k_w$ , for the submergence ratios selected in the presentation of design curves as detailed later in Chapter 5.

All data were plotted onto figures such as those shown in Figures 4.20 and 4.21 as soon as the test had been run and the coefficients computed. Sixty such figures were plotted (two for each model) and these are included in the Appendix.

#### 4.2.6 Error Analysis

##### Calibration of Orifice Meters

Two orifice meters were manufactured and calibrated for the measurement of upstream and grate flow discharges. Calibration equations (Equations 4.2 and 4.3) were determined using power curve regression analysis.

$$Q_u = 0.349 (\Delta h)^{0.500} \quad \dots \text{Eq. 4.2}$$

and

$$Q_g = 0.348 (\Delta h)^{0.505} \quad \dots \text{Eq. 4.3}$$

where  $Q_u$  is the upstream discharge (l/s);  
 $Q_g$  is the grate flow discharge (l/s); and  
 $\Delta h$  is the manometer reading in mm Hg.

Ten volumetric measurements were taken for each calibration and the coefficients of determination ( $r^2$ ) were both recorded as 1.000. With this level of correlation, errors due to meter calibration were considered to be insignificant.

### Reading of Orifice Meter Manometers

Mercury manometers were used on the orifice meters for discharges greater than 2 l/s, using one millimetre divisions. A reading error of one millimetre at this discharge results in a 2 percent error. The diameters of the model pipelines were measured to an accuracy of 0.1 mm, resulting in a possible error in cross sectional area of 0.3 per cent for the 70 mm diameter pipe. Therefore, since the possible error attributable to the flow velocity is the sum of the individual errors of discharge and cross-sectional area, a one millimetre error in manometer reading will yield a total error of 2.3 per cent. For higher discharges, the maximum error is reduced. Provided the manometers were read consistently to an accuracy of 0.5 mm for each column, errors resulting in velocity head calculations could thus be maximized at 4.6 per cent at a discharge of 2 l/s. For discharges less than 2 l/s, water manometers were used. Under these conditions errors in discharge measurements were reduced.

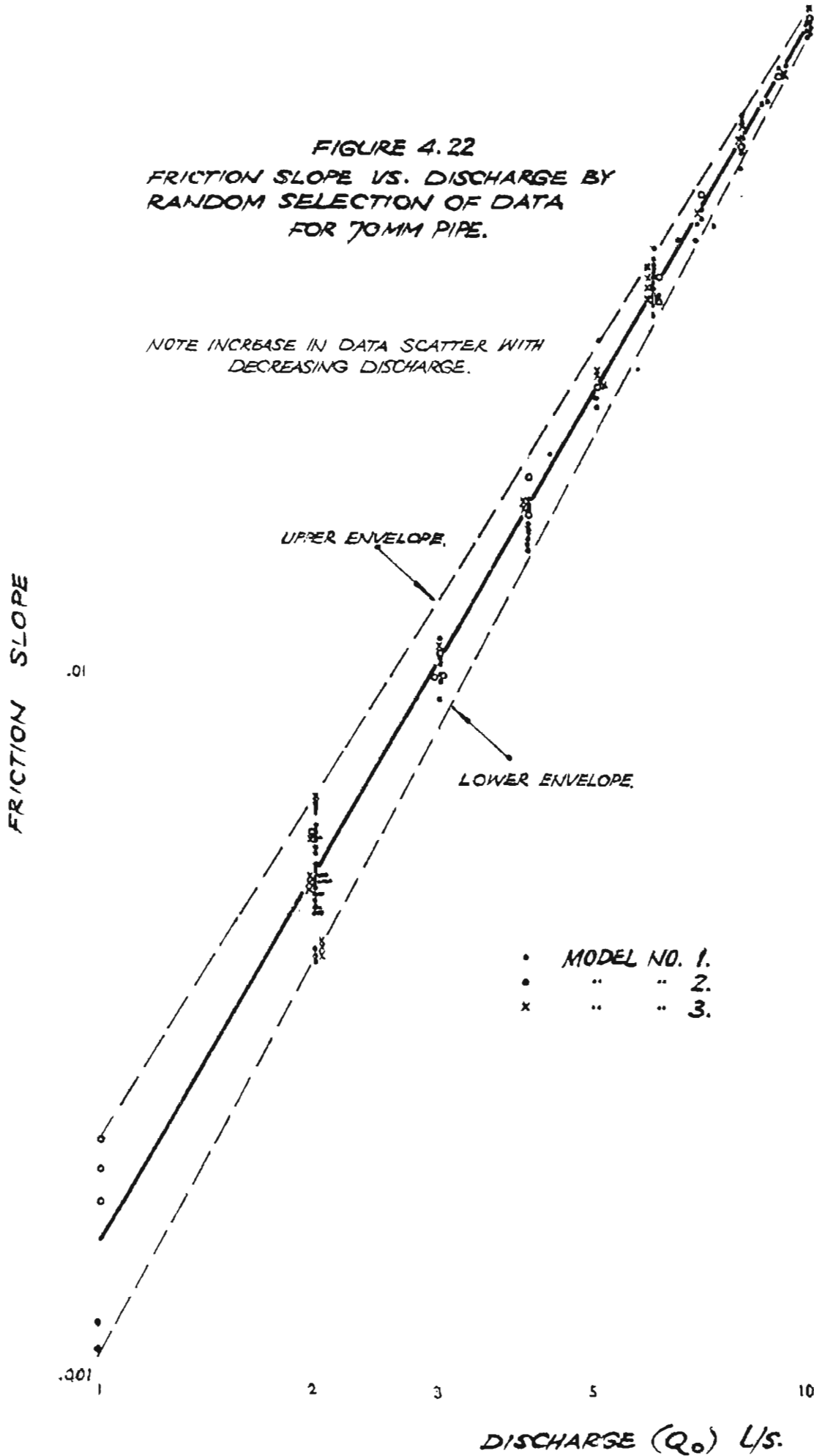
### Piezometer Measurements

In the majority of tests, linear regression analysis for the determination of friction slopes yielded coefficients of determination ( $r^2$ ) greater than or equal to 0.98. Friction slopes for each pipe were determined for each test run and recorded to four decimal places. In Figure 4.22, friction slope has been plotted against the outfall discharge for model numbers 1, 2 and 3 (70 mm diameter pipe). The points plotted are for randomly selected data. The accuracy of piezometer readings increased with increasing discharge (the errors being reflected in the scatter of the data).

At a discharge of 2 l/s, the variation in the outfall friction slope represents a maximum error of 3.6 mm in the

FIGURE 4.22  
 FRICTION SLOPE VS. DISCHARGE BY  
 RANDOM SELECTION OF DATA  
 FOR 70MM PIPE.

NOTE INCREASE IN DATA SCATTER WITH  
 DECREASING DISCHARGE.



ultimate pressure head change over a 2000 mm length of pipe. The error in pressure head change may be set simply as a proportion of the downstream pipe diameter as follows:

$$\text{Maximum Error at } 2 \text{ l/s} = \left( \frac{3.6}{70} \right)^{D_o} = D_o/18$$

which corresponds to an absolute error of 21 mm for a 375 mm diameter prototype, and 50 mm for a 900 mm diameter prototype. This order of accuracy may be considered to be adequate for practical design purposes.

CHAPTER 5EXPERIMENTAL RESULTS

- 5.1 Introduction
- 5.2 Flow Straight Through Junction Pits
- 5.3  $22\frac{1}{2}^{\circ}$  Bends at Pits
- 5.4  $45^{\circ}$  Bends at Pits
- 5.5  $67\frac{1}{2}^{\circ}$  Bends at Pits
- 5.6  $90^{\circ}$  Bends at Pits

## EXPERIMENTAL RESULTS

### 5.1 Introduction

Over 2000 tests were performed on thirty different models of various geometric configurations. All models were tested for three different values of the diameter ratio  $D_u/D_o$  and for a range of values of the hydraulic parameters  $Q_g/Q_o$  and  $S/D_o$ . These data have been processed and the results are set out in graphical form in Figures 5.1 through 5.35. A commentary on the processing of the test data is included in the Appendix. The figures show pressure head change coefficients and/or water surface elevation coefficients plotted against diameter ratios for various submergence and grate flow conditions. The figures have been categorized into five sub-groups:

1. Straight through flow.
2.  $22\frac{1}{2}^\circ$  bend structures
3.  $45^\circ$  bend structures.
4.  $67\frac{1}{2}^\circ$  bend structures.
5.  $90^\circ$  bend structures.

Each category is detailed in Section 5.2 to 5.6 respectively.

In some models, the submergence ratio was restricted due to model limitations. For example, with large downstream pipe sizes, submergence depths significantly greater than three could not be obtained due to low friction losses in the downstream pipe. In these cases, the graphs are shown with dashed lines representing an extrapolation of the curves beyond the range covered by the experimental data.

When interpolating for intermediate grate flow ratios ( $Q_g/Q_o$ ), the pressure head change and water surface elevation coefficients should not be read as a linear function but rather as a function of ( $Q_u/Q_o$ ) in accordance with Equation 5.1:

$$k_g = k_o + 1.33 \cdot \left[ 1 - \left( \frac{Q_u}{Q_o} \right)^2 \right] (k_{s0} - k_o) \quad \dots \text{Eq. 5.1}$$

where



$k_g$  is the coefficient to be calculated for a given grate flow ratio,

$k_o$  is the coefficient value when  $Q_g/Q_o=0$

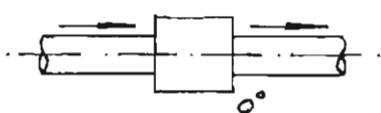
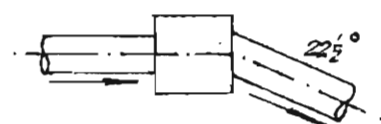
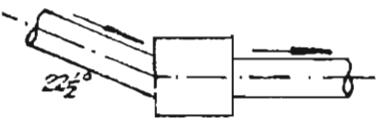
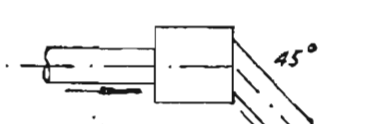
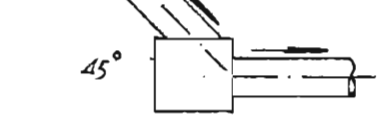
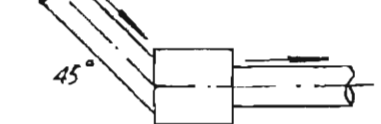
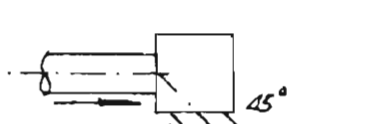
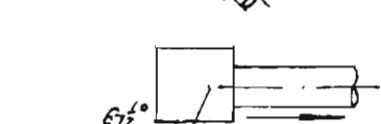

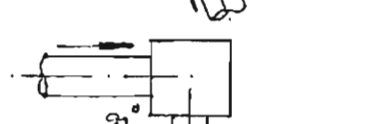
and  $k_{50}$  is the coefficient value when  $Q_g/Q_o=0.50$ .

For submergence values of about 1.5 outfall pipe diameters, experimental evidence suggests that the loss coefficients decrease until the limiting case of pipes not flowing full occurs. In some models tested, loss coefficients started to decrease for submergence depths higher than 1.5 pipe diameters. In the formulation of the charts, the assumption has been made that the pressure head change coefficients will only start to decrease for submergence depths less than 1.5 outfall pipe diameters. This assumption has been made on the basis, first, that errors in experimental readings are potentially larger at low submergence depths (see Section 4.2.6) and, second, that interpolation of coefficient values for submergences between  $1.5 \leq S/D_o \leq 2$  could not be made from the figures if the loss coefficients decrease suddenly within this range. This assumption may lead to conservative results for some geometric configurations but seeks to eliminate the experimental difficulties and subsequent risk of significant errors when the model submergence ratios were tested at values of 1.5 outfall pipe diameters or less.

In the practical application of the graphs, the derived loss coefficients,  $k_u$  and  $k_w$ , must be multiplied by the downstream velocity head to determine the upstream pressure line and water surface elevations respectively.

Table 5.1 provides a quick reference to the various bend geometries tested.

TABLE 5.1 : QUICK REFERENCE GUIDE TO GEOMETRIES TESTED.

	GEOMETRIC CONFIGURATION.	FIGURE NOS.	PAGE NOS.
1.		Fig. 5.1, 5.2 Table 5.2	112, 113, 103
2.		Fig. 5.3, 5.4 Table 5.2	114, 115, 103
3.		Fig. 5.5 - 5.8	116 - 119
4.		Fig. 5.9, 5.10 Table 5.2	120, 121, 103
5.		Fig. 5.9, 5.11 Table 5.2	120, 122, 103
6.		Fig. 5.12 - 5.15	123 - 126
7.		Fig. 5.16 - 5.19	127 - 130
8.		Fig. 5.20 - 5.24	131 - 135
9.		Fig. 5.25 - 5.28	136 - 139
10.		Fig. 5.29 - 5.35	140 - 146

## 5.2 Flow Straight Through Junction Pits

For junction pits in which the inlet and outlet pipes are in-line and which have flow entering through a top grate, Equation 2.19 can be reduced to Equation 5.2:

$$k_u = 2 \left[ 1 - \frac{A_o}{A_u} \left( \frac{Q_u}{Q_o} \right)^2 \right] \quad \dots \text{Eq. 5.2}$$

Equation 5.2 has been plotted in Figure 5.1\* and the results compared with experimental data obtained by the author and by previous investigators. These include Archer (1978) who tested junctions with  $D_u/D_o$  equal to 1.00 and  $Q_g/Q_o$  equal to zero, and Sangster (1958) who presented experimental data for  $Q_g/Q_o$  equal to zero but extrapolated his results for grate flow ratios of up to 50 per cent.

Of particular interest in Figure 5.1 are the negative pressure head change coefficients obtained when  $D_u/D_o < 1.0$  (i.e., at an expansion). At low grate flows the negative coefficients are large in magnitude and are attributable to deceleration of flow across the junction.

### Experimental Results

Experimental results have been plotted in Figure 5.2 for a submergence ratio equal to 2.5 (i.e.  $S/D_o = 2.5$ ). Use of Table 5.2 allows modification of pressure head change coefficients for other values of submergence ( $1.5 < S/D_o < 4.0$ ). Modifications need only be made when  $Q_g/Q_o$  is not equal to zero. The water surface elevation in the pit coincides with the elevation of the pressure line of the upstream pipe at the junction branch point (i.e.,  $k_u = k_w$ ).

---

\* Because of the large number of figures in this Chapter, the figures have been grouped together at the end of the Chapter. Figure 5.1 is located on page 112.

TABLE 5.2

MODIFICATION TABLE FOR VALUES OF  $S/D_0$  OTHER THAN 2.5. ADD MODIFICATION VALUES TO  $K_U$  AND  $K_W$  AS DETERMINED FROM FIGURE 5.2, 5.4, 5.11 OR 5.12. APPLICABLE ONLY TO JUNCTIONS WHERE THE BRANCH POINT OF THE JUNCTION IS LOCATED ON THE DOWNSTREAM FACE OF THE PIT.

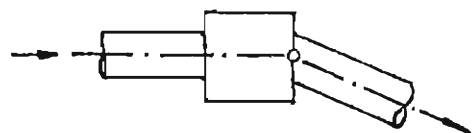
$S/D_0 \backslash Q_c/Q_0$	0.00	0.10	0.20	0.30	0.40	0.50
1.5	0.00	0.11	0.22	0.33	0.44	0.55
2.0	0.00	0.04	0.08	0.12	0.16	0.20
2.5	0.00	0.00	0.00	0.00	0.00	0.00
3.0	0.00	-0.03	-0.06	-0.09	-0.12	-0.15
3.5	0.00	-0.04	-0.08	-0.12	-0.16	-0.20
4.0	0.00	-0.05	-0.10	-0.15	-0.20	-0.25

In most design applications, the ratio  $D_u/D_o$  approaches unity whilst the grate flow ratio  $Q_g/Q_o$  approaches zero. Thus the loss coefficients,  $k_u$  and  $k_w$ , would, in most instances, lie within the range  $-0.5 < k_u, k_w < 0.5$ . For the common case of equal size pipes ( $D_u/D_o = 1.0$ ) and for grate flow,  $Q_g$ , equal to zero, coefficients  $k_u$  and  $k_w$  may be set equal to 0.2, being independent of submergence ratio,  $S/D_o$ . For expansions ( $D_u < D_o$ ), negative pressure head change coefficients will occur. Negative pressure head changes are considered acceptable in design practice provided that the upstream hydraulic grade line elevation, as determined, is located above the upstream pipe invert, thus avoiding negative (less than atmospheric) pipe pressures. For in-line flow, loss coefficients are generally lower than those values which have been used traditionally in design practice. Maximum pressure head changes of two downstream velocity heads are obtained at high grate flow ratios coupled with low submergence depths.

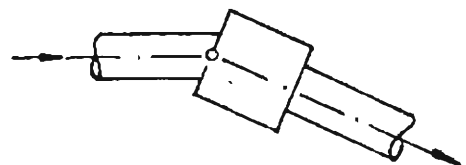
### 5.3 $22\frac{1}{2}^\circ$ Bends at Pits

Two configurations using  $22\frac{1}{2}^\circ$  bends were tested:

- (i) the junction branch point located on the downstream face of the pit.



- (ii) the junction branch point located on the upstream face of the pit.



Configuration (i) : Branch Point Located on Downstream Face of Pit.

For junction pits having the branch point on the downstream face, Equation 2.19 may be reduced to Equation 5.3:

$$k_u = 2 \left[ 1 - \frac{A_o}{A_u} \cdot \left( \frac{Q_u}{Q_o} \right)^2 \cos \theta_u \right] \quad \dots \text{Eq. 5.3}$$

Equation 5.3 is plotted in Figure 5.3 along with the author's experimental data for submergence ratios equal to approximately 2.5. The good correlation which exists between the equation and the data suggests that Equation 5.3 may be used for pits with a  $22\frac{1}{2}^\circ$  bend configuration when the branch is located on the downstream face of the pit and when the submergence depth is relatively high.

Figure 5.4 has been developed from the author's test data, and applies specifically to a submergence depth of  $2.5 D_o$ . For submergence ratios other than 2.5, values obtained from Figure 5.4 should be modified by using Table 5.2.

The elevations of the upstream pressure line and the water surface are coincident. Negative pressure head change coefficients apply to some combinations of pipe sizes and grate flow contributions. Values of pressure head change coefficients, for most design applications, will be less than those values that have been traditionally used in design.

Configuration (ii) : Branch point located on Upstream  
Face of Pit.

When the branch point is located on the upstream face of the pit, the hydraulic efficiency of the junction is reduced since the upstream flow momentum is partially lost in crossing the pit. This interference across the junction precludes the theoretical analysis previously derived.

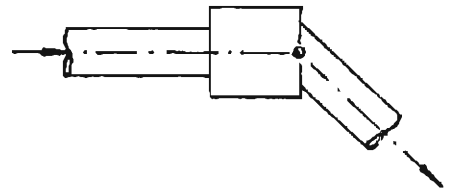
Figures 5.5 through 5.8 have been prepared using experimental data for pressure head change and water surface elevation coefficients for a range of submergence depths ( $1.5 \leq S/D_o \leq 4.0$ ) when the branch point is located on the upstream face of the pit. For this condition, the magnitudes of  $k_u$  and  $k_w$  are considerably greater than values shown in Figure 5.4 for equivalent diameter and grate flow ratios.

All pressure head change coefficients are positive and, in each case, the water surface elevation is located above the upstream pressure line elevation. To improve junction performance, the location of the upstream pipe should be shifted to ensure that the branch point is located on the downstream face of the pit. Under these conditions, hydraulic efficiency similar to case (i) above may be anticipated.

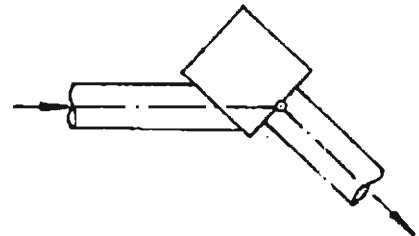
#### 5.4 45° Bends at Pits

For 45° bends, the following junction pit configurations were tested:

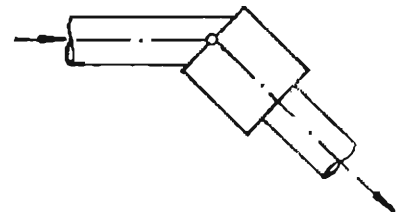
- (i) the junction branch point located on the downstream face of the pit with the downstream pipe on a 45° angle connected to the downstream face of the pit;



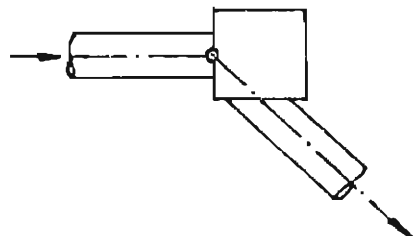
- (ii) the junction branch point located on the downstream face of the pit with the upstream pipe on a 45° angle connected to a side face of the pit;



- (iii) the junction branch point located on the upstream face of the pit with the upstream pipe on a 45° angle connected to the upstream face of the pit;



- (iv) the junction branch point located on the upstream face of the pit with the downstream pipe on a 45° angle connected to a side face of the pit.



Many configurations other than those described above can be obtained by changing the location of the junction branch point and/or the pit-to-pipe orientation. The hydraulic principles can, however, be demonstrated using those configurations described above as examples.

Relative hydraulic efficiencies of the configurations tested can be deduced from Figures 5.10 through 5.19 which have been prepared using the experimental data.

For  $45^\circ$  junction pit configurations (i) and (ii) above, the experimental results may be compared with the theoretical solution obtained using Equation 5.3. This is shown in Figure 5.9.

For the purpose of discussion, each configuration has been considered separately below.

#### Configuration (i)

In Figure 5.9, Equation 5.3 is drawn together with the plot of experimental data for the junction geometry described. Good agreement is observed between the equation and the data. Since the branch point of the junction is located on the downstream face of the pit, the loss coefficients  $k_u$  and  $k_w$  will be equal in magnitude and negative pressure head changes will occur at expansions, i.e., ( $D_u < D_o$ ). Figure 5.10 presents data for submergence depths of  $2.5D_o$ . Adjustments for other submergence ratios may be made in accordance with Table 5.2.

#### Configuration (ii)

Since the branch point of the junction is located on the downstream face of the pit, the hydraulic performance of this junction configuration is similar to that described for case (i). Loss coefficients, however, are marginally larger for case (ii). A comparison between the experimental results for this



configuration and Equation 5.3 is also shown in Figure 5.9. Once again, good agreement is observed. Pressure line and water surface elevations are coincident and negative pressure head change coefficients occur at low values of  $D_u/D_o$ .

Figure 5.11 has been drawn using experimental results for a submergence ratio of 2.5. Loss coefficients for other submergence ratios may be determined using the modification factors in Table 5.2.

### Configuration (iii)

With the branch point of the junction located on the upstream face of the pit, much of the upstream flow momentum is lost within the confines of the pit. Consequently, such a junction configuration does not lend itself to the application of a theoretical solution for the determination of loss coefficients. The experimental results show that the coefficients are higher than those for corresponding values of  $D_u/D_o$  in configurations (i) and (ii). Negative pressure head change coefficients are not developed and the water surface elevation will be located above the upstream pressure line elevation (i.e.,  $k_w > k_u$ ). Of interest, however, is the fact that the loss coefficients can decrease with increased grate flow (see Figure 5.12 for example). This may be explained by an increased pressure component acting in the upstream direction when the upstream flow jet strikes the side face of the pit. This upstream force (or backpressure) will increase the loss coefficients. Increasing grate flow ratios will, by reducing the upstream flow momentum, reduce the backpressure effects and lower the loss coefficients.

Figures 5.12 through 5.15 have been developed using the experimental results. Loss coefficients  $k_u$  and  $k_w$  have been evaluated for a submergence range of  $1.5 < S/D_o < 4.0$ .

Configuration (iv)

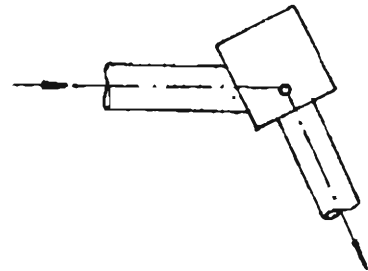
This junction pit geometry is characterized by an upstream pipe perpendicular to an opposing pit face, creating a strong backpressure effect in the upstream pipe and a corresponding rise in the hydraulic grade line. In addition, flow across the junction is hampered severely by what amounts to a  $135^\circ$  deflection angle once the jet hits and is reflected off the opposing face of the pit.

For this configuration, Figures 5.16 through 5.19 present pressure head change and water surface elevation coefficients for a submergence range of  $1.5 \leq S/D_o \leq 4.0$ . For the most common design applications ( $D_u$  equal to  $D_o$ ,  $Q_g$  approaching zero), loss coefficients would generally lie within the range  $2 \leq k_u, k_w \leq 2.5$ . Such values greatly exceed those that have been traditionally used in design practice.

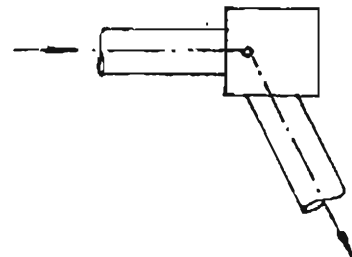
5.5  $67\frac{1}{2}^\circ$  Bends at Pits

Two  $67\frac{1}{2}^\circ$  bend configurations were tested:

- (i) the upstream pipe angled at  $67\frac{1}{2}^\circ$  such that the junction branch point was located near the downstream face of the pit;



- (ii) the downstream pipe angled at  $67\frac{1}{2}^\circ$  such that the junction branch point was located near the upstream face of the pit.

Configuration (i)

Of the two  $67\frac{1}{2}^\circ$  bend geometries tested, this configuration, with the branch point of the junction located near the downstream face of the pit, was found to be more hydraulically efficient.

Even though the branch point is not located on the downstream face, a trend toward a theoretical solution is evident from Figure 5.20. Negative pressure head change coefficients will occur for low values of  $D_u/D_o$ . Water surface elevation coefficients,  $k_w$ , however, will be greater than the corresponding pressure head change coefficients,  $k_u$ . A closer agreement between experimental results and the theoretical solution (Equation 5.2) may be anticipated by shifting the upstream pipe so that the branch point of the junction coincides with the downstream face of the pit.

Experimental results have been plotted in Figures 5.21 through 5.24 for both pressure head change and water surface elevation coefficients for a submergence range  $1.5 \leq S/D_o \leq 4.0$ .

#### Configuration (ii)

With the branch point of the junction located near the upstream face of the pit, hydraulic efficiency is reduced. The configuration is characterized by high losses attributable to backpressure effects.

Figures 5.25 through 5.28 present experimental results for loss coefficients,  $k_u$  and  $k_w$ , for a submergence range of  $1.5 \leq S/D_o \leq 4.0$ . A theoretical solution is not applicable since the upstream flow momentum does not cross the structure without severe disturbance. Water surface elevation coefficients will be significantly greater than the pressure head change coefficient values for the same geometric and flow conditions.

#### 5.6 Flow at 90° Bends

On discussion flow characteristics at 90° bends, Sangster (1958) states:

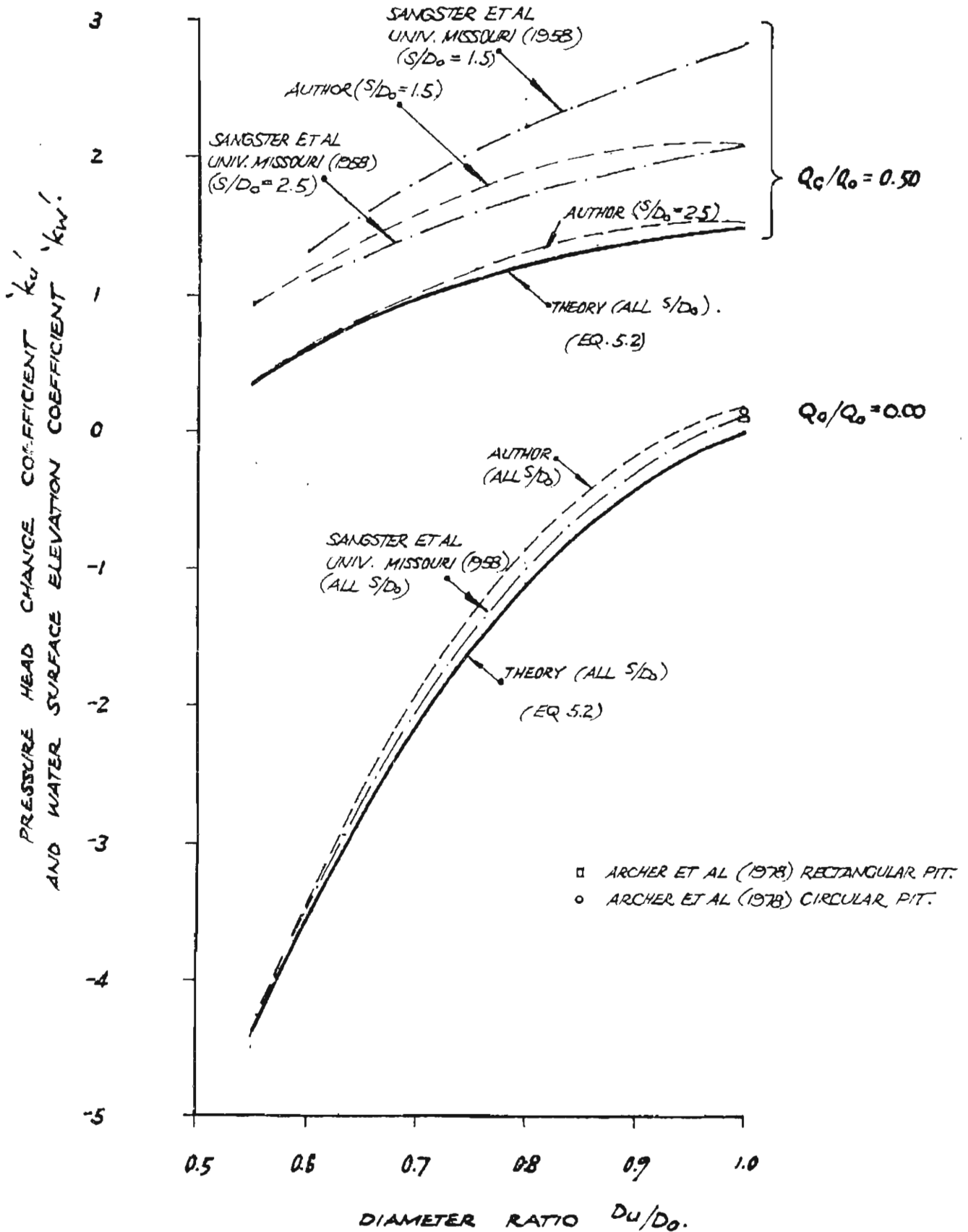
"It is unlikely that a sound and general theoretical analysis can be devised for the manhole problem." (p. 63)

Experimental results by both Sangster (1958) and by the author have been plotted along with the theoretical solutions in Figures 5.30 and 5.31 and support Sangster's view. Variations between experimental and theoretical results are attributable to a disturbance of the upstream flow momentum in crossing the structure. (Fully undisturbed flow is not possible unless the branch point is located on the downstream face of the pit).

Experimental results have been plotted, for both  $k_u$  and  $k_w$ , in Figures 5.32 through 5.35. Water surface elevation coefficients will be significantly larger than the corresponding pressure head change coefficients.

Typical design values of loss coefficients would lie within the range  $1.5 \leq k_u, k_w \leq 1.9$ . Loss coefficients may be reduced by using deflection devices such as those proposed by Sangster (1958) or by changing to junction geometries such as those shown in Figure 5.29.

**FIGURE 5.1 : COMPARISON OF EXPERIMENTAL RESULTS WITH THOSE OF OTHER INVESTIGATORS AND WITH THE THEORETICAL ANALYSIS FOR STRAIGHT THROUGH FLOW.**



**FIGURE 5.2 : COEFFICIENTS FOR STRAIGHT THROUGH FLOW.**  
**FOR SUBMERGENCE RATIO  $S/D_0 = 2.5$**

(FOR OTHER SUBMERGENCE RATIOS, MODIFY ACCORDING TO TABLE 5.2)

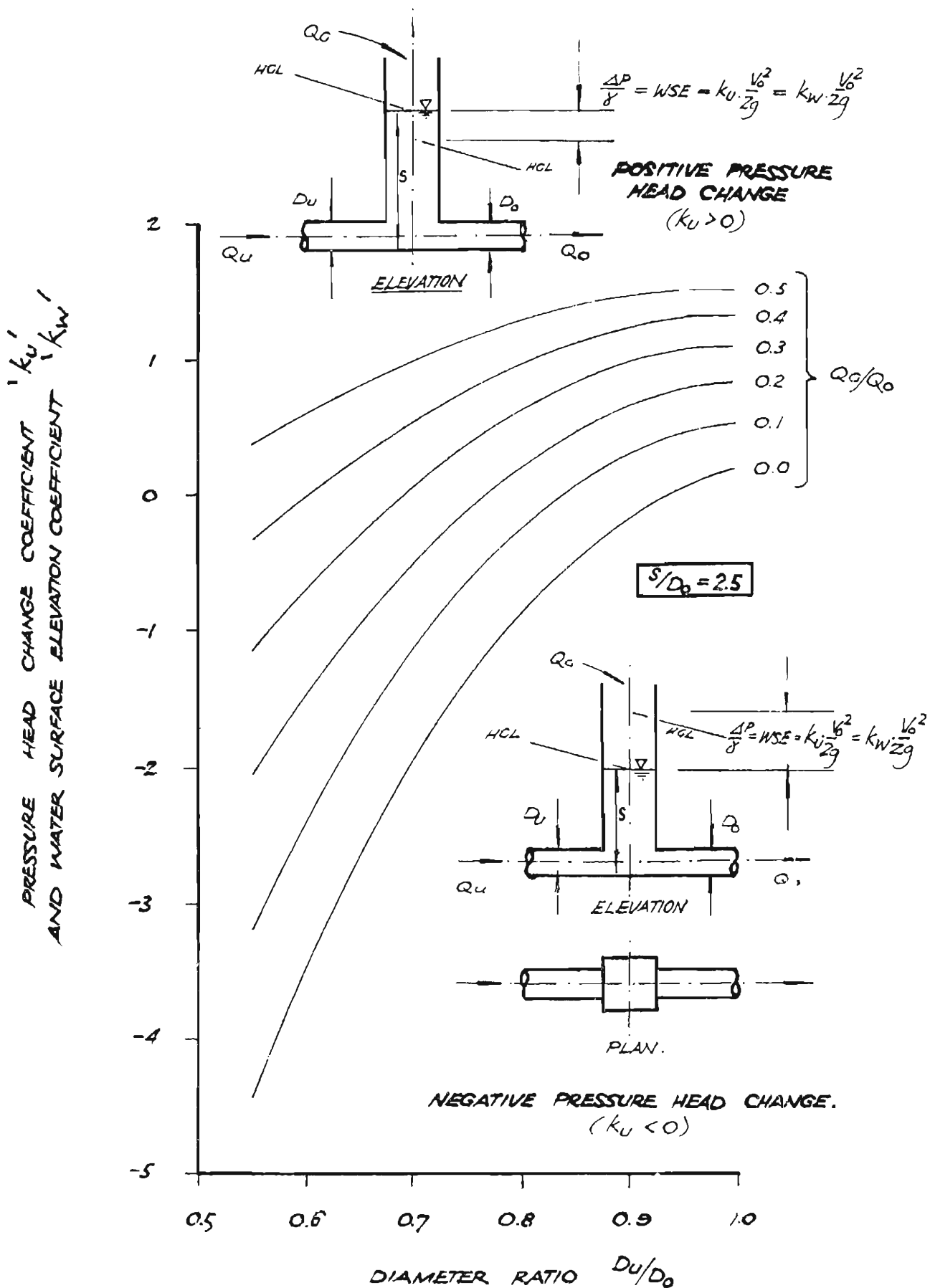
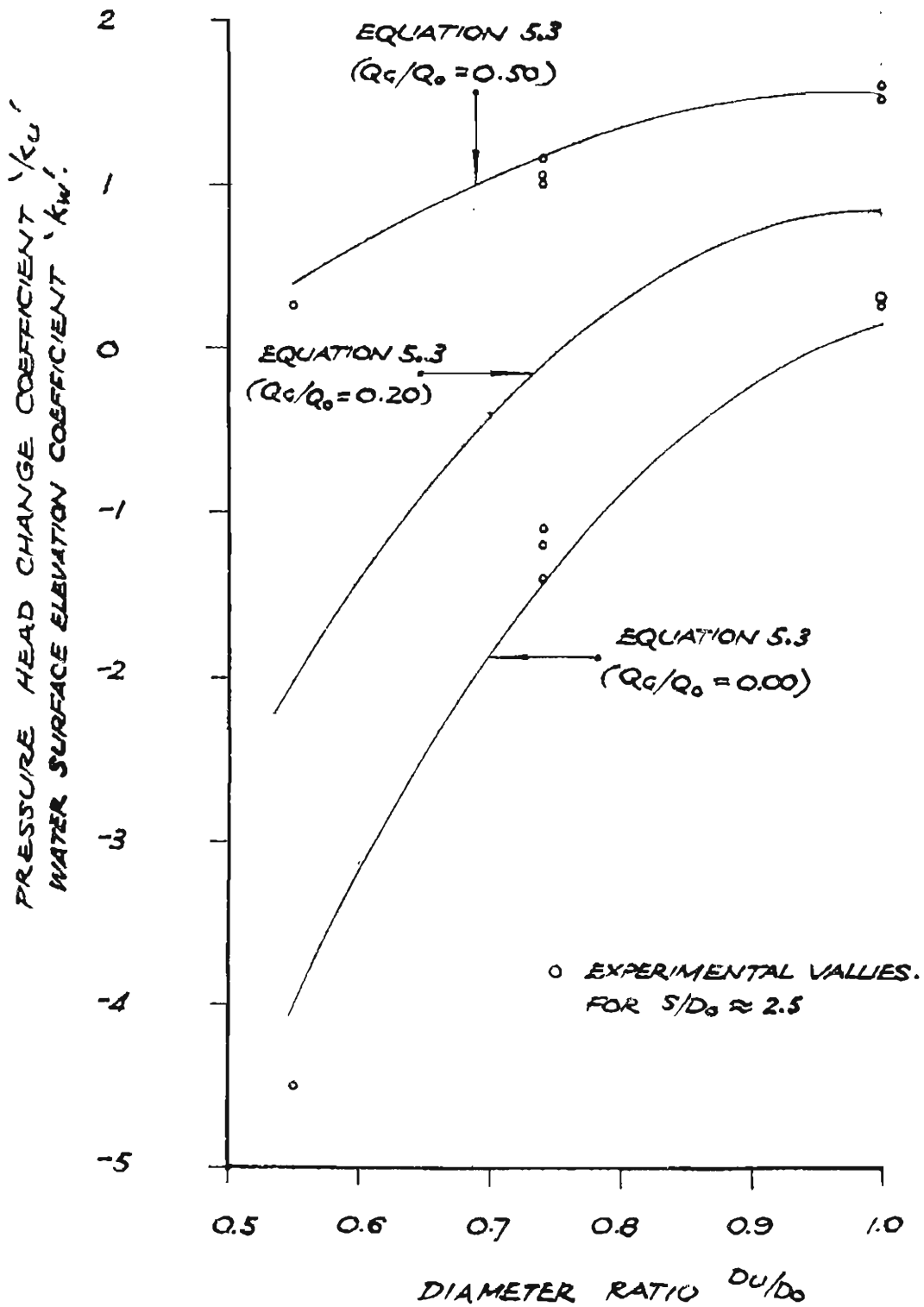
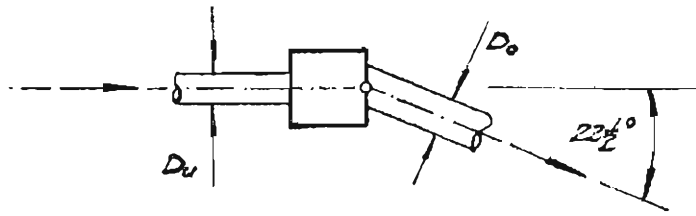
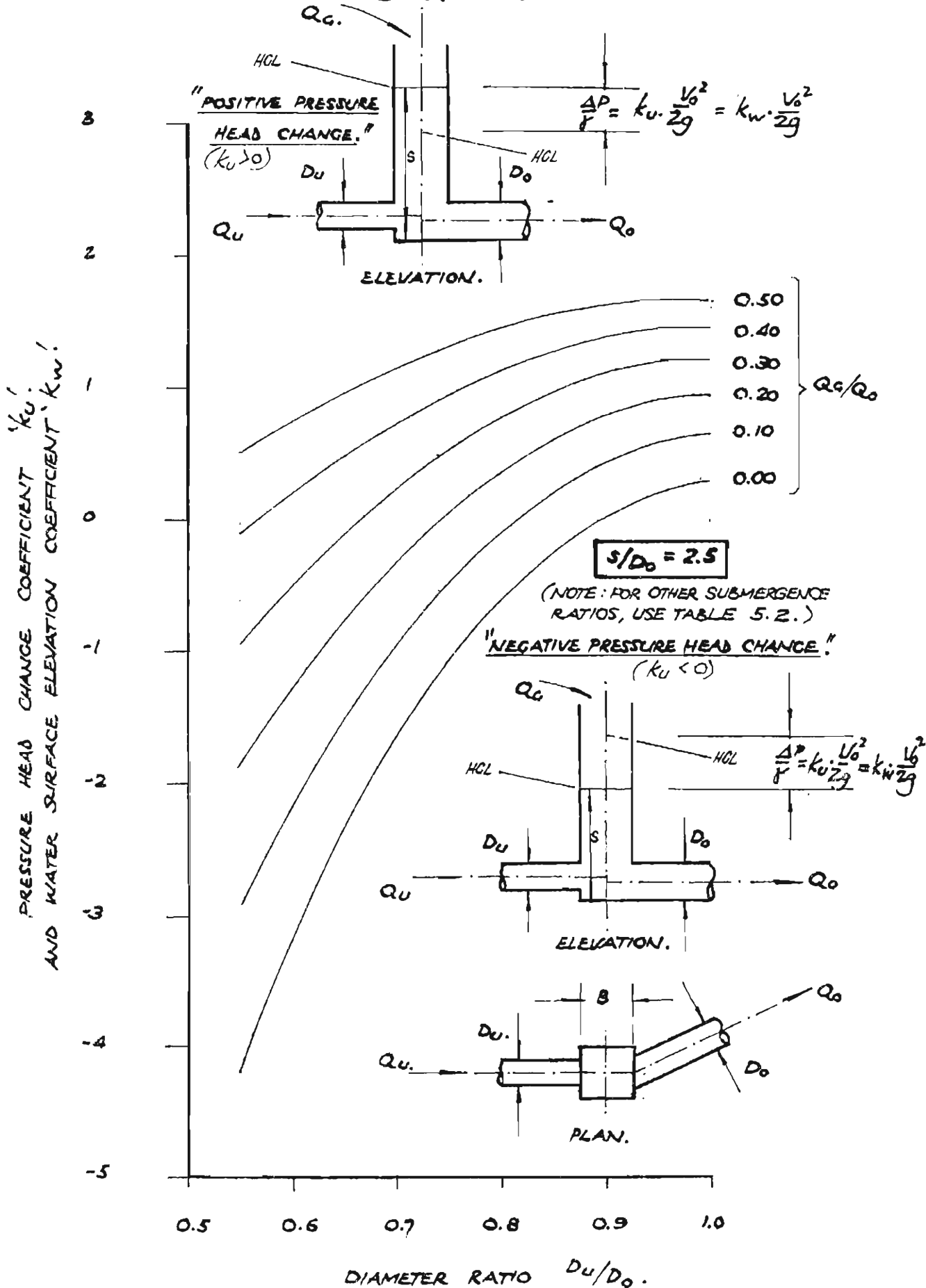


FIGURE 5.3

COMPARISON OF THEORETICAL ANALYSIS WITH EXPERIMENTAL

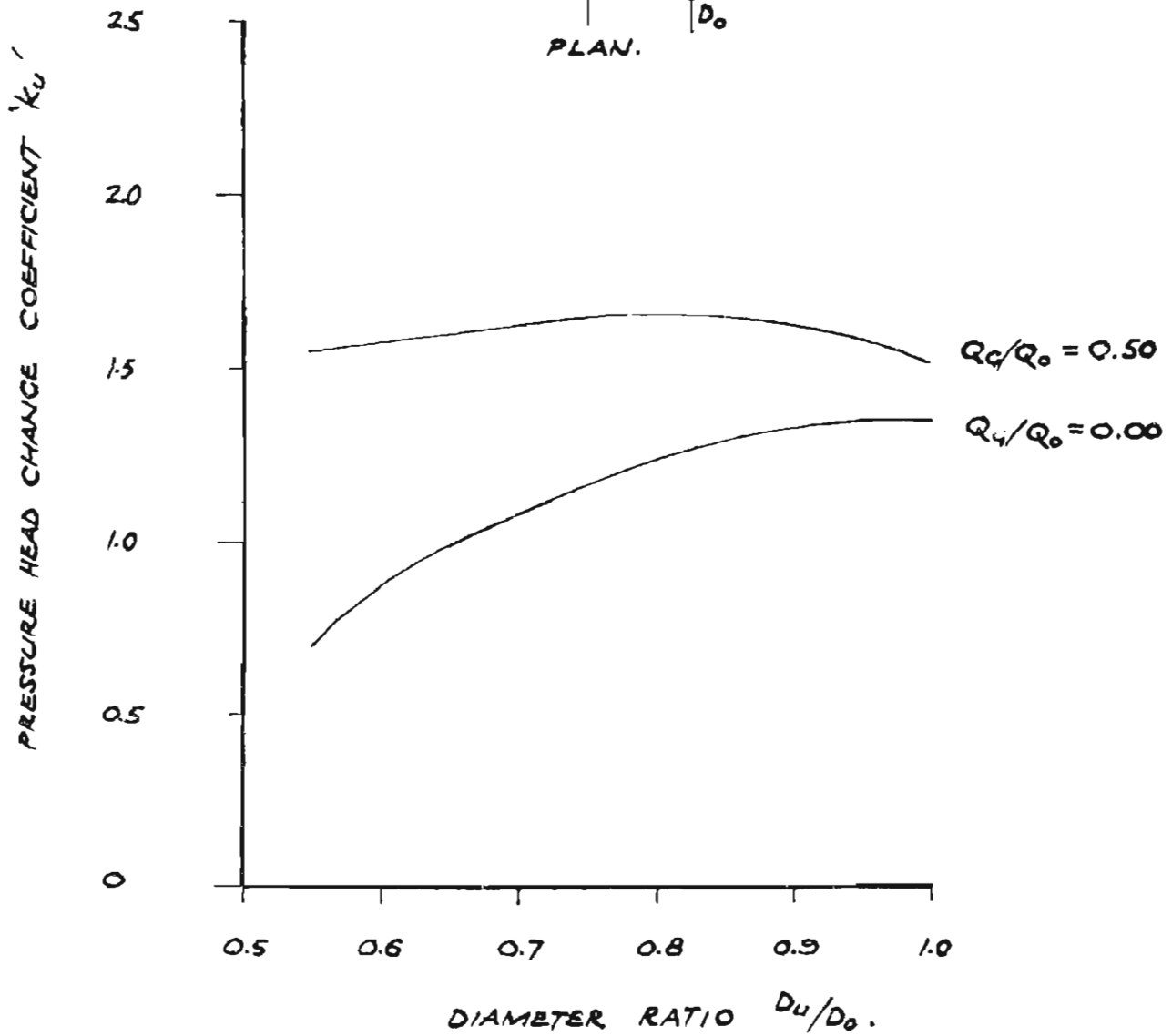
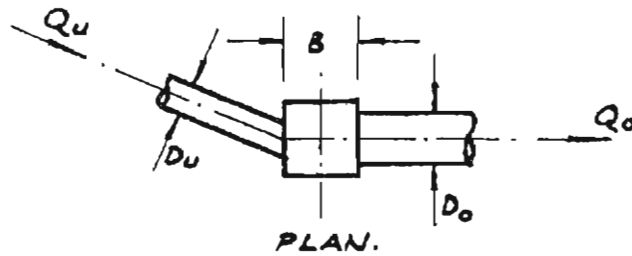
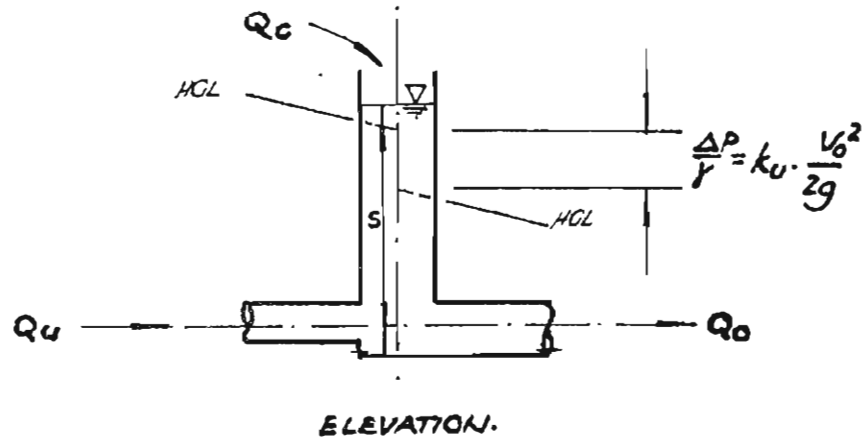
RESULTS FOR  $\theta = 22\frac{1}{2}^\circ$ .

**FIGURE 5.4: PRESSURE HEAD CHANGE AND WATER SURFACE ELEVATION COEFFICIENTS FOR  $22\frac{1}{2}^\circ$  BENDS AT PIT JUNCTIONS—BRANCH POINT ON DOWNSTREAM FACE OF PIT—FOR SUBMERGENCE RATIO OF 2.5.**

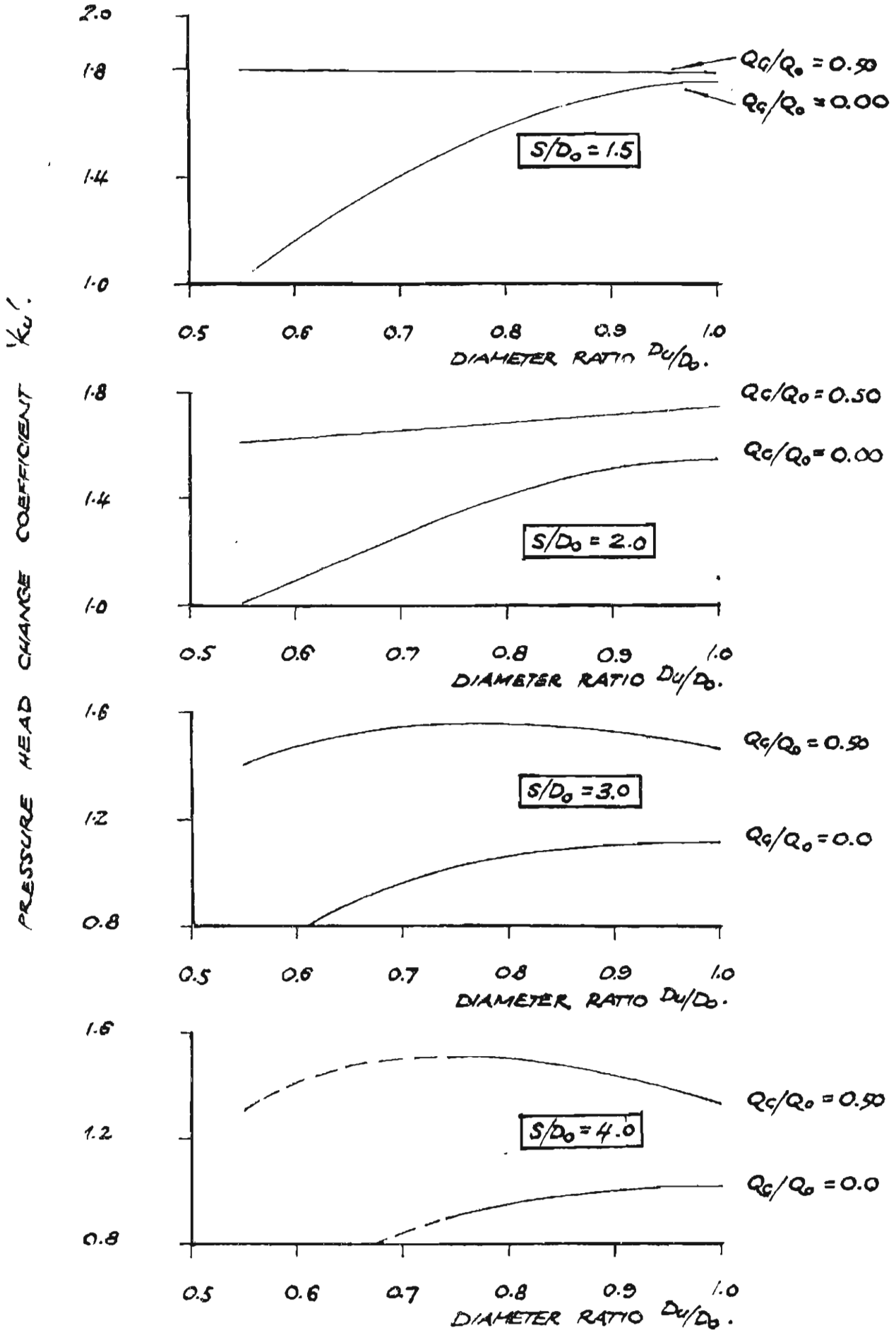




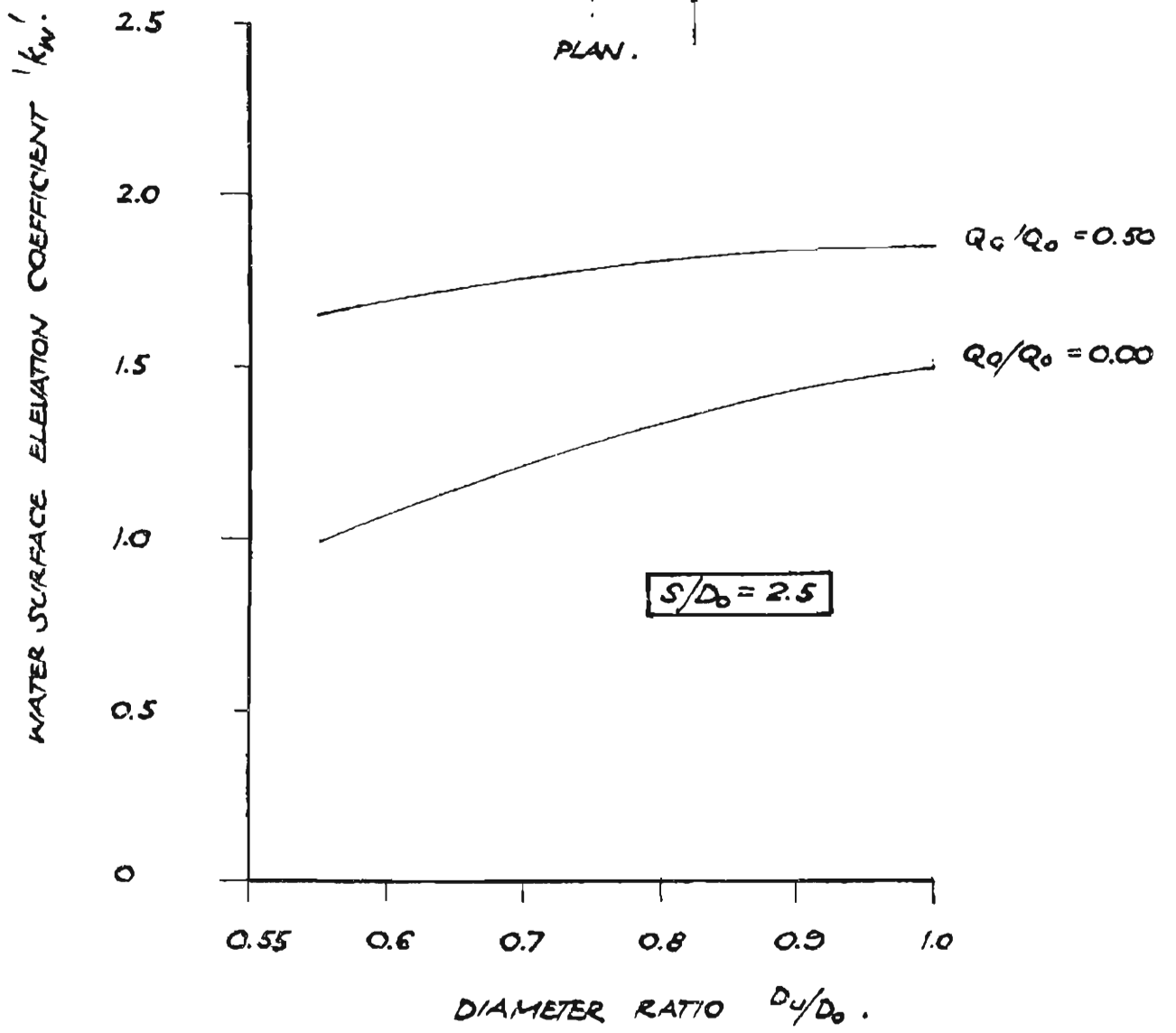
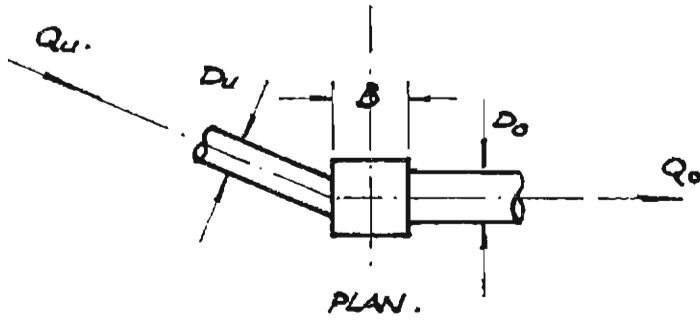
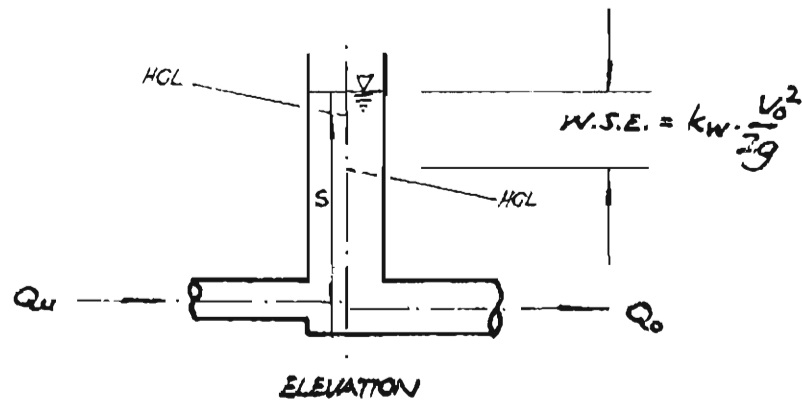
**FIGURE 5.5: PRESSURE HEAD CHANGE COEFFICIENTS ( $k_u$ ) FOR  $22\frac{1}{2}^\circ$  BENDS AT PIT JUNCTIONS — BRANCH POINT LOCATED ON UPSTREAM FACE OF PIT. — FOR SUBMERGENCE RATIO OF 2.5.**



**FIGURE 5.6 : PRESSURE HEAD CHANGE COEFFICIENTS ( $k_u$ ) FOR  $22\frac{1}{2}^\circ$  BENDS AT PIT JUNCTIONS — BRANCH POINT LOCATED ON UPSTREAM FACE OF PIT. — SUBMERGENCE RATIOS OF 1.5, 2.0, 3.0 AND 4.0**

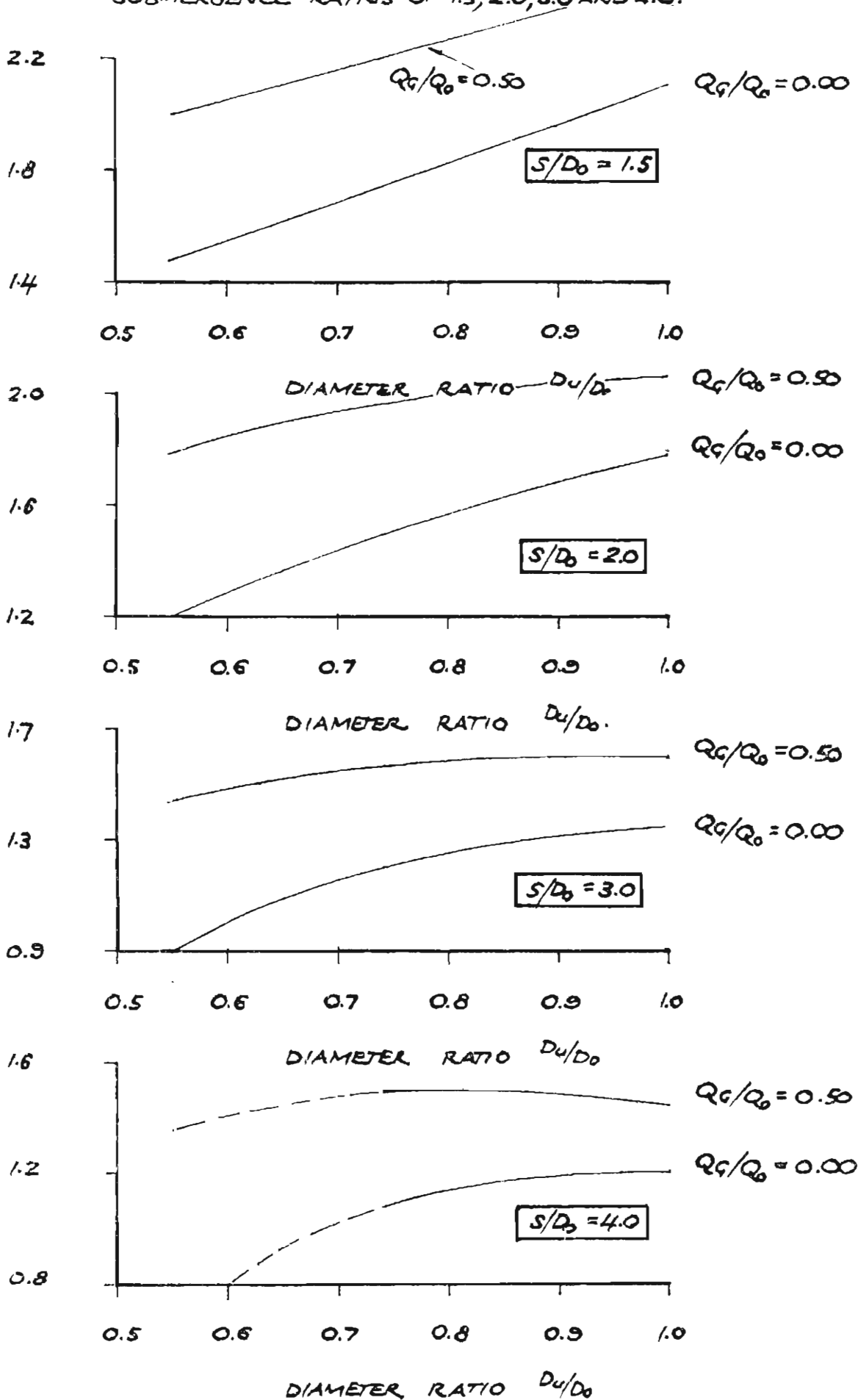


**FIGURE 5.7: WATER SURFACE ELEVATION COEFFICIENTS ( $k_w$ ) FOR  $22\frac{1}{2}^\circ$  BENDS AT PIT JUNCTIONS — BRANCH POINT LOCATED ON UPSTREAM FACE OF PIT — FOR SUBMERGENCE RATIO OF 2.5.**

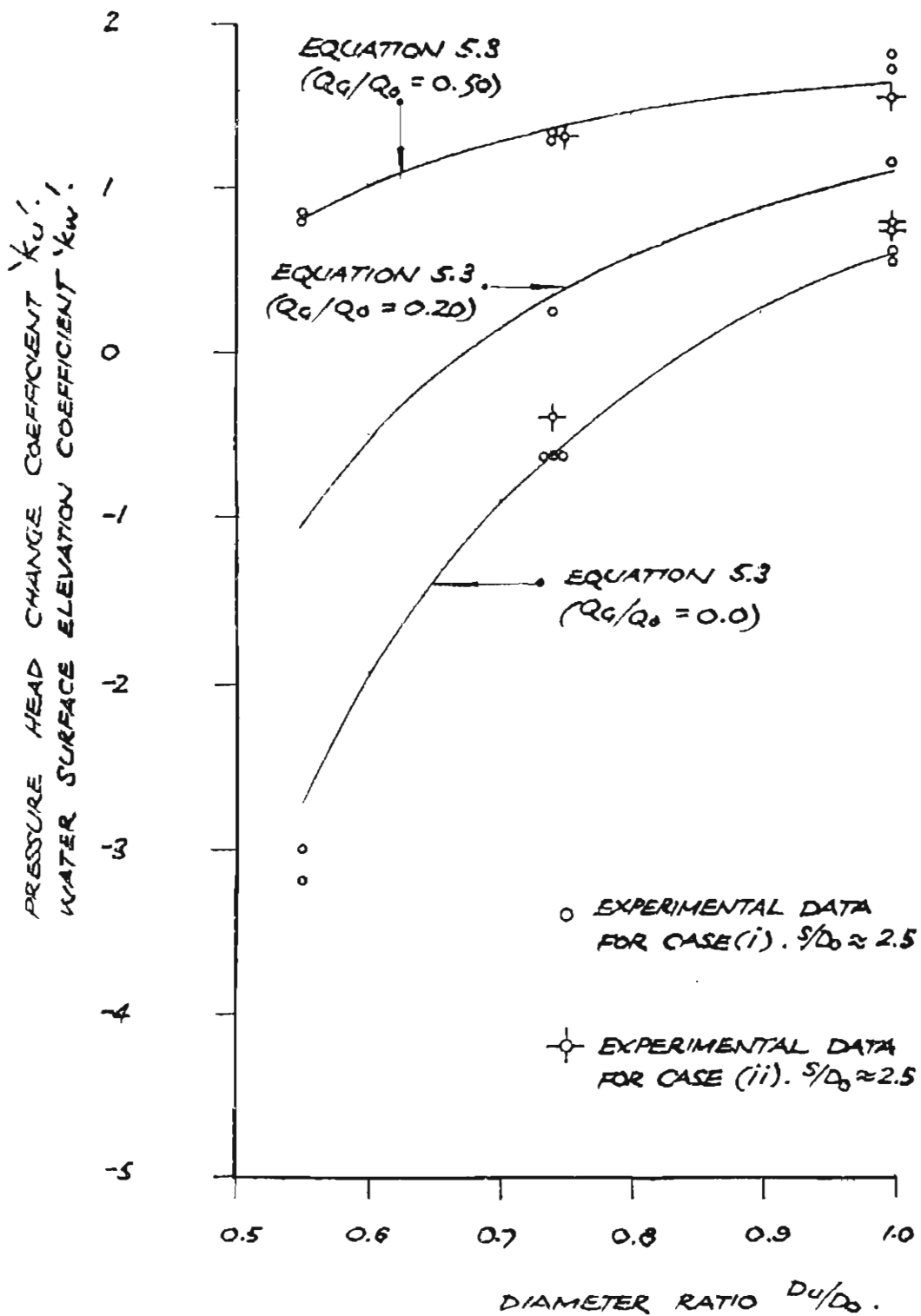
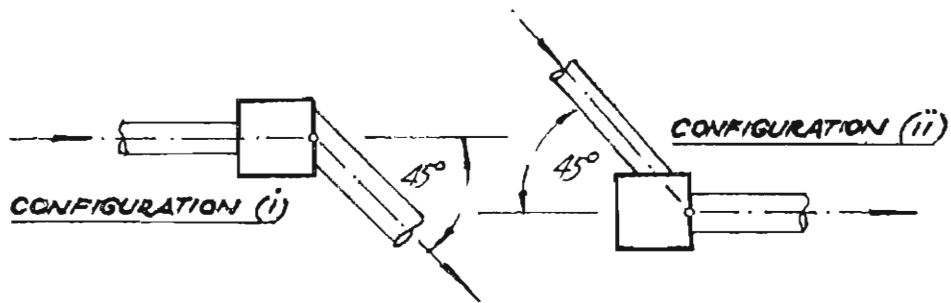


**FIGURE 5.8 : WATER SURFACE ELEVATION COEFFICIENTS ( $k_w$ ) FOR  $22\frac{1}{2}^\circ$  BENDS AT PIT JUNCTIONS — BRANCH POINT LOCATED ON UPSTREAM FACE OF PIT — FOR SUBMERGENCE RATIOS OF 1.5, 2.0, 3.0 AND 4.0.**

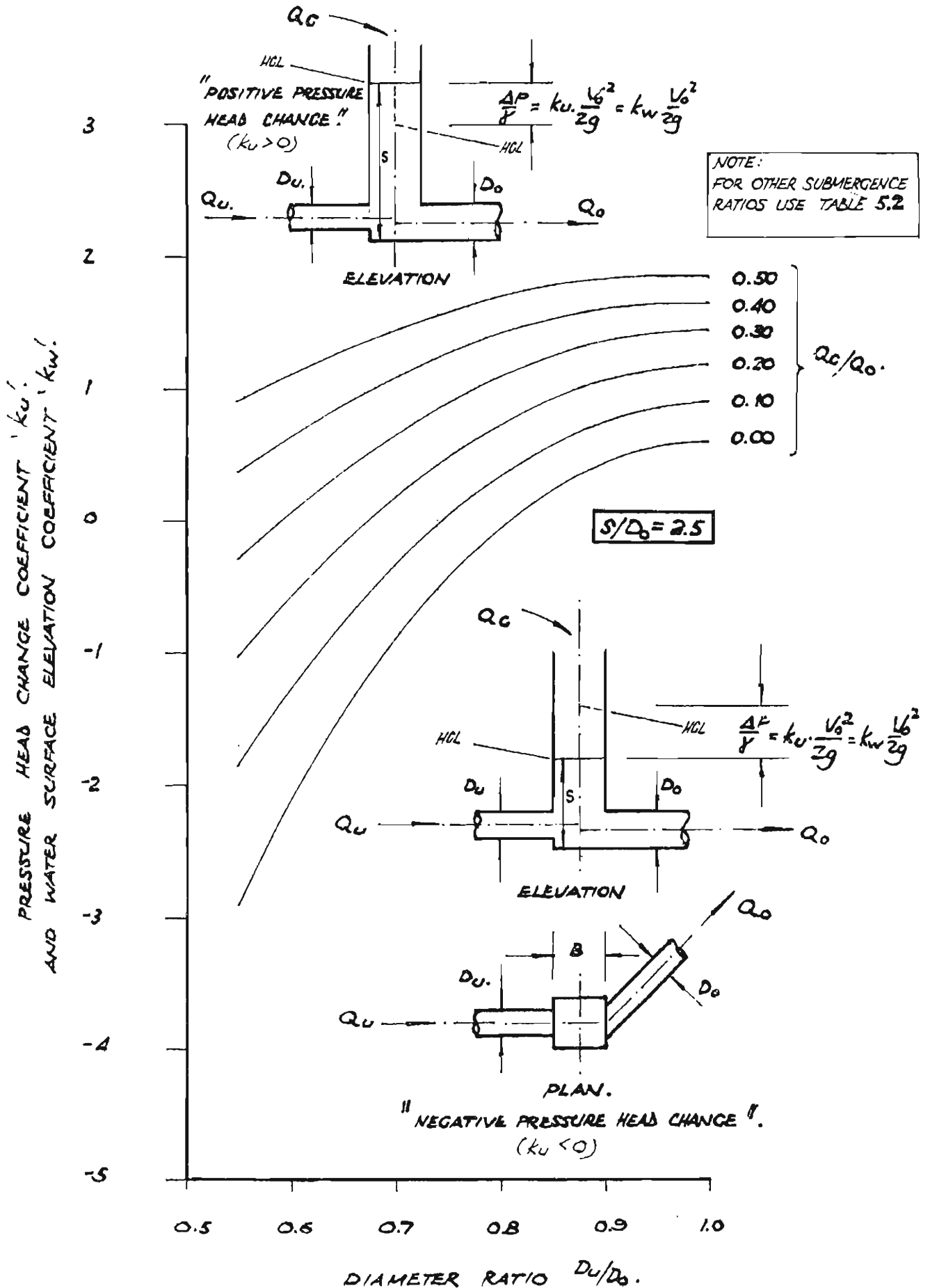
WATER SURFACE ELEVATION COEFFICIENTS ' $k_w$ '.



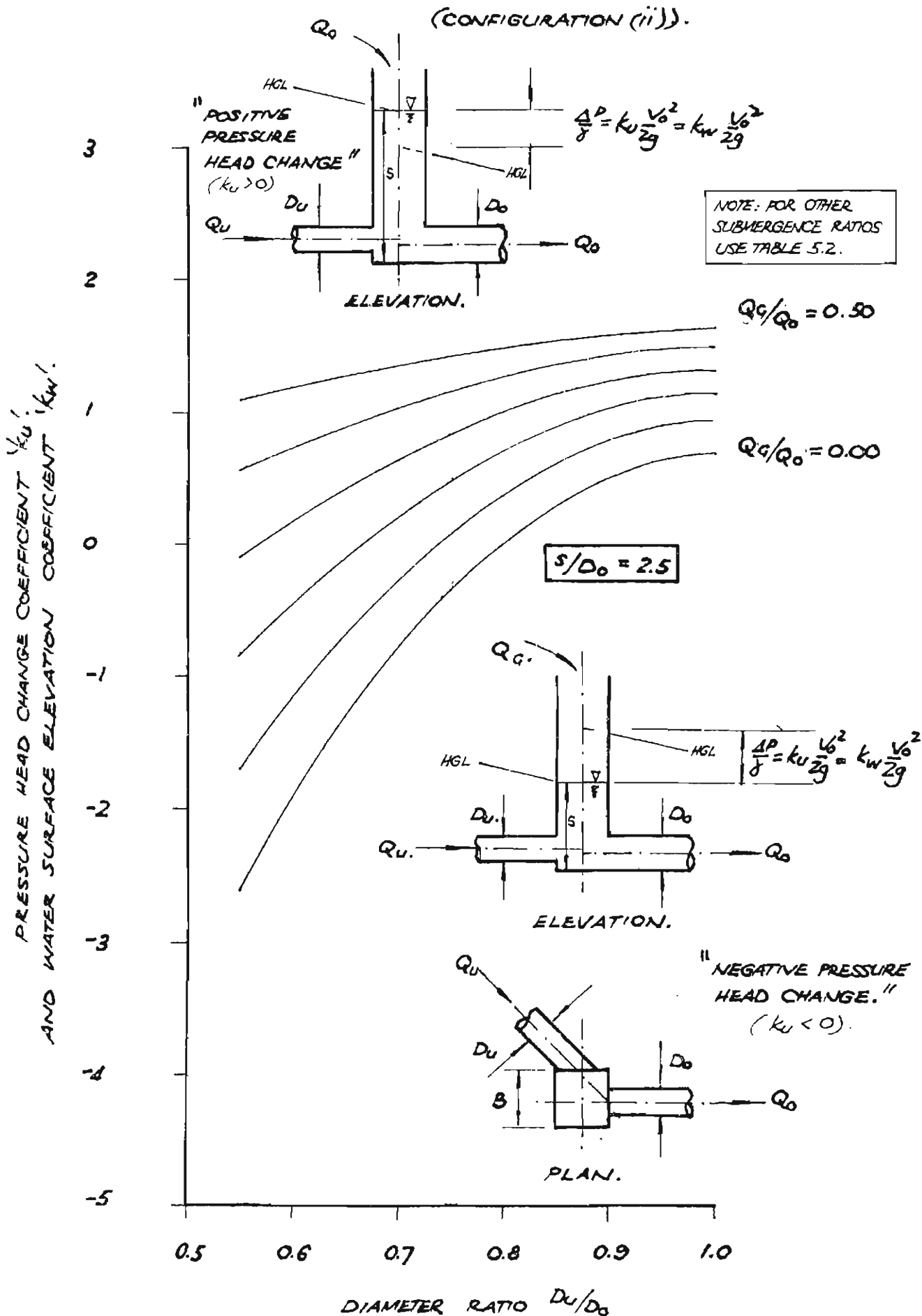
**FIGURE 5.9 : COMPARISON OF THEORETICAL ANALYSIS WITH EXPERIMENTAL RESULTS FOR  $\theta = 45^\circ$**



**FIGURE 5.10: PRESSURE HEAD CHANGE AND WATER SURFACE ELEVATION COEFFICIENTS FOR 45° BENDS AT FIT JUNCTIONS — BRANCH POINT LOCATED ON DOWNSTREAM FACE OF FIT — FOR SUBMERGENCE RATIO OF 2.5. (CONFIGURATION (1)).**



**FIGURE 5.11 : PRESSURE HEAD CHANGE AND WATER SURFACE ELEVATION COEFFICIENTS FOR 45° BEND AT PIT JUNCTIONS — BRANCH POINT LOCATED ON DOWNSTREAM FACE OF PIT FOR SUBMERGENCE RATIO OF 2.5.**



**FIGURE 5.12 : PRESSURE HEAD CHANGE COEFFICIENTS ( $k_u$ ) FOR 45° BENDS AT PIT JUNCTIONS ——— BRANCH POINT LOCATED ON UPSTREAM FACE OF PIT . ——— FOR SUBMERGENCE RATIO OF 2.5.  
(CONFIGURATION (iii))**

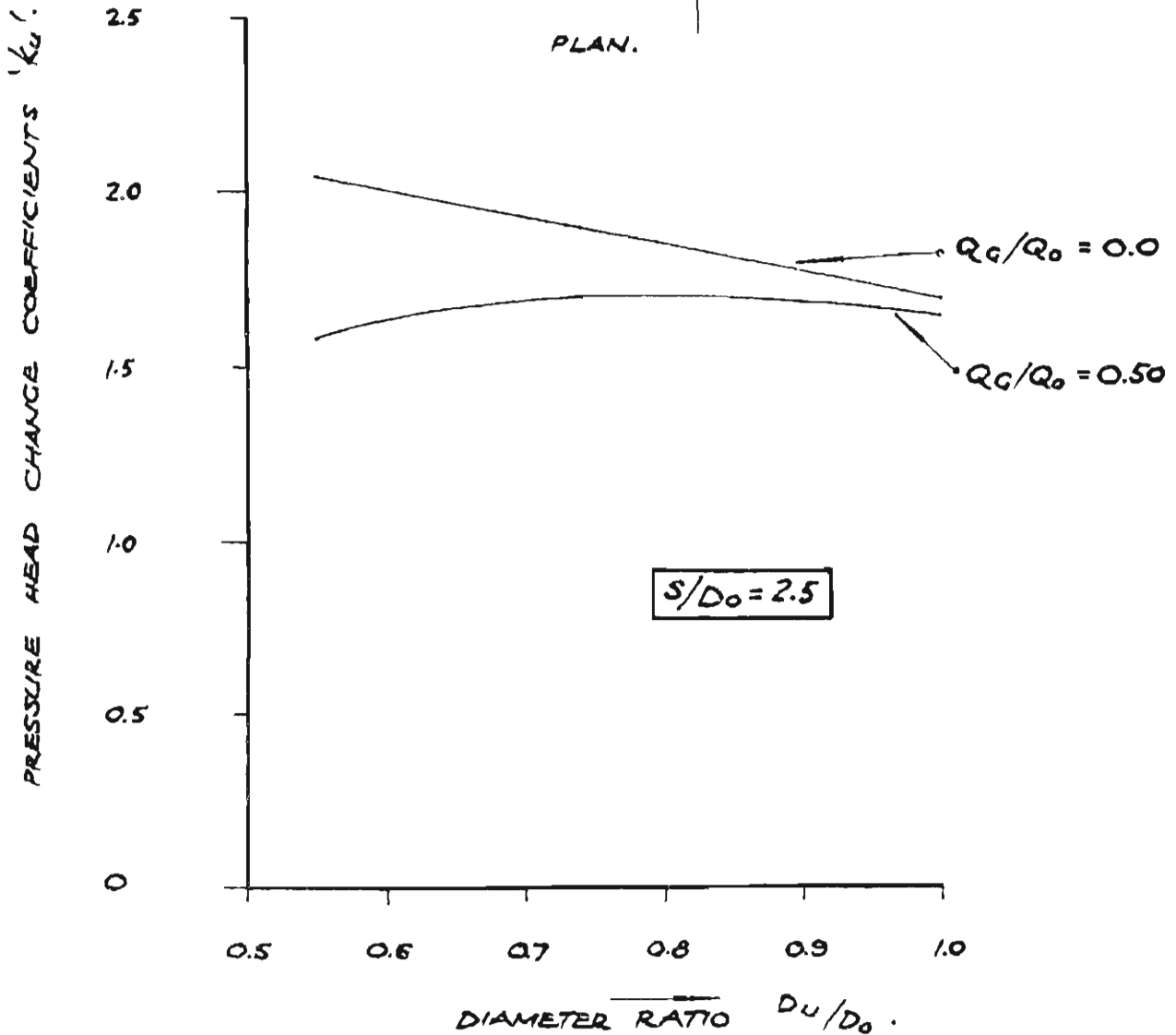
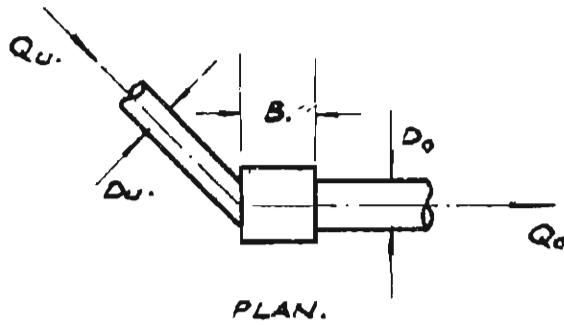
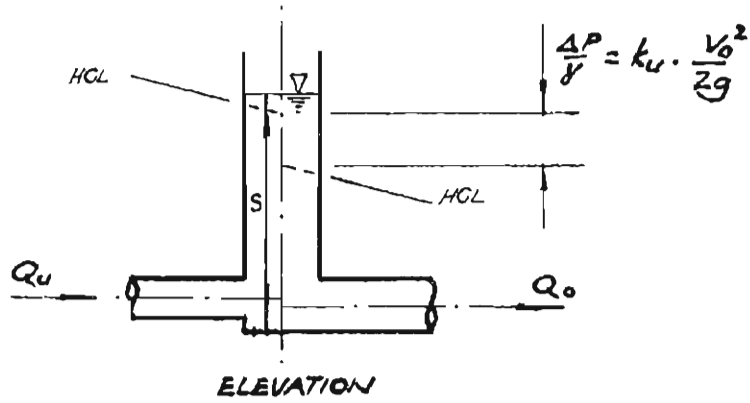
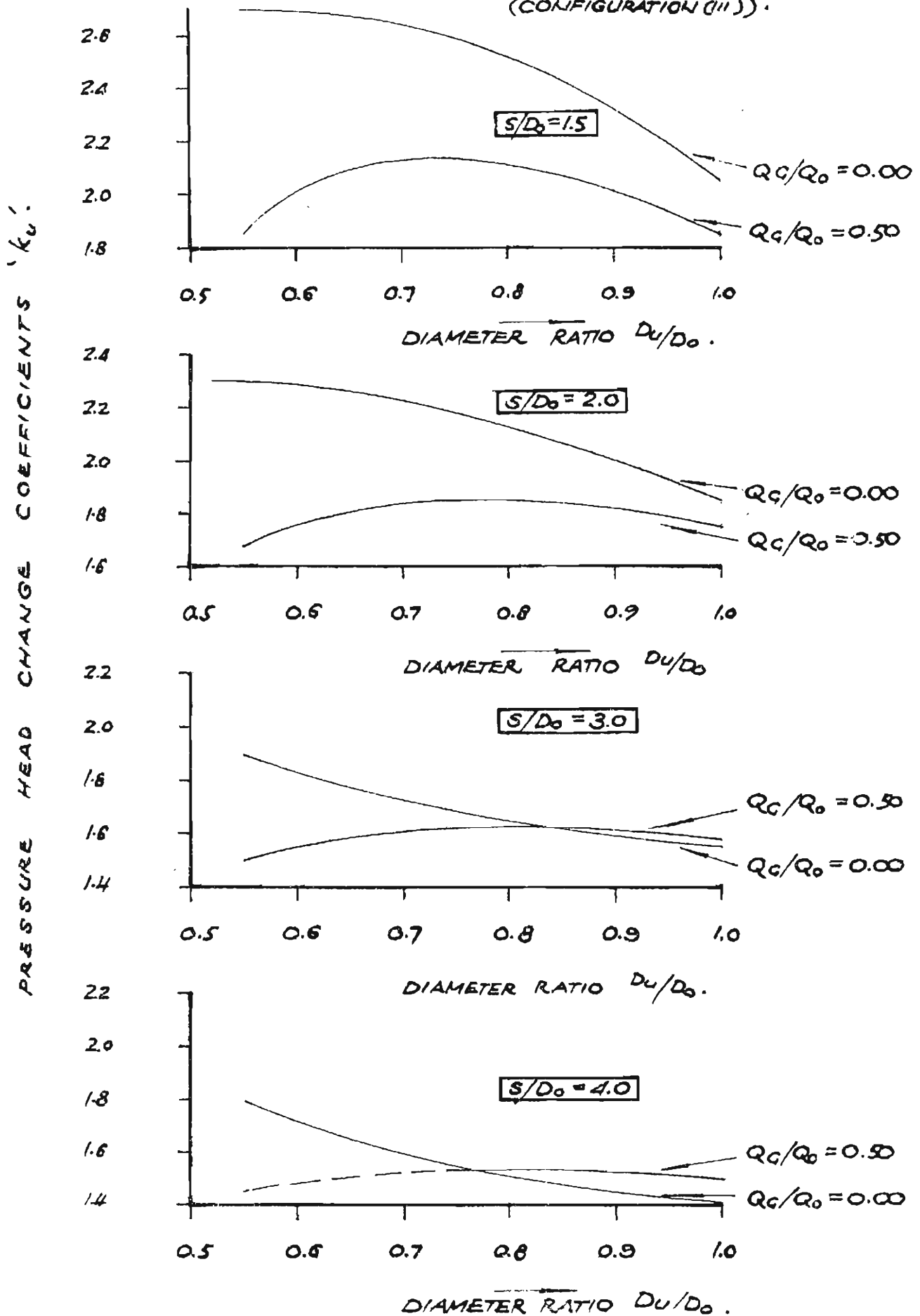


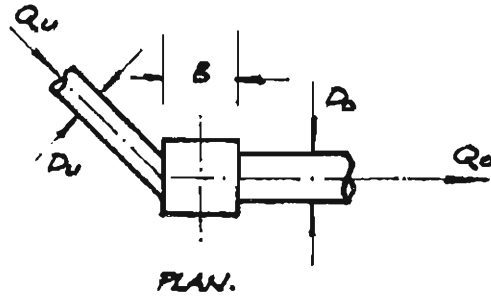
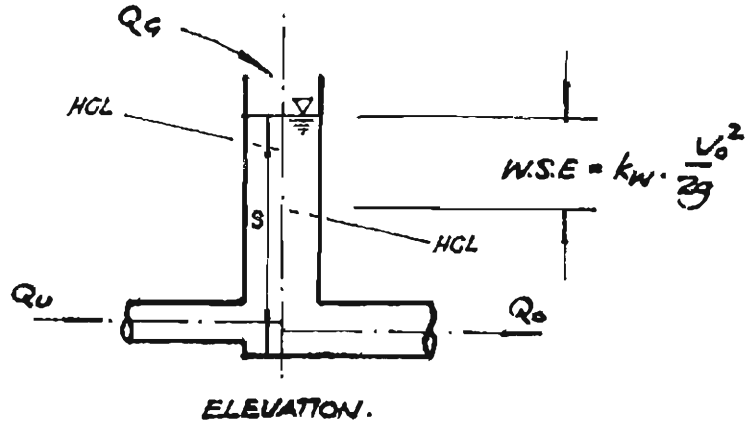


FIGURE 5.13 : PRESSURE HEAD CHANGE COEFFICIENTS ( $k_u$ ) FOR 45° BENDS AT PIT JUNCTIONS — BRANCH POINT LOCATED ON UPSTREAM FACE OF PIT — FOR SUBMERGENCE RATIOS OF 1.5, 2.0, 3.0 AND 4.0. (CONFIGURATION (ii)).

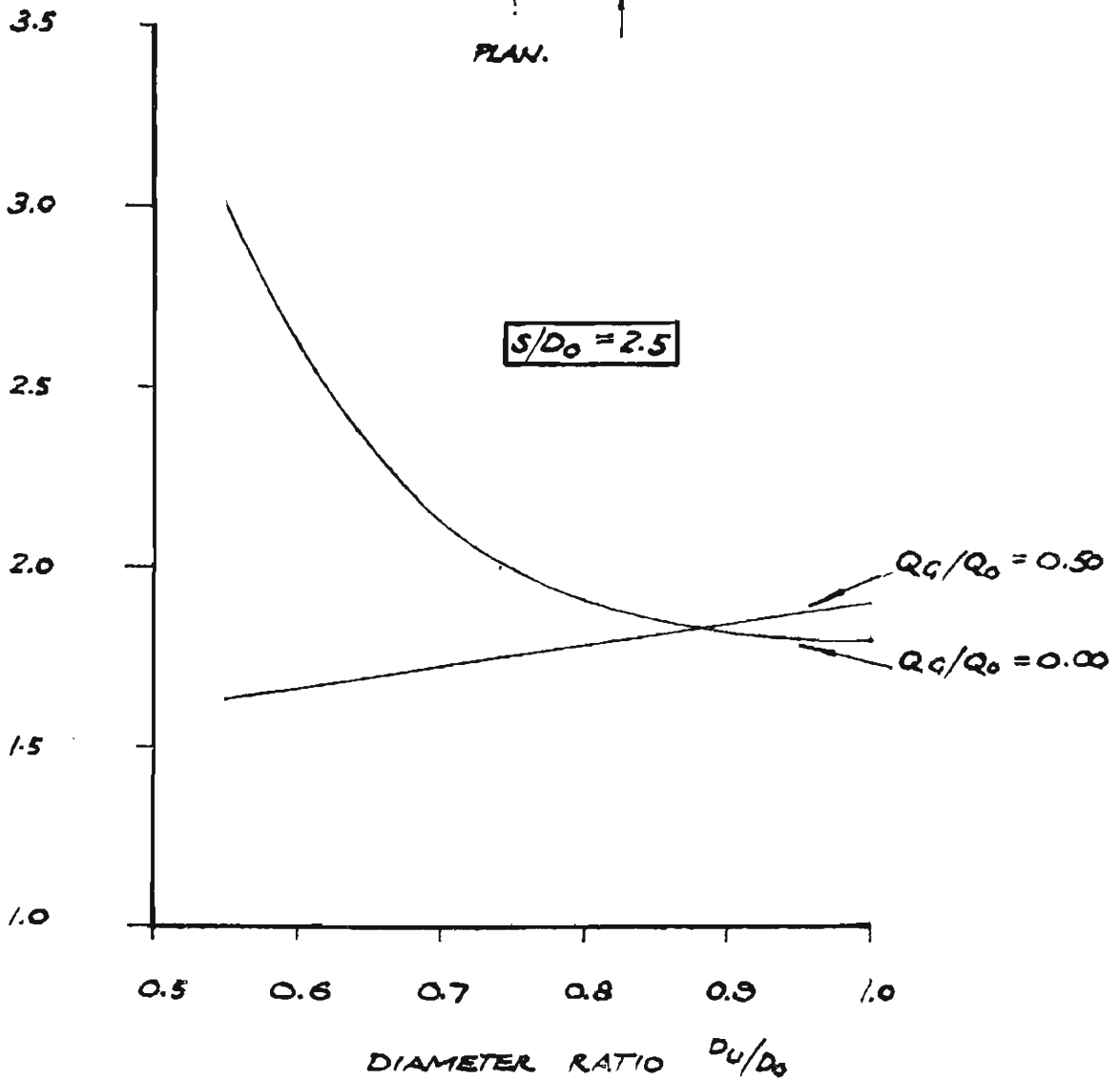


**FIGURE 5.16 : WATER SURFACE ELEVATION COEFFICIENTS ( $k_w$ ) FOR 45° BENDS AT FIT JUNCTIONS — BRANCH POINT LOCATED ON UPSTREAM FACE OF PIT — FOR SUBMERGENCE RATIO OF 2.5**

(CONFIGURATION (iii))

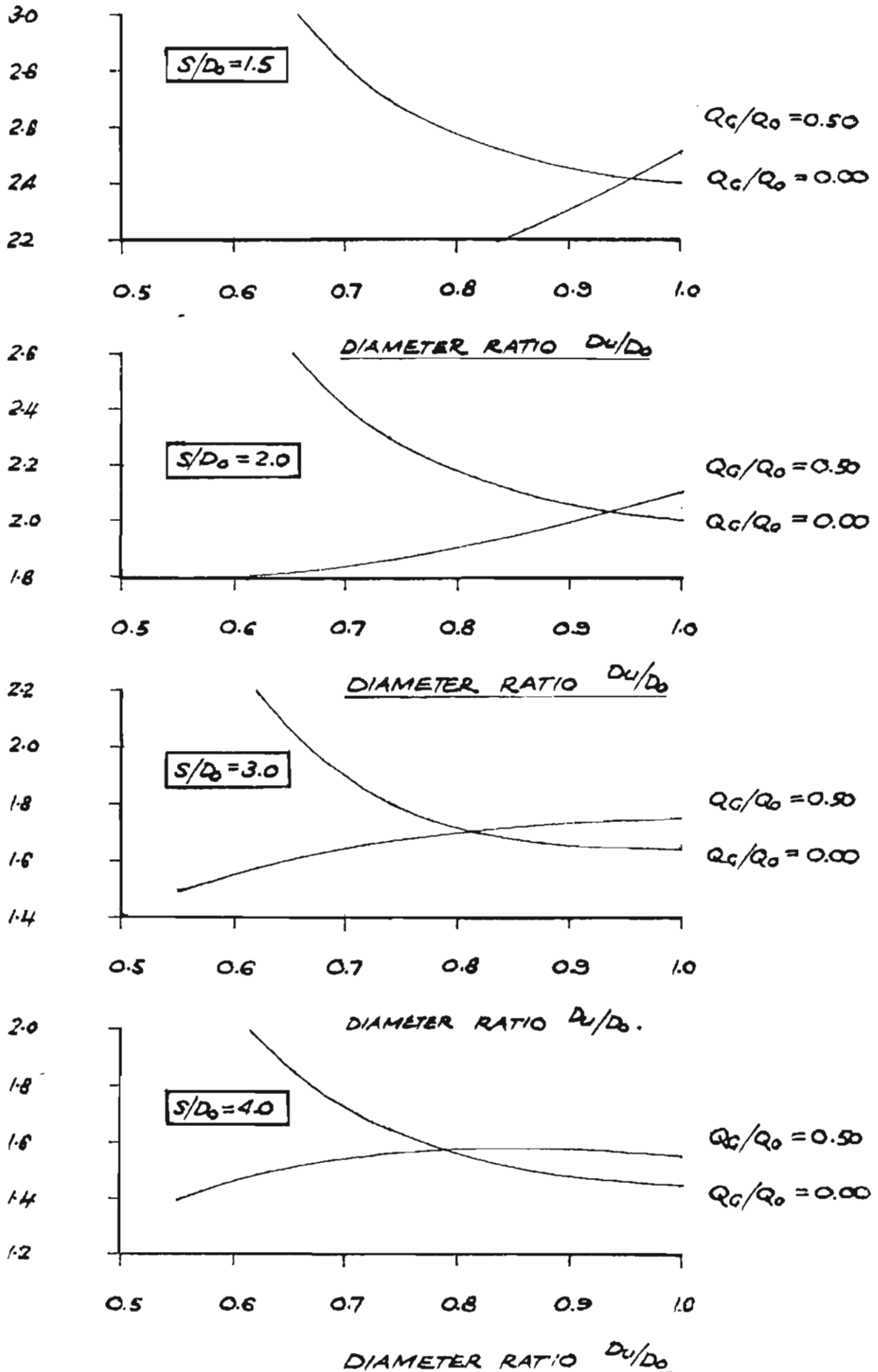


WATER SURFACE ELEVATION COEFFICIENT ' $k_w$ '



**FIGURE 5.15: WATER SURFACE ELEVATION COEFFICIENTS ( $k_w$ ) FOR 45° BENDS AT PIT JUNCTIONS — BRANCH POINT LOCATED ON UPSTREAM FACE OF PIT — FOR SUBMERGENCE RATIOS OF 1.5, 2.0, 3.0 AND 4.0 (CONFIGURATION (ii)).**

WATER SURFACE ELEVATION COEFFICIENTS ' $k_w$ '



**FIGURE 5.16 : PRESSURE HEAD CHANGE COEFFICIENTS ( $k_u$ ) FOR 45° BENDS AT PIT JUNCTIONS — BRANCH POINT LOCATED ON THE UPSTREAM FACE OF THE PIT — FOR SUBMERGENCE RATIO OF 2.5.**

(CONFIGURATION (IV))

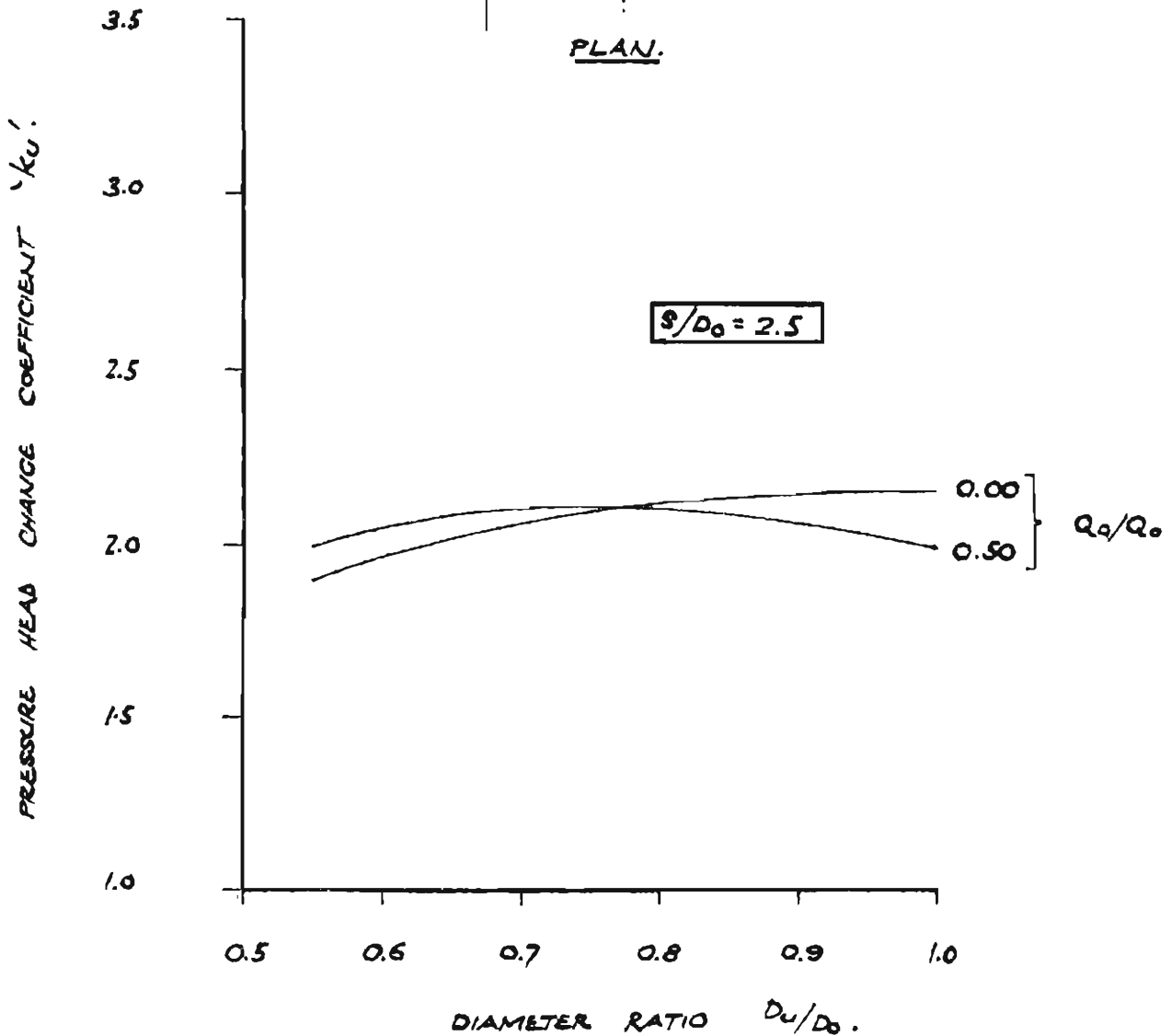
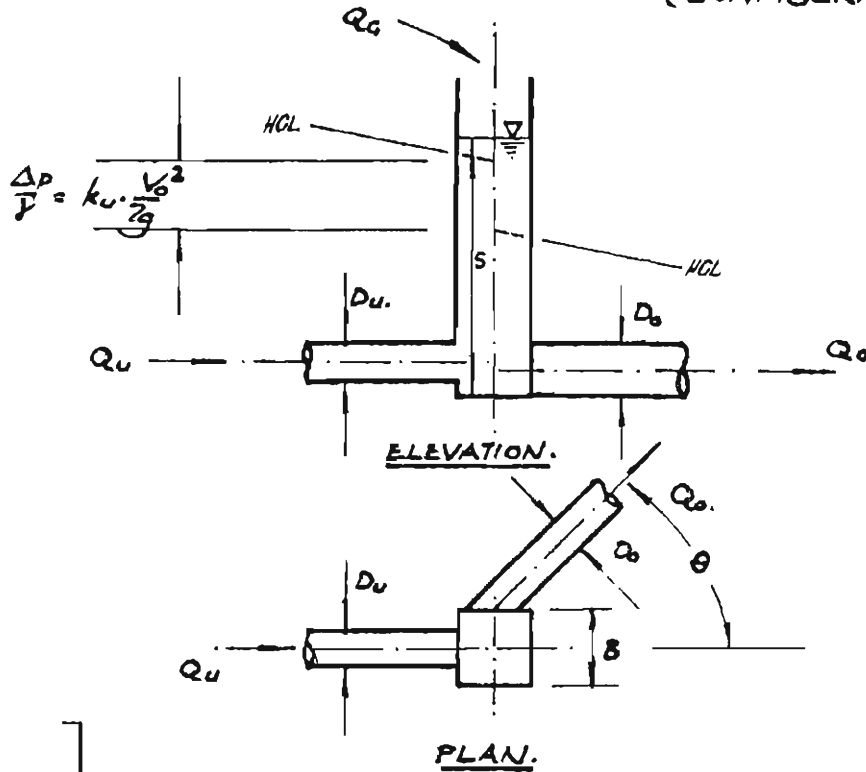
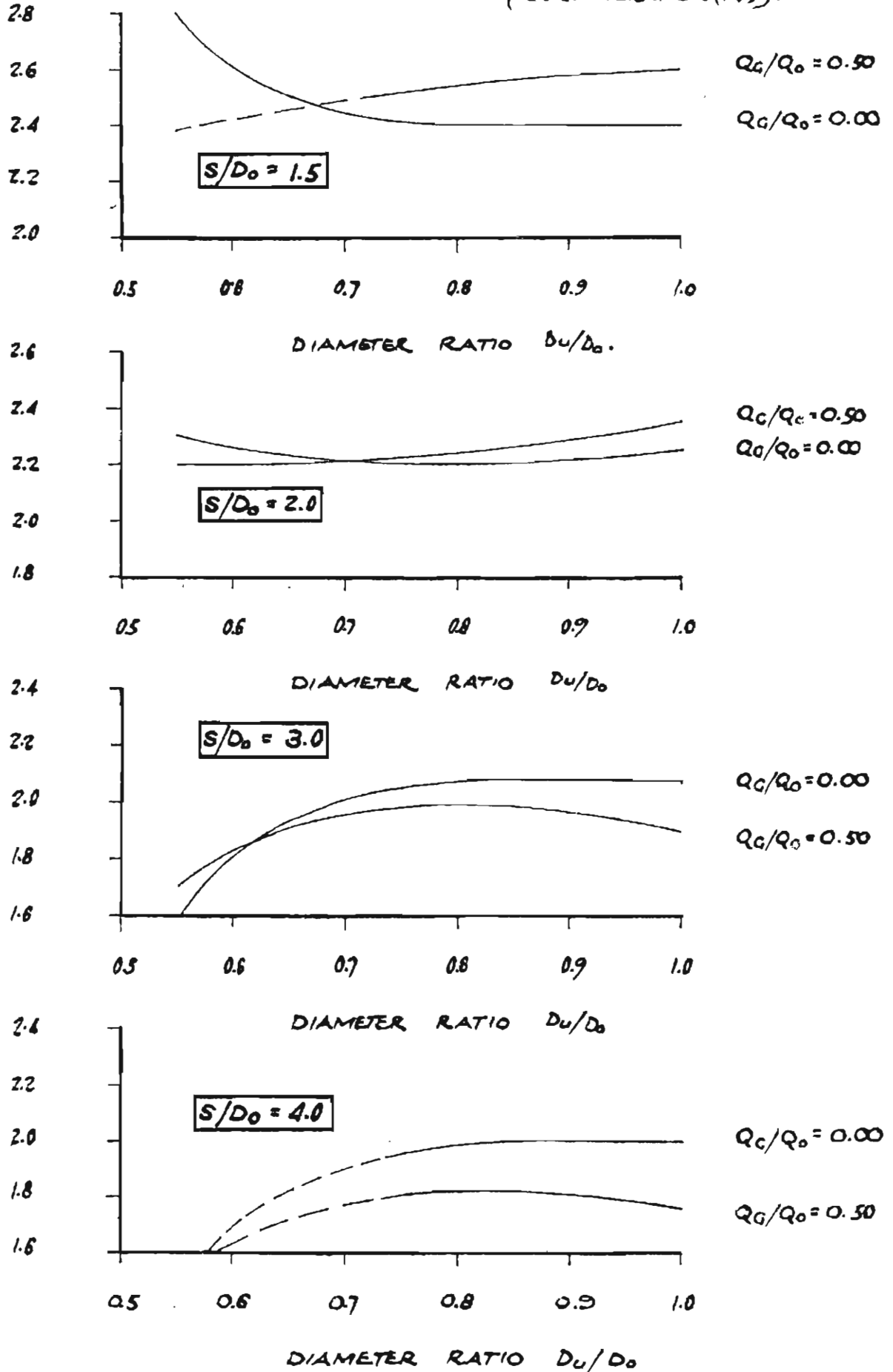


FIGURE 5.17 : PRESSURE HEAD CHANGE COEFFICIENTS ( $k_u$ ) FOR 45° BENDS AT PIT JUNCTIONS. —

BRANCH POINT LOCATED ON UPSTREAM FACE OF PIT —  
 FOR SUBMERGENCE RATIOS OF 1.5, 2.0, 3.0 AND 4.0  
 (CONFIGURATION (iv)).

PRESSURE HEAD CHANGE COEFFICIENTS ( $k_u$ )



**FIGURE 5.18 : WATER SURFACE ELEVATION COEFFICIENTS ( $k_w$ ) FOR 45° BENDS AT PIT JUNCTIONS — BRANCH POINT LOCATED ON UPSTREAM FACE OF THE PIT — FOR SUBMERGENCE RATIO OF 2.5. (CONFIGURATION (iv))**

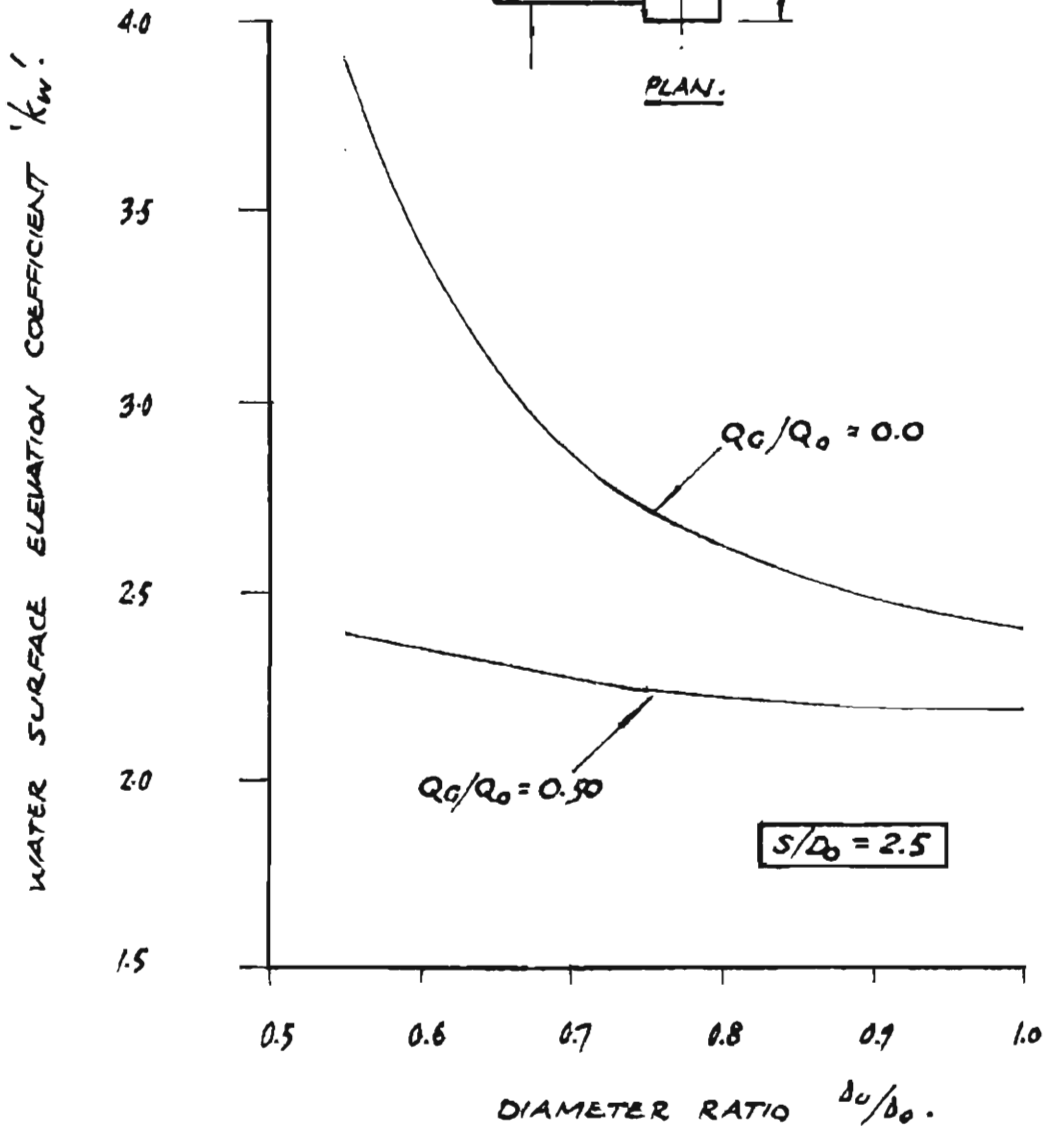
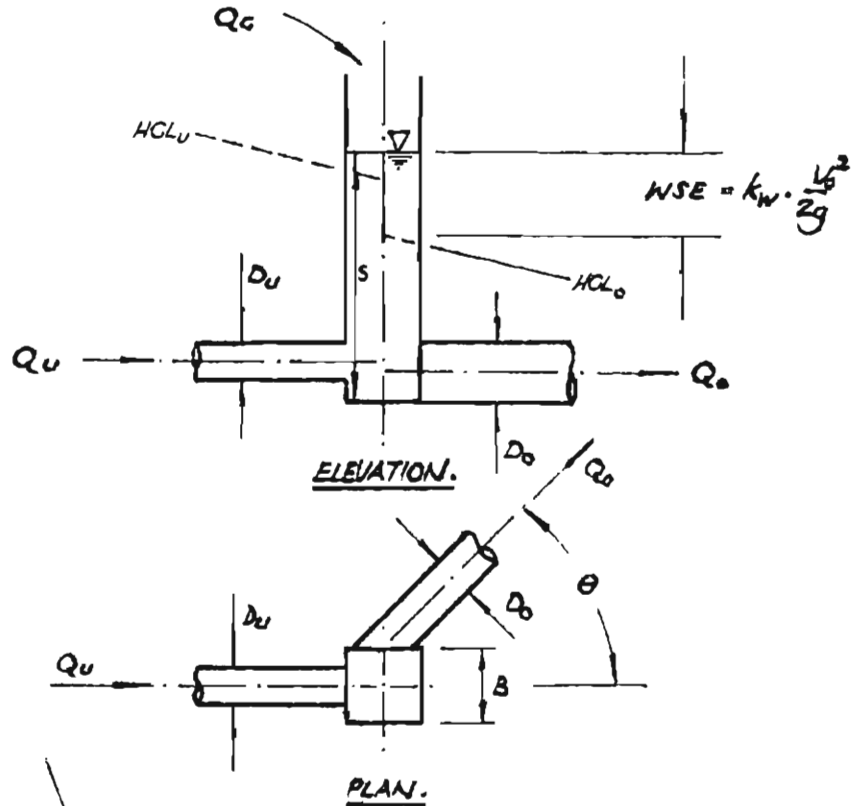
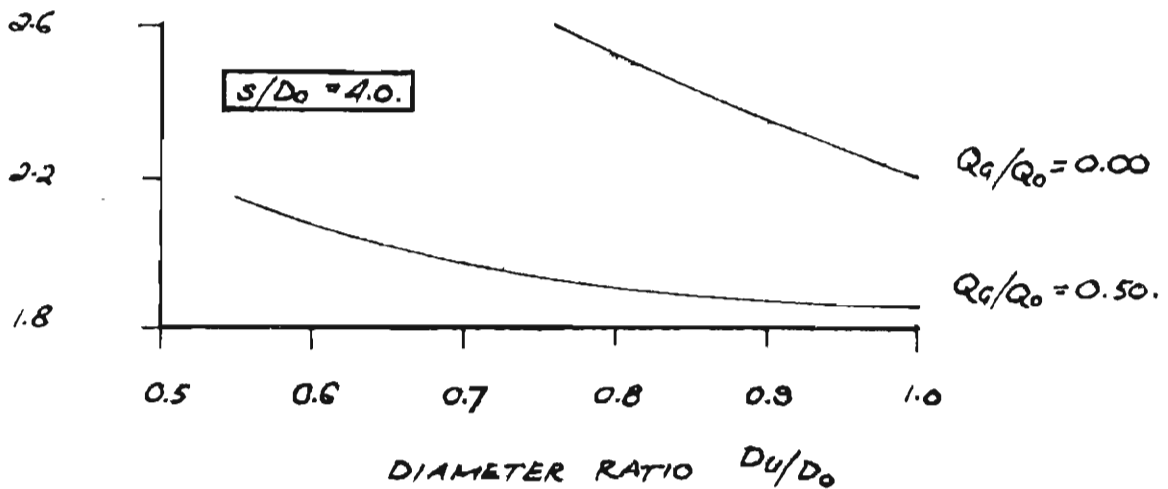
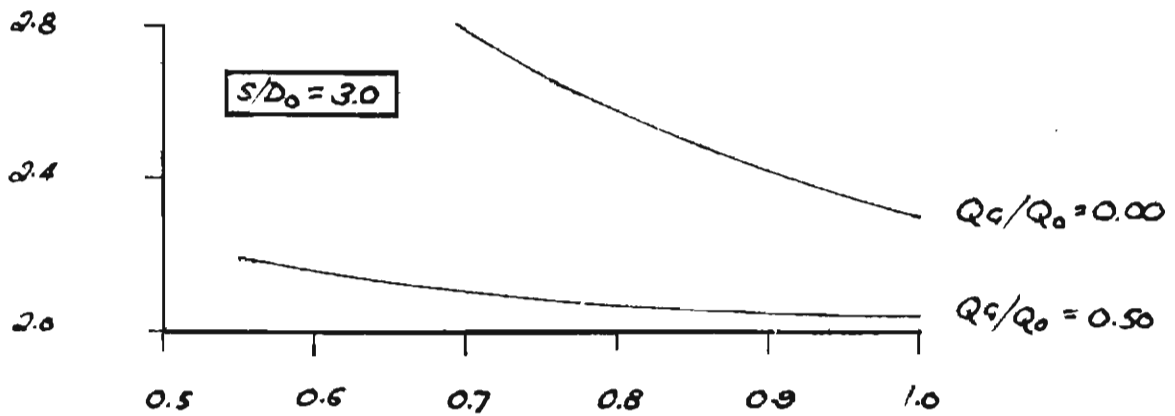
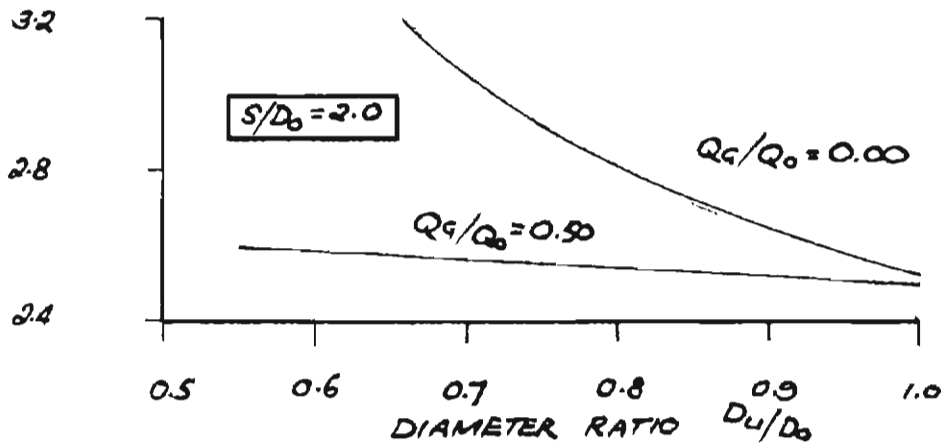
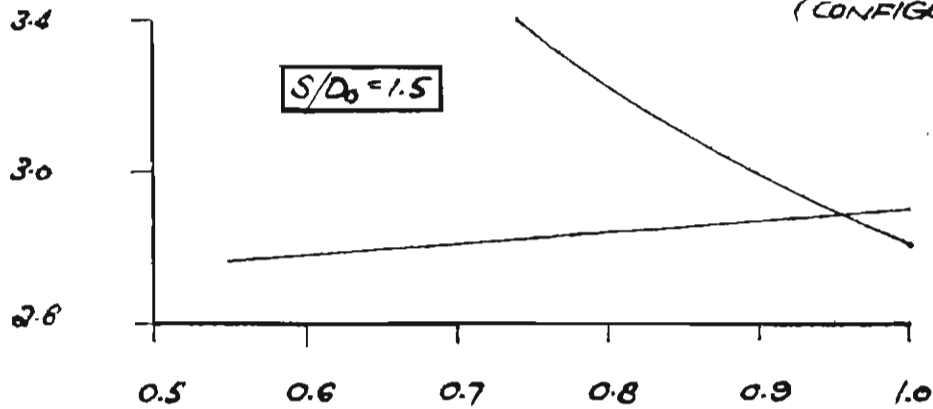


FIGURE 5.19 : WATER SURFACE ELEVATION COEFFICIENTS ( $k_w$ ) FOR 45° BENDS AT PIT JUNCTIONS — BRANCH POINT LOCATED ON UPSTREAM FACE OF PIT. — FOR SUBMERGENCE RATIOS OF 1.5, 2.0, 3.0 AND 4.0

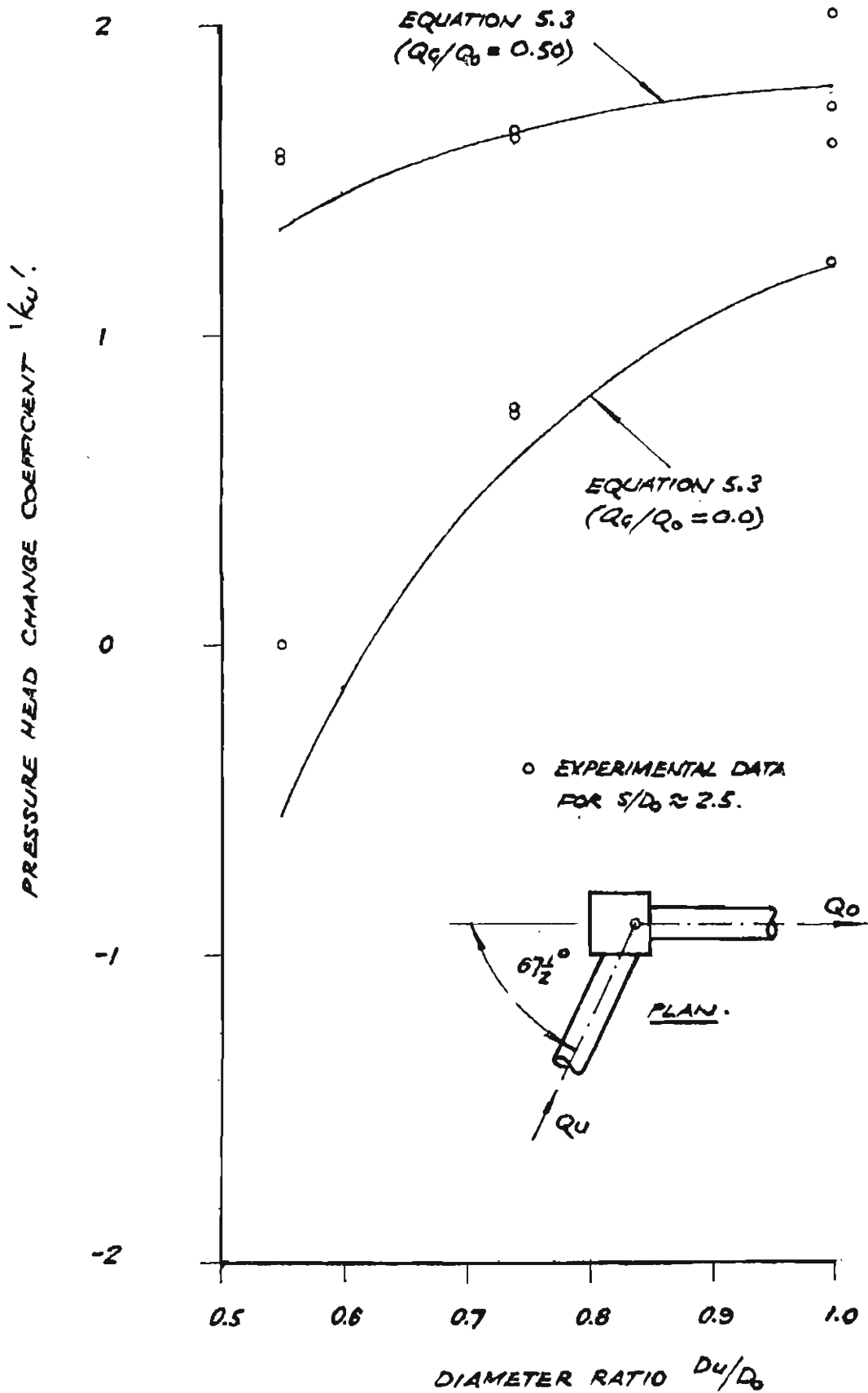
(CONFIGURATION (iv)).

WATER SURFACE ELEVATION COEFFICIENT  $k_w$ .



**FIGURE 5.20 : COMPARISON OF THEORETICAL ANALYSIS WITH EXPERIMENTAL RESULTS FOR**

$$\theta = 67\frac{1}{2}^\circ$$





**FIGURE 5.21 : PRESSURE HEAD CHANGE COEFFICIENTS ( $k_u$ ) FOR  $87\frac{1}{2}^\circ$  BENDS AT PIT JUNCTIONS — BRANCH POINT LOCATED NEAR DOWNSTREAM FACE OF PIT — FOR SUBMERGENCE RATIO OF 2.5.**

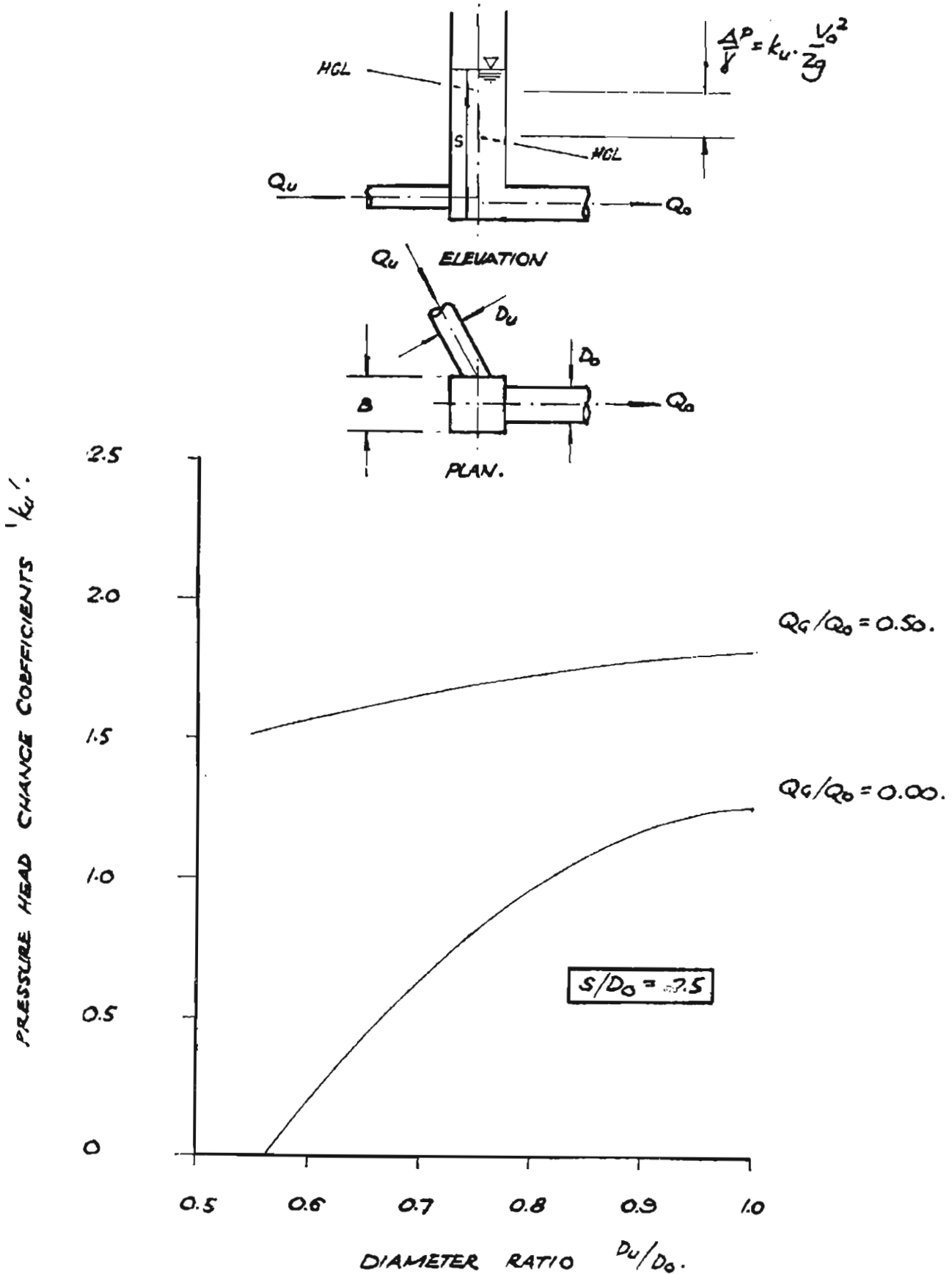
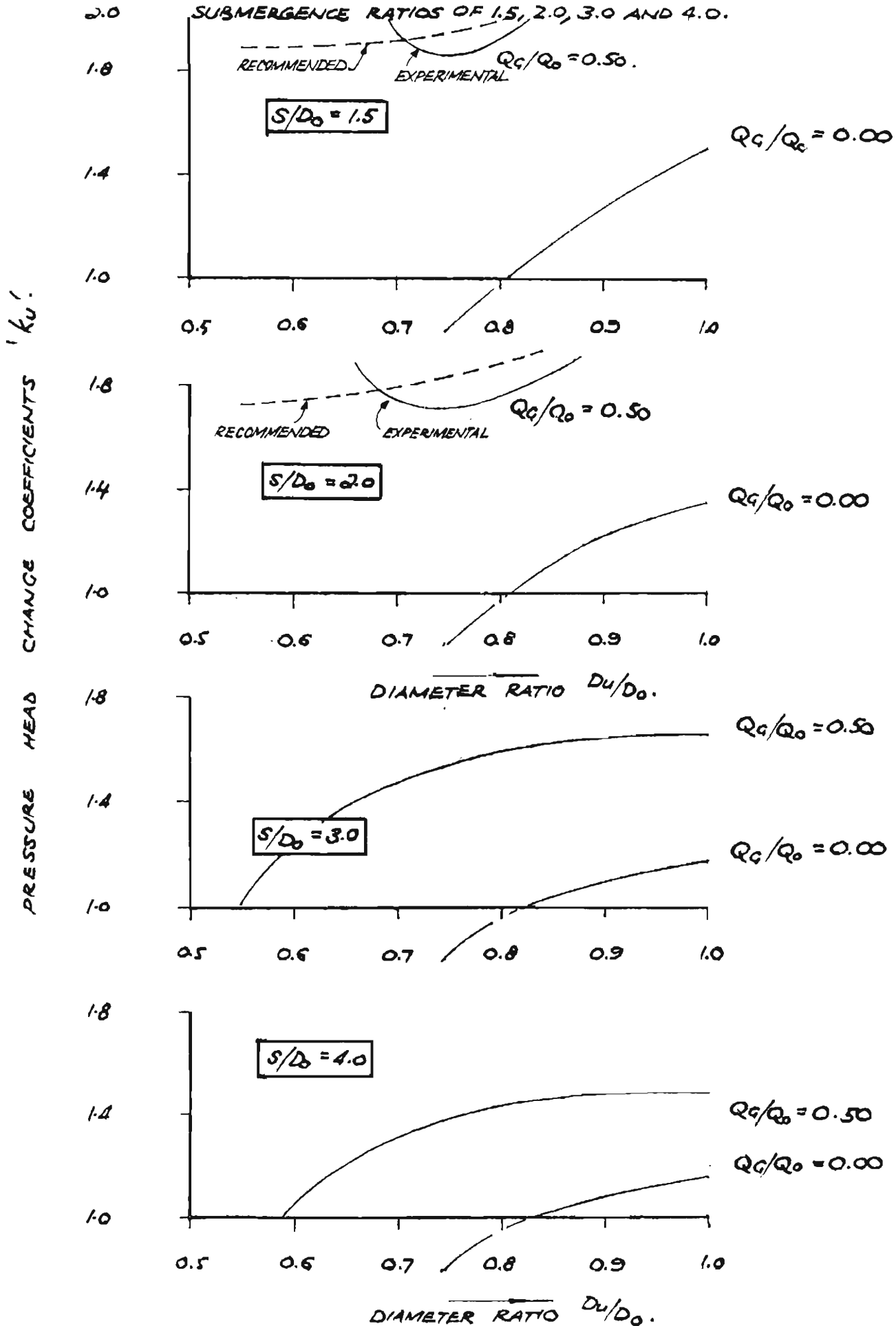


FIGURE 5.22 : PRESSURE HEAD CHANGE COEFFICIENTS ( $K_u$ ) FOR  $67\frac{1}{2}^\circ$  BENDS AT PIT JUNCTIONS BRANCH POINT LOCATED NEAR DOWNSTREAM FACE OF PIT FOR SUBMERGENCE RATIOS OF 1.5, 2.0, 3.0 AND 4.0.



**FIGURE 5.23: WATER SURFACE ELEVATION COEFFICIENTS ( $k_w$ ) FOR  $67\frac{1}{2}^\circ$  BENDS AT PIT JUNCTIONS — BRANCH POINT LOCATED NEAR DOWNSTREAM FACE OF PIT — FOR SUBMERGENCE RATIO OF 2.5.**

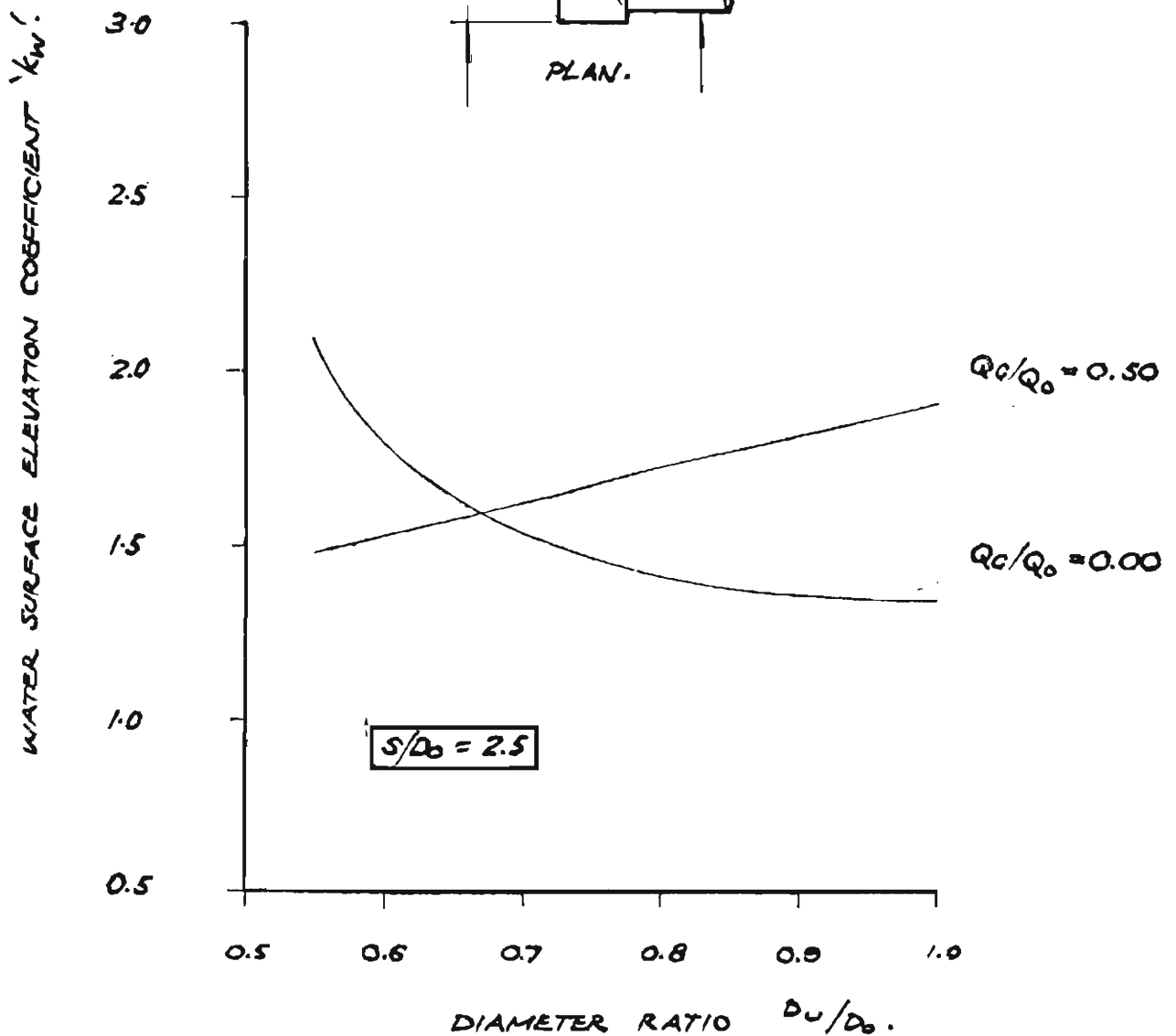
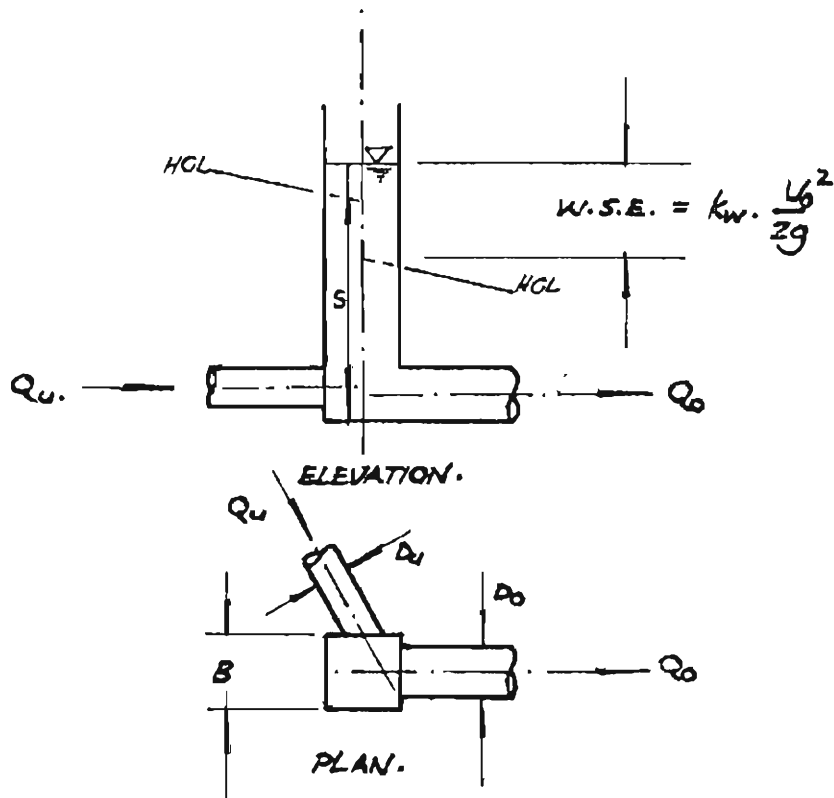
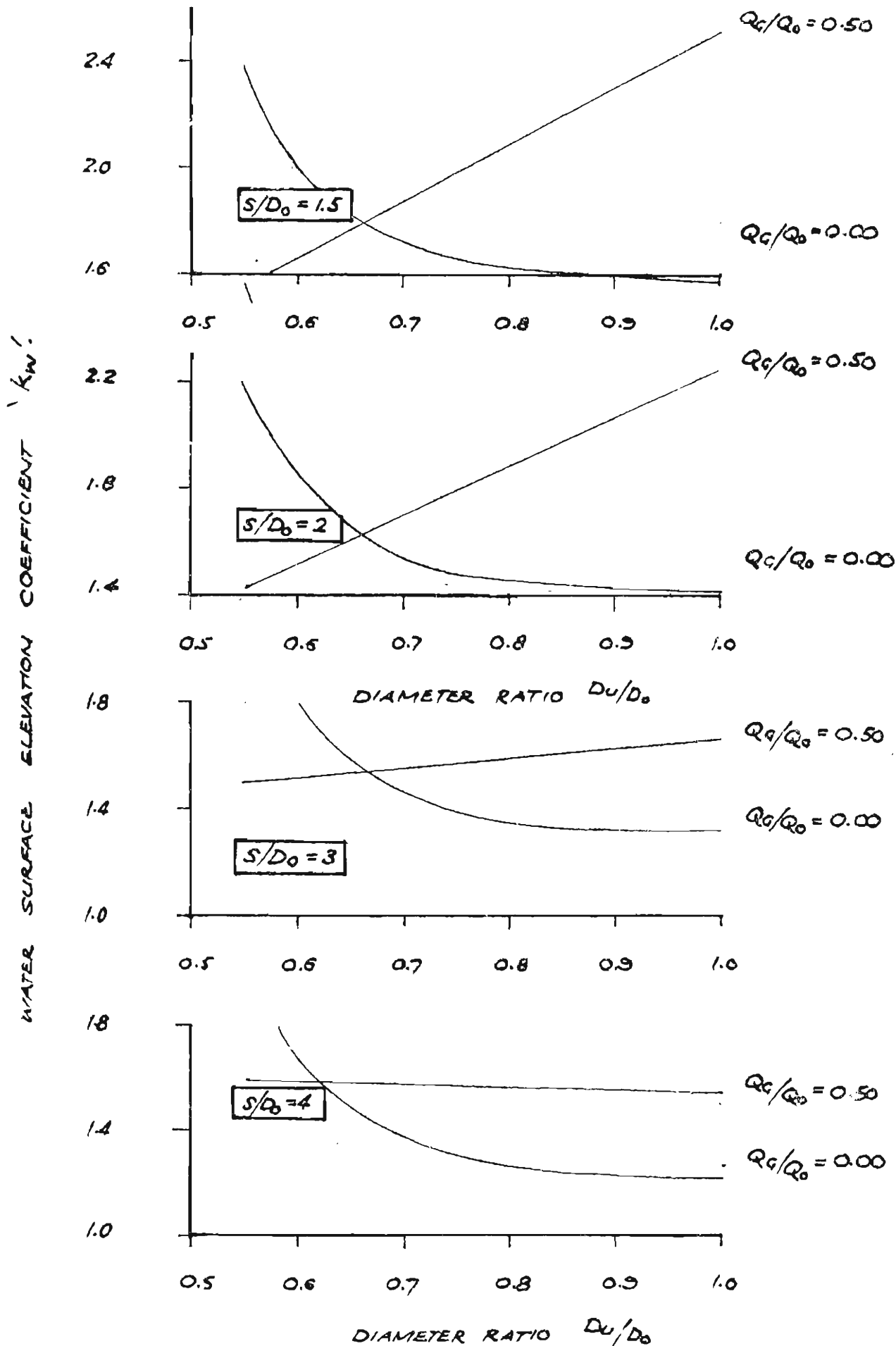
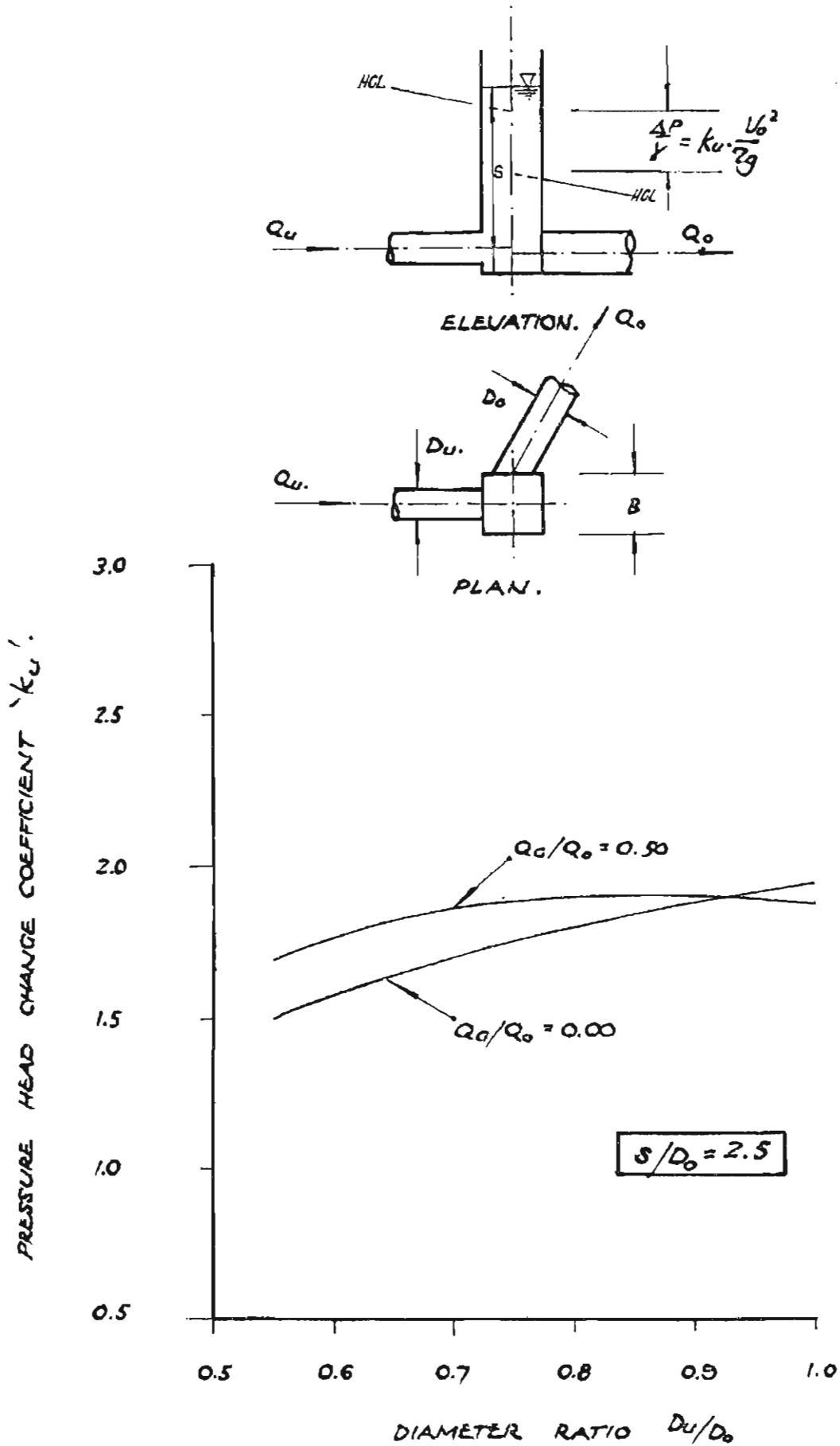


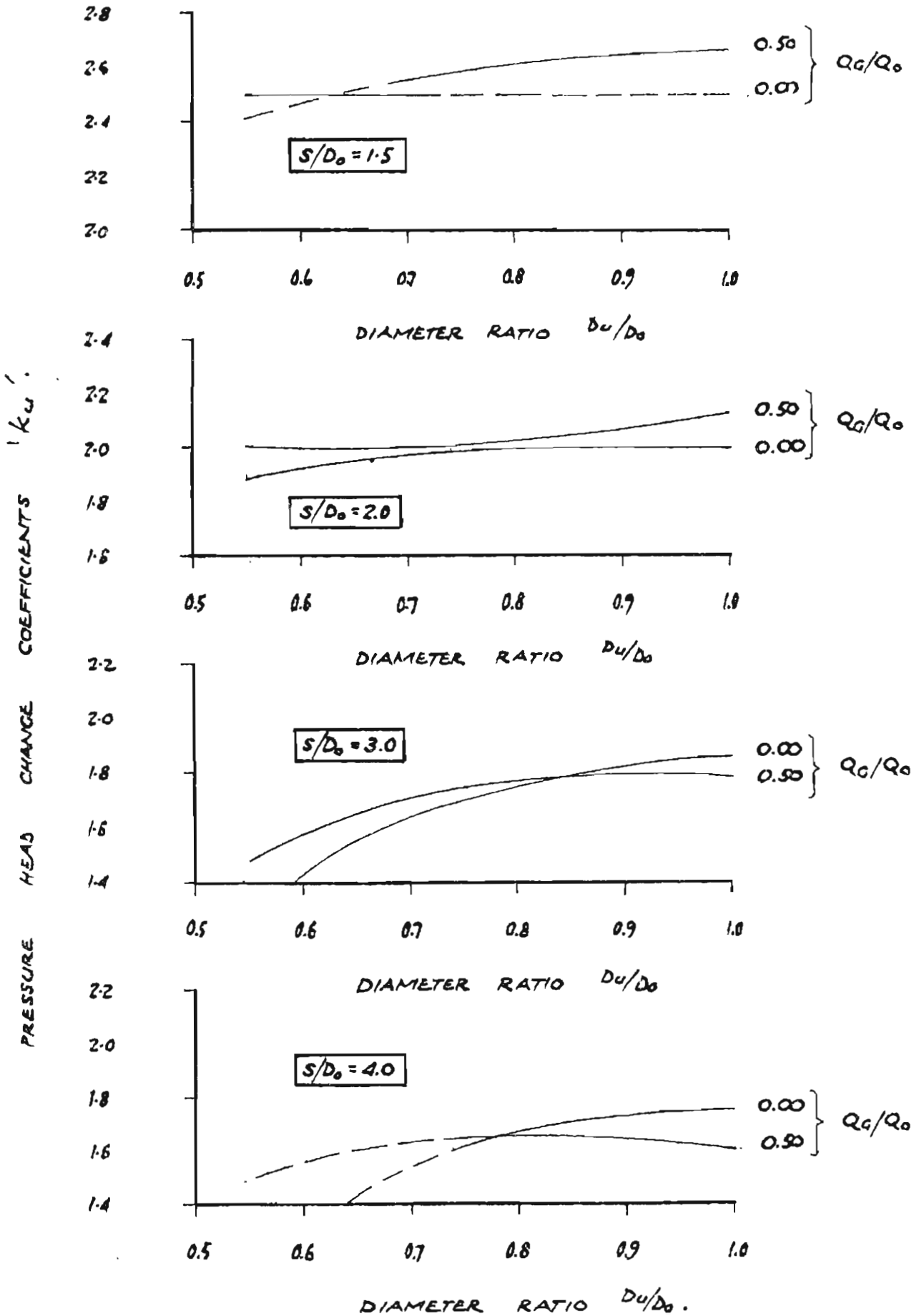
FIGURE 5.24 : WATER SURFACE ELEVATION COEFFICIENTS ( $k_w$ )— BRANCH POINT LOCATED NEAR DOWNSTREAM FACE OF PIT— FOR SUBMERGENCE RATIOS 1.5, 2.0, 3.0 AND 4.0



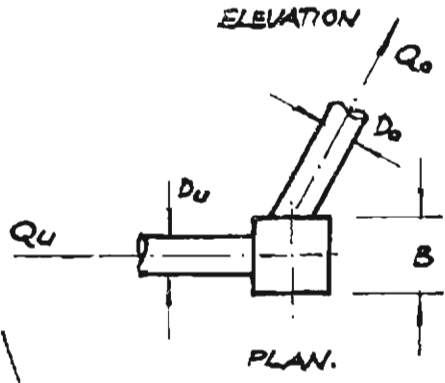
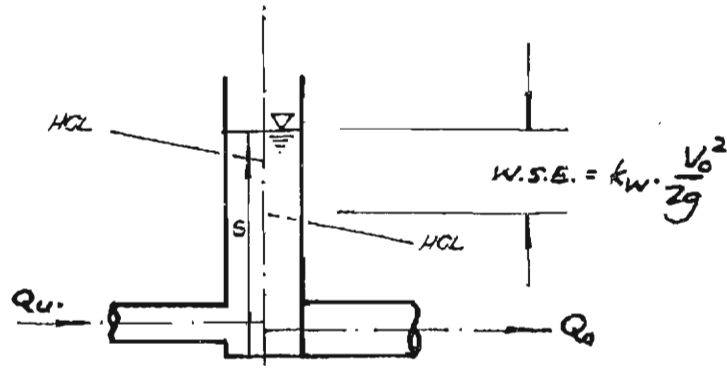
**FIGURE 5.25 : PRESSURE HEAD CHANGE COEFFICIENTS ( $k_u$ ) FOR  $67\frac{1}{2}^\circ$  BENDS AT PIT JUNCTIONS — BRANCH POINT LOCATED NEAR THE UPSTREAM FACE OF THE PIT. PIT — FOR SUBMERGENCE RATIO OF 2.5.**



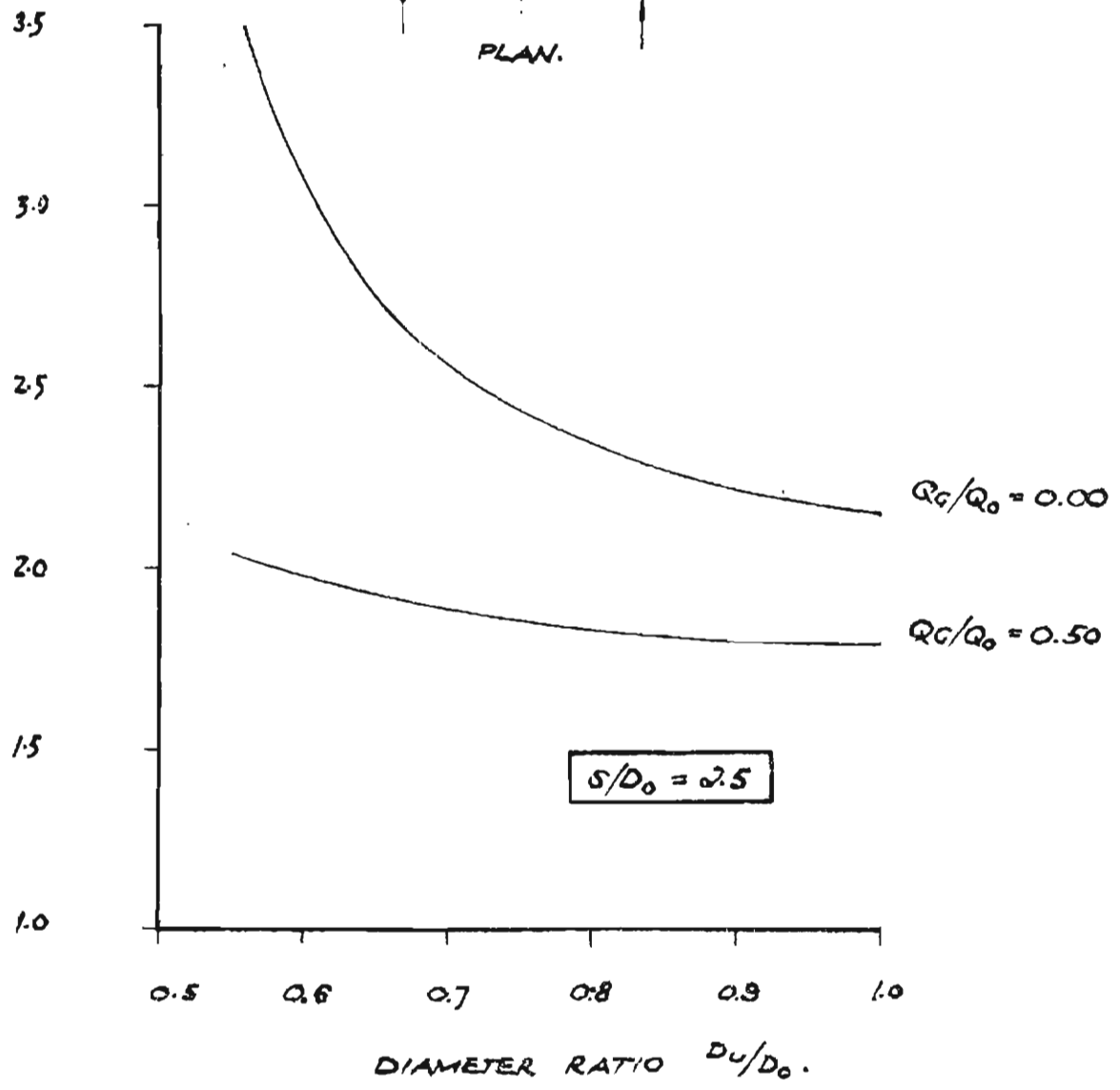
**FIGURE 5.26: PRESSURE HEAD CHANGE COEFFICIENTS ( $k_u$ ) FOR  $67\frac{1}{2}^\circ$  BENDS AT PIT JUNCTIONS — BRANCH POINT LOCATED NEAR THE UPSTREAM FACE OF PIT — FOR SUBMERGENCE RATIOS OF 1.5, 2.0, 3.0 AND 4.0**



**FIGURE 5.27: WATER SURFACE ELEVATION COEFFICIENTS ( $k_w$ ) FOR  $67\frac{1}{2}^\circ$  BENDS AT PIT JUNCTIONS.—BRANCH POINT LOCATED NEAR UPSTREAM FACE OF PIT—FOR SUBMERGENCE RATIO OF 2.5.**



WATER SURFACE ELEVATION COEFFICIENTS  $k_w$ .



**FIGURE 5.28 : WATER SURFACE ELEVATION COEFFICIENTS ( $k_w$ ) FOR  $67\frac{1}{2}^\circ$  BENDS AT PIT JUNCTIONS — BRANCH POINT LOCATED NEAR UPSTREAM FACE OF PIT — FOR SUBMERGENCE RATIOS OF 1.5, 2.0, 3.0 AND 4.0**

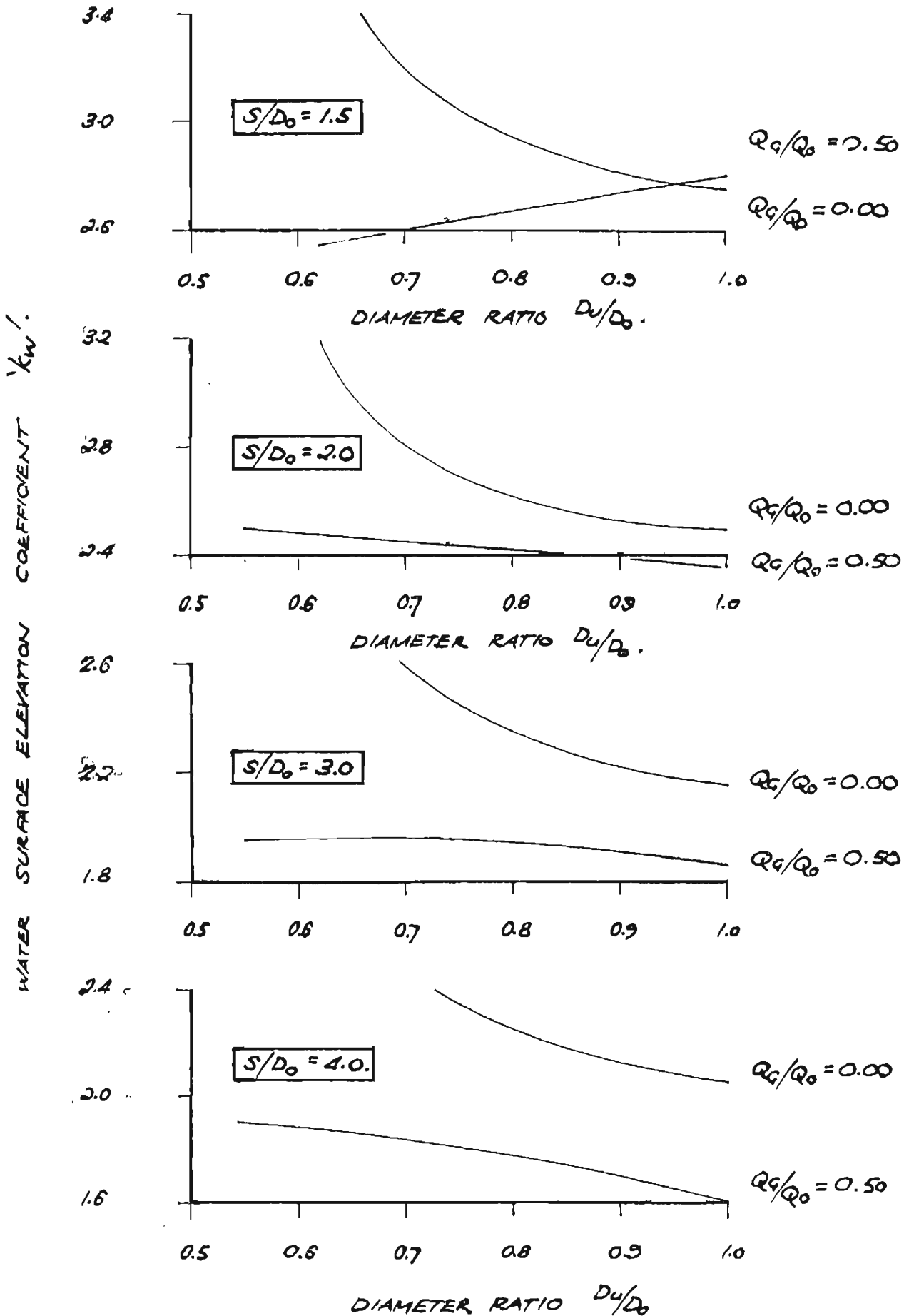




FIGURE 5.29 : HYDRAULIC IMPROVEMENT OF 90°  
BENDS AT PIT JUNCTIONS.

○ JUNCTION BRANCH POINT.

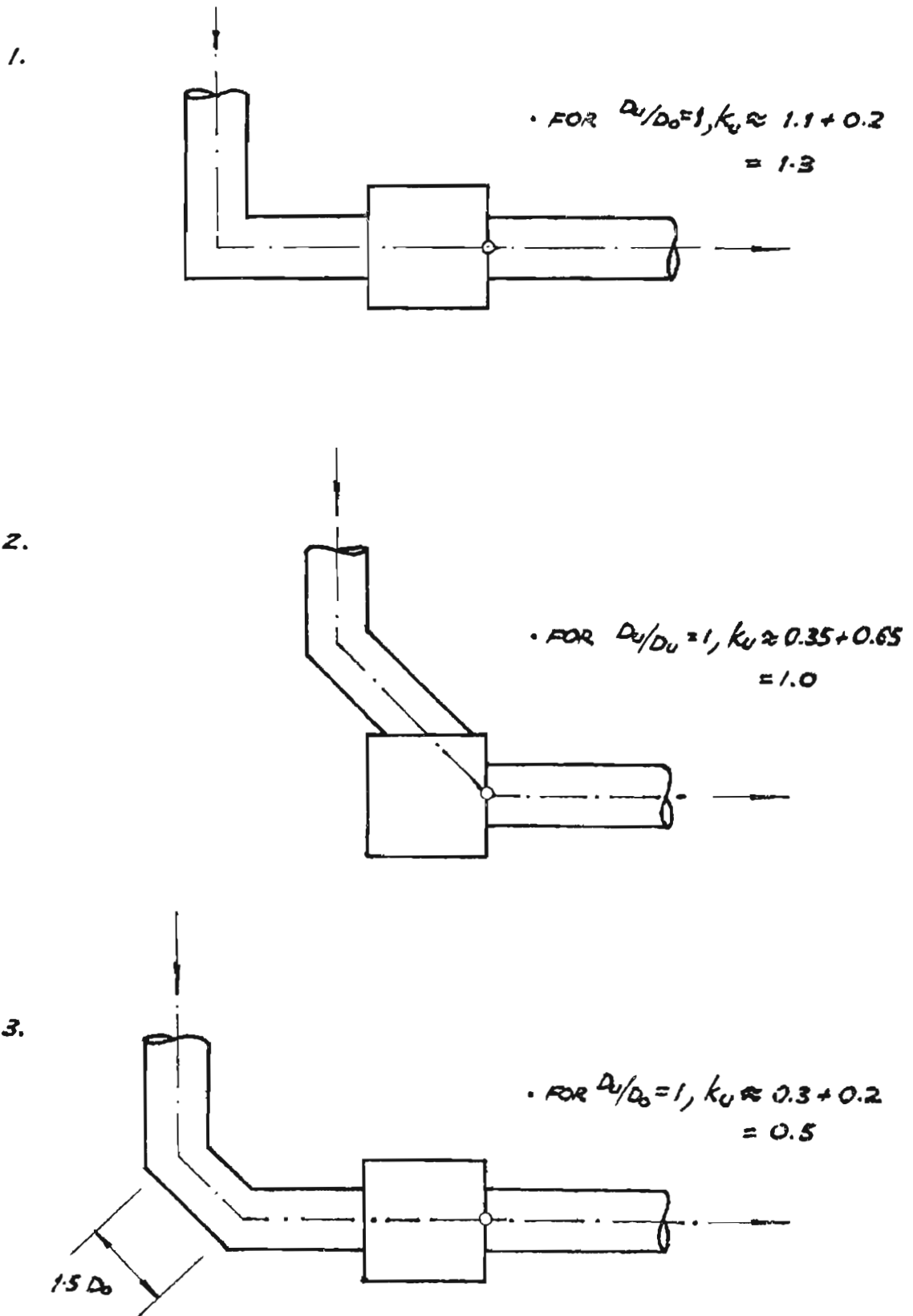


FIGURE 5.30 : COMPARISON OF EXPERIMENTAL RESULTS WITH THOSE OF OTHER INVESTIGATORS. (PRESSURE HEAD CHANGE COEFFICIENTS AT 90° JUNCTIONS)

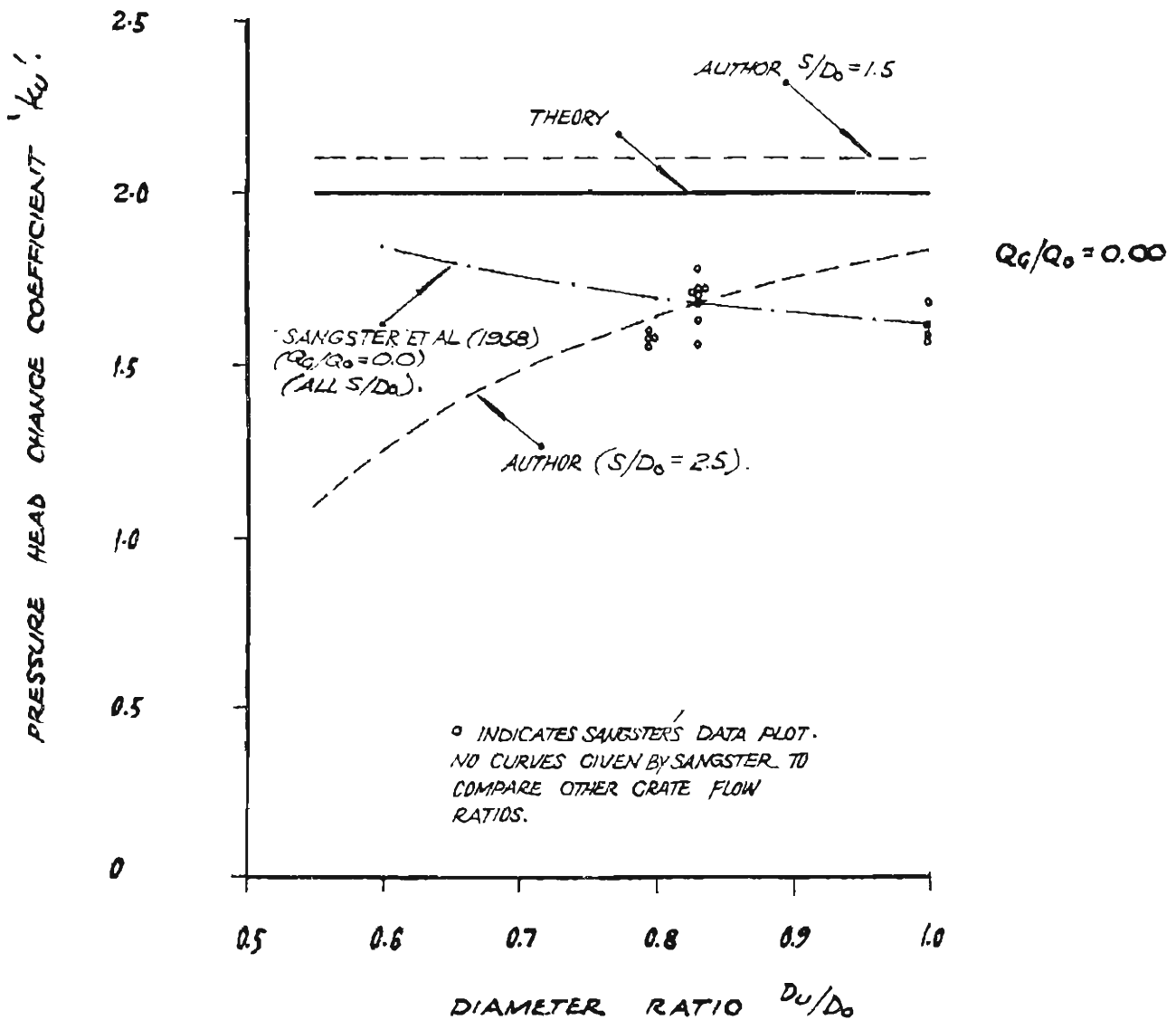
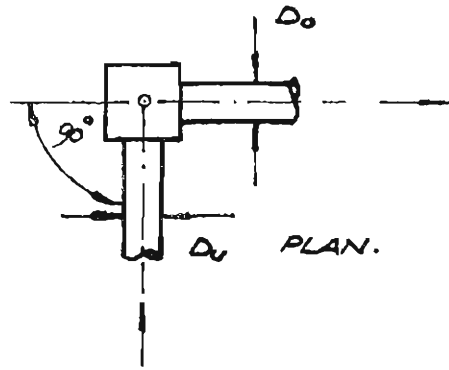
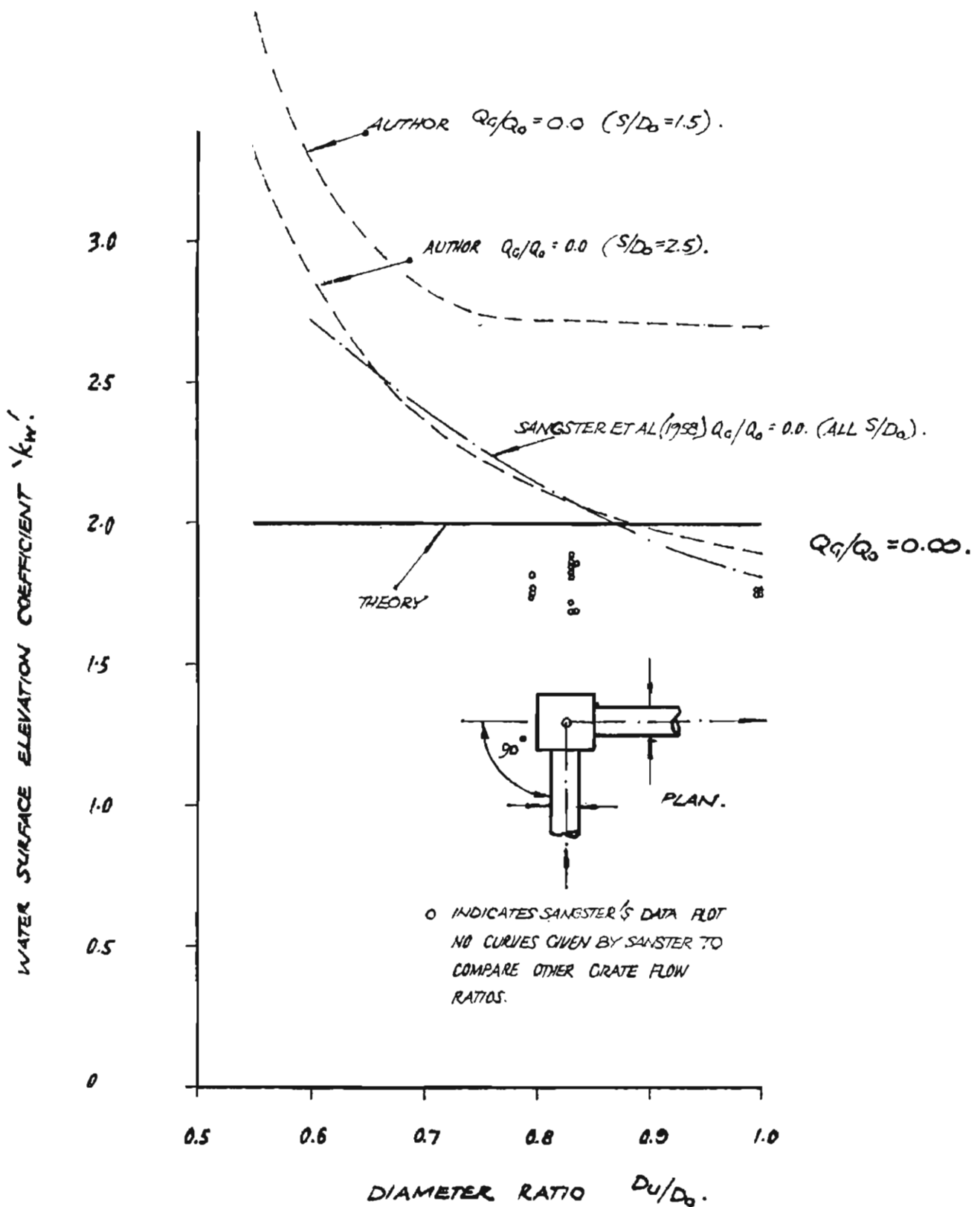
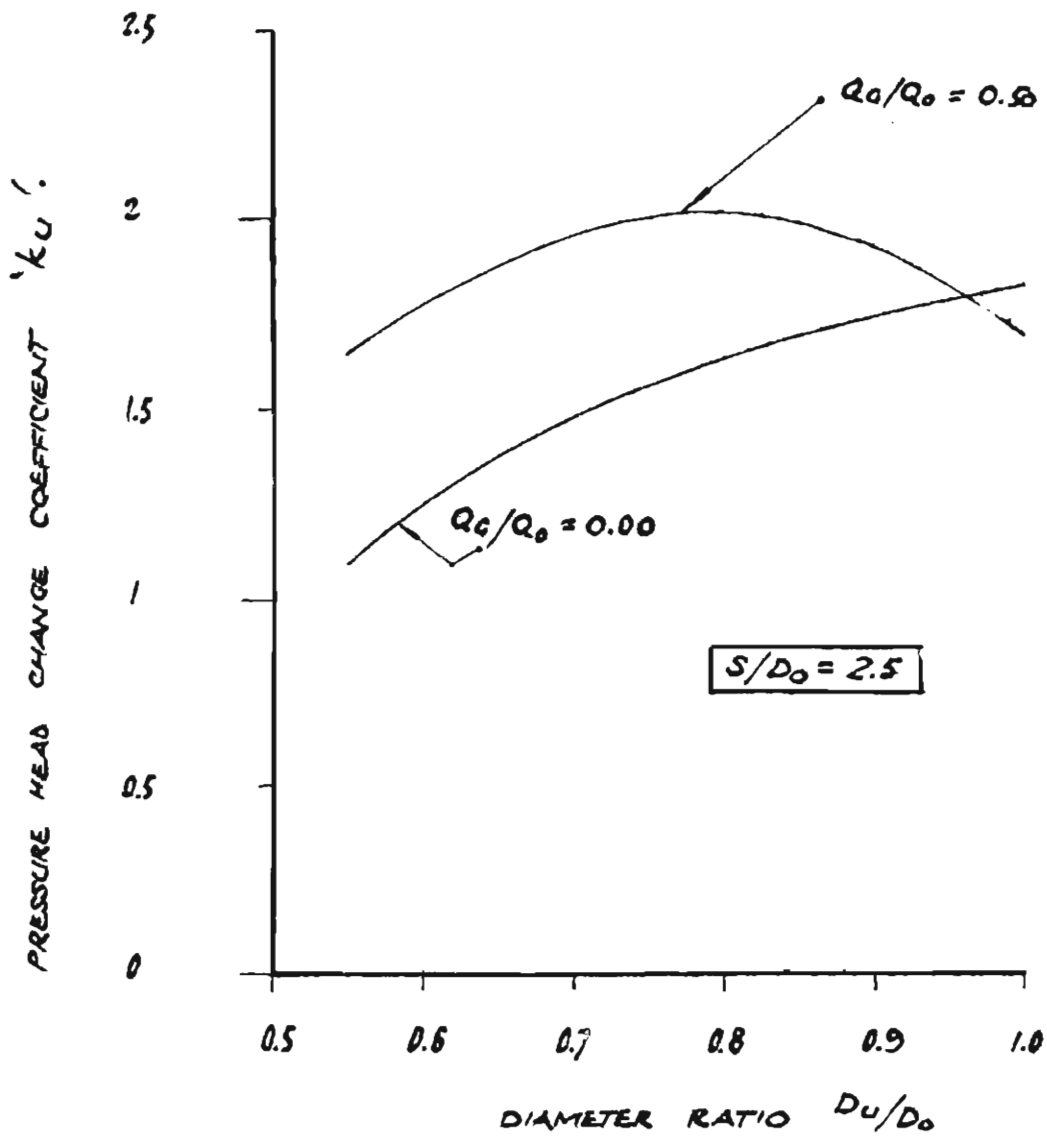
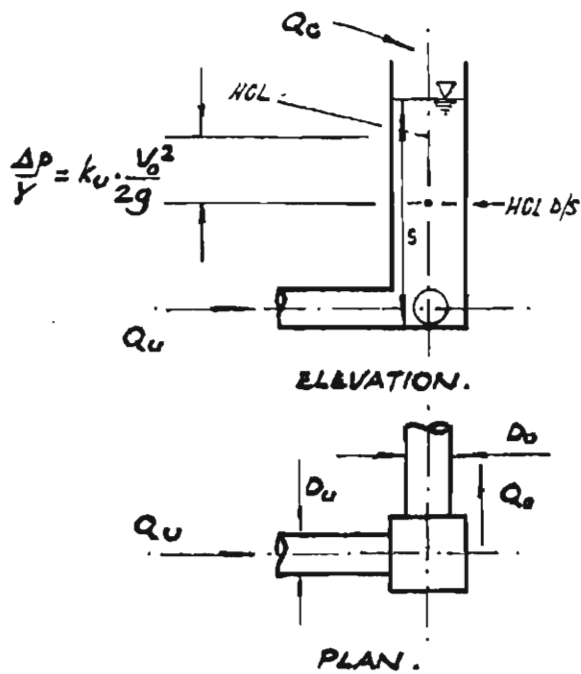


FIGURE 5.31 : COMPARISON OF EXPERIMENTAL RESULTS WITH THOSE OF OTHER INVESTIGATORS (WATER SURFACE ELEVATION COEFFICIENTS AT 90° JUNCTIONS).



**FIGURE 5.32 : PRESSURE HEAD CHANGE COEFFICIENTS ( $k_u$ ) FOR 90° BENDS AT PIT JUNCTIONS — FOR SUBMERGENCE RATIO OF 2.5**



**FIGURE 5.33 : PRESSURE HEAD CHANGE COEFFICIENTS ( $k_u$ ) FOR 90° BENDS AT PIT JUNCTIONS—FOR SUBMERGENCE RATIOS OF 1.5, 2.0, 3.0 AND 4.0.**

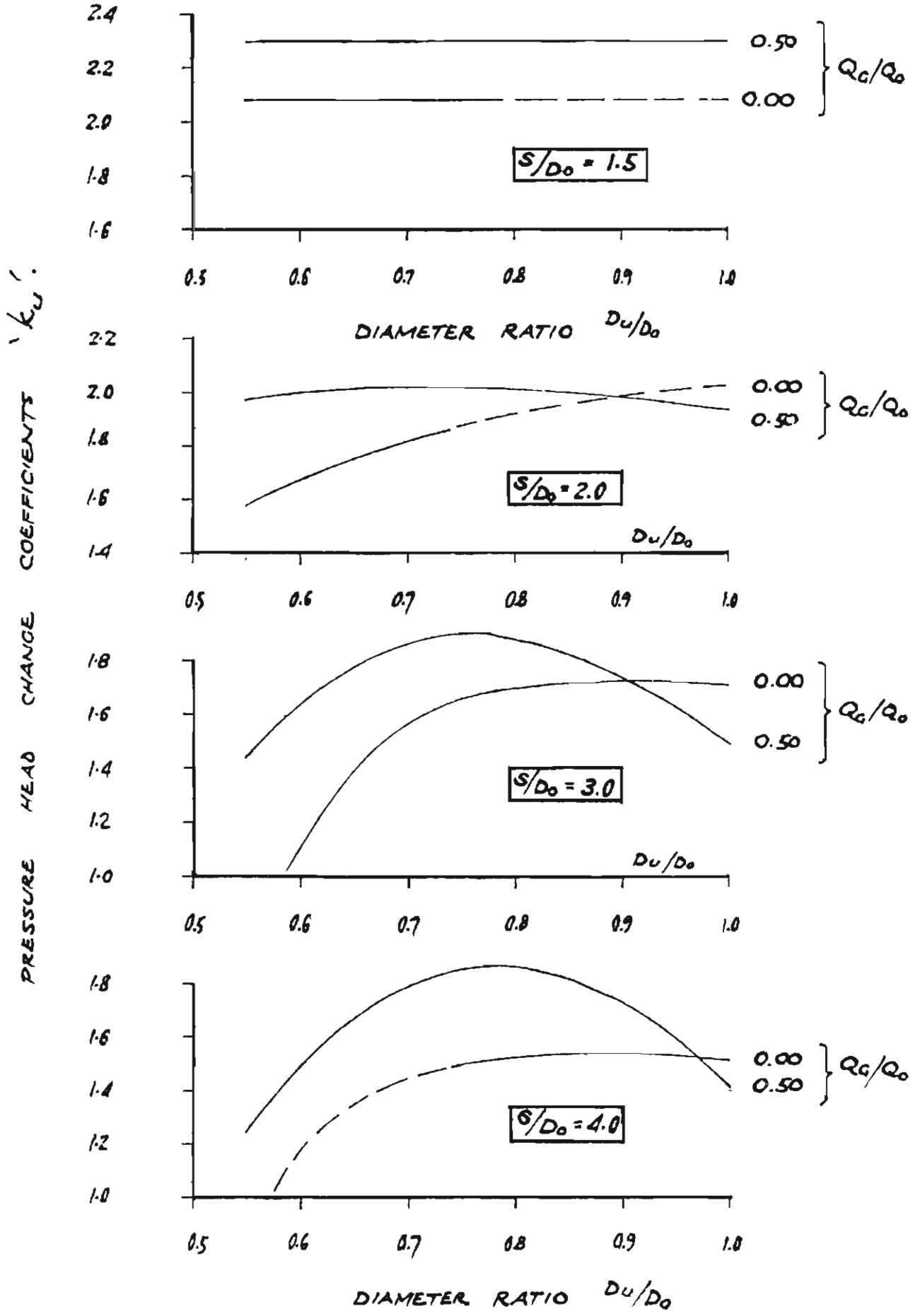
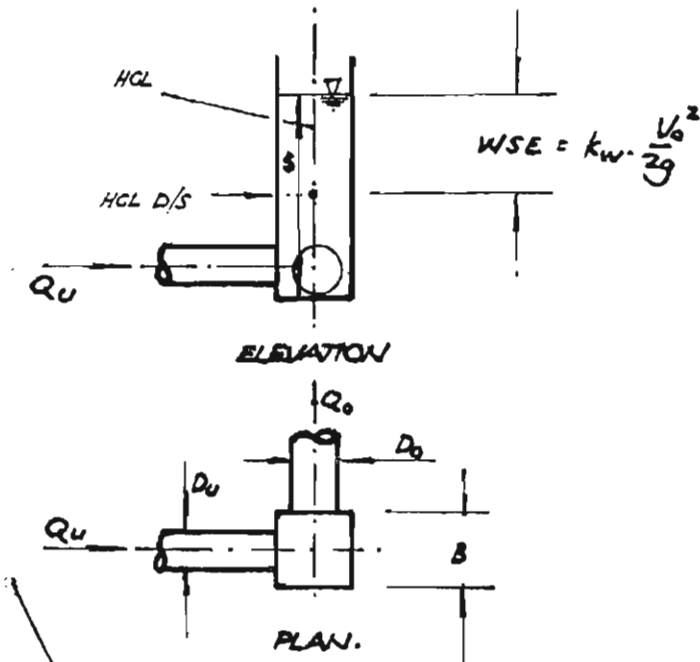


FIGURE 5.34 : WATER SURFACE ELEVATION COEFFICIENTS ( $k_w$ ) FOR 90° BENDS AT PIT JUNCTIONS — FOR SUBMERGENCE RATIO OF 2.5



WATER SURFACE ELEVATION COEFFICIENT ' $k_w$ '.

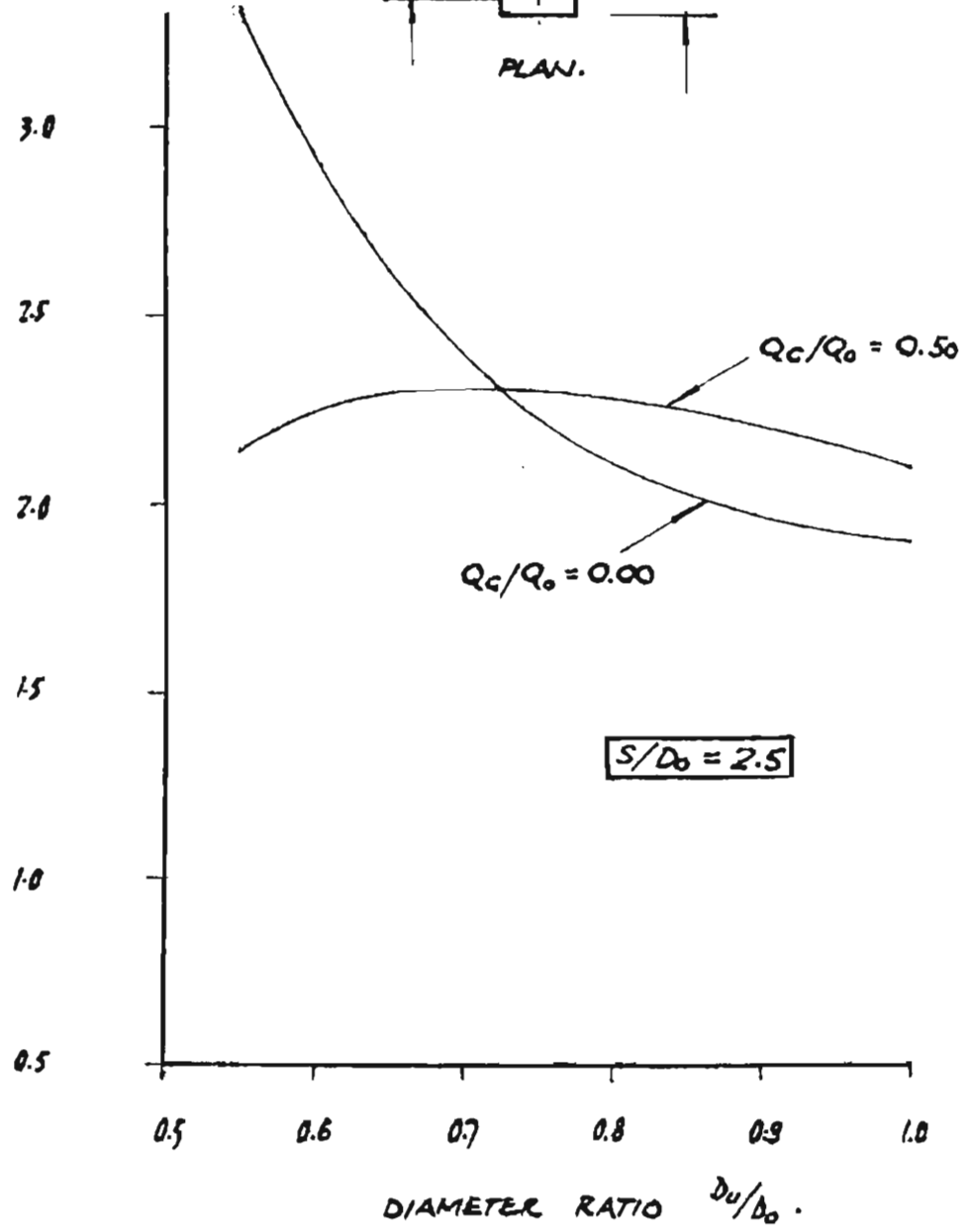
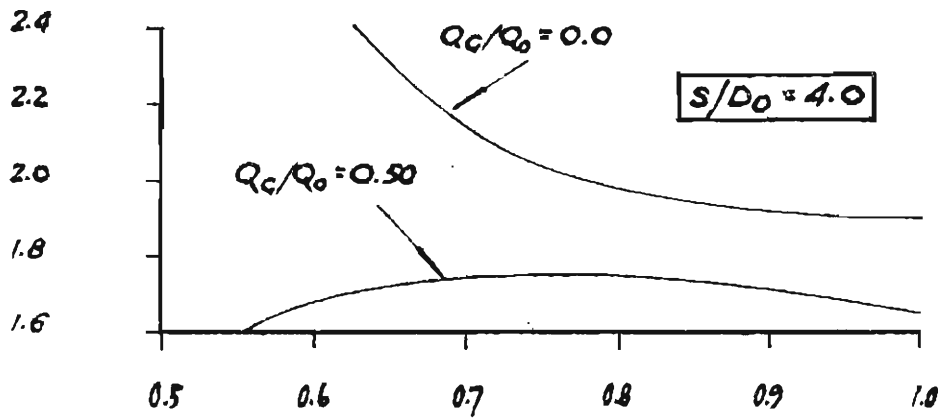
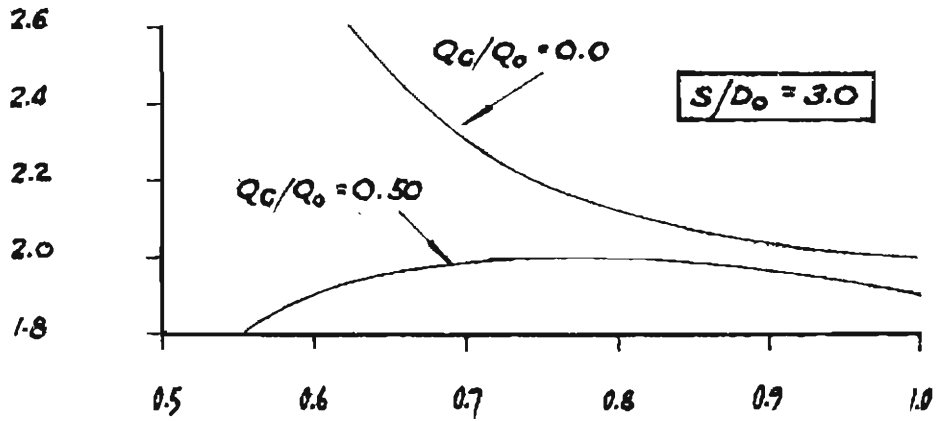
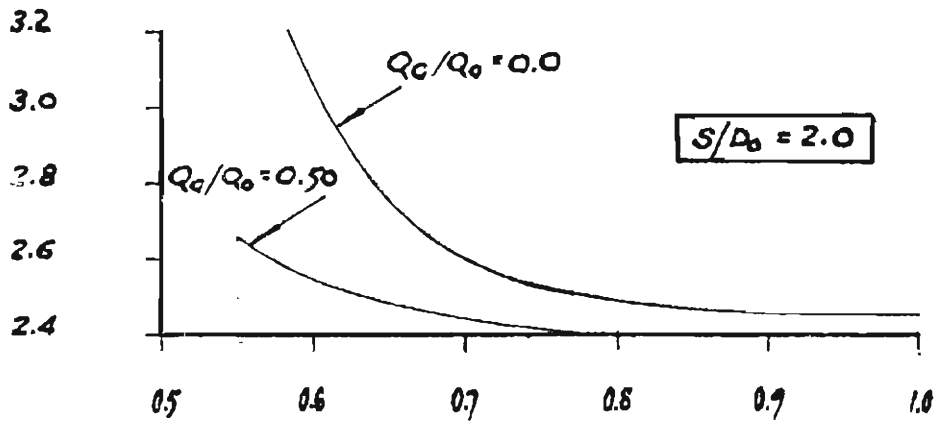
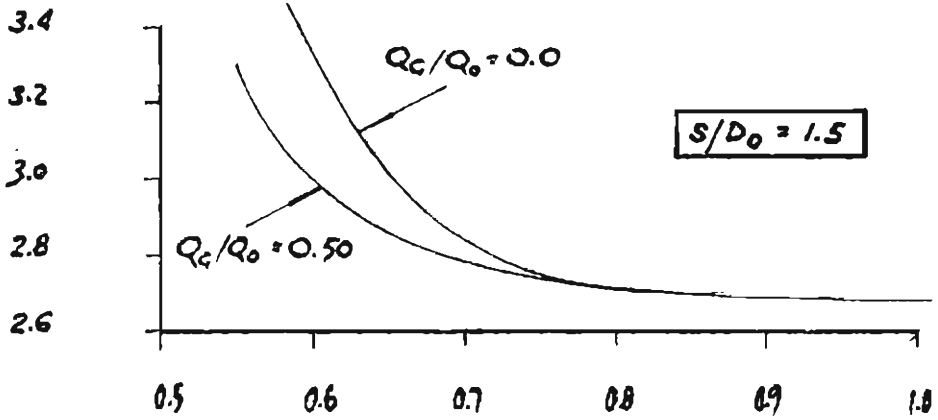


FIGURE 5.35: WATER SURFACE ELEVATION COEFFICIENTS ( $K_w$ ) FOR 90° BENDS AT PIT JUNCTIONS — FOR SUBMERGENCE RATIOS OF 1.5, 2.0, 3.0 AND 4.0.

WATER SURFACE ELEVATION COEFFICIENT  $K_w$ .



DIAMETER RATIO  $d_u/d_0$ .

CHAPTER 6

CONCLUSIONS



### CONCLUSIONS

The work contained in this thesis includes a consideration of closed pipe and open pit junction structures used in stormwater drainage systems. Hydraulic losses at such junctions constitute a significant proportion of total system losses, but the lack of design data to estimate these losses does not always permit the use of an accurate design method based on energy principles.

The purpose of this study has been to research the magnitude of hydraulic losses at junction structures and to provide data which could be used in storm drainage system design.

A general theoretical solution has been developed to determine the magnitude of pressure head change coefficients at closed pipe junctions. Data which have been published for a wide range of commercially available pipe junctions show that the theoretical solutions proposed yield values of energy loss and pressure head change coefficients which could be used for design purposes. Similarly, losses at closed pipe junction structures for which data have not been determined experimentally may be evaluated using the theoretical solutions derived in this thesis. In such instances, derived loss coefficients will generally produce conservative results.

For pit junctions, few data have been published and an experimental programme was undertaken to expand the available data which could be used for design purposes. An important conclusion which may be drawn from the results of this test programme is that the location of the branch point of the junction (i.e., the intersection of the centre lines of the upstream and downstream pipes) has a controlling effect on the hydraulic operation and efficiency of the junction pit.

The junction pit tests conducted in the programme covered a range of configurations and it was noted that the efficiency of the pit structure increased when the branch point was located close to or on the downstream face of the pit.

The most hydraulically efficient structures were those which had the branch point located on the downstream face.

By assertion, it would appear that the same basic principle would apply for junction pit structures which are characterized by more than two connecting pipes converging to a single junction branch point. Such an assertion is not currently supported by experimental evidence but is a logical extension of the conclusions drawn within the scope of this thesis.

For structures where the branch point is located on the downstream face of the pit, several points may be noted:

1. Pressure head change coefficients are considerably less than those values which have been traditionally used in storm drain design practice. In Australia, a requirement of 1.5 downstream velocity heads has been set as a design standard by both local government and road authorities alike. Typical values of coefficients (for zero grate flow) derived in this study are given in Table 6.1:

TABLE 6.1 : Typical Values of  $k_u$  and  $k_w$  for Branch Point on Downstream Face of Pit.

$D_u/D_o$	$\theta = 0^\circ$	$\theta = 22\frac{1}{2}^\circ$	$\theta = 45^\circ$
0.7	- 1.95	- 1.60	- 0.90
0.8	- 0.95	- 0.60	0.00
0.9	- 0.20	0.00	0.45
1.0	0.20	0.30	0.60

2. Negative values of the pressure head change coefficients develop when the diameter ratio  $D_u/D_o$  is less than one. This is evidenced in Table 6.1. A deceleration of flow (i.e., the

---

\* Values extracted from Figures 5.2, 5.4 and 5.10

provision of an expansion) may be used, therefore, to overcome other (positive) losses attributable to changes in flow direction or the addition of a secondary (grate) flow.

3. For practical purposes, the water surface elevation in a junction pit may be considered to be coincident with the upstream hydraulic grade line elevation (i.e.,  $k_u = k_w$ ).
4. The pit size and shape does not significantly affect the magnitude of the loss coefficients.
5. A closed pipe junction theoretical solution can be applied to determine pressure head changes at junction pit structures provided that, (a) an allowance ( $\Delta k_p$ ) is made for the presence of the pit structure itself (0.20 downstream velocity heads for two-pipe junctions and, say, 0.3 downstream velocity heads for three-pipe junctions; and (b) an allowance ( $\Delta k_s$ ) is made for submergence effects in accordance with Table 5.2. Alternatively a modification for submergence may be made to the theoretical solution given in Equation 2.19 using Equation 6.1:

$$\Delta k_s = \left[ 4.4 \left( S/D_o \right)^{-1.18} - 1.75 \left( S/D_o \right)^{-0.18} \right] \left( Q_z/Q_o \right) \quad \dots \text{Eq. 6.1}$$

The junction pressure head change coefficient can thus be derived from Equation 6.2 :

$$k_u = k_{u(\text{theory})} + \Delta k_p + \Delta k_s \quad \dots \text{Eq. 6.2}$$

where  $k_{u(\text{theory})}$  can be developed from Equation 2.19:

$$\begin{aligned}
k_{u(\text{theory})} = & 2 - 2 \left( \frac{A_o}{A_u} \right) \cos \theta_u + 4 \left( \frac{Q_b}{Q_o} \right) \left( \frac{A_o}{A_u} \right) \cdot \cos \theta_u \\
& - 2A_o \left( \frac{\cos \theta_b}{A_b} + \frac{\cos \theta_u}{A_u} \right) \left( \frac{Q_b}{Q_o} \right)^2 - \frac{2p_u A_o}{\rho Q_o V_o} + \frac{2R_x}{\rho Q_o V_o}
\end{aligned}$$

(... Eq. 2.19)

For a two-pipe junction, setting  $p_u$  and  $R_x$  equal to zero,

$$k_{u(\text{theory})} = 2 \left[ 1 - \frac{A_o}{A_u} \left( \frac{Q_u}{Q_o} \right)^2 \cos \theta_u \right] \quad \dots \text{Eq. 6.3}$$

and, similarly, for a three-pipe junction,  $k_{u(\text{theory})}$  is given by Equation 6.4:

$$\begin{aligned}
k_{u(\text{theory})} = & 2 - 2 \left( \frac{A_o}{A_u} \right) \cos \theta_u + 4 \left( \frac{Q_b + Q_g}{Q_o} \right) \left( \frac{A_o}{A_u} \right) \cdot \cos \theta_u \\
& - 2A_o \left( \frac{\cos \theta_b}{A_b} + \frac{\cos \theta_u}{A_u} \right) \left( \frac{Q_b + Q_g}{Q_o} \right)^2
\end{aligned}$$

... Eq. 6.4

(For a three-pipe junction, it must be assumed, pending further investigation, that the lateral pressure line coefficient,  $k_b$ , will correspond to  $k_u$  and  $k_w$  when the branch point of the junction is located on the downstream face of the pit.

These conclusions do not apply to pit junction structures where the branch point of the junction is not located on the downstream face of the pit and consideration should be given to the following points:

1. Loss coefficients are generally higher than those values that have been traditionally used in design practice. Typical values determined in this study are set out in Table 6.2.

TABLE 6.2 : Typical Values\* of  $k_u$  and  $k_w$  for Branch Point

Not on Downstream Face of Pit						
$D_u/D_o$	$\theta = 45^0$		$\theta = 67\frac{1}{2}^0$		$\theta = 90^0$	
	$k_u$	$k_w$	$k_u$	$k_w$	$k_u$	$k_w$
0.7	2.05	2.90	1.70	2.50	1.50	2.40
0.8	2.10	2.60	1.80	2.35	1.65	2.10
0.9	2.15	2.50	1.90	2.25	1.75	2.00
1.0	2.20	2.40	2.00	2.20	1.85	1.90

- The water surface elevation within the pit is located above the upstream hydraulic grade line by a distance of up to 0.3 upstream velocity heads. (This value, however, may increase for very low submergence depths). For a three-pipe tee junction, the water surface elevation will correspond to the upstream in-line pressure line. The lateral pressure line elevation will be located below the water surface by up to 0.3 upstream velocity heads. Thus,  $k_u$  equals  $k_w$ , and  $k_b < k_u, k_w$ .
- The pit size is an important factor in determining the magnitude of loss coefficients. These coefficients are minimized when pit sizes are kept to a minimum.
- A closed pipe junction theoretical solution is not applicable. Data should be extracted from the appropriate figures.

Where it is not possible to locate the junction branch point on the downstream face of the pit, consideration should be given to the use of deflection devices such as those outlined by Sangster *et al* (1958) and to keep pit dimensions as small as is practically feasible allowing for access and maintenance.

\* Values extracted from Figures 5.16, 5.18, 5.25, 5.27, 5.32, 5.34

In summary, either experimental results or empirically derived equations have been developed for the range of pit junctions that were tested in the experimental programmes. It is envisaged that this data will be adopted in urban storm drain design and will eventually be included in a manual that will lead to an accurate design approach for surcharged storm drain systems.

CHAPTER 7

SELECTED BIBLIOGRAPHY

1. ACKERS, P. Investigation of Head Losses at Sewer Manholes, *Civil Engineering (London)*, Vol. 54, No. 637, 639, July, Aug., 1959, pp. 882-887, Sept. 1959, pp. 1033 - 1036.
2. AMBROSE, H. H., Head Losses in Miter Bends, Univ. of Iowa, *Studies in Engineering Bulletin*, No. 35, 1953.
3. ANDERSON, A. G., STRAUB, L. G., Hydraulics of Conduit Bends, St. Anthony Falls Hydraulic Laboratory, *Bulletin*, No. 1., Univ. of Minnesota, Minneapolis, Minnesota, Dec. 1948.
4. ARCHER, B., BETTESS, F. AND COLYEK, P.J., Head Loss and Air Entrainment at Surcharged Manholes, Hydraulics Research Station, *Report*, IT 185, Wallingford, England, Nov. 1978.
5. ARCHER, W. H., Loss of Head Due to Enlargement in Pipes, *Transactions*, A.S.C.E., Vol. 76, 1913, pp. 999 - 1026.
6. BALTIMORE COUNTY DEPARTMENT OF PUBLIC WORKS, Bureau of Engineering, *Design Manual for Sanitary Sewers*, Towson, Baltimore County, Maryland, USA, 1964.
7. BLAISDELL, F. W., MANSON, P.W., Energy Losses at Pipe Junctions, *Proceedings*, A.S.C.E. Vol. 93, No. IR3, Sept., 1967, pp. 59 - 78.
8. BLAISDELL, F. W., MANSON, P.W., Loss of Energy at Sharp Edged Pipe Junctions, *Technical Bulletin No. 1283*, U.S. Dept. of Agriculture, Washington, D.C., 1963.
9. CHOW, YEN TE, *Open Channel Hydraulics*, McGraw Hill Book Co., N.Y., 1959.
10. CHOW, YEN TE (Ed.), *Handbook of Applied Hydrology*, McGraw Hill Book Co., N.Y., 1964.
11. CITY OF LOS ANGELES DEPARTMENT OF PUBLIC WORKS, Bureau of Engineering Manual *Storm Drain Design*, Part G, Dec., 1973, Office Standard No. 115, Hydraulic Analysis of Junctions, Storm Drain Design Division, 1968.
12. CLARK, J.W., VIEMANN, W., HAMMER, M.J., *Water Supply and Pollution Control*, 2nd Ed., International Textbook Co., 1971.
13. COLYER, P.J., The Effect of Surcharging on Discharge Through a Pipe, *Chartered Municipal Engineer*, Journal of the Institution of Municipal Engineers, April 1977, pp. 60 - 62.



14. COLYER, P. J., PELNICK, R.W., Storm Drainage Design Methods - A Literature Review, *Report INT 154*, Hydraulics Research Station, 1976.
15. CROLEY, T. E., *Hydrologic and Hydraulic Computations on Small Programmable Calculators*, Iowa Institute of Hydraulic Research, Univ. of Iowa, 1977.
16. CROW, D. A., WHARTON, R., A Review of the Literature on the Division and Combination of Flow in Closed Conduits, B.H.R.A., *Bulletin TN 937*, Jan., 1968.
17. DEPARTMENT OF MAIN ROADS, N.S.W., *Waterway Calculations for Urban Drainage*, M.R. Form 371B, Aug., 1963.
18. FAVRE, H. On the Laws Governing the Movement of Fluids in Conduits under Pressure with Lateral Flow. *Revue Universelle des Mines*, Eighth Series, Vol. XIII No. 12, Dec. 1937 [Translated from the French by Agricultural Research Service, St. Anthony Falls Hydraulic Laboratory, Univ. of Minnesota].
19. GARDEL, A., The Loss of Head in the Flow Through Tee Branches, *Bulletin Technique de la Suisse Romande*, No. 9 and 10, 1957 [Translation supplied by Agricultural Research Service, St. Anthony Falls Hydraulic Laboratory, Univ. of Minnesota].
20. GIBSON, A. H., *Hydraulics and its Applications*, Constable and Co., London, 1961.
21. KARAKI, S., *Fundamentals of Fluid Flow in Closed Conduits*, Paper presented at Symposium on Control of Flow in Closed Conduits, Fort Collins, Colorado, 1971 (see ref. Tullis, J.P. (Ed.) )
22. INSTITUTION OF ENGINEERS, AUST., *Australian Rainfall & Runoff*, Sydney, Aust., 1977.
23. JENS, S.W. (Ed.), *Design of Urban Highway Drainage*, U.S. Dept. of Transportation Federal Highway Administration, Washington, D.C., 20590, Aug. 1979.
24. KING, H. W., *Handbook of Hydraulics*, Fifth Edition, McGraw-Hill Book Co., 1963.
25. KINNE, E., *Contribution to the Hydraulic Losses in Branches*, Bureau of Reclamation, US Dept. of the Interior, Washington, D.C., 1955.

26. KIRCHBACH, W., Loss of Energy in Mitre Bends, Trans. of the Munich Institute of Hydraulics *Bulletin* 3 (1929). Translation by A.S.M.E., pp. 43-64 (1935).
27. McNOWN, J. S., Mechanics of Manifold Flow" *Transactions*, A.S.C.E., Vol. 119, 1954, pp. 1103 - 1142.
28. MERRIMAN, M., *Treatise on Hydraulics*, 10th Edition, John Wiley & Sons, N.Y. 1916.
29. MILLER, D. S., *Internal Flow - A Guide to Losses in Pipes and Duct Systems*, B.H.R.A., England, 1971.
30. NIAZ, S. M., *A Study of Converging Flow in Pipelines*, thesis presented to Iowa State University, Iowa City, 1947.
31. PETERMANN, F., Loss in Oblique-angled Pipe Branches, *Special Publication*, A.S.M.E., 1935.
32. PRINS, R., *Storm Sewer Junction Geometry and Related Energy Losses*, M. App. Sc. Thesis presented to Univ. of Ottawa, Ontario, Canada, Dec., 1975.
33. QUEENSLAND DEPARTMENT OF MAIN ROADS, *Urban Road Design Manual*, 2 volumes, 1975.
34. ROUSE, H., *Fluid Mechanics for Hydraulic Engineers*, Dover Publications, N.Y., 1961.
35. ROUSE, H. (Ed.), *Engineering Hydraulics*, John Wiley and Sons Inc., N.Y., 1950.
36. SANGSTER, W.M., WOOD, H.W., SMERDON, E.T., BOSSY, H.G., Pressure Changes at Storm Drain Junctions, *Bulletin* No. 41, Engineering Experiment Station, University of Missouri (1958).
37. SANGSTER, W.M., WOOD, H.W., SMERDON, E.T., BOSSY, H.G., Pressure Changes at Open Junctions in Conduits, A.S.C.E. *Trans.* Vol. 126, pt. 1, 1961, pp. 364-396.
38. SCHUBART, W., Energy Loss in Smooth and Rough Surfaced Bends and Curves in Pipe Lines, *Transactions of the Munich Hydraulics Institute, Bulletin* 3 1929, [Translation A.S.M.E. pp. 81-99 (1935)]

39. STANDARDS ASSOCIATION OF AUSTRALIA, *Design Charts for Water Supply and Sewerage*, Australian Standard, A.S. 2200, 1978 .
40. STAROSOLSZKY, O., *Vizugyi Kozlemenyek [Hydraulic Engineering]* No. 1958, Imprimerie Universitaire, Budapest, 1958. [Translation supplied by Agricultural Research Service, St. Anthony Falls Hydraulic Laboratory, University of Minnesota].
41. STEVENS, J. C., Theoretical Energy Losses in Intersecting Pipes, *Engineering News Record*, Vol. 97, No. 4., July 22, 1928.
42. TULLIS, J. P. (Ed), Control of Flow in Closed Conduits, *Proceedings* of the Institute, held at Colorado State Univ., Aug., 1970.
43. VAZSONYI, A., Pressure Losses in Elbows and Duct Branches, *Trans.*, A.S.M.E., Vol. 66, Apr. 1944, pp. 177-183.
44. VENNARD, J. K., *Elementary Fluid Mechanics*, Wiley, N.Y., 1961.
45. VOGEL, G., Experiments to Determine the Loss in Right-angle Pipe Tees, *Technical Memorandum* 299, U.S. Dept. of the Interior, Denver, Colorado, 1932.
46. WEBBER, N. B., *Fluid Mechanics for Civil Engineers*, S.I Edition, Chapman and Hall, 1971, London.
47. WRIGHT-McLAUGHLIN ENGINEERS, *Urban Storm Drainage Criteria Manual*, Vol. I & II, Denver, Colorado, March 1969.
48. YEVSEVICH, V., BARNES, A.H., Flood Routing through Storm Drains (Part III) - Evaluation of Geometric and Hydraulic Parameters, *Hydrology Papers*, Colorado State University, Nov. 1970.
49. ZANKER, K. H., BROCK, T.E., A Review of the Literature on Fluid Flow through Closed Conduit Bends, B.H.R.A., *Bulletin*, No. TN 901, July, 1967.

APPENDIX

TEST DATA

TEST DATA

Test data determined from the experimental programme are plotted in Figures A1 to A60. Two data plots have been prepared for each of the thirty models tested, being pressure head change coefficient ( $k_u$ ) versus discharge, and water surface elevation coefficient ( $k_w$ ) versus discharge respectively. For each data plot, grate flow ratio ( $Q_g/Q_o$ ) and submergence ratio ( $S/D_o$ ) have been used as secondary parameters.

The data contained in this Appendix have been interpreted to produce the experimental results presented in Chapter 5.

For most models, the grate flow ratio ( $Q_g/Q_o$ ) was tested for values of 0.00 and 0.50. In some models, intermediate values were also tested to verify the interpolation of the test data. The effects of the grate flow ratio has been established from this information and reported on in Section 5.1. For each grate flow ratio, a submergence range of  $1.5 < S/D_o < 4.0$  was also tested. Submergence ratios have been numbered on both data plots for each model.

Thus, for example, in Figure A1 (Model No. 1), pressure head change coefficients have been determined for grate flow ratios of  $0.00 \leq Q_g/Q_o \leq 0.50$ . For each of these grate flow ratios, a range of submergence has also been examined. Likewise, in Figure A2, water surface elevation coefficients have been determined for similar ranges of grate flow and submergence ratios.

In the interpretation of the data, the effect of discharge  $Q_o$  was considered to be reflected primarily by the submergence ratio ( $S/D_o$ ), since, in prototype application, the submergence will vary only with variable discharge. Where variations in derived loss coefficients occurred for constant submergence but with variable discharge, test results have been interpreted for discharges of approximately 6 l/s. This selection eliminated the higher

potential for experimental error at low discharges and represents a medium value of discharge and velocity in the prototype application (for example, 6 l/s flowing in a 94 mm diameter model represents a velocity of 2.44 m/s in a 750 mm diameter prototype).

The effects of variations in the diameter ratio ( $D_u/D_o$ ) are reflected in the data plots for constant angle of deflection  $\theta$ . Thus, for example, Figure 5.2 has been derived from an interpretation of Figures A1, A2, A13, A14, A25 and A26 which have all been plotted for  $\theta$  equal to  $0^\circ$ .

All experimental results included in Chapter 5 have been produced from a similar interpretation of all other data plots.

FIGURE A1: DATA PLOT FOR MODEL N°1.

PRESSURE HEAD CHANGE COEFFICIENT VS. DISCHARGE  $Q_0$

$\theta = 0^\circ$ ,  $D_0 = 70$  MM,  $D_U = 70$  MM,  $A_0/A_U = 1.00$ .

(FIGURES INDICATE SUBMERGENCE RATIOS.)

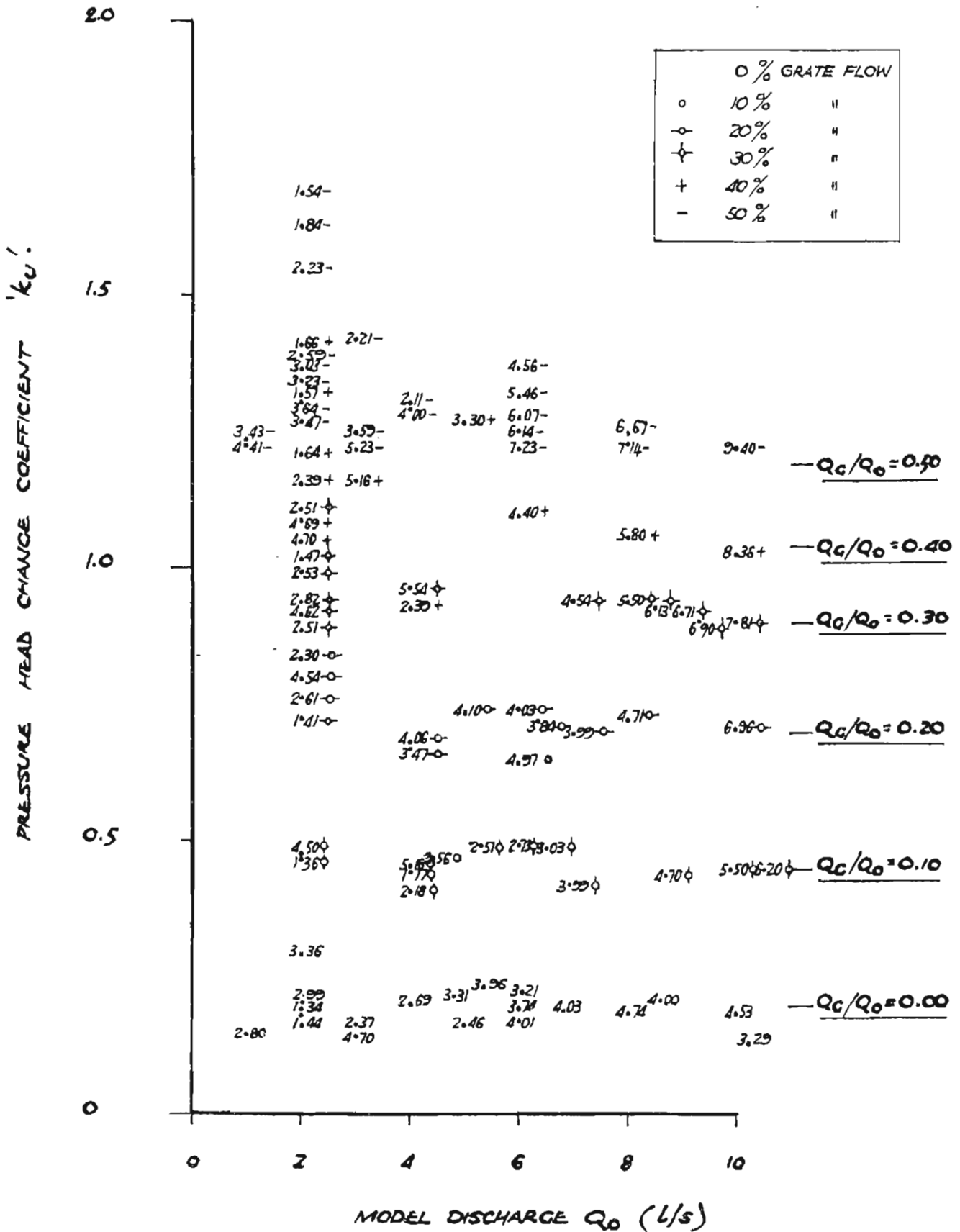


FIGURE A2 : DATA PLOT FOR MODEL NO. 1.

WATER SURFACE ELEVATION COEFFICIENT VS DISCHARGE  $Q_0$ .

$\theta = 0^\circ$ ,  $D_0 = 70$  MM,  $D_U = 70$  MM,  $A_0/A_u = 1.00$

(FIGURES INDICATE SUBMERGENCE RATIOS)

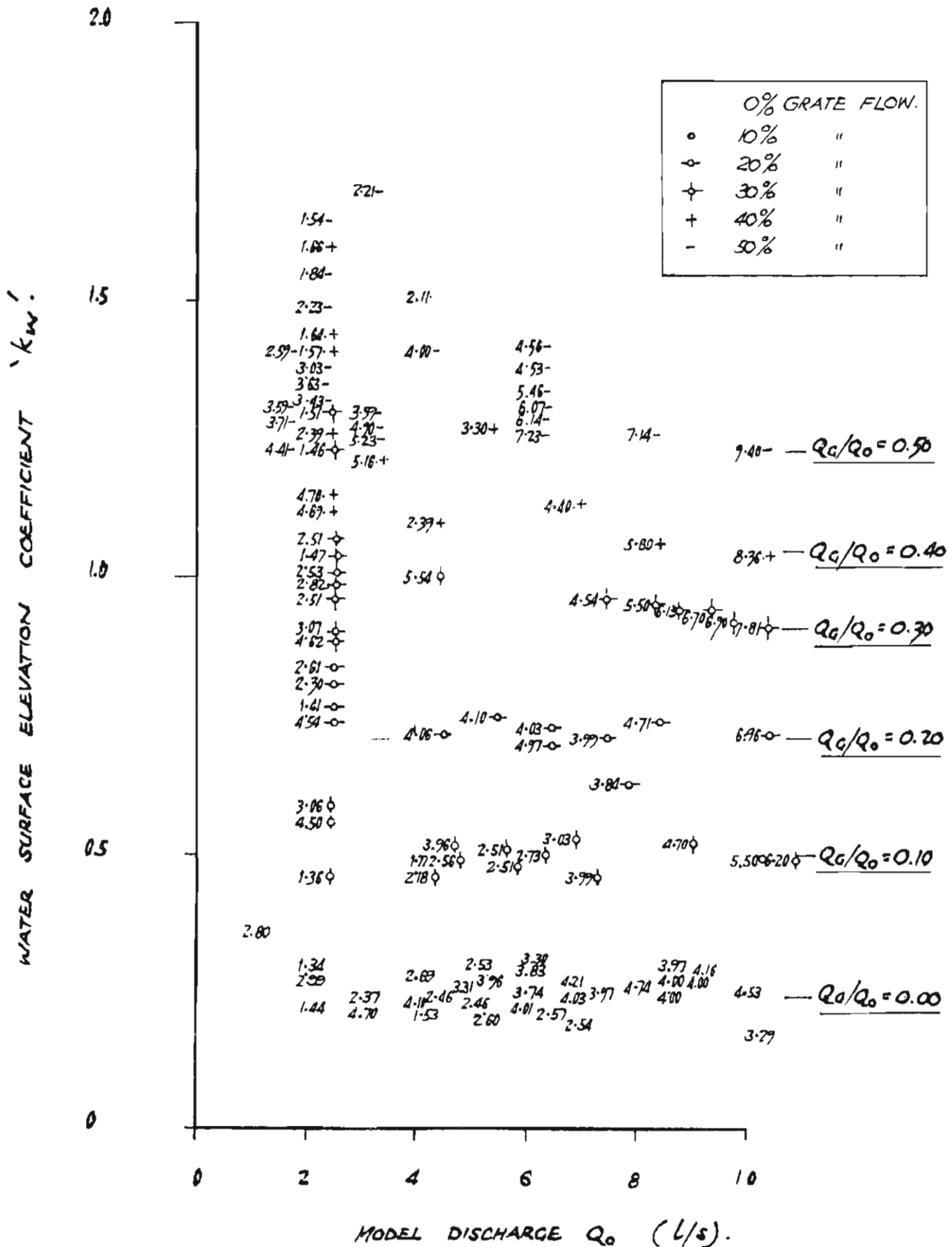




FIGURE A3: DATA PLOT FOR MODEL NO. 2.

PRESSURE HEAD CHANGE COEFFICIENT VS. DISCHARGE  $Q_0$ .

$\theta = 22\frac{1}{2}^\circ$ ,  $D_0 = 70$  MM,  $D_u = 70$  MM,  $A_0/A_u = 1.00$

(FIGURES INDICATE SUBMERGENCE RATIOS.)

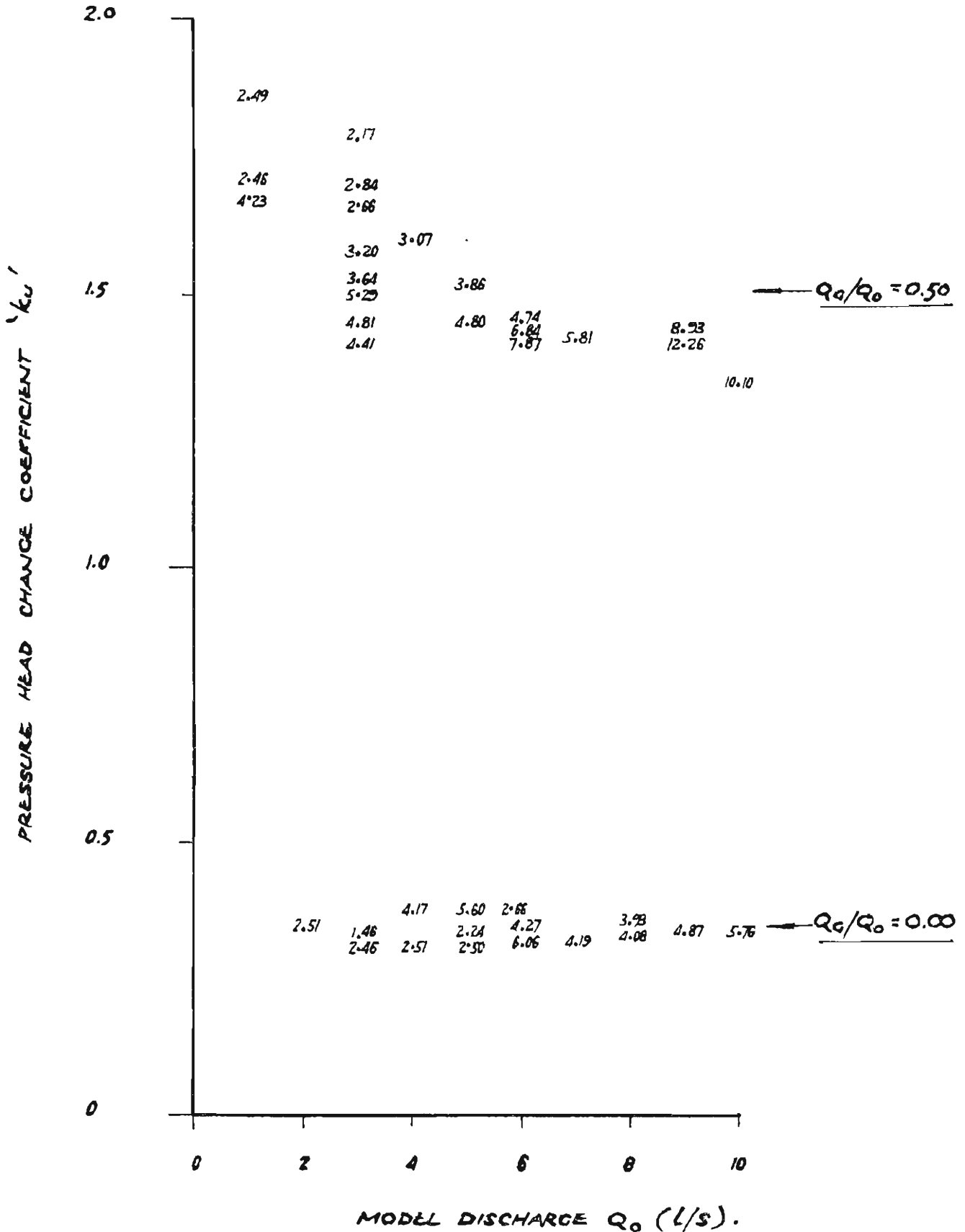


FIGURE A4: DATA PLOT FOR MODEL NO. 2.

WATER SURFACE ELEVATION COEFFICIENT VS DISCHARGE  $Q_0$ .

$\Theta = 22\frac{1}{2}^\circ$ ,  $D_0 = 70$  MM,  $D_u = 70$  MM,  $A_0/A_u = 1.00$ .

(FIGURES INDICATE SUBMERGENCE RATIOS.)

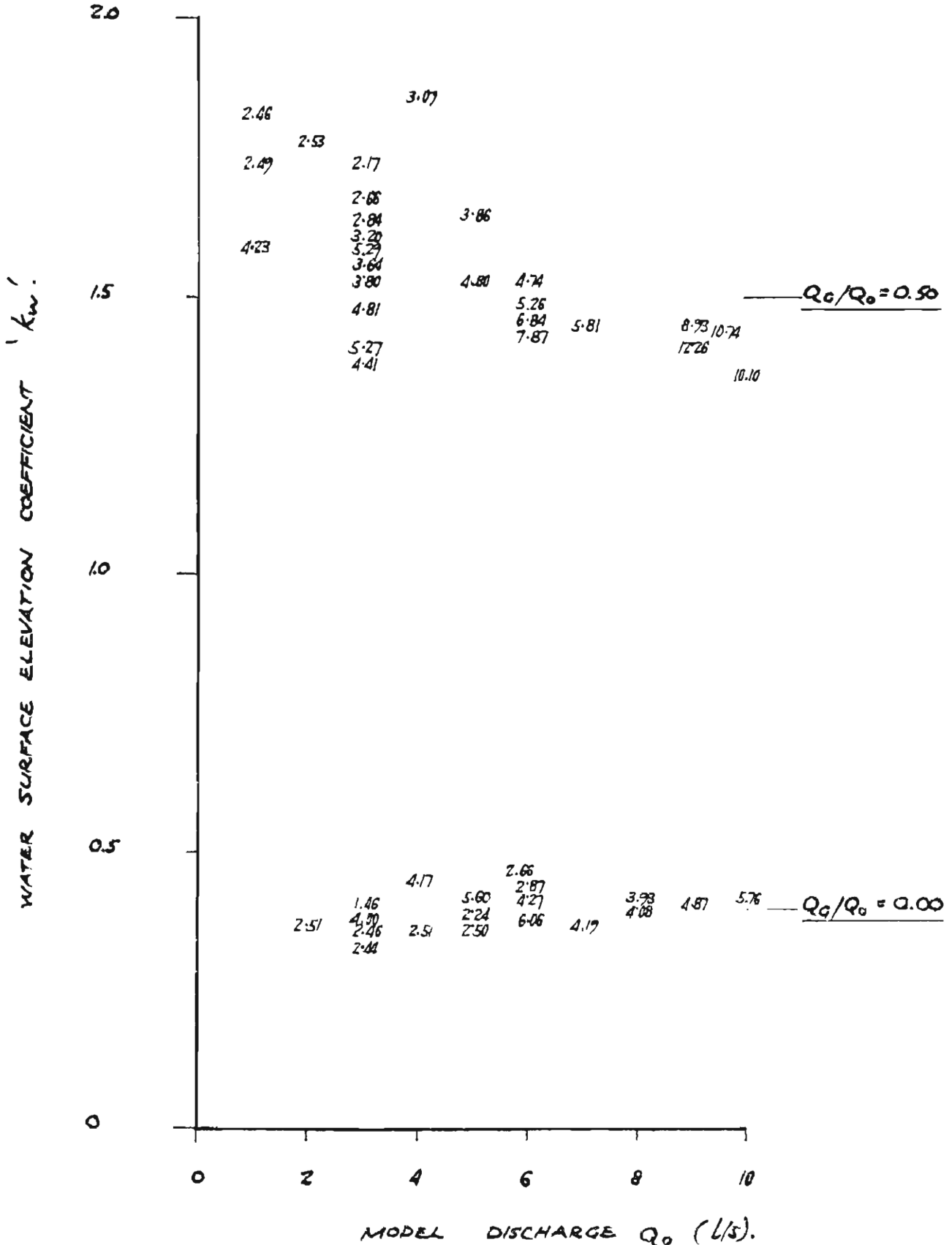


FIGURE A5: DATA PLOT FOR MODEL NO. 3.

PRESSURE HEAD CHANGE COEFFICIENT VS. DISCHARGE

$\theta = 45^\circ$ ,  $D_0 = 70$  MM,  $D_u = 70$  MM  $A_0/A_u = 1.0$

(FIGURES INDICATE SUBMERGENCE RATIOS).

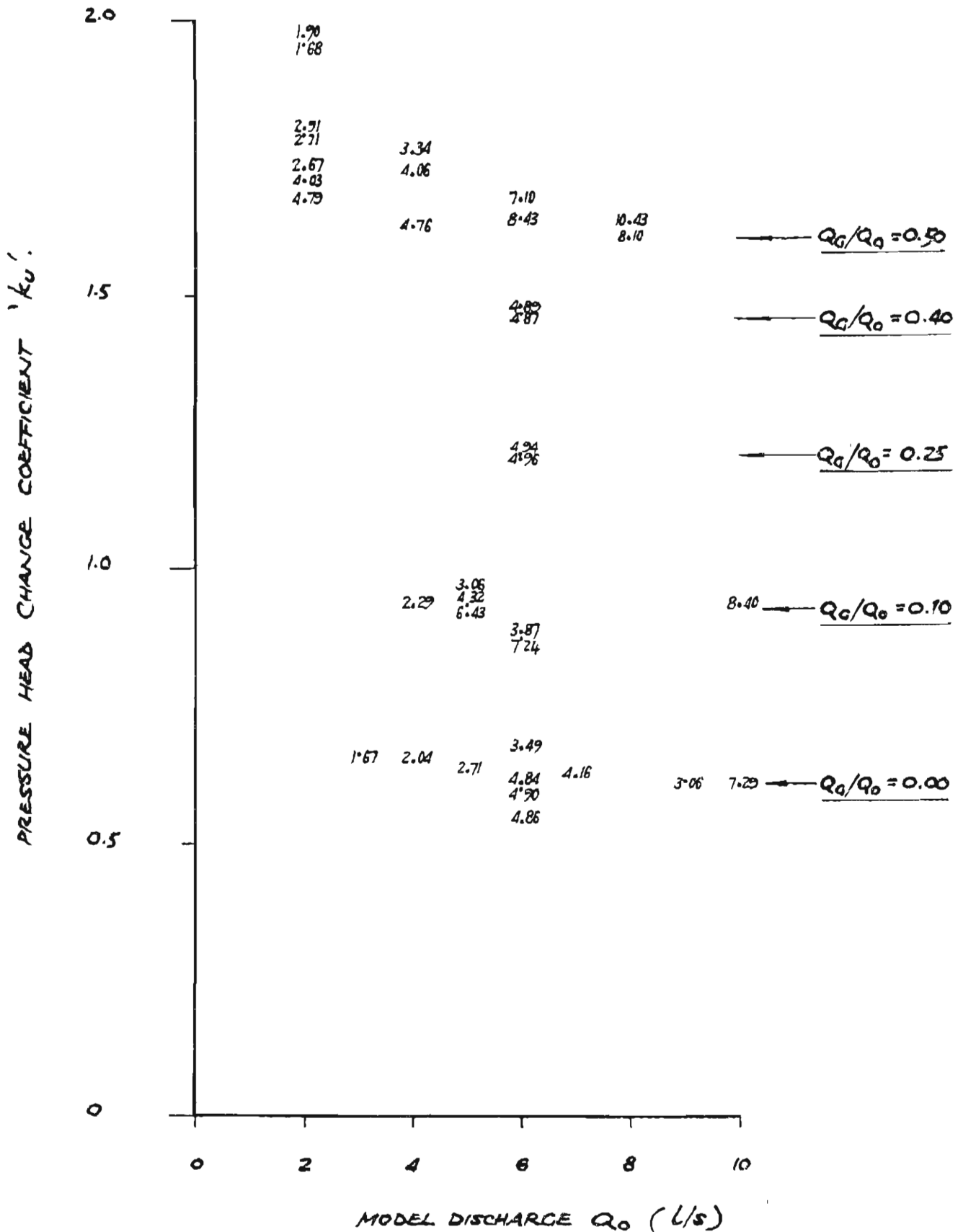


FIGURE A6: DATA PLOT FOR MODEL NO. 3

WATER SURFACE ELEVATION COEFFICIENT ' $K_w$ ' VERSUS DISCHARGE  $Q_0$ .

$\theta = 45^\circ$ ,  $D_u = 70$  MM,  $D_d = 70$  MM,  $A_0/A_u = 1.00$ .

(FIGURES INDICATE SUBMERGENCE RATIOS).

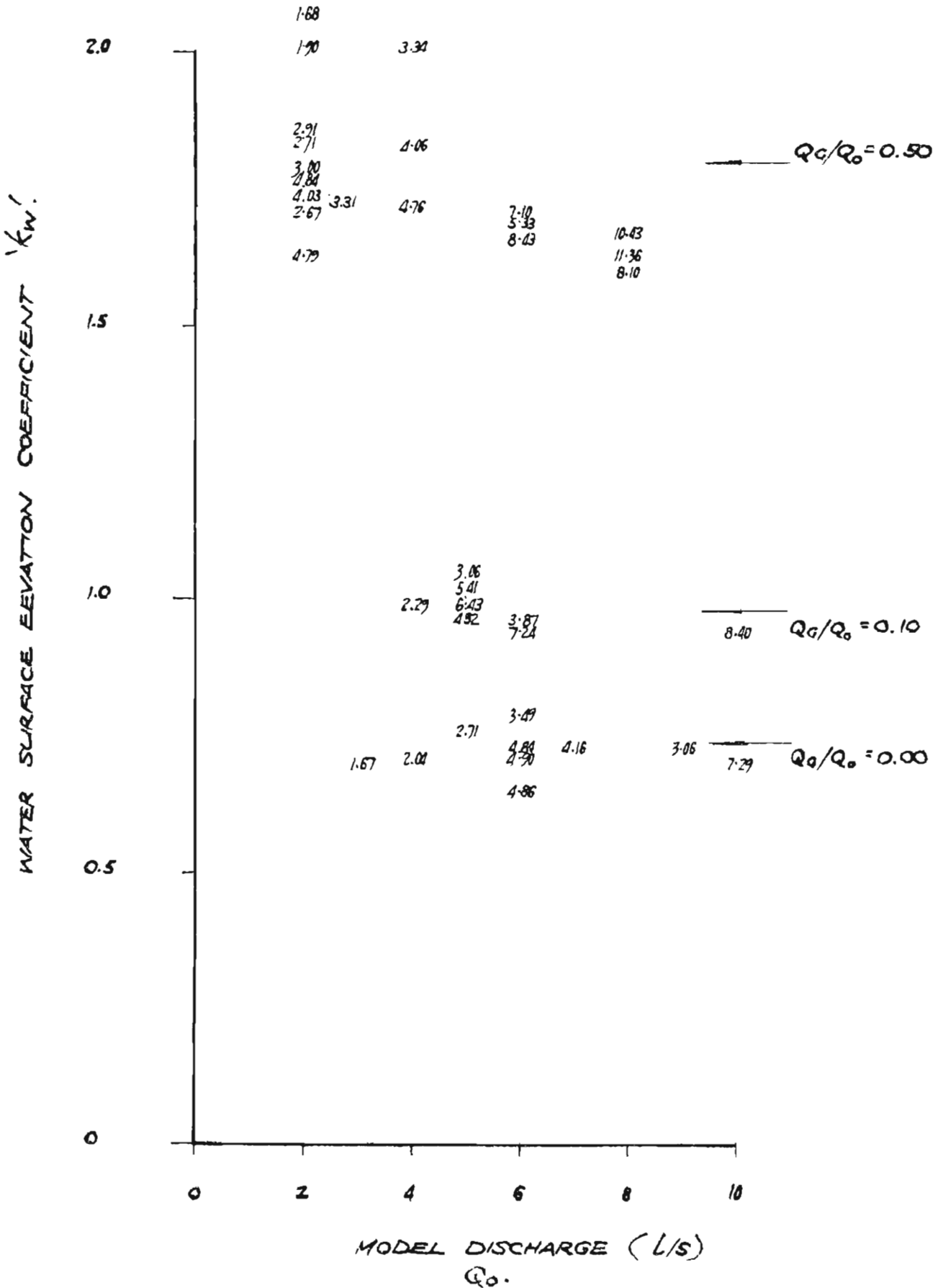


FIGURE A7: DATA PLOT FOR MODEL NO. 4.

PRESSURE HEAD CHANGE COEFFICIENT VS DISCHARGE  $Q_0$ .

$\theta = 45^\circ$ ,  $D_0 = 70 \text{ MM}$ ,  $D_u = 70 \text{ MM}$ ,  $A_0/A_u = 1.00$

(FIGURES INDICATE SUBMERGENCE RATIOS).

(- INDICATES  $Q_G/Q_0 = 0.50$ ).

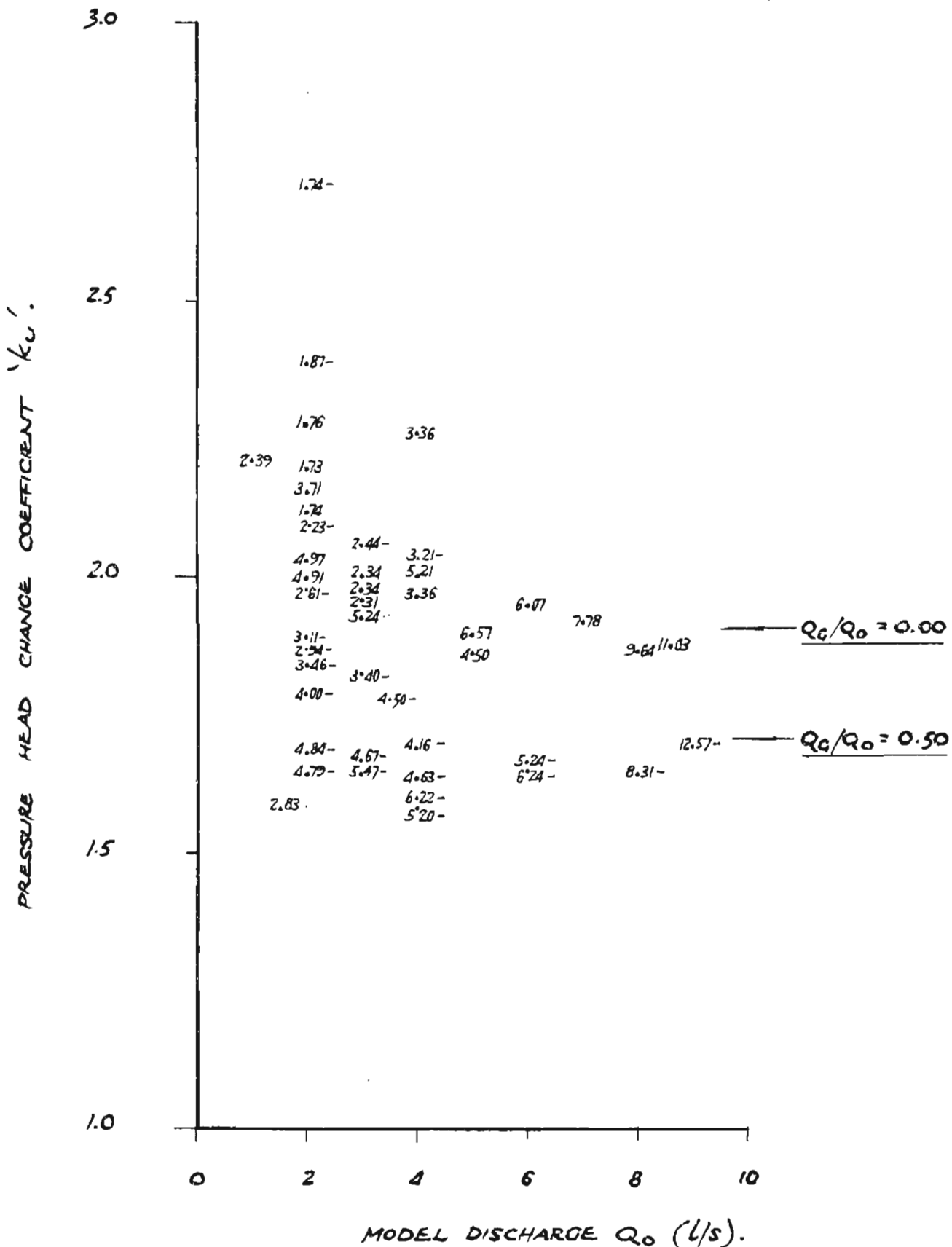


FIGURE A8: DATA PLOT FOR MODEL NO. 4

WATER SURFACE ELEVATION COEFFICIENT VS DISCHARGE  $Q_0$ .

$\Theta = 45^\circ$ ,  $D_0 = 70 \text{ MM}$ ,  $D_u = 70 \text{ MM}$ ,  $A_0/A_u = 1.00$

(FIGURES INDICATE SUBMERGENCE RATIOS)

(- INDICATES  $Q_0/Q_0 = 0.50$ .)

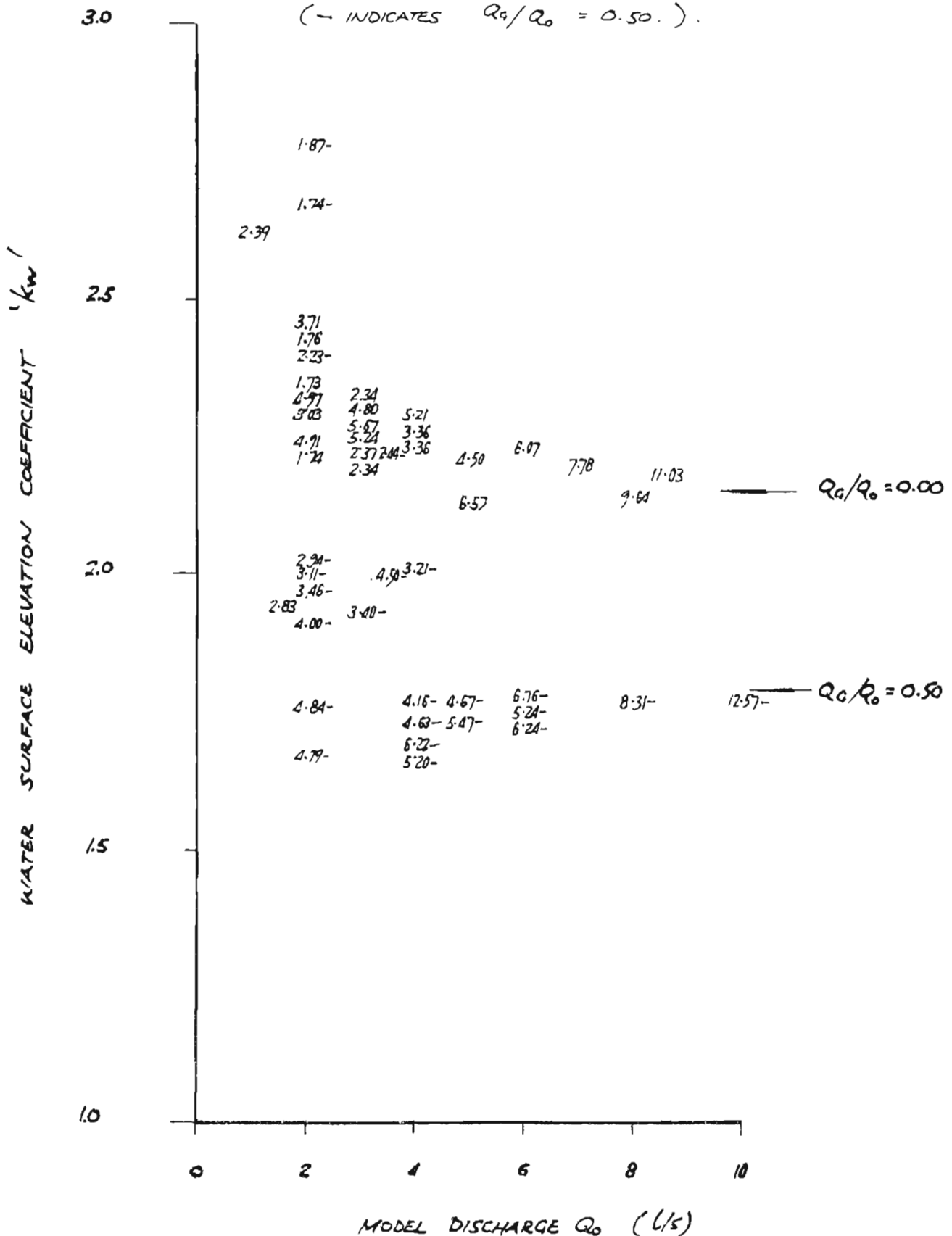


FIGURE A9: DATA PLOT FOR MODEL NO. 5.

PRESSURE HEAD CHANGE COEFFICIENT VS DISCHARGE  $Q_0$ .

$\theta = 67\frac{1}{2}^\circ$ ,  $D_0 = 70$  MM,  $D_1 = 70$  MM,  $A_0/A_1 = 1.00$

(FIGURES INDICATE SUBMERGENCE RATIOS).

(- INDICATES  $Q_C/Q_0 = 0.50$ ).

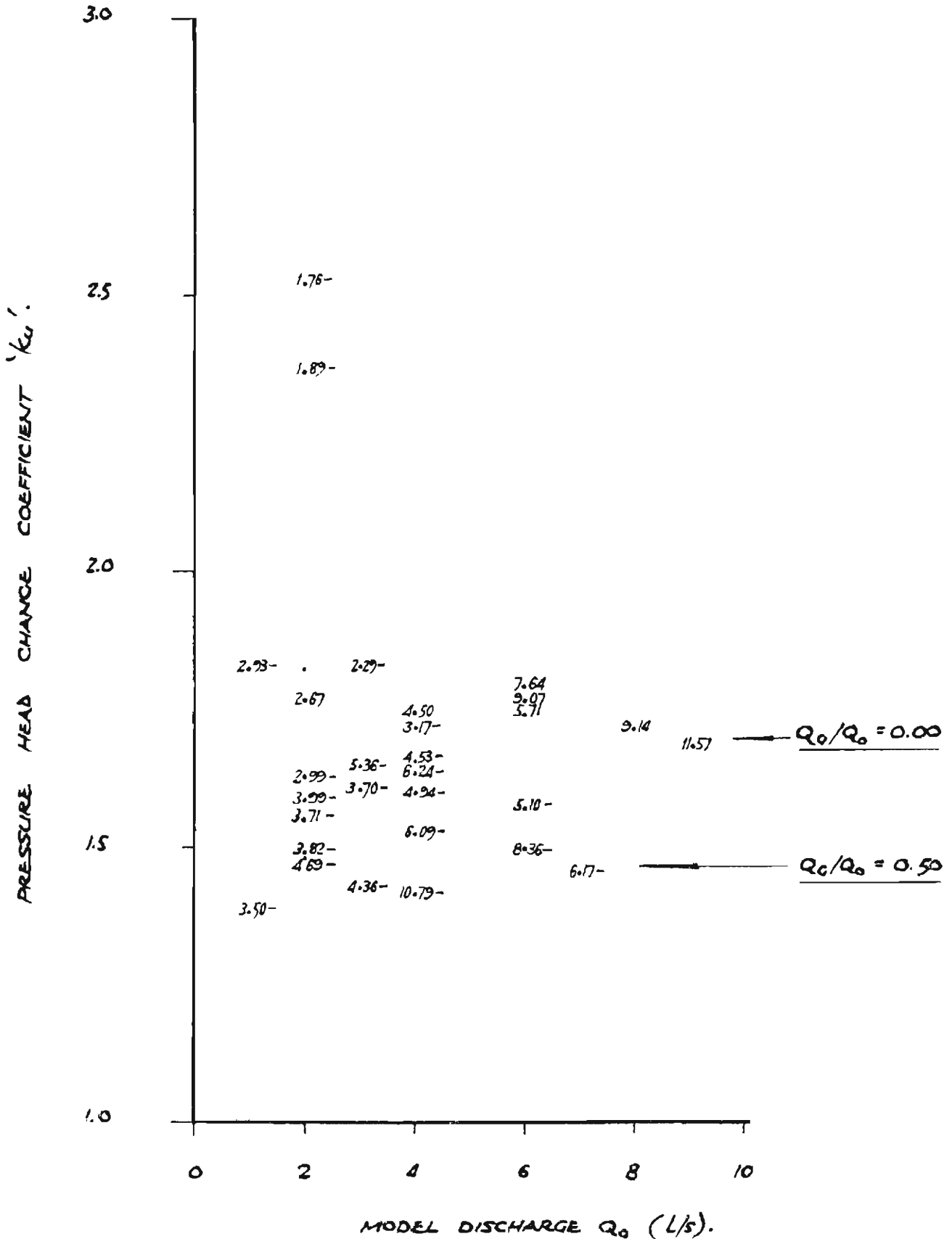


FIGURE A10: DATA PLOT FOR MODEL NO. 5

WATER SURFACE ELEVATION COEFFICIENT VS. DISCHARGE  $Q_0$ .

$\theta = 67\frac{1}{2}^\circ$ ,  $D_0 = 70 \text{ MM}$ ,  $D_U = 70 \text{ MM}$ ,  $A_0/A_u = 1.00$ .

(FIGURES INDICATE SUBMERGENCE RATIOS)

(- INDICATES  $Q_G/Q_0 = 0.50$ ).

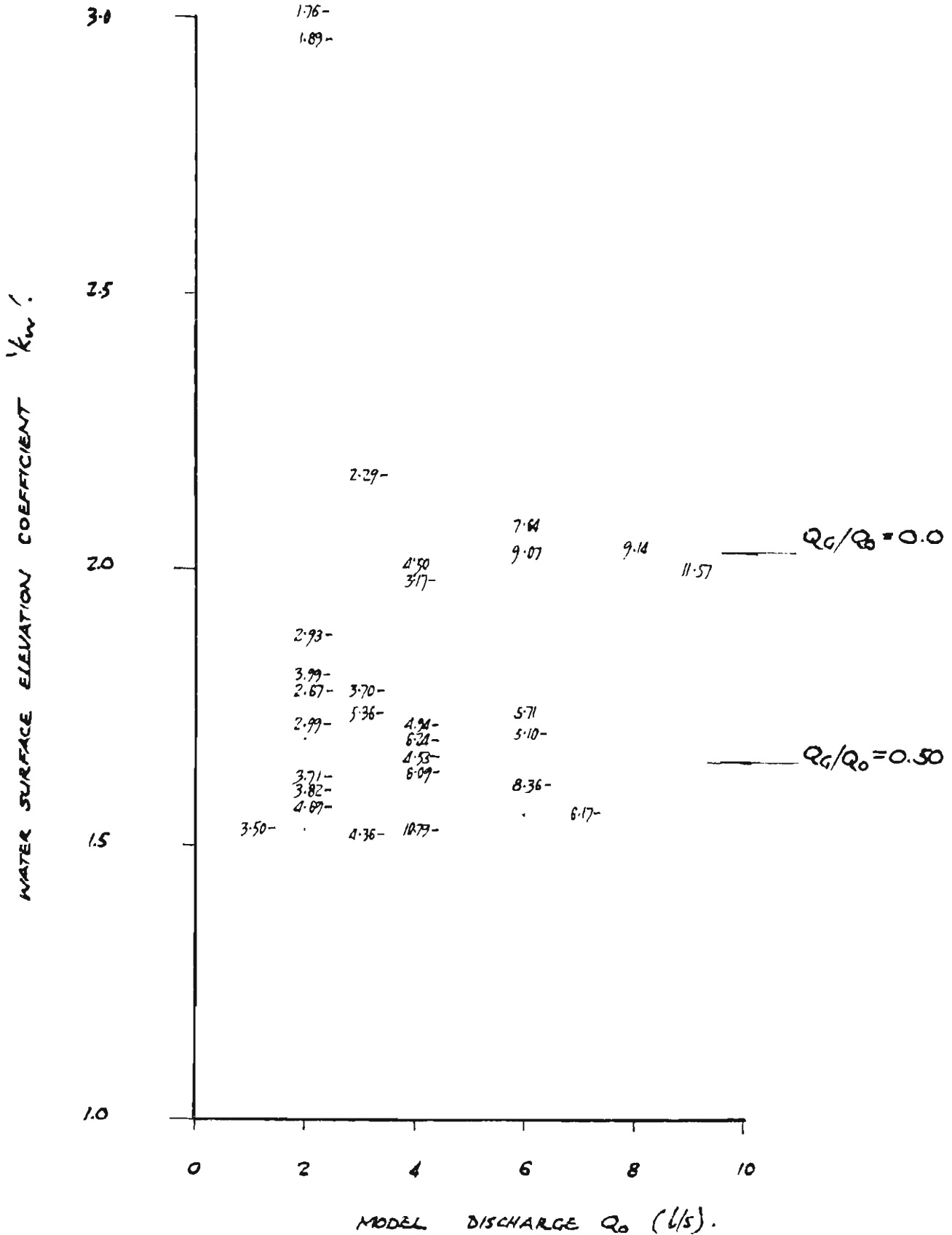




FIGURE A11: DATA PLOT FOR MODEL NO. 6

PRESSURE HEAD CHANGE COEFFICIENT VS. DISCHARGE  $Q_0$ .

$\theta = 90^\circ$ ,  $D_0 = 70$  MM,  $D_u = 70$  MM,  $A_0/A_u = 1.00$

(FIGURES INDICATE SUBMERGENCE RATIOS).

(- INDICATES  $Q_0/Q_0 = 0.50$ ).

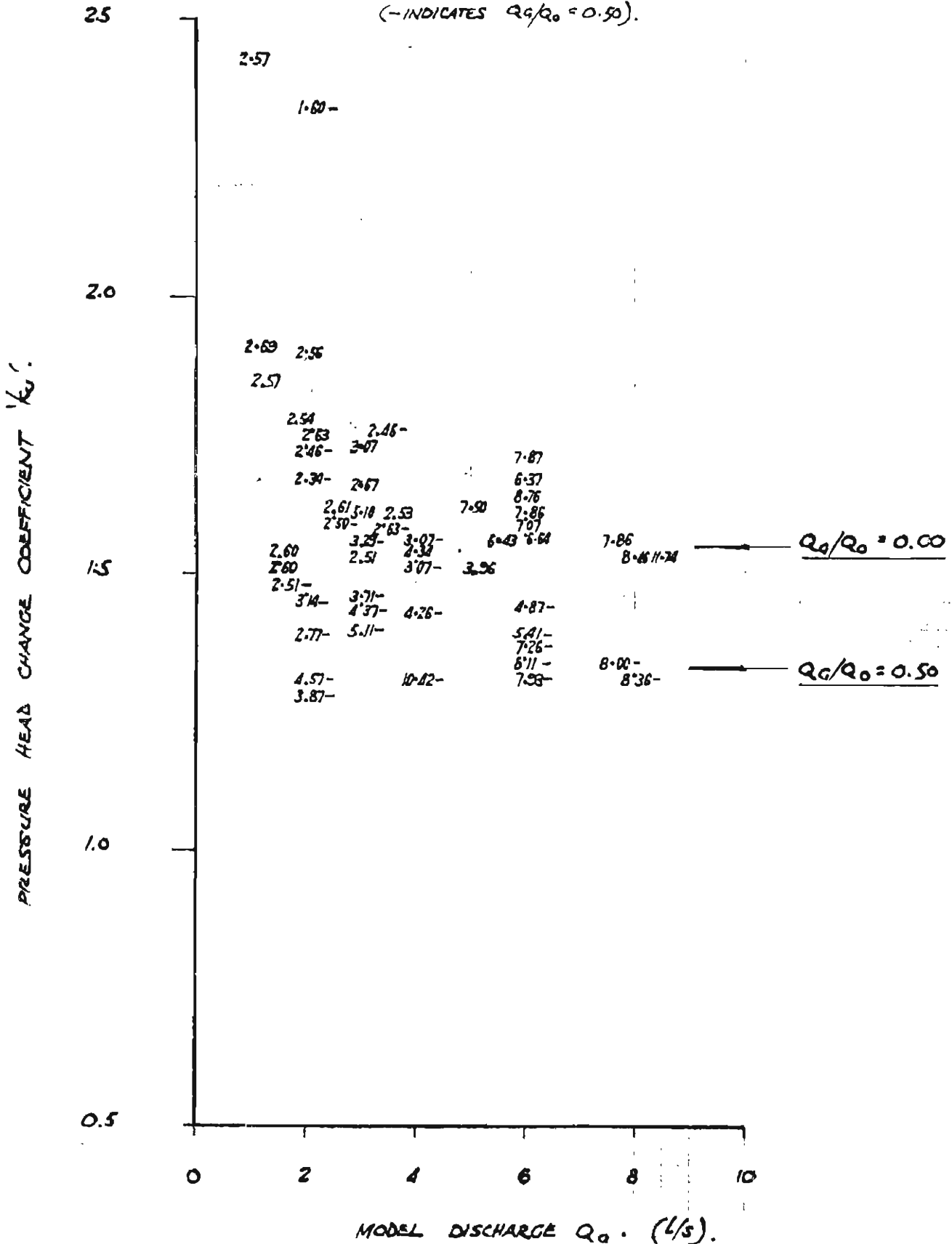


FIGURE A12 : DATA PLOT FOR MODEL NO: 6

WATER SURFACE ELEVATION COEFFICIENT ' $k_w$ ' VS DISCHARGE  $Q_0$ .

$\theta = 90^\circ$ ,  $D_u = 70 \text{ MM}$ ,  $D_o = 70 \text{ MM}$ ,  $A_o/A_u = 1.00$ .

(FIGURES INDICATE SUBMERGENCE RATIOS)  
 (- INDICATES  $Q_c/Q_0 = 0.50$ ).

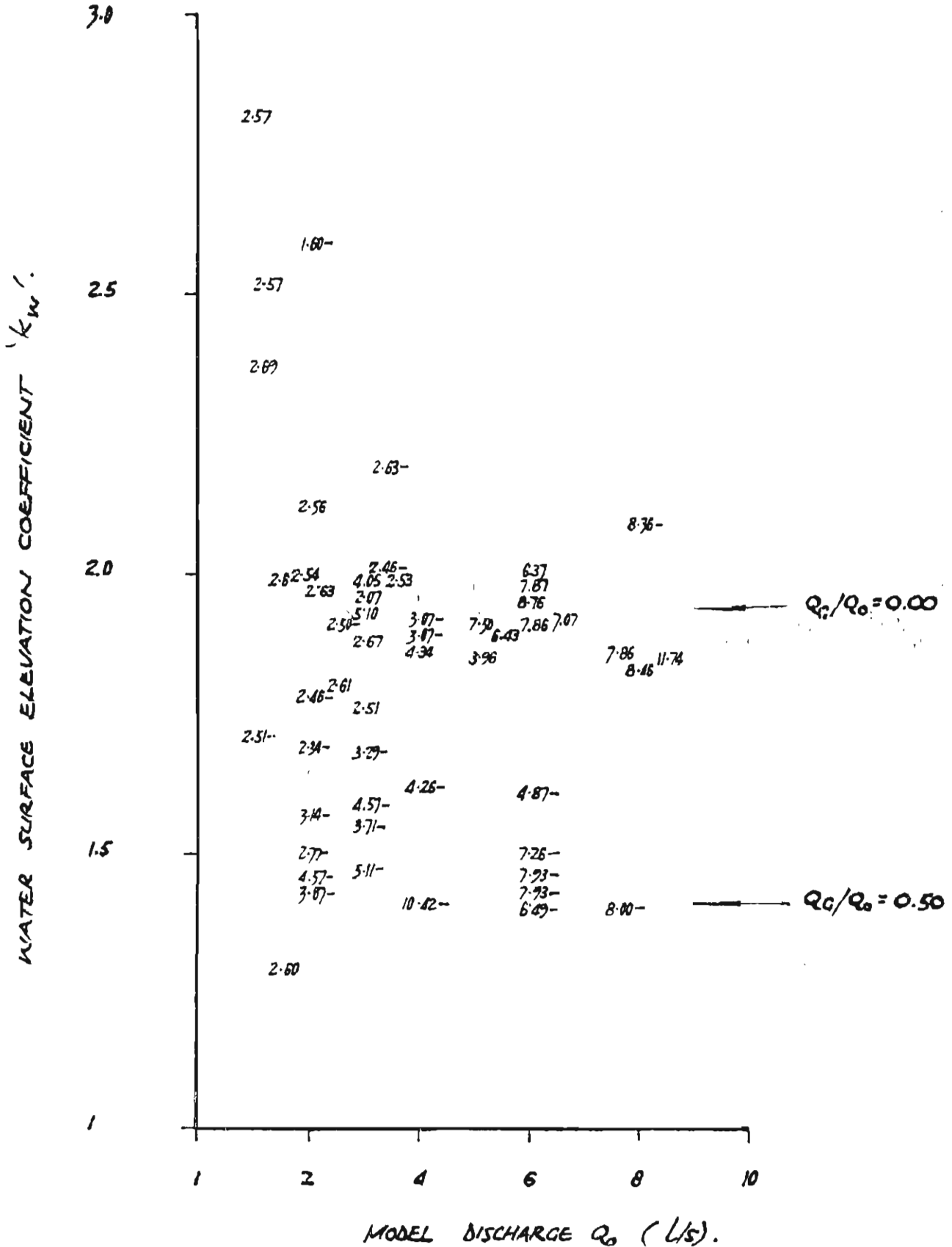


FIGURE A13: DATA PLOT FOR MODEL NO. 7.

PRESSURE HEAD CHANGE COEFFICIENT  $k_u$  VS. DISCHARGE  $Q_0$ .

$\theta = 0^\circ$ ,  $D_0 = 94 \text{ MM}$ ,  $D_u = 70 \text{ MM}$ ,  $A_0/A_u = 1.803$

(FIGURES INDICATE SUBMERGENCE RATIOS).

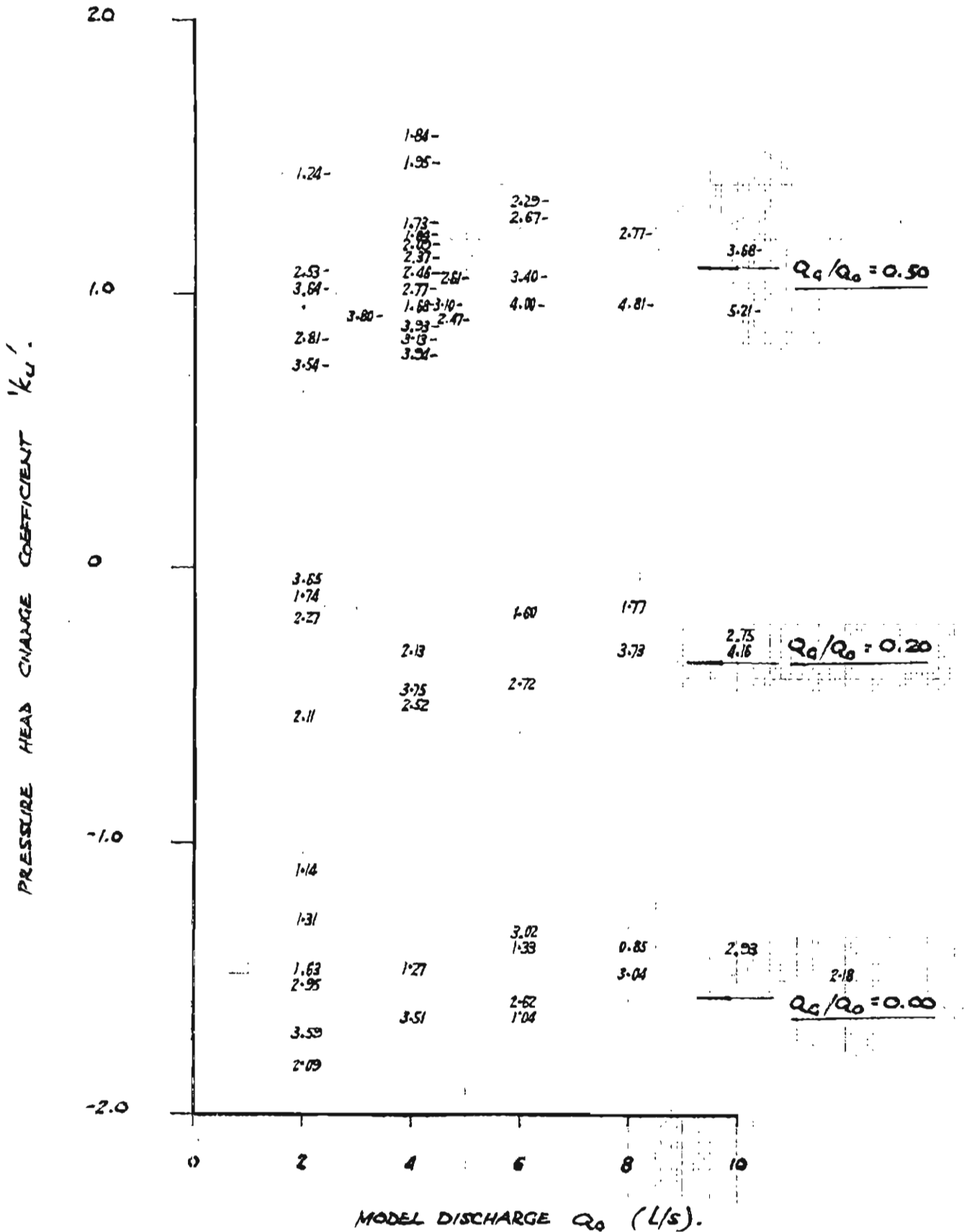


FIGURE A14: DATA PLOT FOR MODEL NO. 7.

WATER SURFACE ELEVATION COEFFICIENT VS. DISCHARGE  $Q_0$ .

$\theta = 0^\circ$ ,  $D_0 = 94 \text{ MM}$ ,  $D_U = 70 \text{ MM}$ ,  $A_0/A_u = 1.803$ .

(FIGURES INDICATE SUBMERGENCE RATIOS).

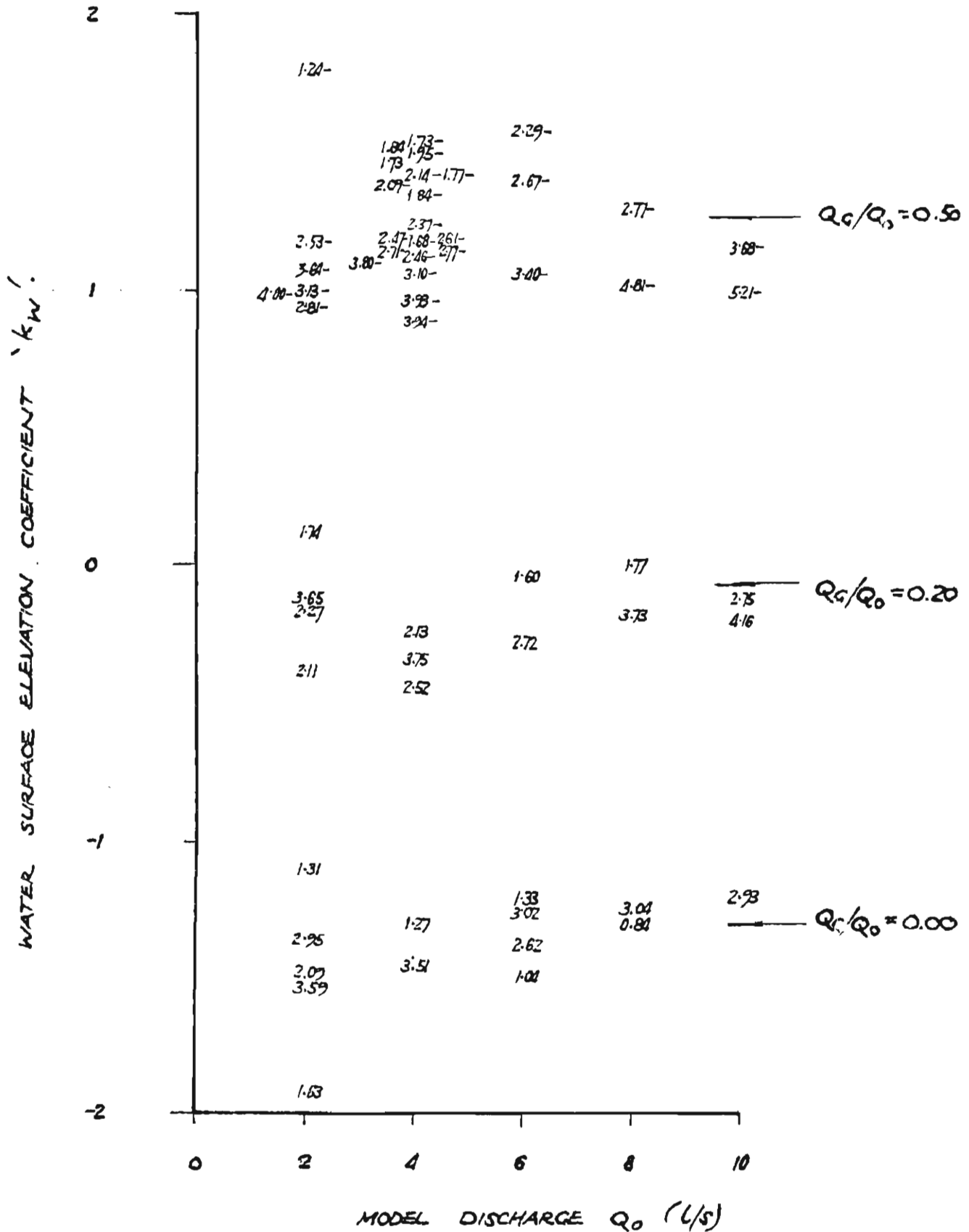


FIGURE A15: DATA PLOT FOR MODEL NO. 8.

PRESSURE HEAD CHANGE COEFFICIENT VS. DISCHARGE  $Q_0$ .

$\theta = 22\frac{1}{2}^\circ$ ,  $D_0 = 94 \text{ MM}$ ,  $D_u = 70 \text{ MM}$ ,  $A_0/A_u = 1.803$

(FIGURES INDICATE SUBMERGENCE RATIOS).

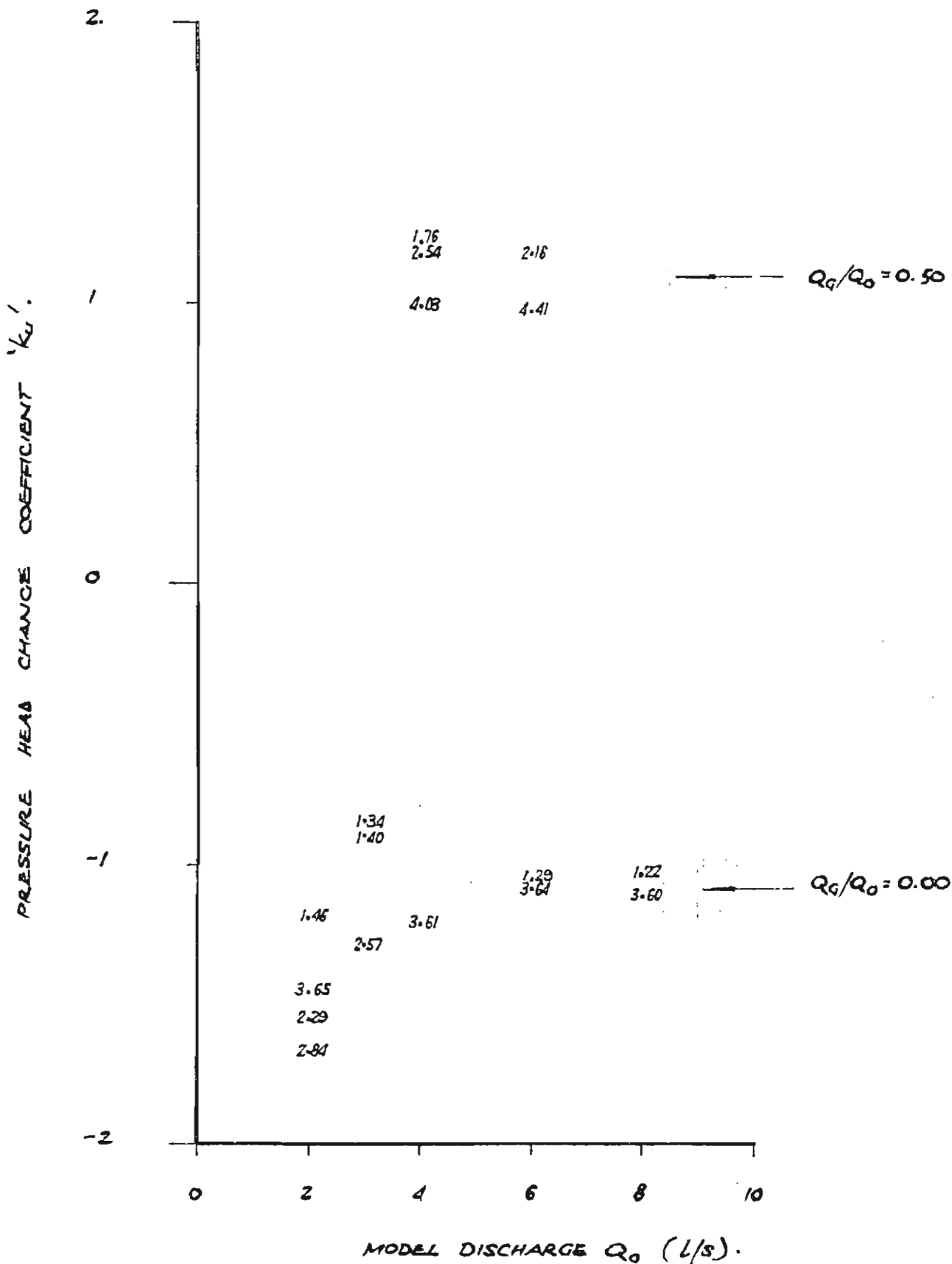


FIGURE A16: DATA PLOT FOR MODEL NO. 8

WATER SURFACE ELEVATION COEFFICIENT ' $k_w$ ' VS DISCHARGE  $Q_0$ .

$\Theta = 22\frac{1}{2}^\circ$ ,  $D_u = 70\text{MM}$ ,  $D_o = 91\text{MM}$ ,  $A_o/A_u = 1.803$ .

(FIGURES INDICATE SUBMERGENCE RATIOS)

(- INDICATES  $Q_c/Q_0 = 0.50$ )

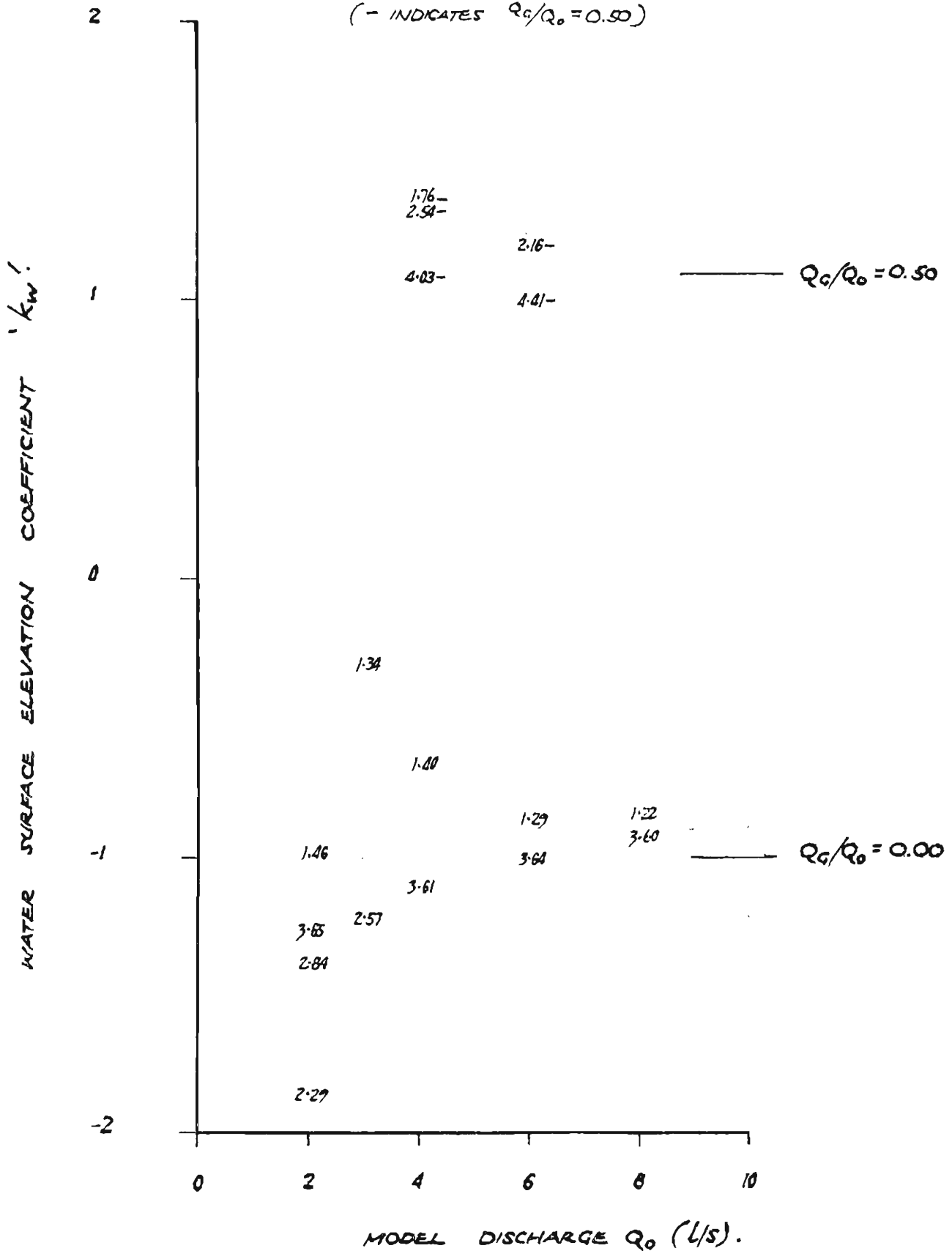


FIGURE A17: DATA PLOT FOR MODEL NO. 9

PRESSURE HEAD CHANGE COEFFICIENTS VS DISCHARGE  $Q_0$ .

$\theta = 45^\circ$ ,  $D_u = 70\text{MM}$ ,  $D_o = 94\text{MM}$ ,  $A_o/A_u = 1.803$ .

(FIGURES INDICATE SUBMERGENCE RATIOS).

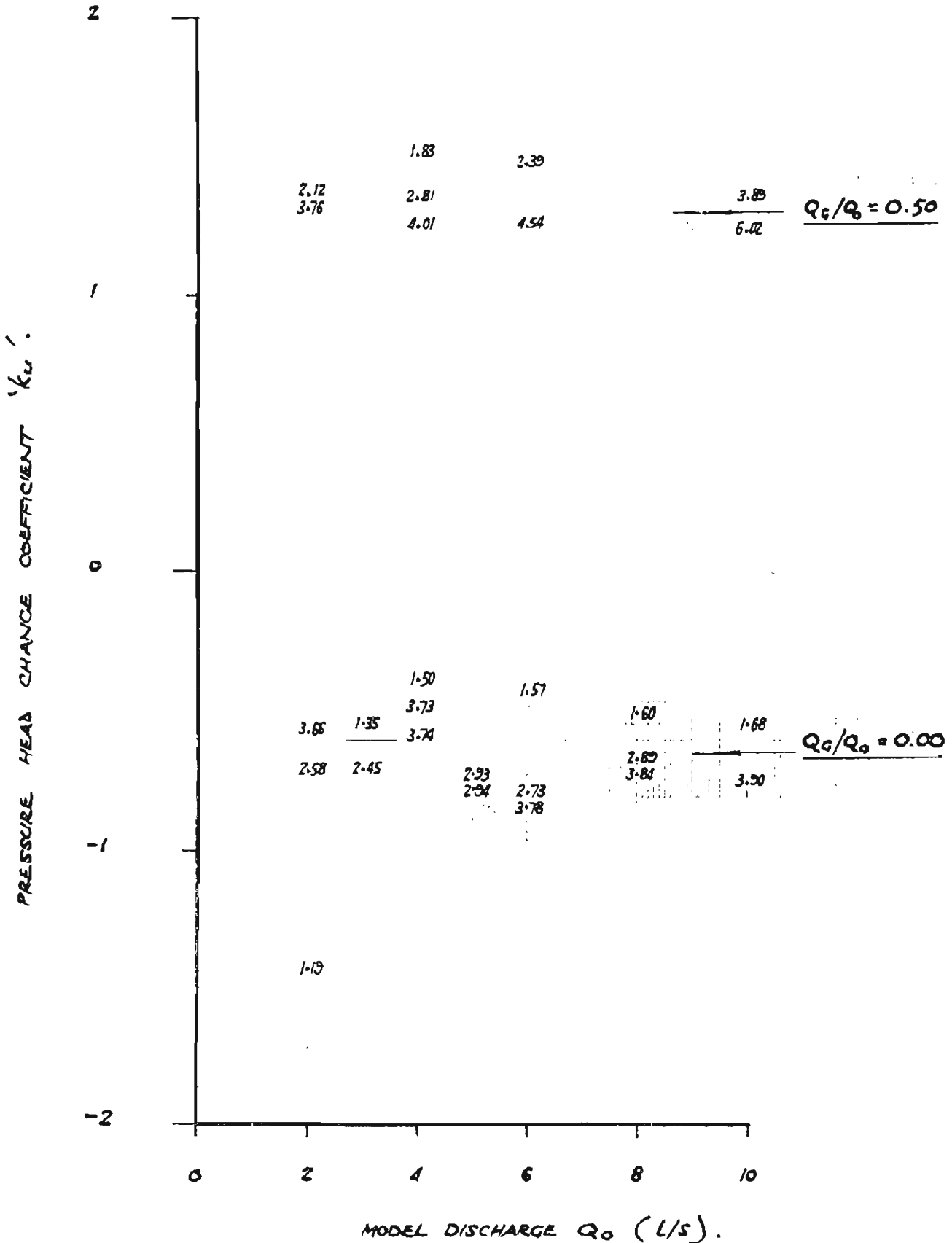


FIGURE A18 : DATA PLOT FOR MODEL NO. 9.

WATER SURFACE ELEVATION COEFFICIENT 'k<sub>w</sub>' VS DISCHARGE Q<sub>0</sub>

$\theta = 45^\circ, D_u = 70 \text{ MM } D_o = 94 \text{ MM } A_o/A_u = 1.803$

(FIGURES INDICATE SUBMERGENCE RATIOS).

(- INDICATES Q<sub>G</sub>/Q<sub>0</sub> = 0.50).

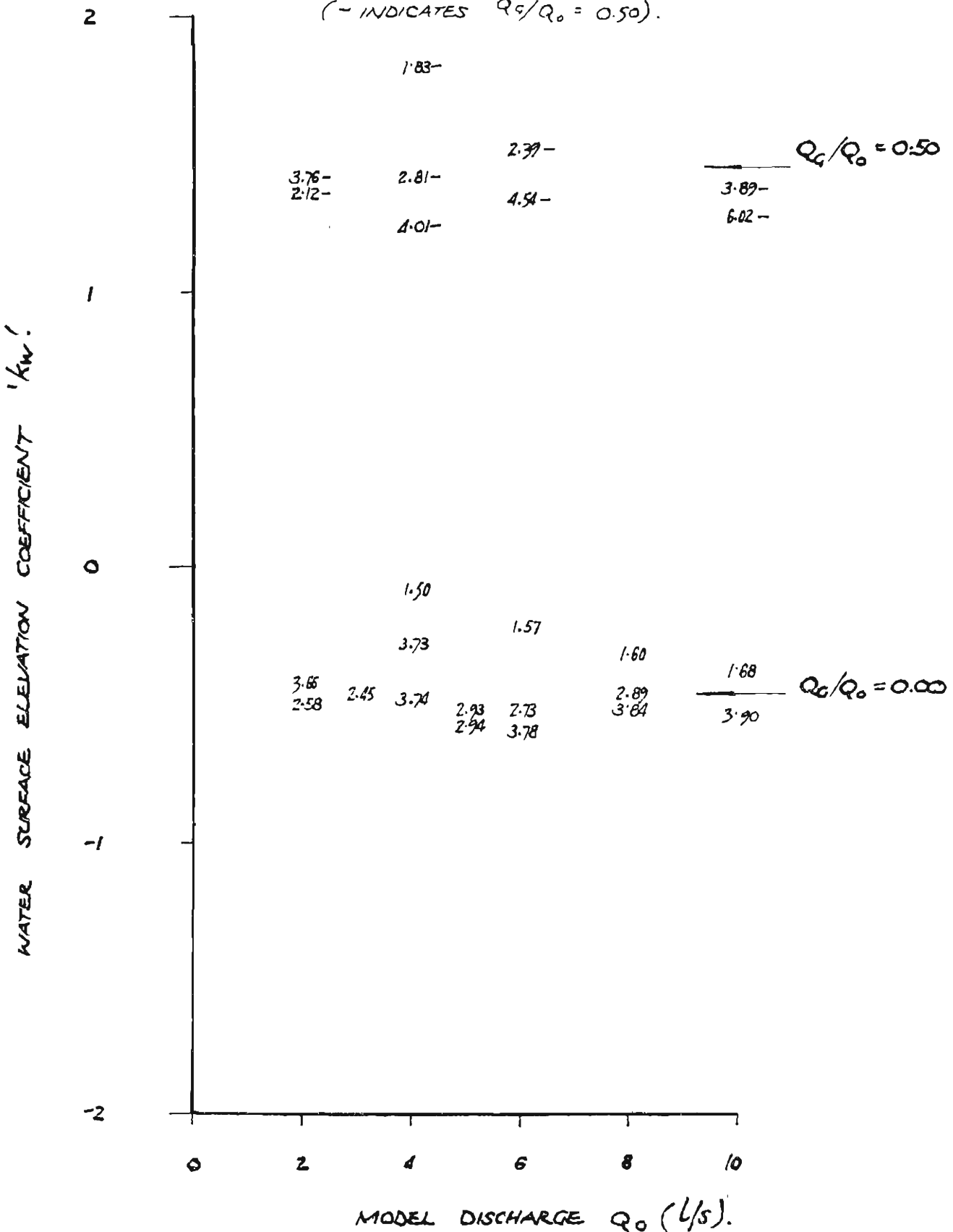




FIGURE A19: DATA PLOT FOR MODEL NO. 10

PRESSURE HEAD CHANGE COEFFICIENT VS. DISCHARGE  $Q_0$

$\Theta = 45^\circ$ ,  $D_u = 70 \text{ MM}$ ,  $D_o = 94 \text{ MM}$ ,  $A_o/A_u = 1.803$ .

(FIGURES INDICATE SUBMERGENCE RATIOS)

(- INDICATES  $Q_1/Q_0 = 0.50$ )

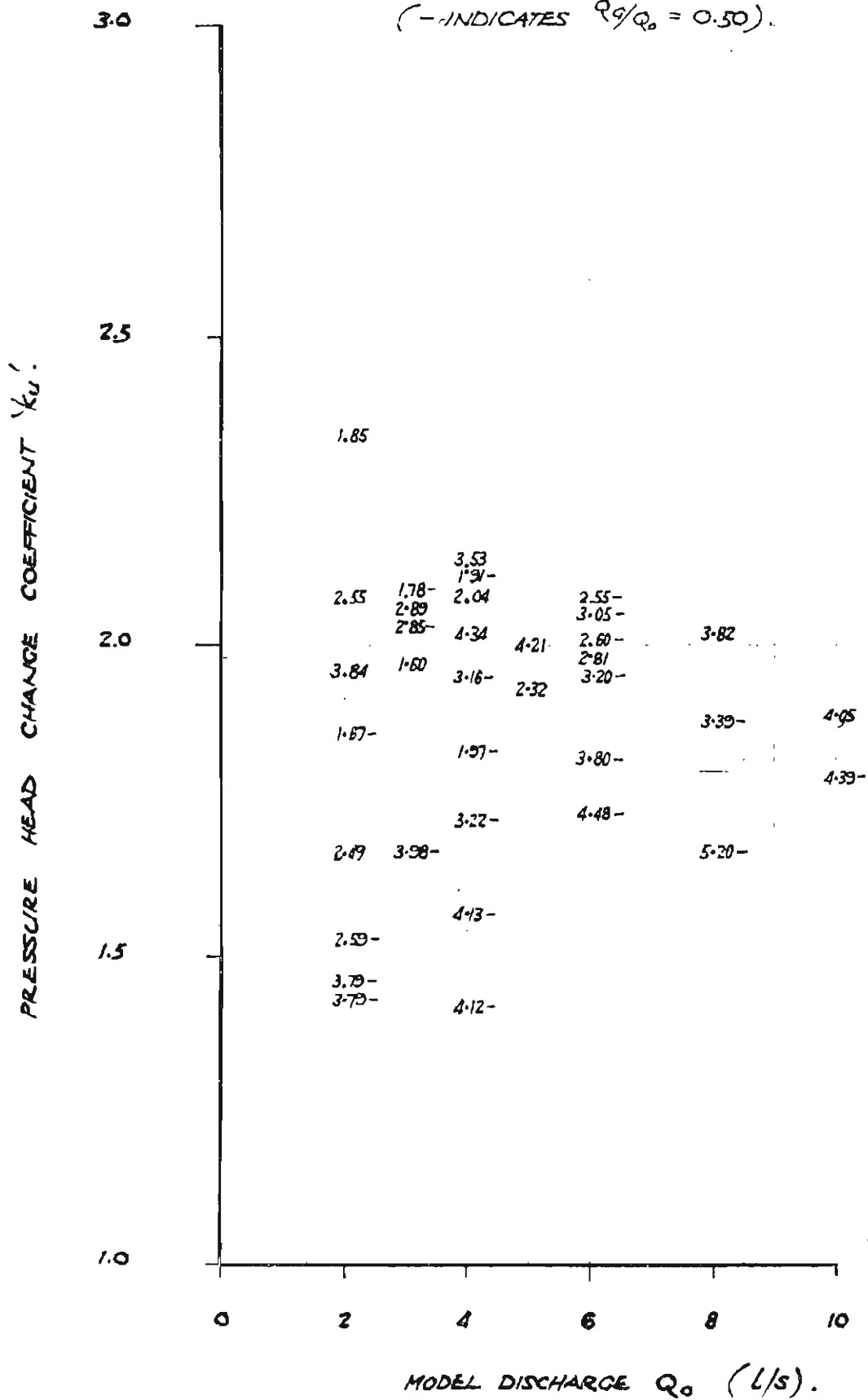


FIGURE A20 : DATA PLOT FOR MODEL NO. 10.WATER SURFACE ELEVATION COEFFICIENTS VS DISCHARGE  $Q_0$ .

$$\theta = 45^\circ, D_u = 70 \text{ MM}, D_o = 94 \text{ MM}, A_o/A_u = 1.803.$$

(FIGURES INDICATE SUBMERGENCE RATIOS)  
 (- INDICATES  $Q_c/Q_0 = 0.50$ )

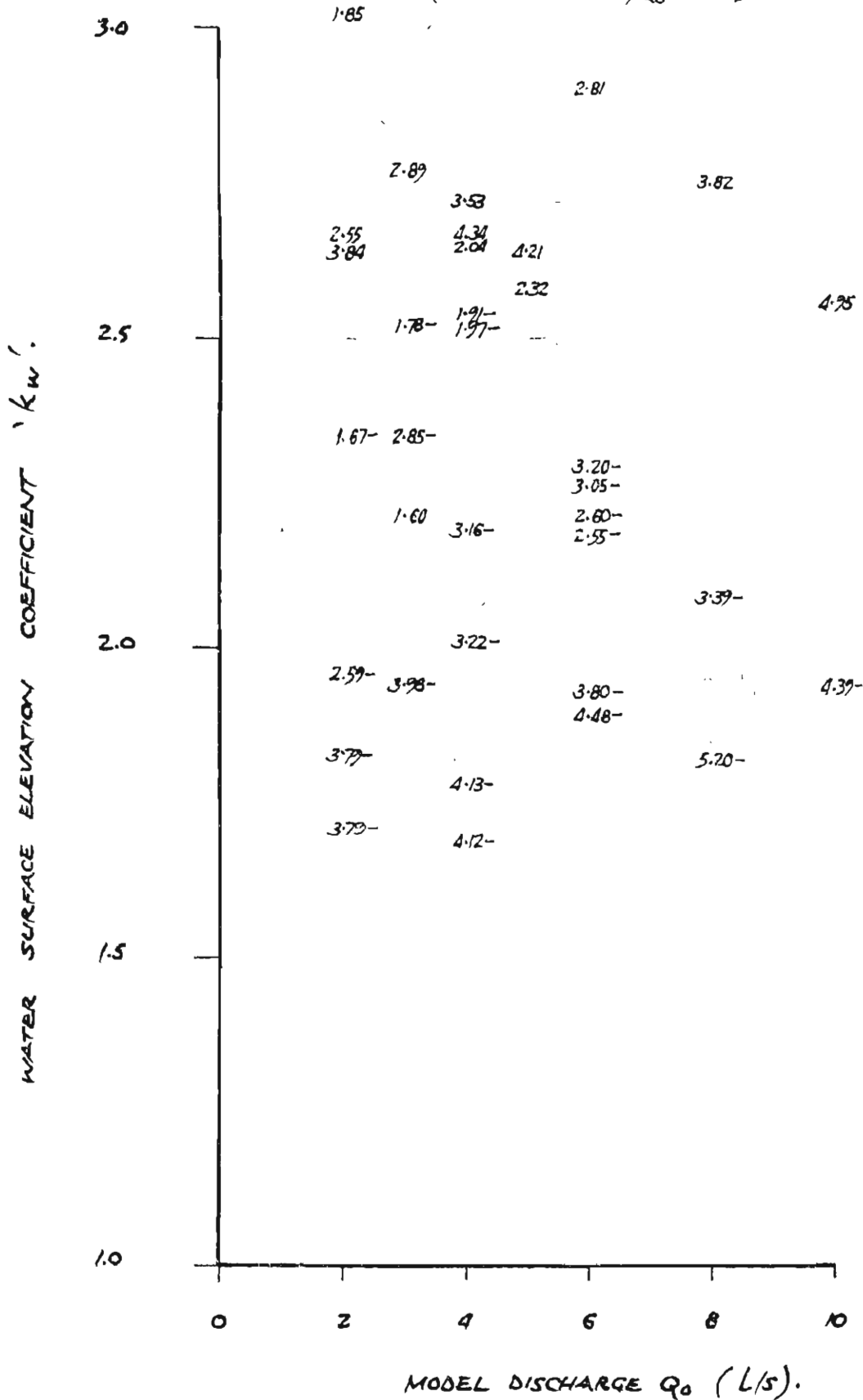


FIGURE A21: DATA PLOT FOR MODEL NO. 11.

PRESSURE HEAD CHANGE COEFFICIENT VS. DISCHARGE  $Q_0$ .

$\theta = 67\frac{1}{2}^\circ$ ,  $D_u = 70\text{MM}$ ,  $D_o = 91\text{MM}$ ,  $A_o/A_u = 1.803$ .

(FIGURES INDICATE SUBMERGENCE RATIOS).

(- INDICATES  $Q_c/Q_0 = 0.50$ ).

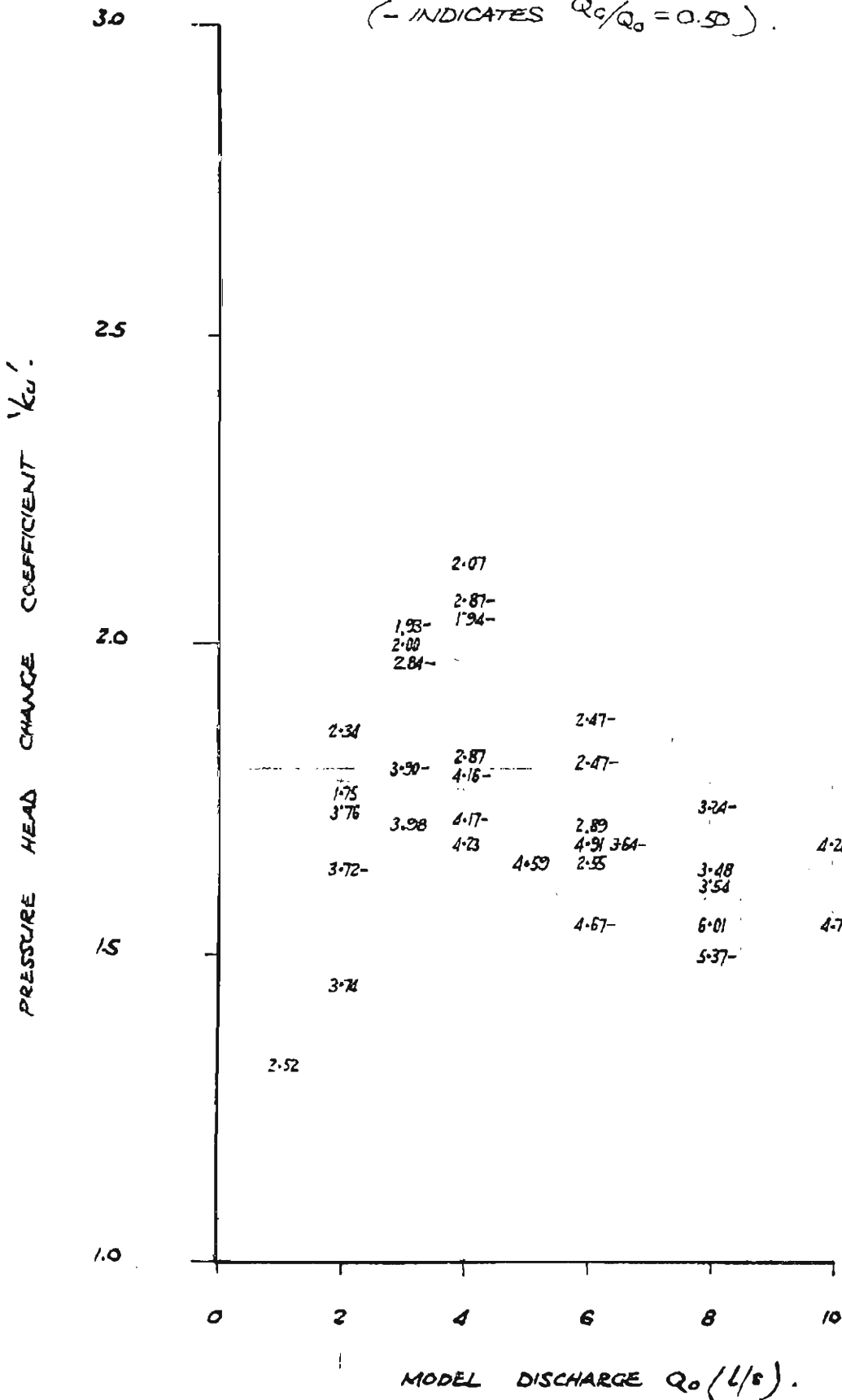


FIGURE A22 : DATA PLOT FOR MODEL NO.11

WATER SURFACE ELEVATION COEFFICIENT VS. DISCHARGE  $Q_0$ .

$\theta = 67\frac{1}{2}^\circ$ ,  $D_u = 70\text{MM}$ ,  $D_o = 94\text{MM}$ ,  $A_o/A_u = 1.803$

(FIGURES INDICATE SUBMERGENCE RATIOS).

(- INDICATES  $Q_G/Q_0 = 0.50$ ).

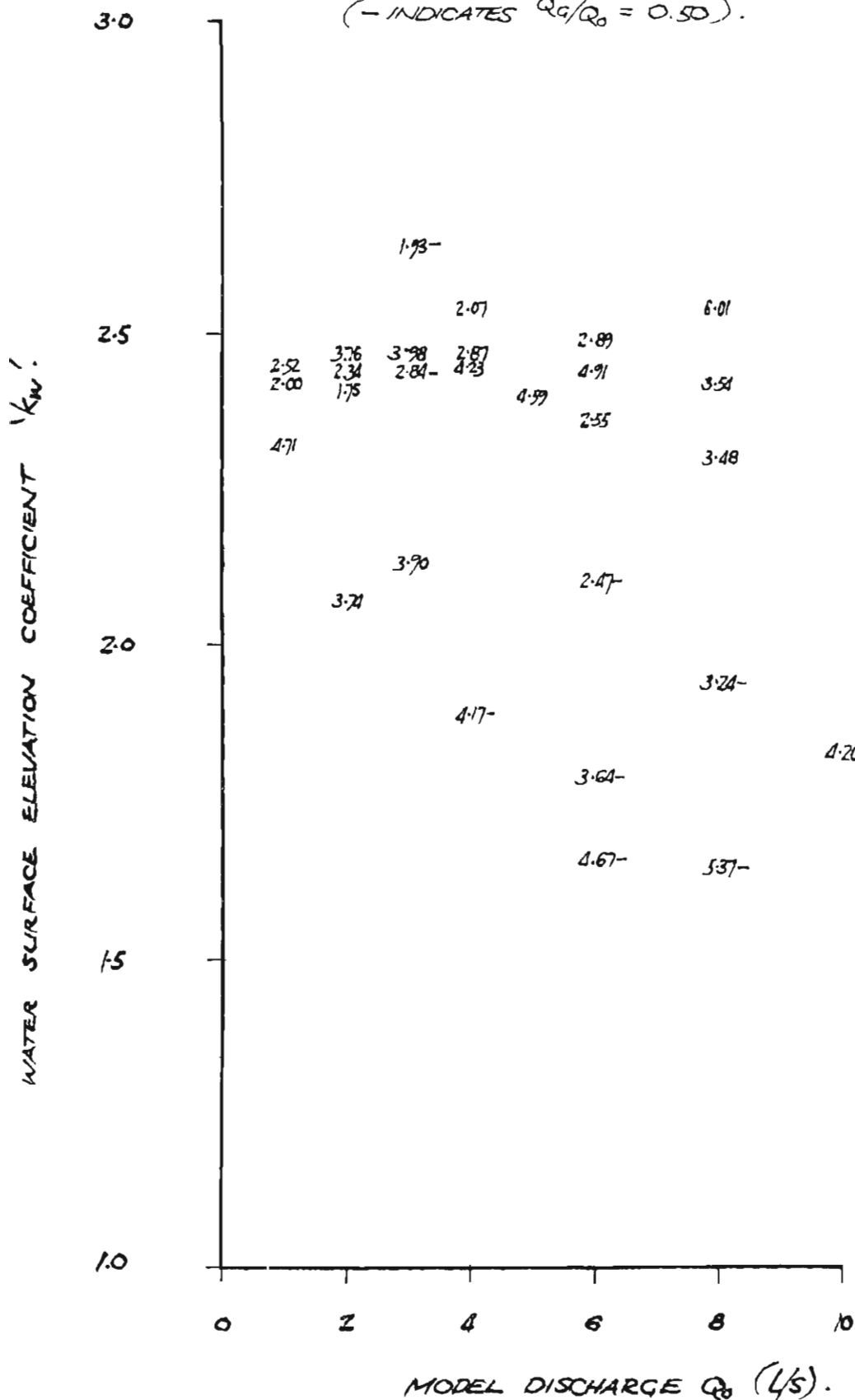


FIGURE A23 : DATA PLOT FOR MODEL NO. 12

PRESSURE HEAD CHANGE COEFFICIENT VS DISCHARGE  $Q_0$ .

$\theta = 90^\circ$ ,  $D_o = 94 \text{ MM}$ ,  $D_u = 70 \text{ MM}$ ,  $A_o/A_u = 1.803$ .

(FIGURES INDICATE SUBMERGENCE RATIOS)

(- INDICATES  $Q_0/Q_0 = 0.50$ )

(+ " " = 1.00)

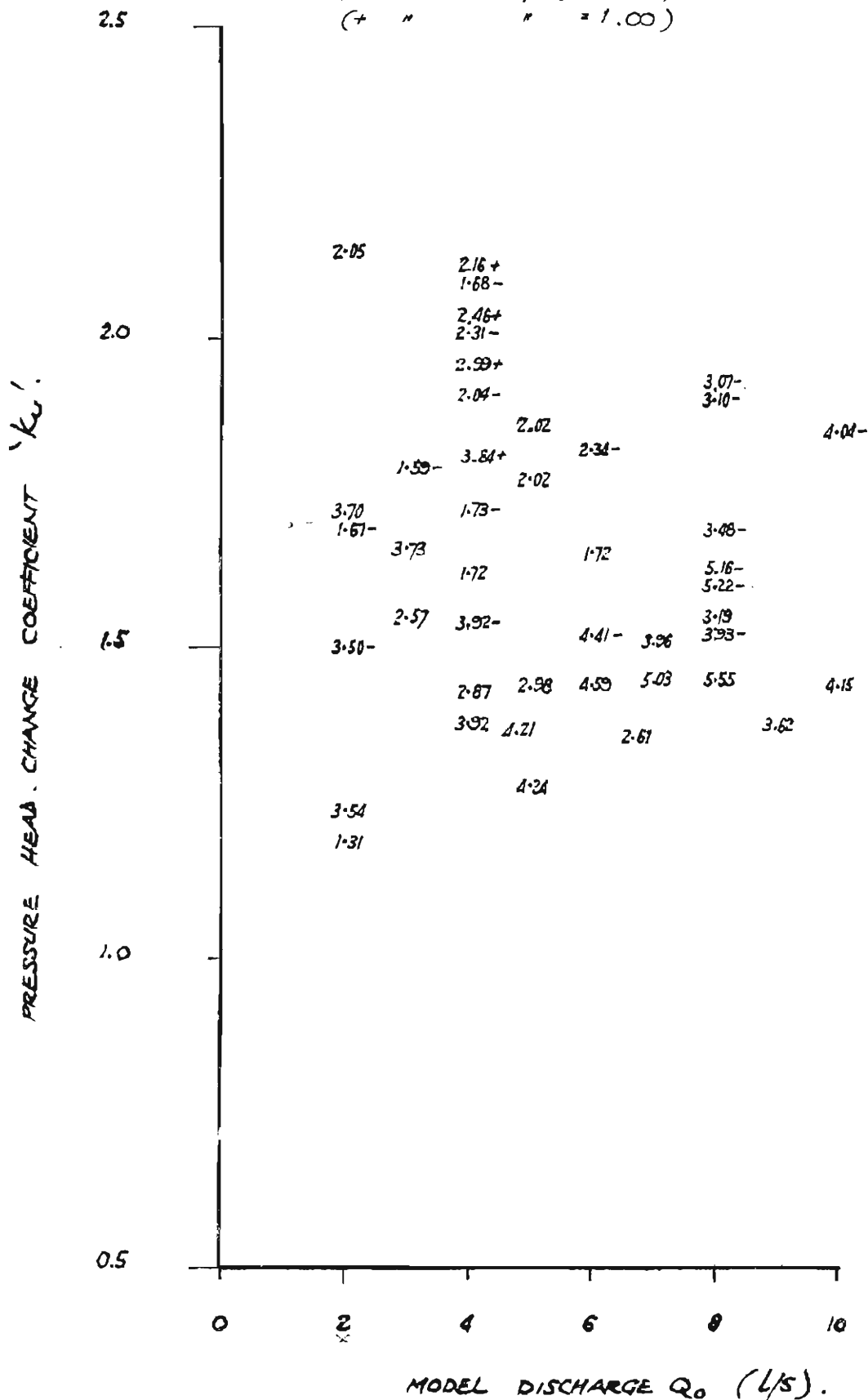


FIGURE A24 : DATA PLOT FOR MODEL NO. 12.

WATER SURFACE ELEVATION COEFFICIENT VS. DISCHARGE  $Q_0$

$\theta = 90^\circ$ ,  $D_U = 70$  MM,  $D_0 = 94$  MM,  $A_0/A_U = 1.803$ .

(FIGURES INDICATE SUBMERGENCE RATIOS)

(-  $Q_0/Q_0 = 0.50$ ).

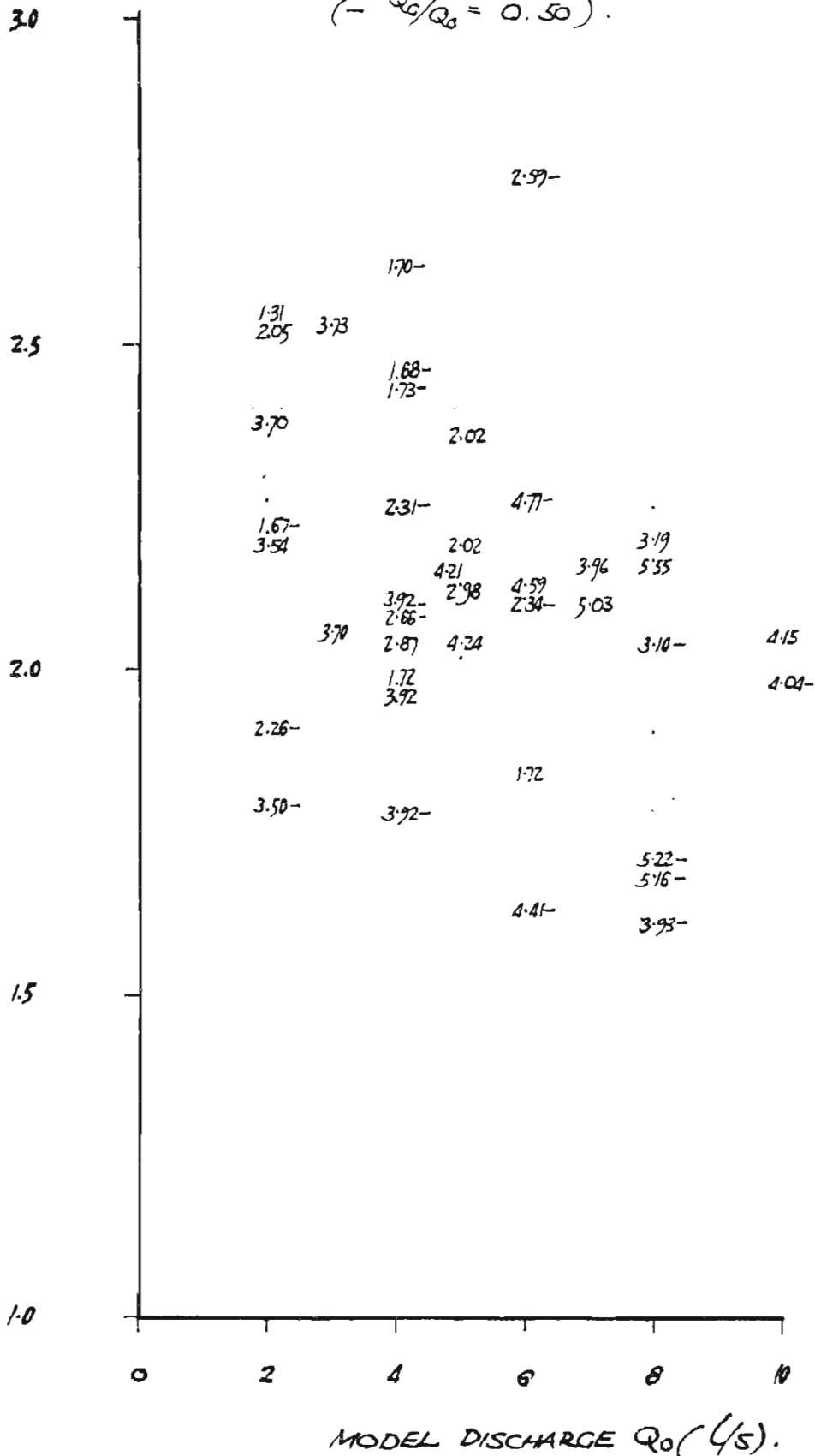


FIGURE A25: DATA PLOT FOR MODEL NO. 13

PRESSURE HEAD CHANGE COEFFICIENT  $k_u$  VS DISCHARGE  $Q_0$ .

$\theta = 0^\circ$ ,  $D_0 = 127 \text{ MM}$ ,  $D_u = 70 \text{ MM}$ ,  $A_0/A_u = 3.292$

(FIGURES INDICATE SUBMERGENCE RATIOS).

(INDICATES  $Q_1/Q_0 = 0.50$ ).

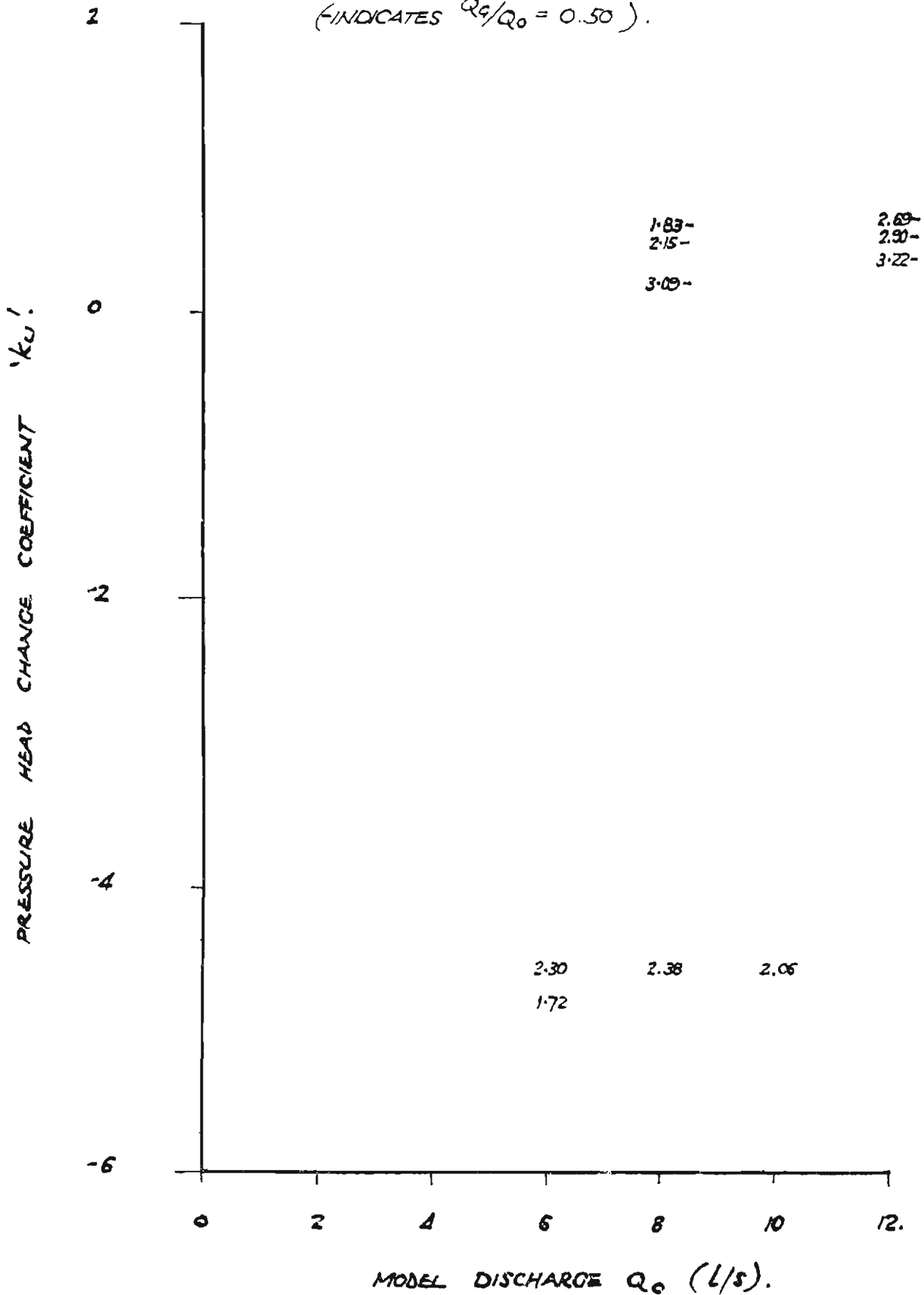


FIGURE A26: DATA PLOT FOR MODEL NO. 13.

WATER SURFACE ELEVATION COEFFICIENT VS. DISCHARGE  $Q_0$ .

$\theta = 0^\circ$ ,  $D_u = 70 \text{ MM}$ ,  $D_o = 127 \text{ MM}$ ,  $A_o/A_u = 3.292$ .

(FIGURES INDICATE SUBMERGENCE RATIOS)

(- INDICATES  $Q_0/Q_0 = 0.50$ ).

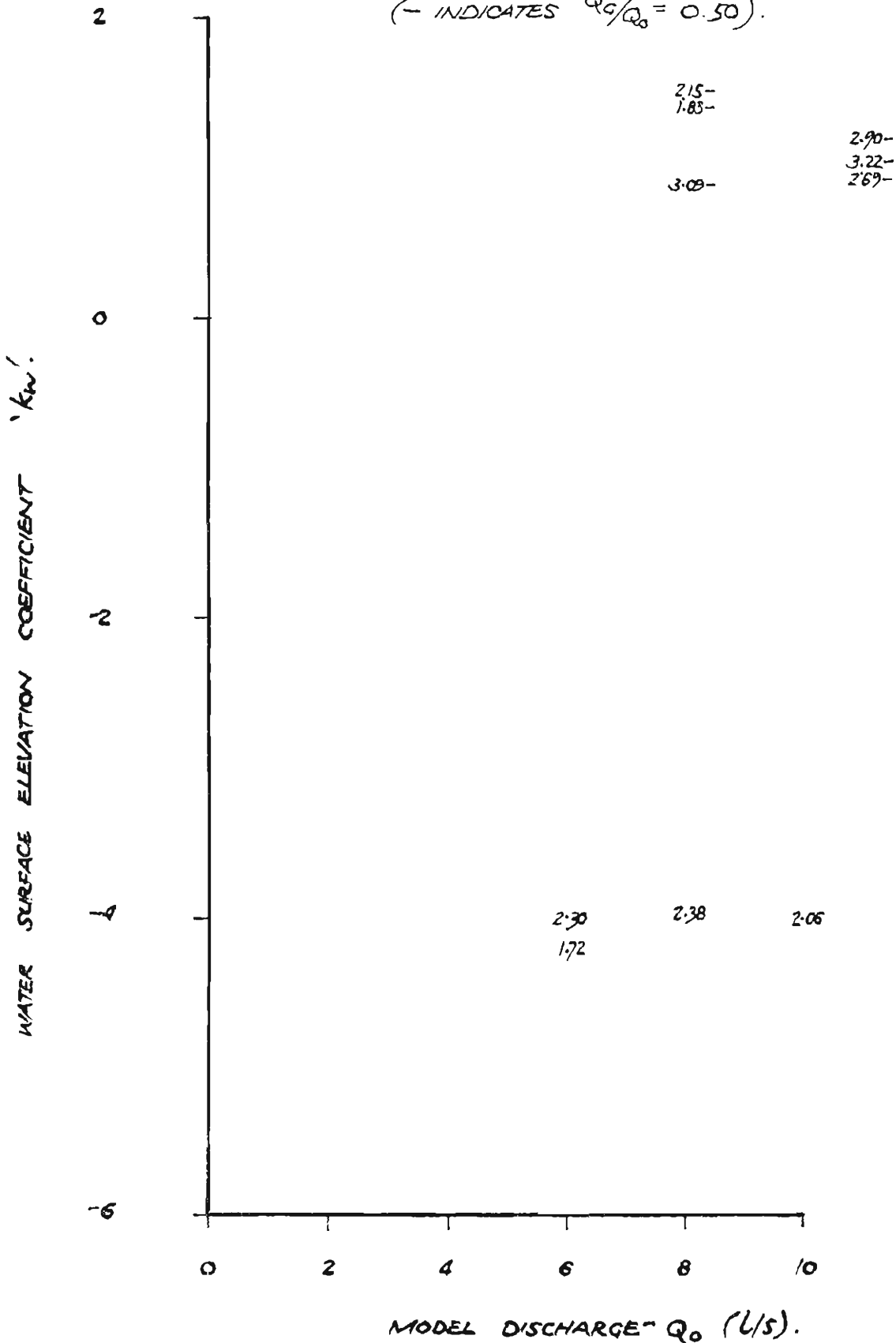




FIGURE A27: DATA PLOT FOR MODEL NO. 14

PRESSURE HEAD CHANGE COEFFICIENT  $K_u$  VS. DISCHARGE  $Q_0$ .

$\theta = 22\frac{1}{2}^\circ$ ,  $D_u = 70$  MM,  $D_o = 127$  MM,  $A_o/A_u = 3.292$ .

(FIGURES INDICATE SUBMERGENCE RATIOS)

(- INDICATES  $Q_1/Q_0 = 0.50$ ).

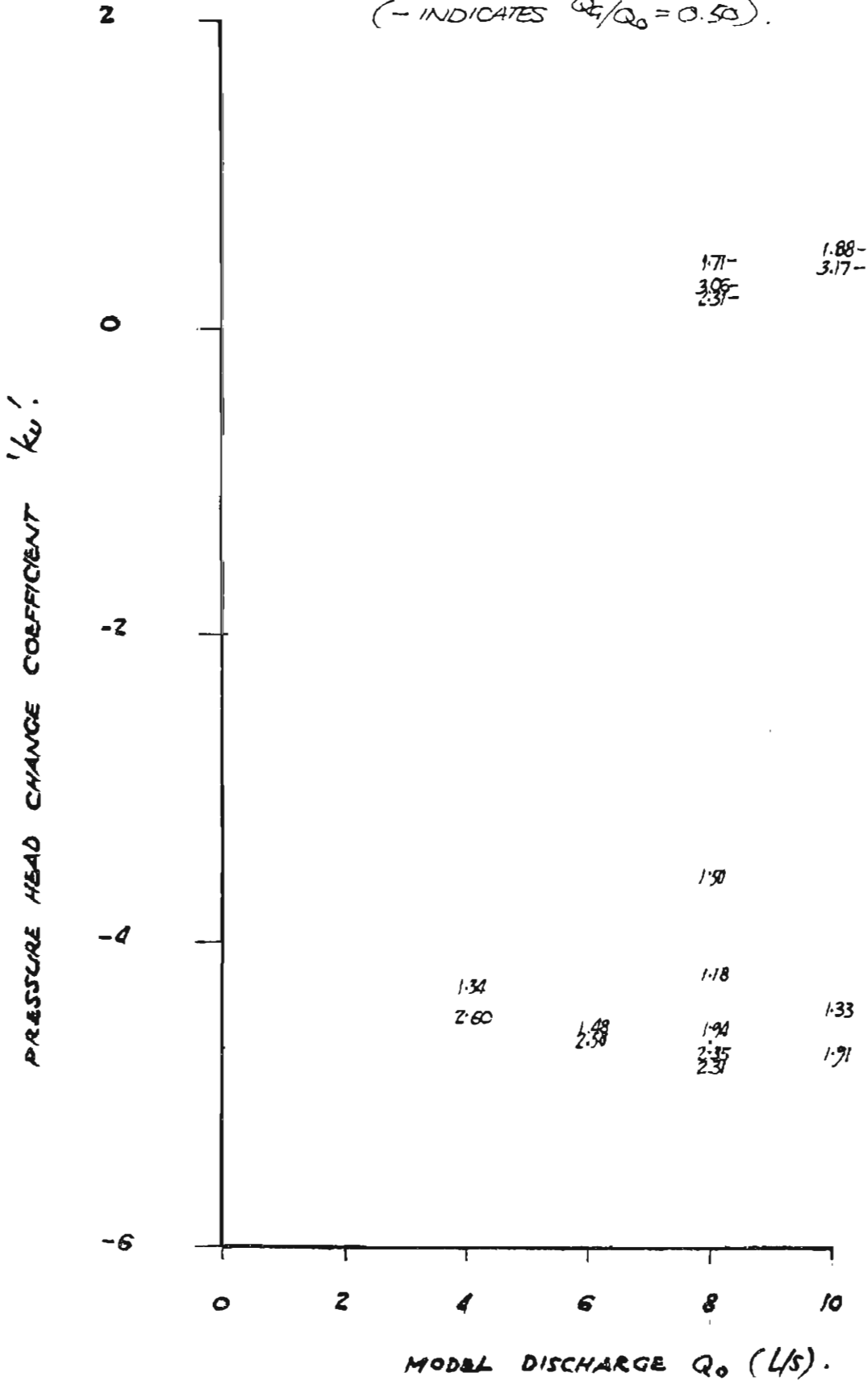


FIGURE A28 : DATA PLOT FOR MODEL NO. 14.

WATER SURFACE ELEVATION COEFFICIENT VS. DISCHARGE  $Q_0$ .

$\theta = 22\frac{1}{2}^\circ$ ,  $D_u = 70$  MM,  $D_o = 127$  MM,  $A_o/A_u = 3.292$ .

(FIGURES INDICATE SUBMERGENCE RATIOS)

(- INDICATES  $Q_1/Q_0 = 0.50$ ).

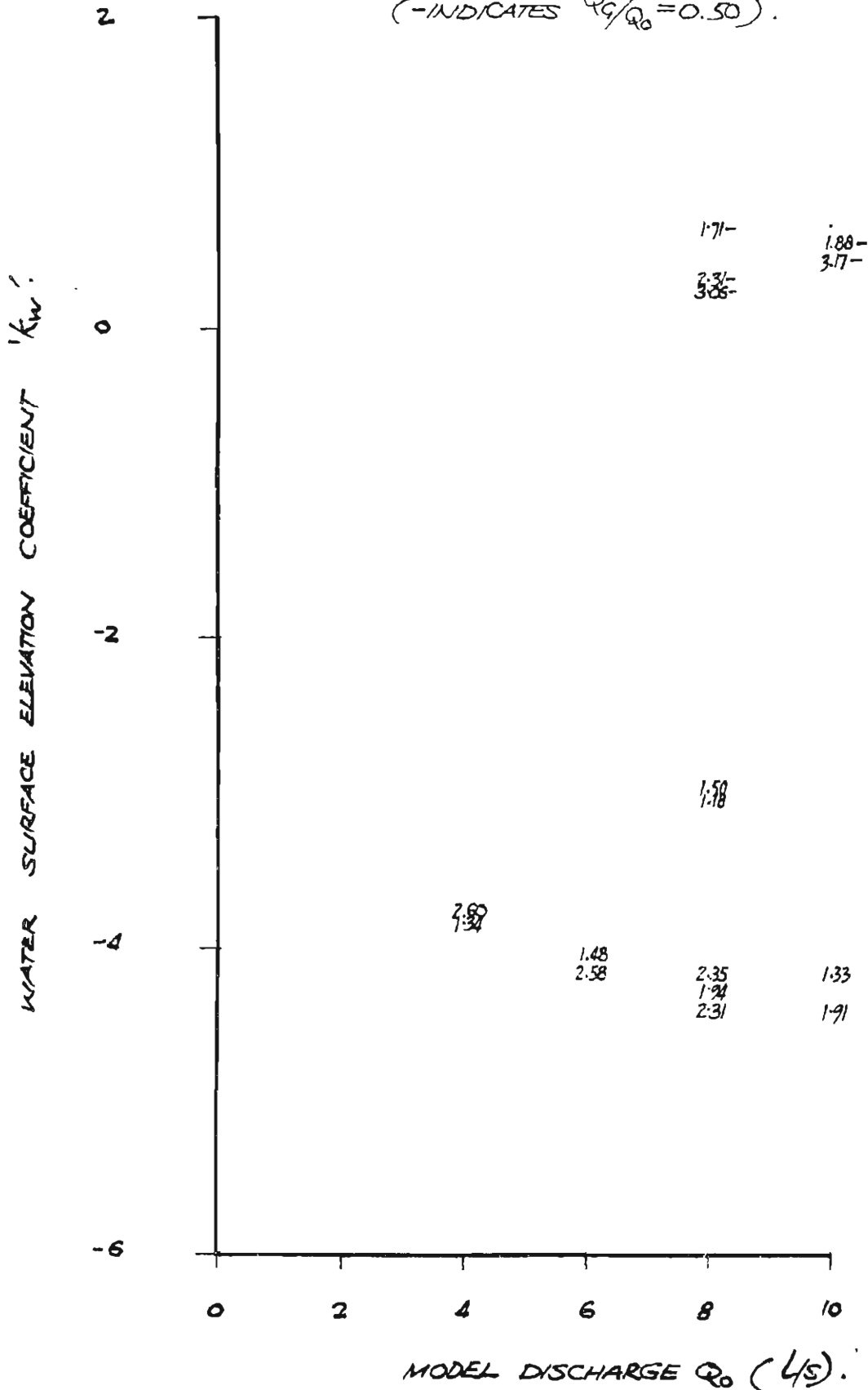


FIGURE A29: DATA PLOT FOR MODEL NO. 15

PRESSURE HEAD CHANGE COEFFICIENT VS DISCHARGE  $Q_0$ .

$\theta = 45^\circ$ ,  $D_o = 127 \text{ MM}$ ,  $D_u = 70 \text{ MM}$ ,  $A_o/A_u = 3.292$

(FIGURES INDICATE SUBMERGENCE RATIOS).

(- INDICATES  $Q_g/Q_0 = 0.50$ ).

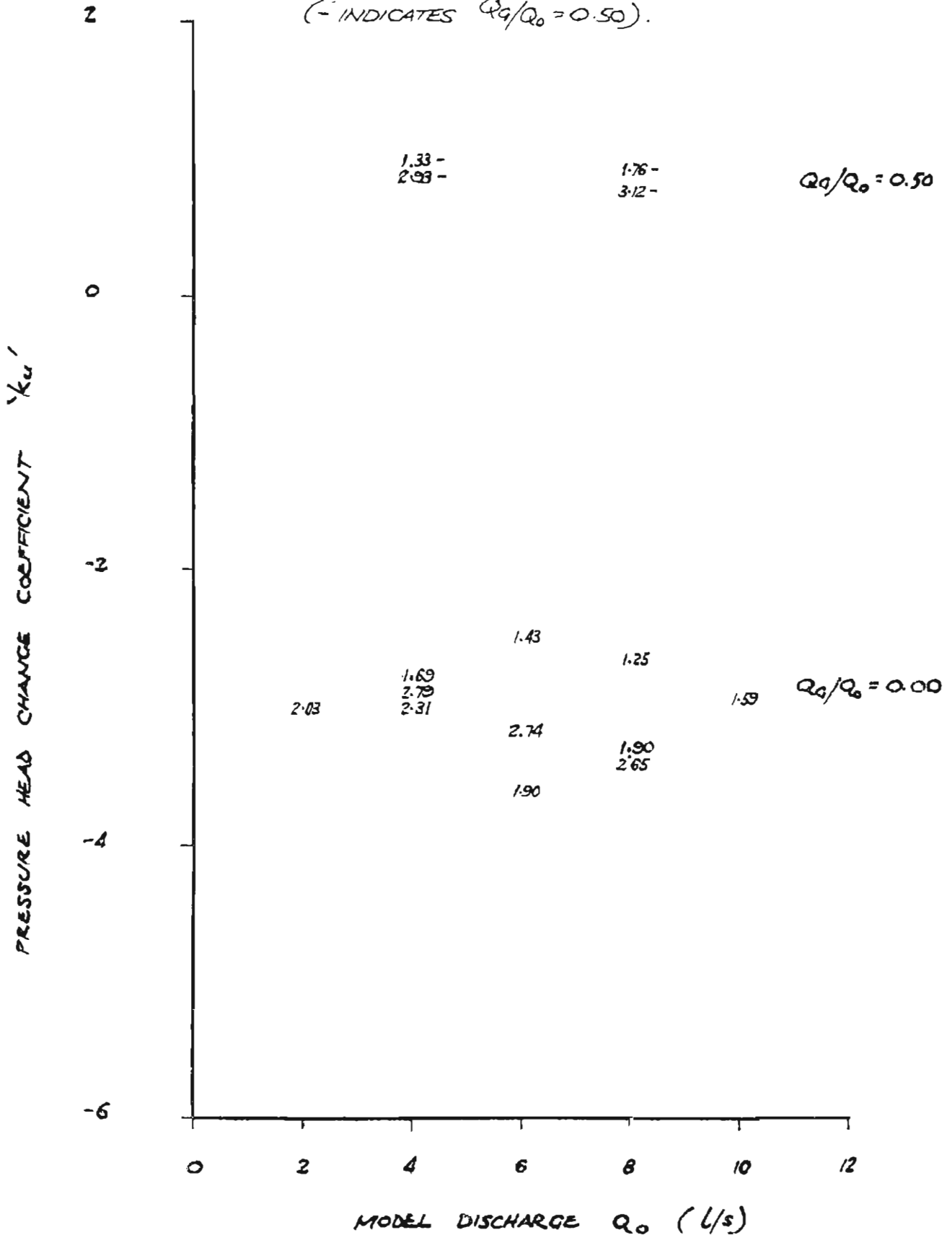


FIGURE A30 : DATA PLOT FOR MODEL NO. 15.

WATER SURFACE ELEVATION COEFFICIENT VS DISCHARGE  $Q_0$ .

$\theta = 45^\circ$ ,  $D_0 = 127 \text{ MM}$ ,  $D_U = 70 \text{ MM}$ ,  $A_0/A_u = 3.292$ .

(FIGURES INDICATE SUBMERGENCE RATIOS)

(- INDICATES  $Q_G/Q_0 = 0.50$ ).

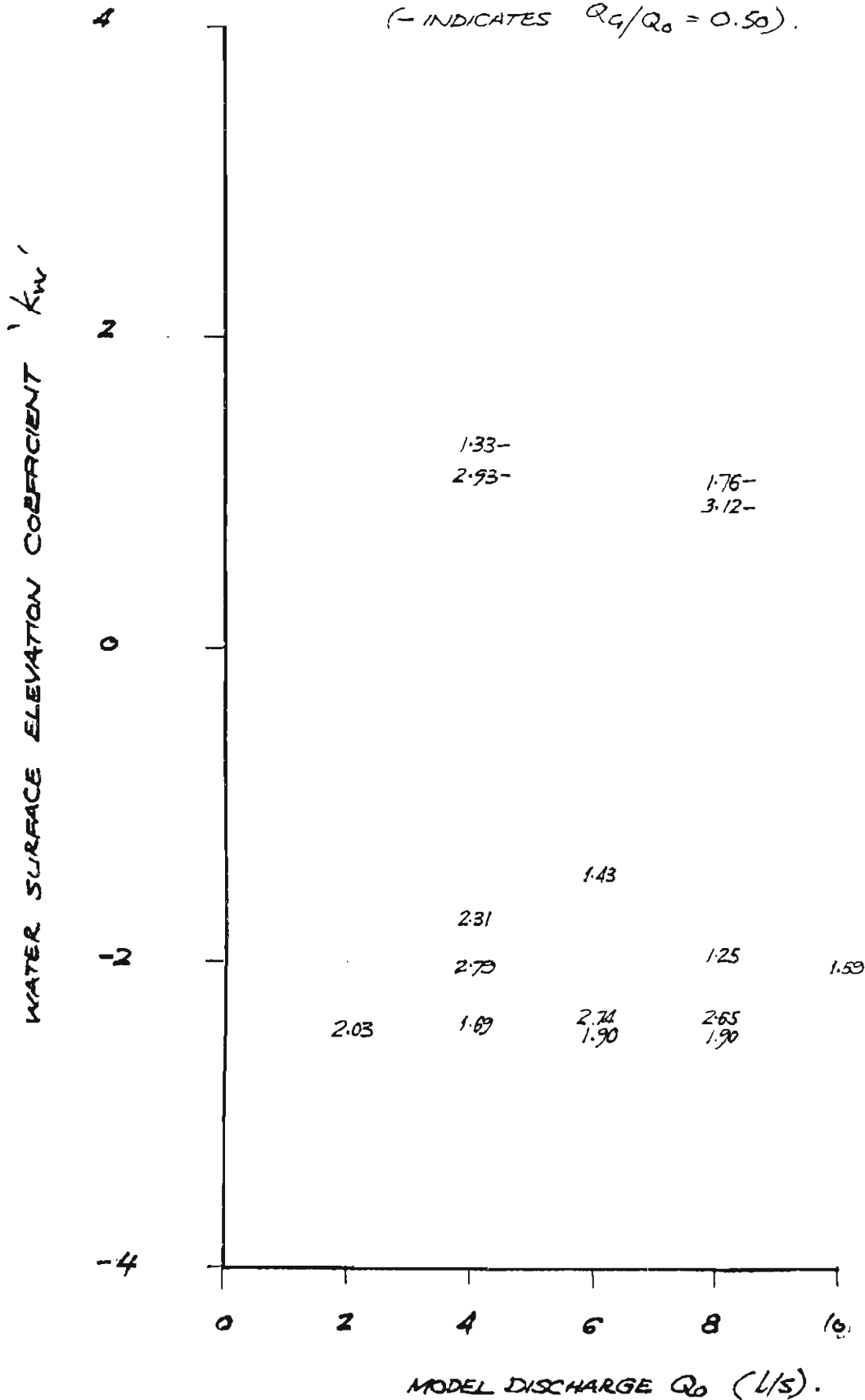


FIGURE A31: DATA PLOT FOR MODEL NO. 16

PRESSURE HEAD CHANGE COEFFICIENT VS. DISCHARGE  $Q_0$ .

$\theta = 45^\circ$ ,  $D_0 = 127\text{MM}$ ,  $D_1 = 70\text{MM}$ ,  $A_0/A_1 = 3.292$ .

(FIGURES INDICATE SUBMERGENCE RATIOS)

(- INDICATES  $Q_0/Q_0 = 0.50$ )

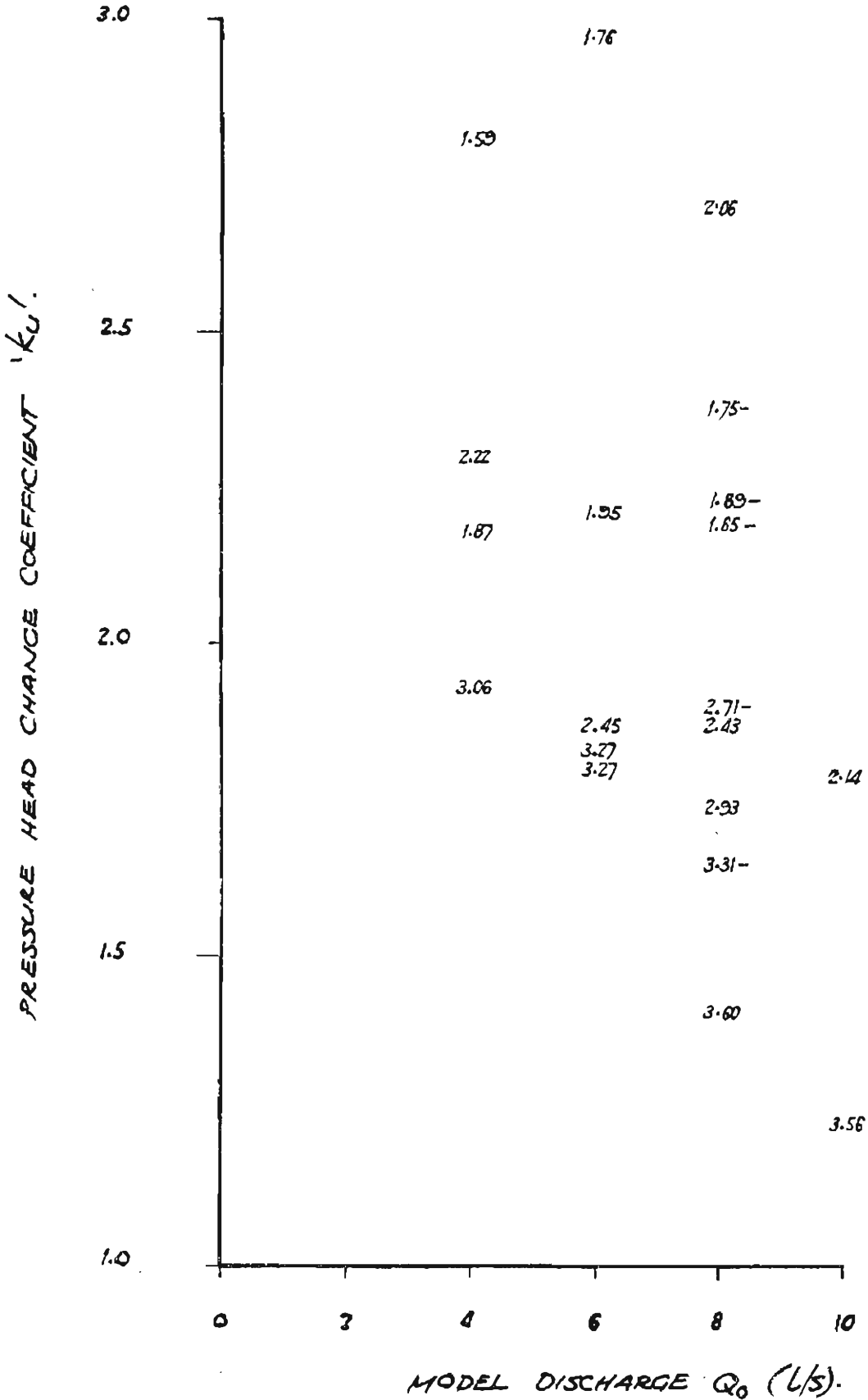


FIGURE A32 : DATA PLOT FOR MODEL NO. 16

WATER SURFACE ELEVATION COEFFICIENT VS. DISCHARGE  $Q_0$ .

$\theta = 45^\circ$ ,  $D_o = 127 \text{ MM}$ ,  $D_u = 70 \text{ MM}$ ,  $A_o/A_u = 3.292$ .

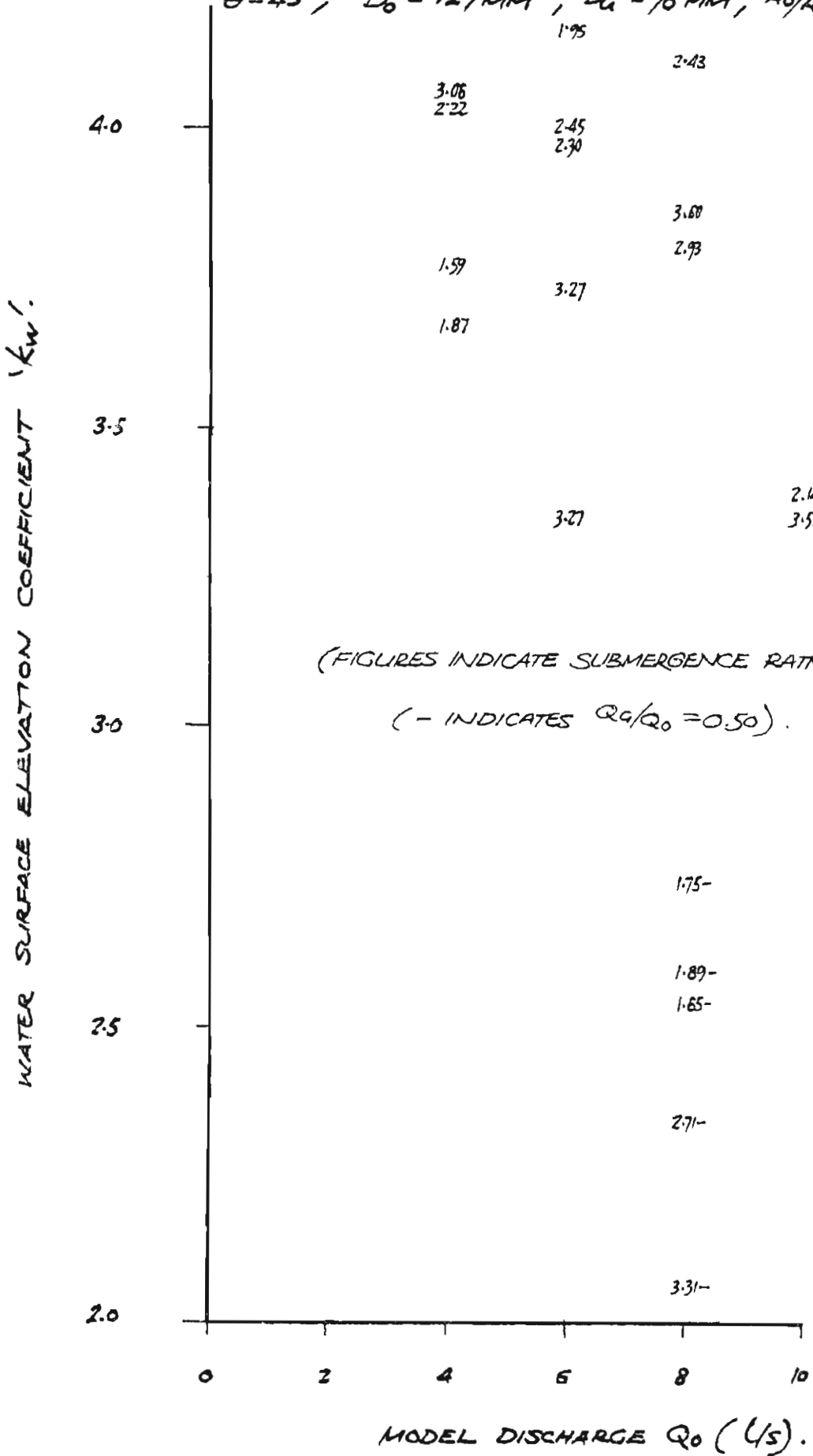


FIGURE A33 : DATA PLOT FOR MODEL NO. 17PRESSURE HEAD CHANGE COEFFICIENT VS. DISCHARGE  $Q_0$ .

$$\theta = 67\frac{1}{2}^\circ, D_0 = 127 \text{ MM}, D_u = 70 \text{ MM}, A_0/A_u = 3.292.$$

(FIGURES INDICATE SUBMERGENCE RATIOS)

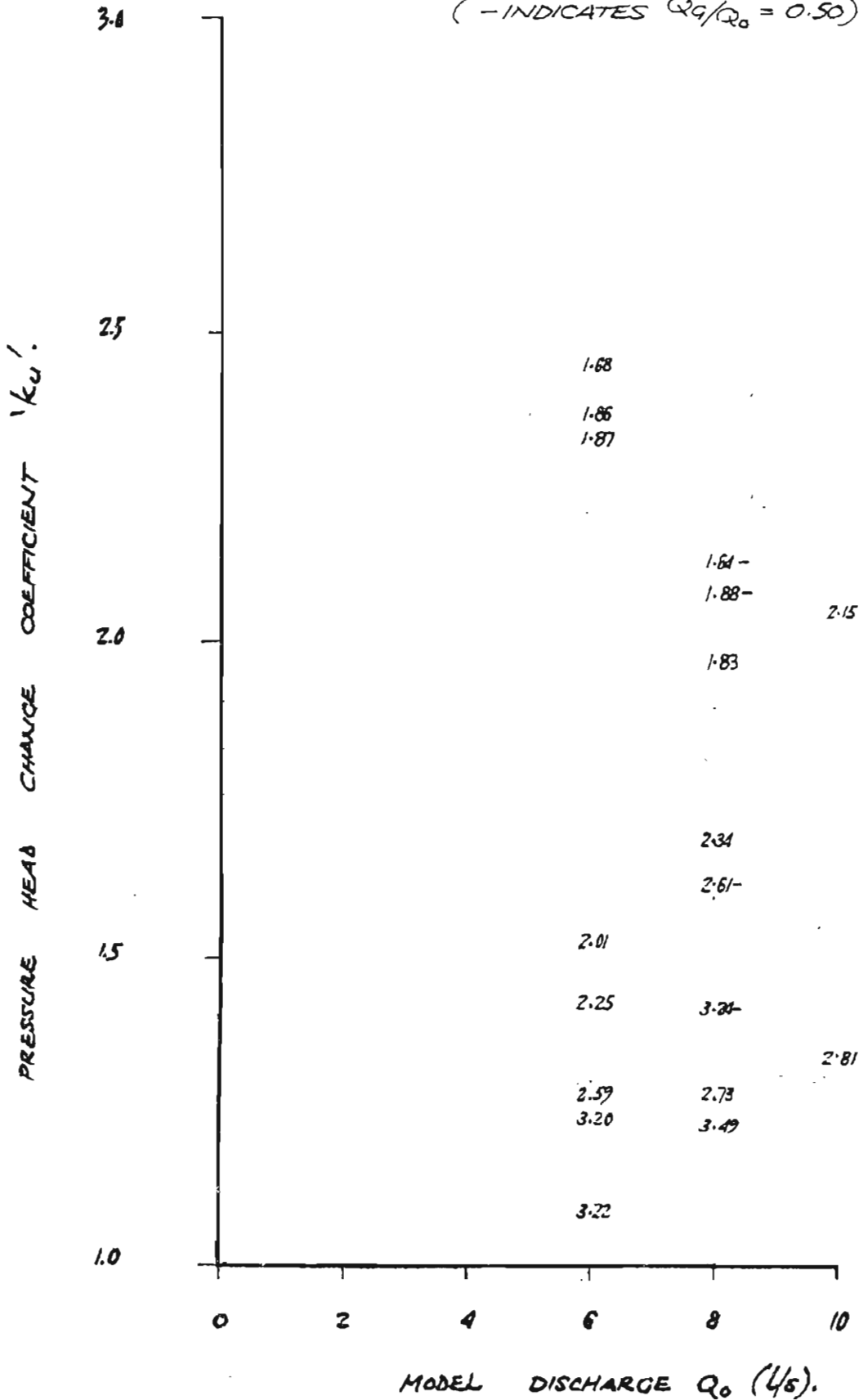
(- INDICATES  $Q_0/Q_0 = 0.50$ ).

FIGURE A3A: DATA PLOT FOR MODEL NO. 17

WATER SURFACE ELEVATION COEFFICIENT VS. DISCHARGE  $Q_0$ .

$\theta = 67\frac{1}{2}^\circ$ ,  $D_0 = 127$  MM,  $D_c = 70$  MM,  $A_0/A_c = 3.292$ .

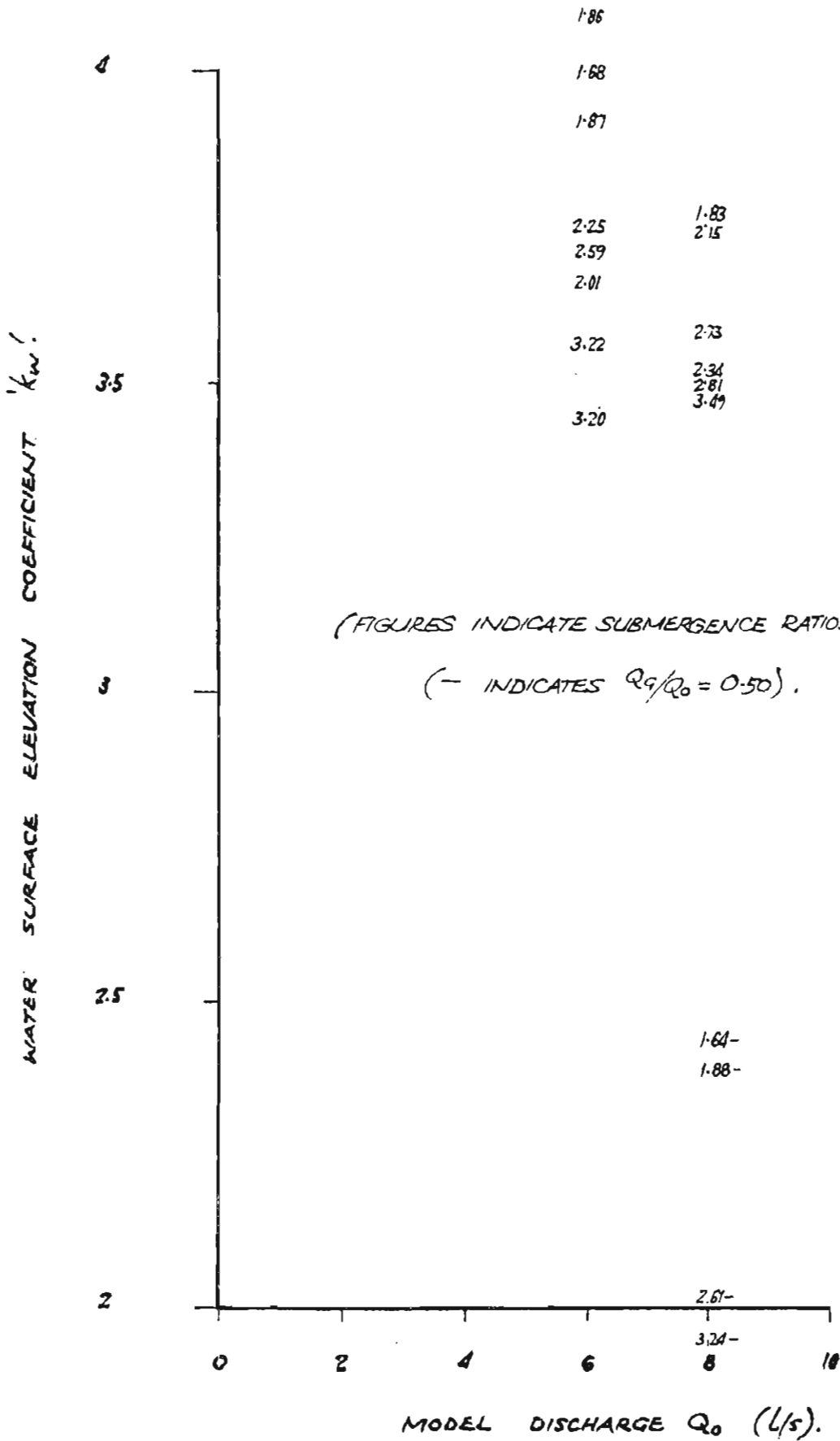




FIGURE A35 : DATA PLOT FOR MODEL NO. 18.

PRESSURE HEAD CHANGE COEFFICIENTS VS. DISCHARGE  $Q_0$ .

$\theta = 90^\circ$ ,  $D_0 = 127 \text{ MM}$ ,  $D_u = 76 \text{ MM}$ ,  $A_0/A_u = 3.292$ .

(FIGURES INDICATE SUBMERGENCE RATIOS)

(+ INDICATES  $Q_g/Q_0 = 0.25$ )

(- INDICATES  $Q_g/Q_0 = 0.50$ )

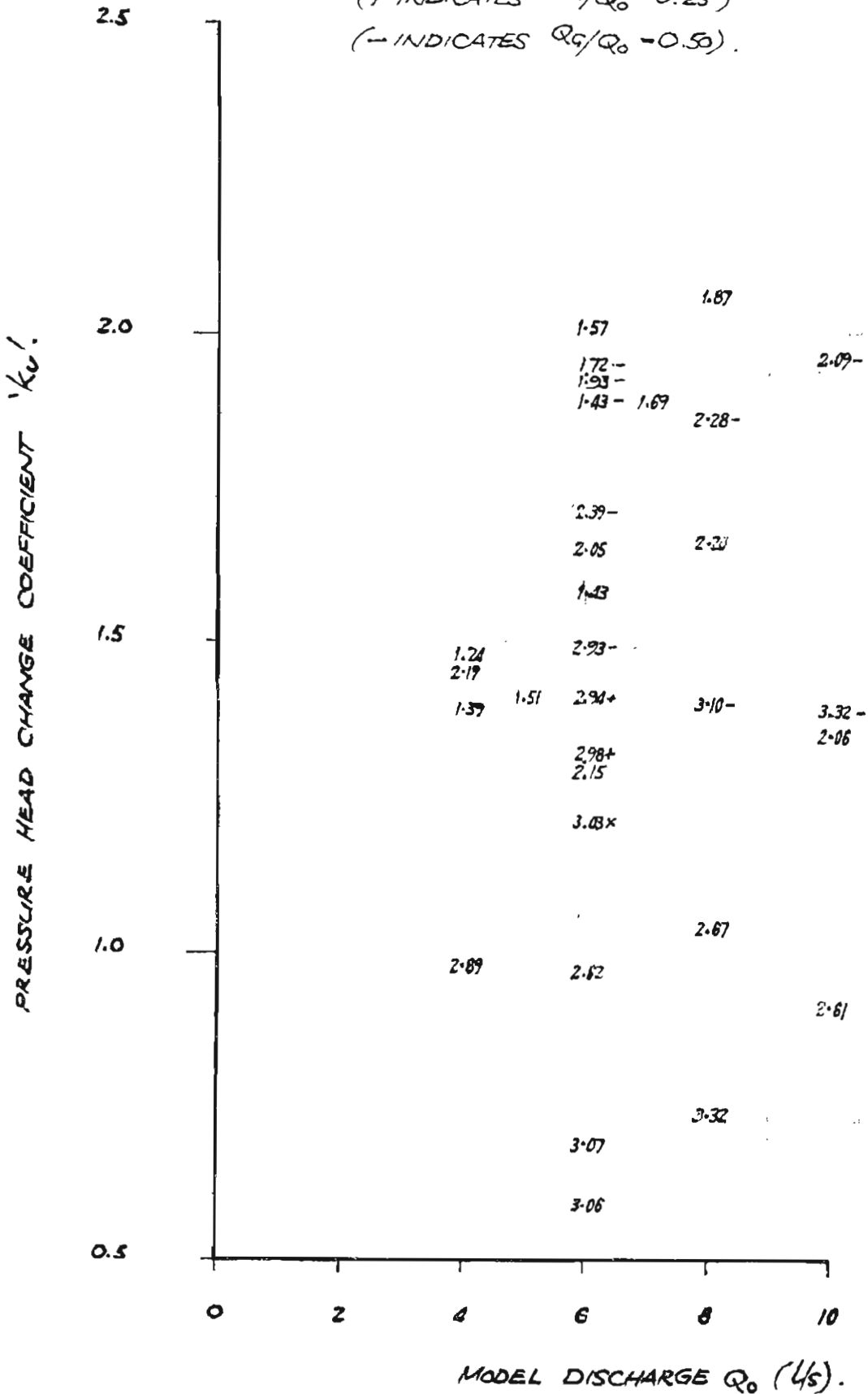


FIGURE A36 : DATA PLOT FOR MODEL NO. 18.

WATER SURFACE ELEVATION COEFFICIENT VS. DISCHARGE  $Q_0$

$\theta = 90^\circ$  ,  $D_0 = 127\text{MM}$  ,  $D_u = 70\text{MM}$   $A_0/A_u = 3.222$ .

(FIGURES INDICATE SUBMERGENCE RATIOS)  
 (- INDICATES  $Q_0/Q_0 = 0.50$  ) .

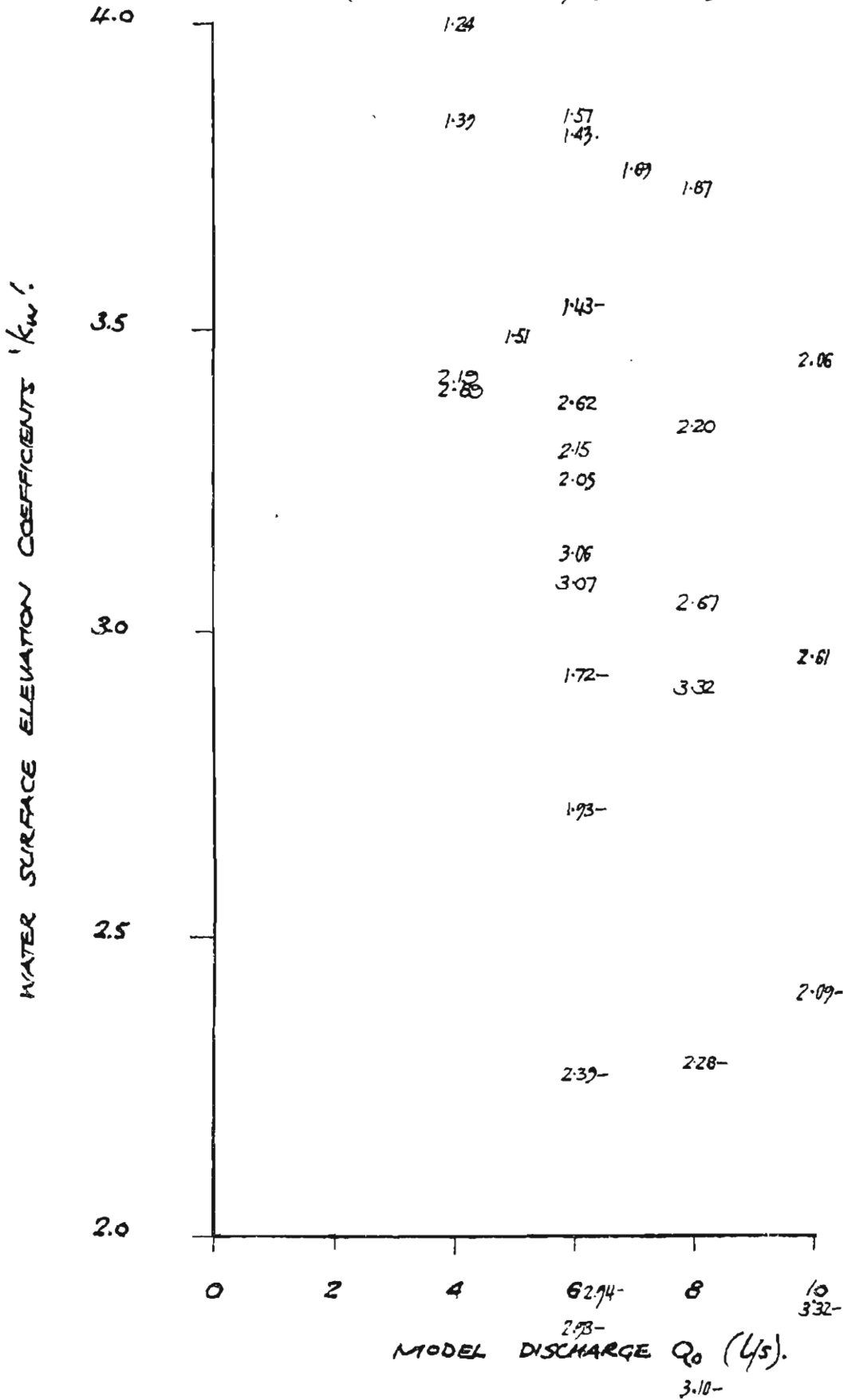


FIGURE A37 : DATA PLOT FOR MODEL NO. 19.

PRESSURE HEAD CHANGE COEFFICIENT VS. DISCHARGE  $Q_0$

$\theta = 22\frac{1}{2}^\circ$ ,  $D_0 = 70 \text{ MM}$ ,  $D_u = 70 \text{ MM}$ ,  $A_0/A_u = 1.00$ .

(FIGURES INDICATE SUBMERGENCE RATIOS)

(- INDICATES  $Q_c/Q_0 = 0.50$ ).

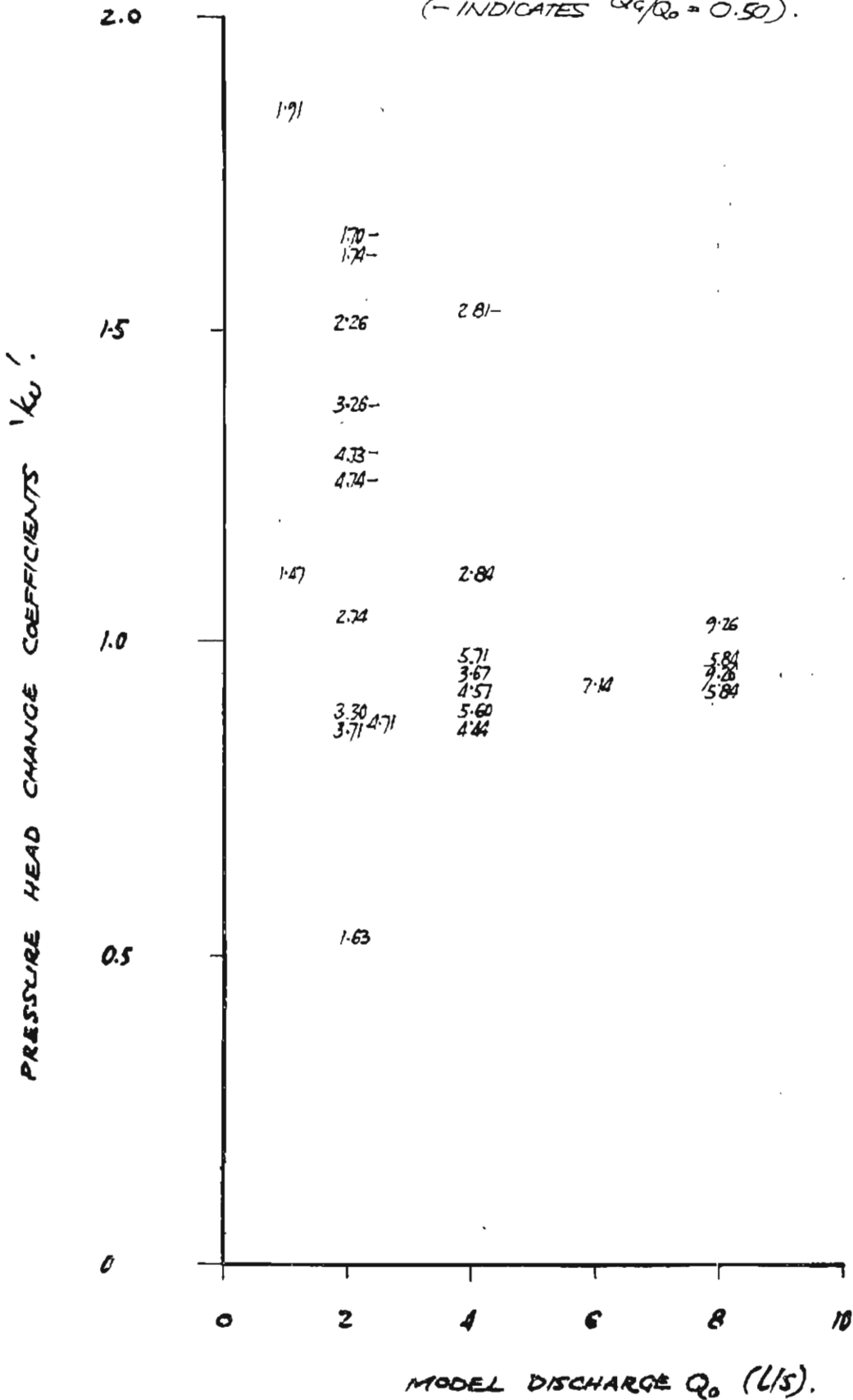


FIGURE A33 : DATA PLOT FOR MODEL NO. 19

WATER SURFACE 170- ELEVATION COEFFICIENT VS. DISCHARGE  $Q_0$ .

$\theta = -22\frac{1}{2}^\circ$   $D_0 = 70$  MM,  $D_u = 70$  MM,  $A_0/A_u = 1.00$

(FIGURES INDICATE SUBMERGENCE RATIOS)

(-- INDICATES  $Q_1/Q_0 = 0.50$ ).

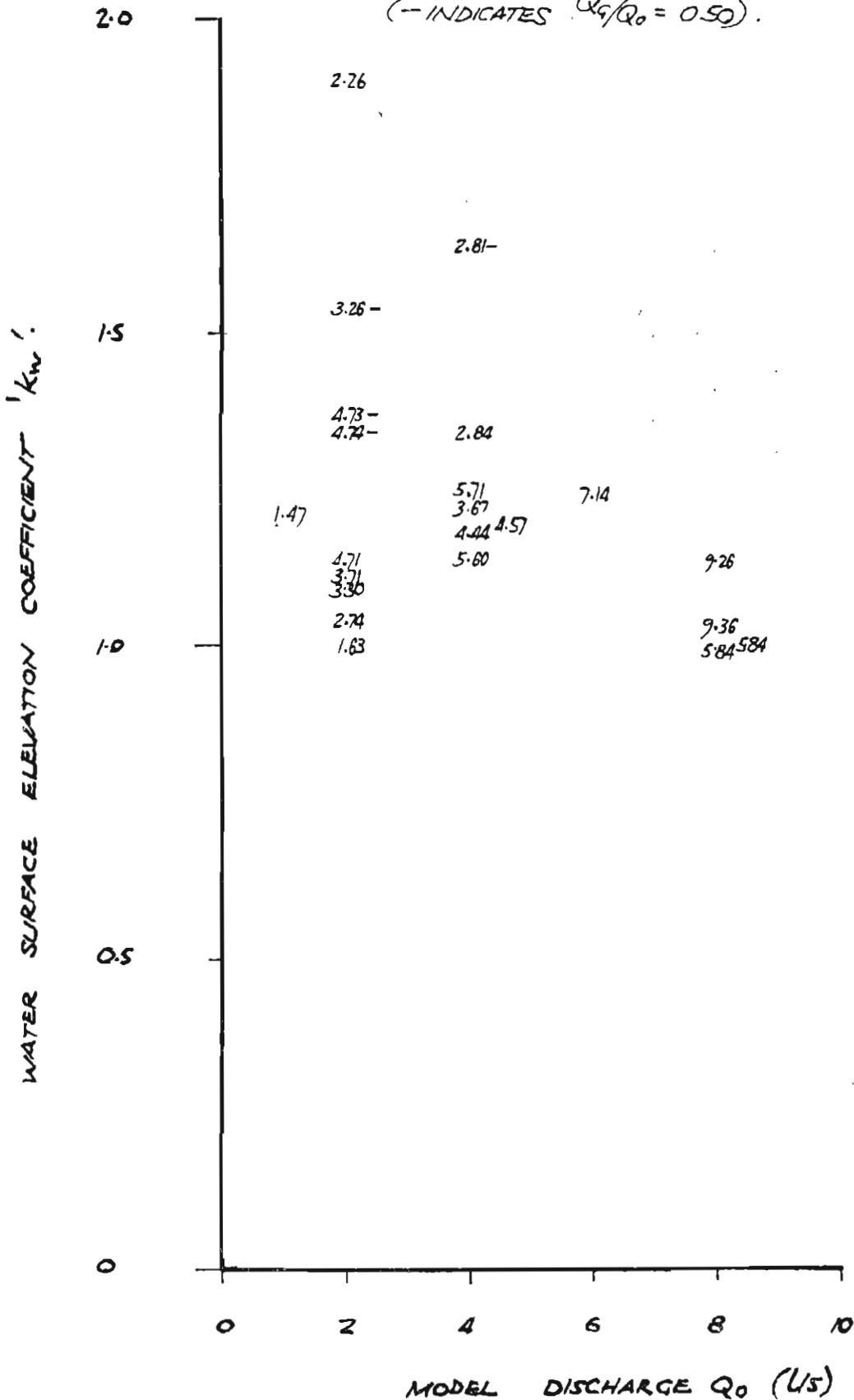


FIGURE A39: DATA PLOT FOR MODEL NO. 20.PRESSURE HEAD CHANGE COEFFICIENT VS. DISCHARGE  $Q_0$ .

$$\theta = 45^\circ, D_0 = 70 \text{ MM}, D_u = 70 \text{ MM}, A_0/A_u = 1.00$$

(FIGURES INDICATE SUBMERGENCE RATIOS)

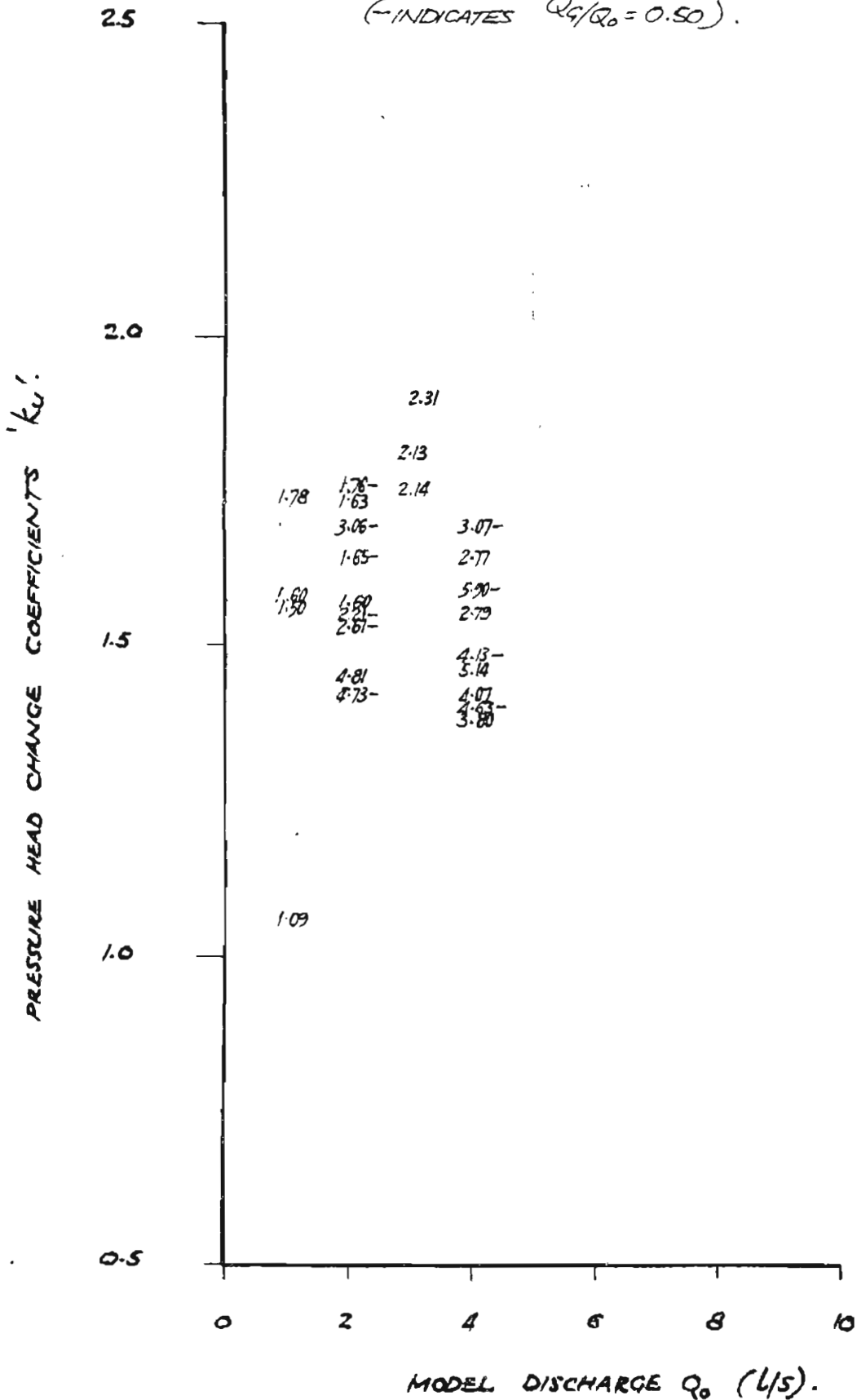
(- INDICATES  $Q_1/Q_0 = 0.50$ ).

FIGURE A40: DATA PLOT FOR MODEL NO. 20.

WATER SURFACE ELEVATION COEFFICIENT VS DISCHARGE  $Q_0$ .

$\theta = 45^\circ$ ,  $D_0 = 70\text{MM}$ ,  $D_u = 70\text{MM}$ ,  $A_0/A_u = 1.00$ .

(FIGURES INDICATE SUBMERGENCE RATIOS)

(- INDICATES  $Q_0/Q_0 = 0.50$ ).

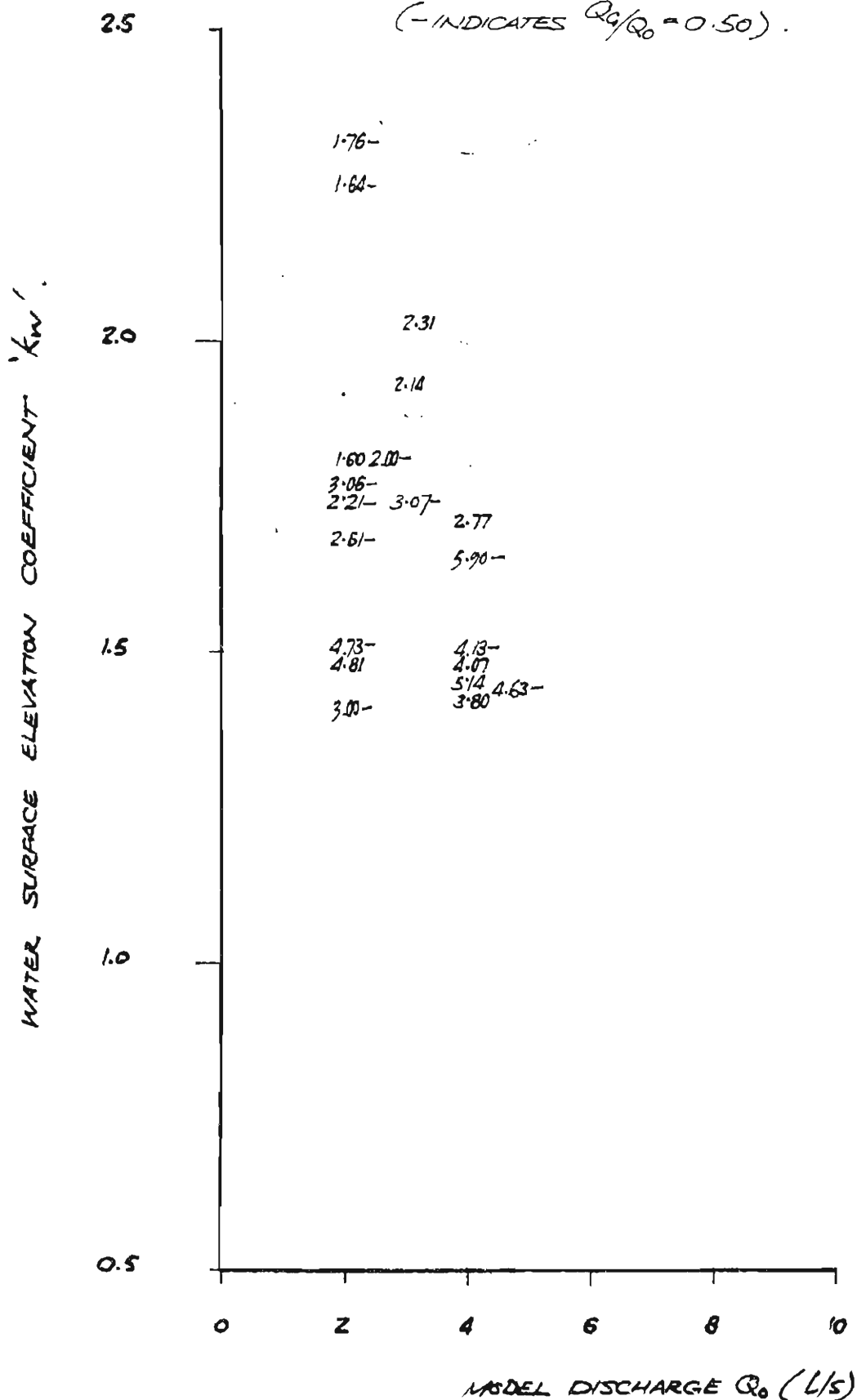


FIGURE A41 : DATA PLOT FOR MODEL NO. 21

PRESSURE HEAD CHANGE COEFFICIENTS VS. DISCHARGE,  $Q_0$ .

1.71-

$\theta = 45^\circ$ ,  $D_u = 70 \text{ MM}$ ,  $D_o = 70 \text{ MM}$ ,  $A_o/A_u = 1.0$

(FIGURES INDICATE SUBMERGENCE RATIOS)

(- INDICATES  $Q_1/Q_0 = 0.50$ ).

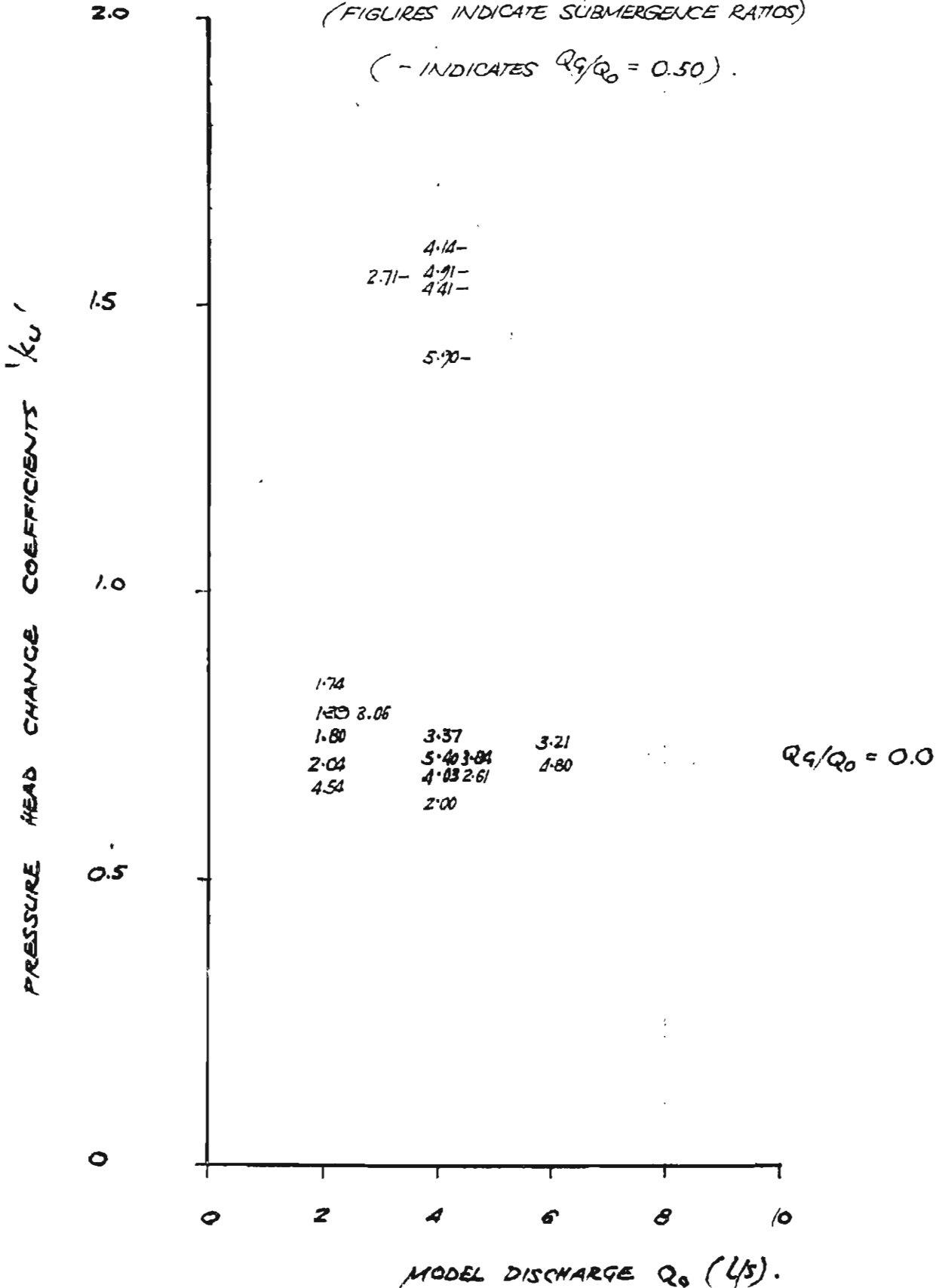


FIGURE A42 : DATA PLOT FOR MODEL NO. 21.

WATER SURFACE ELEVATION COEFFICIENTS VS. DISCHARGE  $Q_0$ .

$\theta = 45^\circ$ ,  $D_0 = 70\text{MM}$ ,  $D_U = 70\text{MM}$ ,  $A_0/A_u = 1.0$   
1.71-

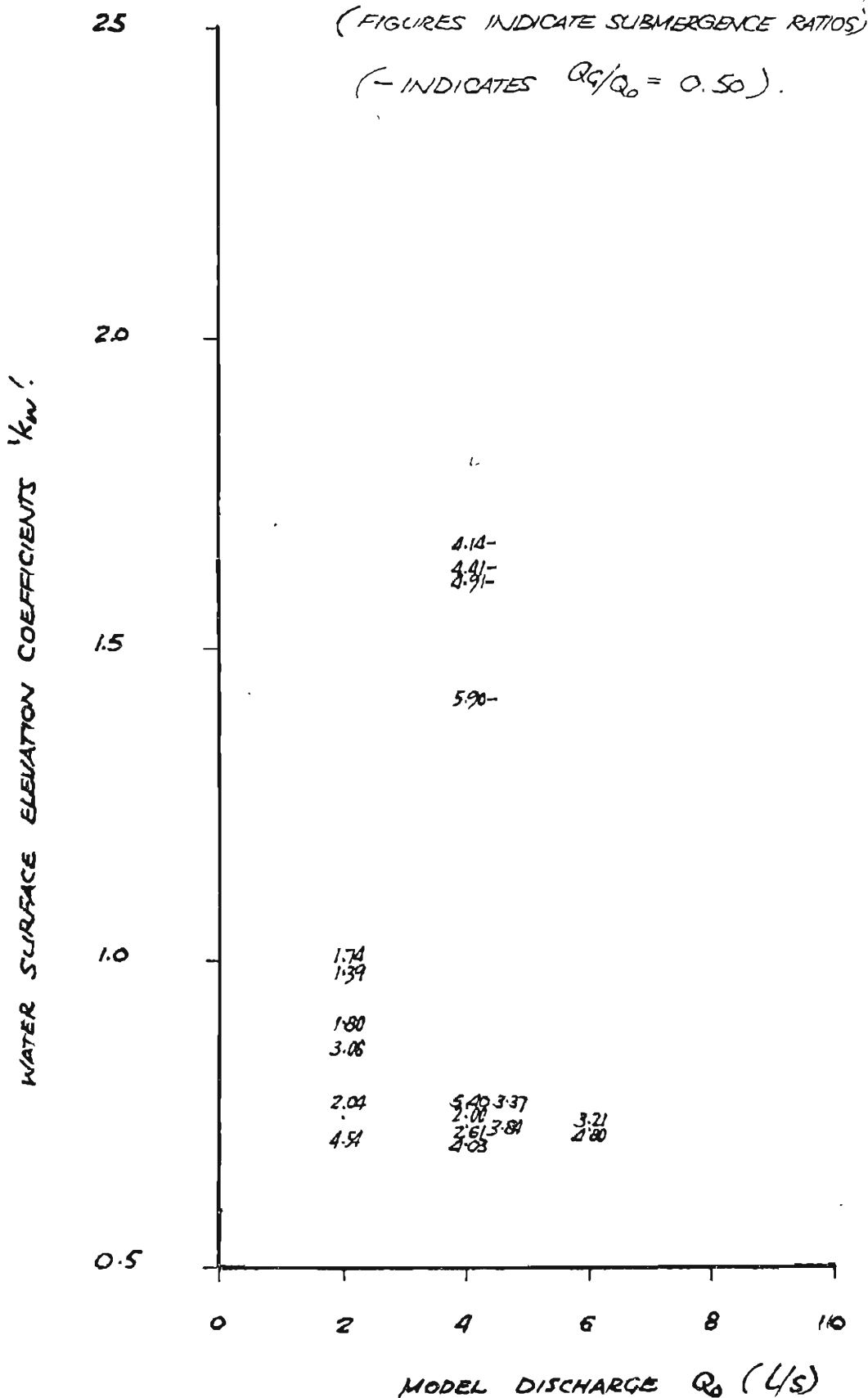




FIGURE A43 : DATA PLOT FOR MODEL NO. 22.

PRESSURE HEAD CHANGE COEFFICIENT VS. DISCHARGE  $Q_0$ .

$\theta = 67\frac{1}{2}^\circ$ ,  $D_o = 70\text{MM}$ ,  $D_u = 70\text{MM}$ ,  $A_o/A_u = 1.00$

(FIGURES INDICATE SUBMERGENCE RATIOS).

(- INDICATES  $Q_1/Q_0 = 0.50$ ).

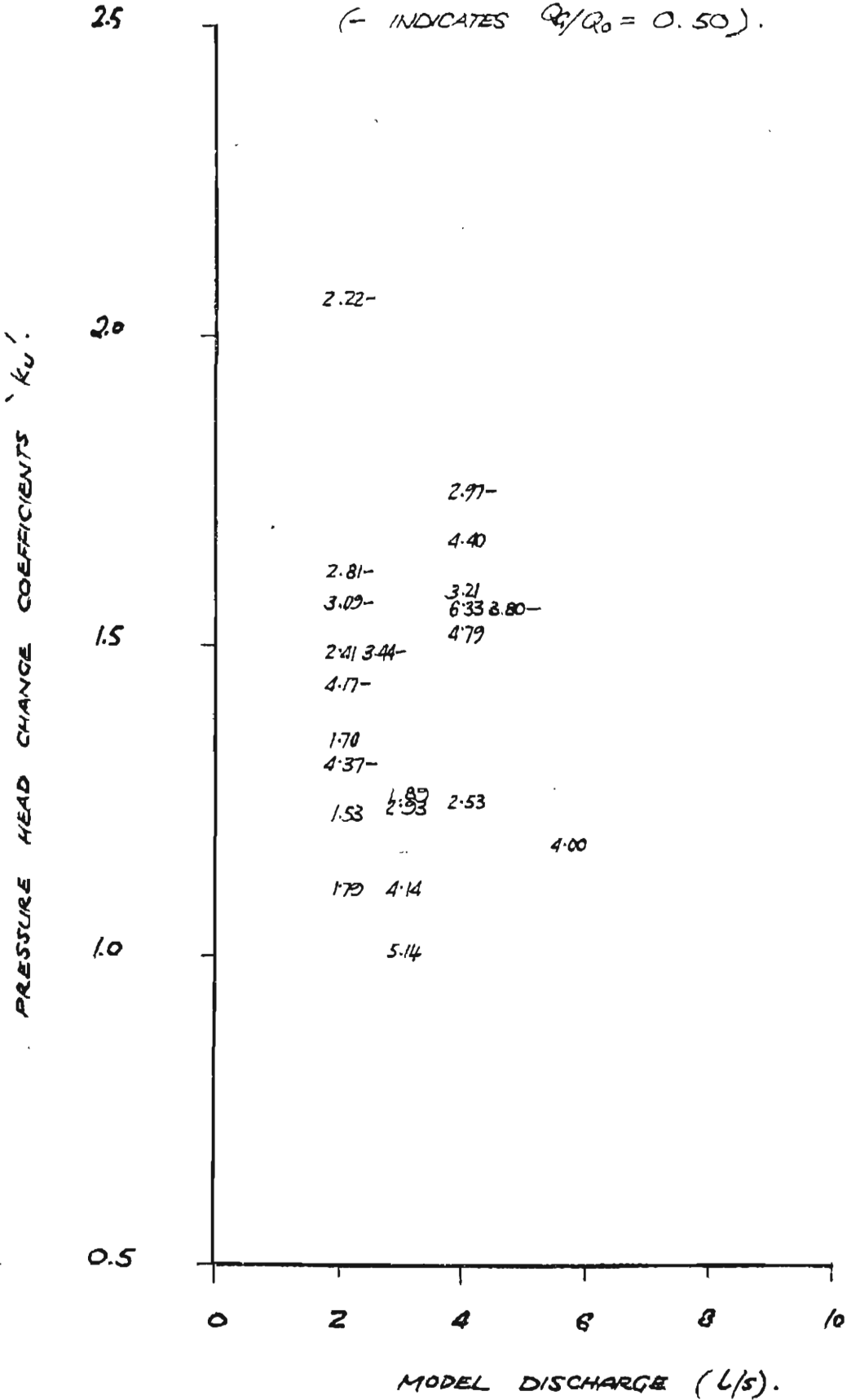


FIGURE A44 : DATA PLOT FOR MODEL NO. 22.

WATER SURFACE ELEVATION COEFFICIENT VS. DISCHARGE  $Q_0$ .

$\theta = 67\frac{1}{2}^\circ$ ,  $D_0 = 70\text{MM}$ ,  $D_u = 70\text{MM}$ ,  $A_0/A_u = 1.00$

(FIGURES INDICATE SUBMERGENCE RATIOS).

(- INDICATES  $Q_1/Q_0 = 0.50$ ).

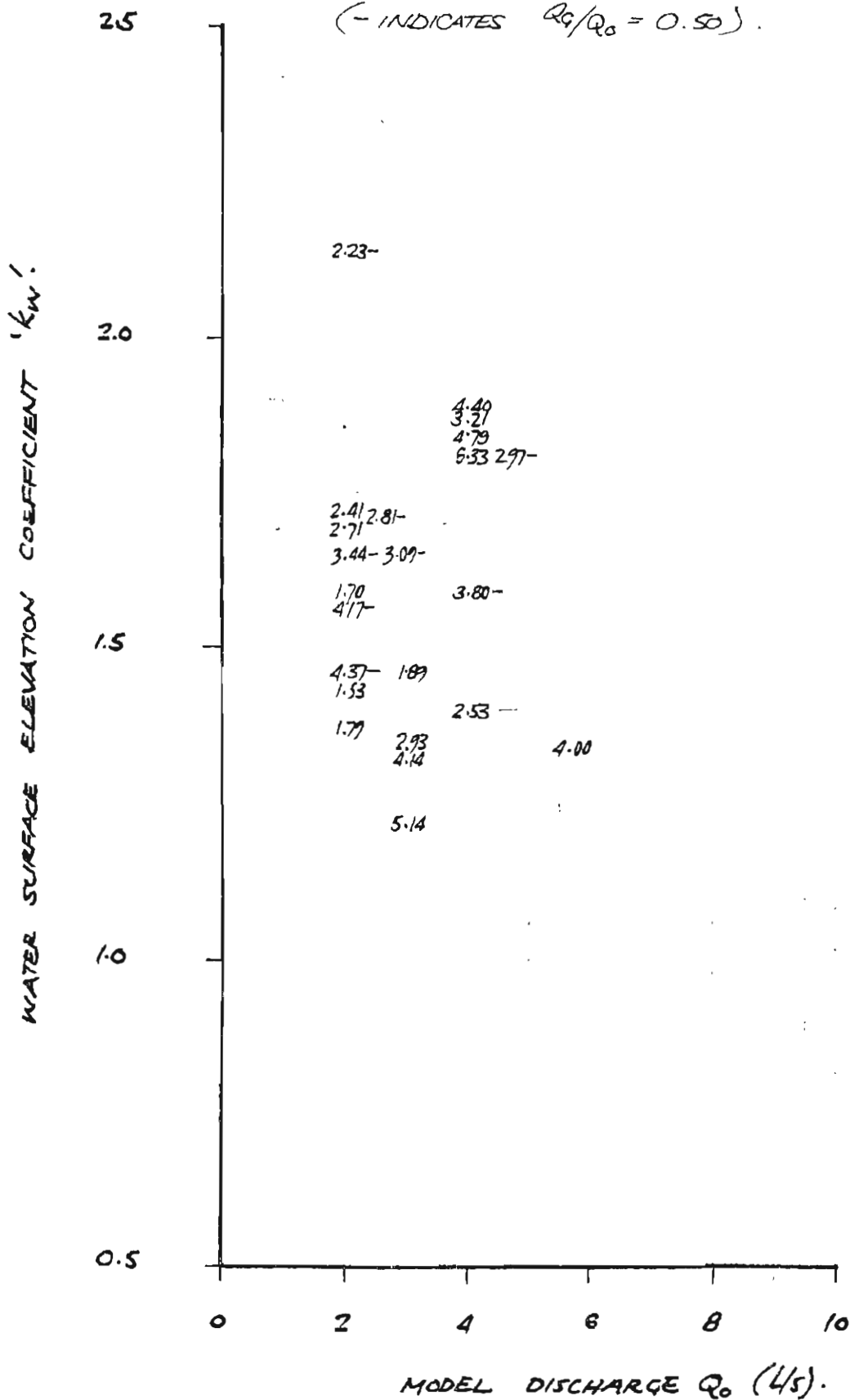


FIGURE A45 : DATA PLOT FOR MODEL NO. 23

PRESSURE HEAD CHANGE COEFFICIENT VS. DISCHARGE  $Q_0$ .

$\theta = 22\frac{1}{2}^\circ$ ,  $D_0 = 94 \text{ MM}$ ,  $D_u = 70 \text{ MM}$ ,  $A_0/A_u = 1.803$

(FIGURES INDICATE SUBMERGENCE RATIOS)

(- INDICATES  $Q_1/Q_0 = 0.50$ ).

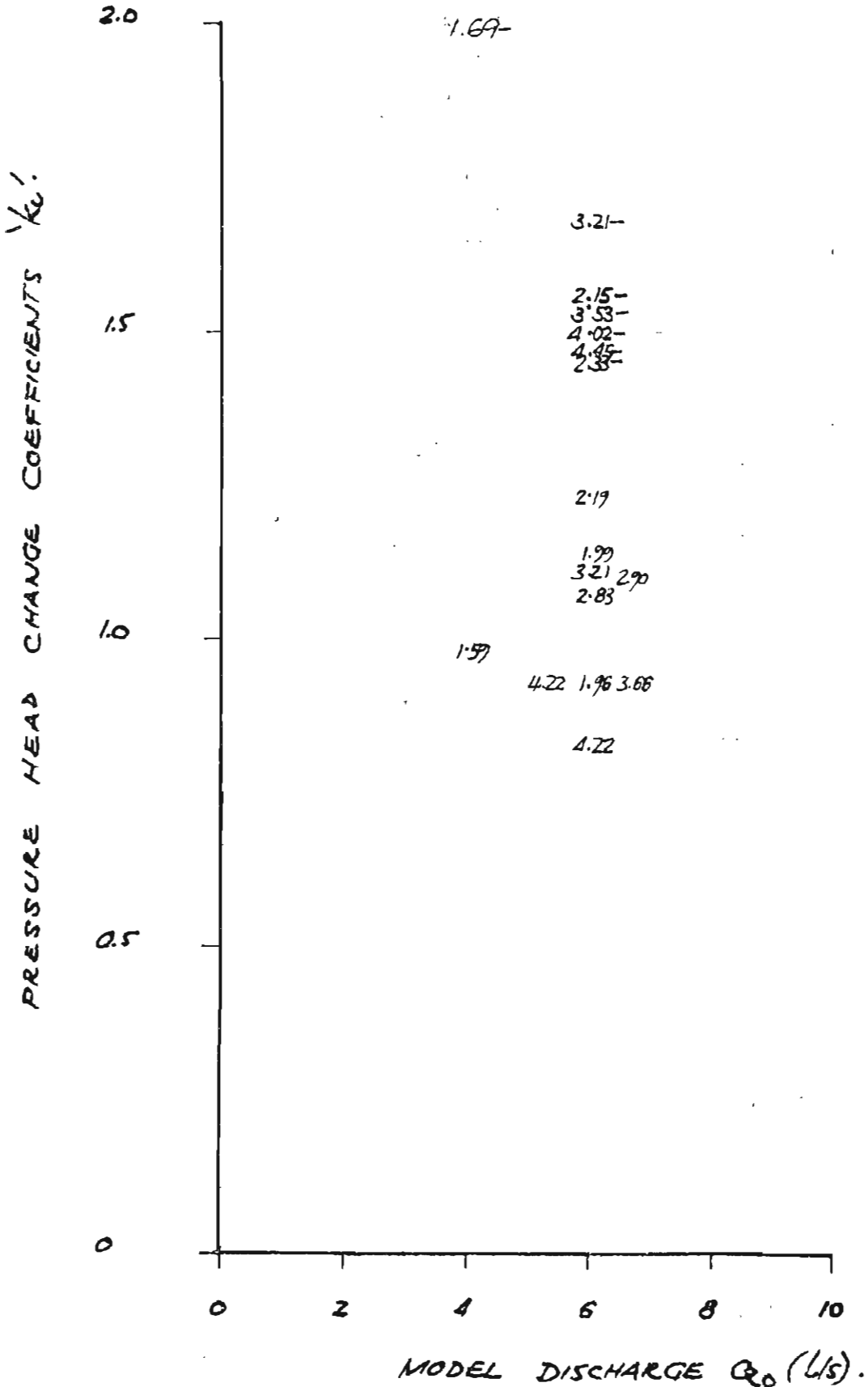


FIGURE A46 : DATA PLOT FOR MODEL NO. 23.

WATER SURFACE ELEVATION COEFFICIENT VS DISCHARGE  $Q_0$ .

$\theta = 22\frac{1}{2}^\circ$ ,  $D_0 = 94 \text{ MM}$ ,  $D_c = 70 \text{ MM}$ ,  $A_0/A_u = 1.803$

(FIGURES INDICATE SUBMERGENCE RATIOS)

(- INDICATES  $Q_9/Q_0 = 0.50$ ).

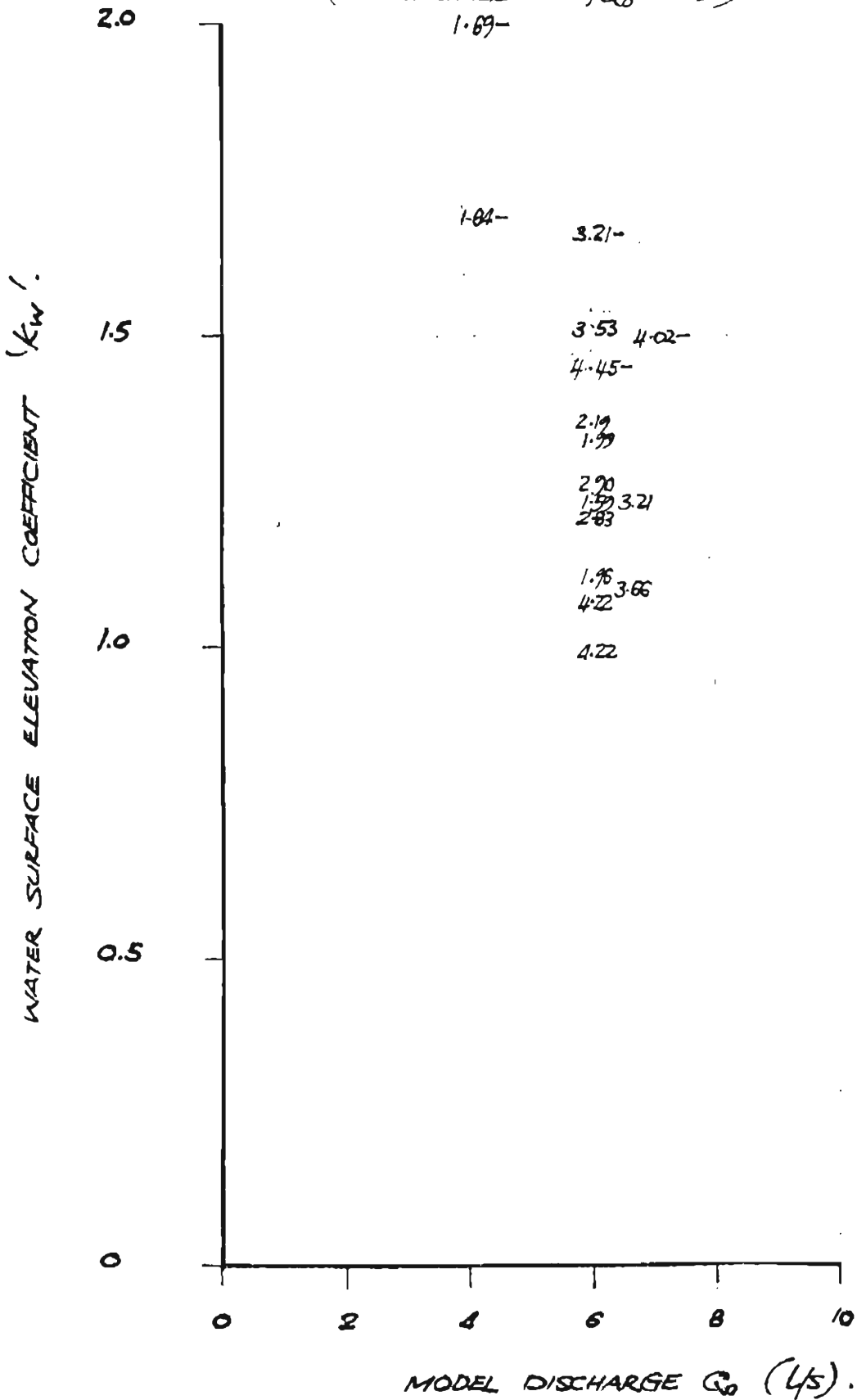




FIGURE A48 : DATA PLOT FOR MODEL NO. 24

WATER SURFACE ELEVATION COEFFICIENT VS. DISCHARGE  $Q_0$ .

$\theta = 45^\circ$ ,  $D_0 = 94 \text{ MM}$ ,  $D_u = 70 \text{ MM}$ ,  $A_0/A_u = 1.803$ .

(FIGURES INDICATE SUBMERGENCE RATIOS)

(- INDICATES  $Q_1/Q_0 = 0.50$ ).

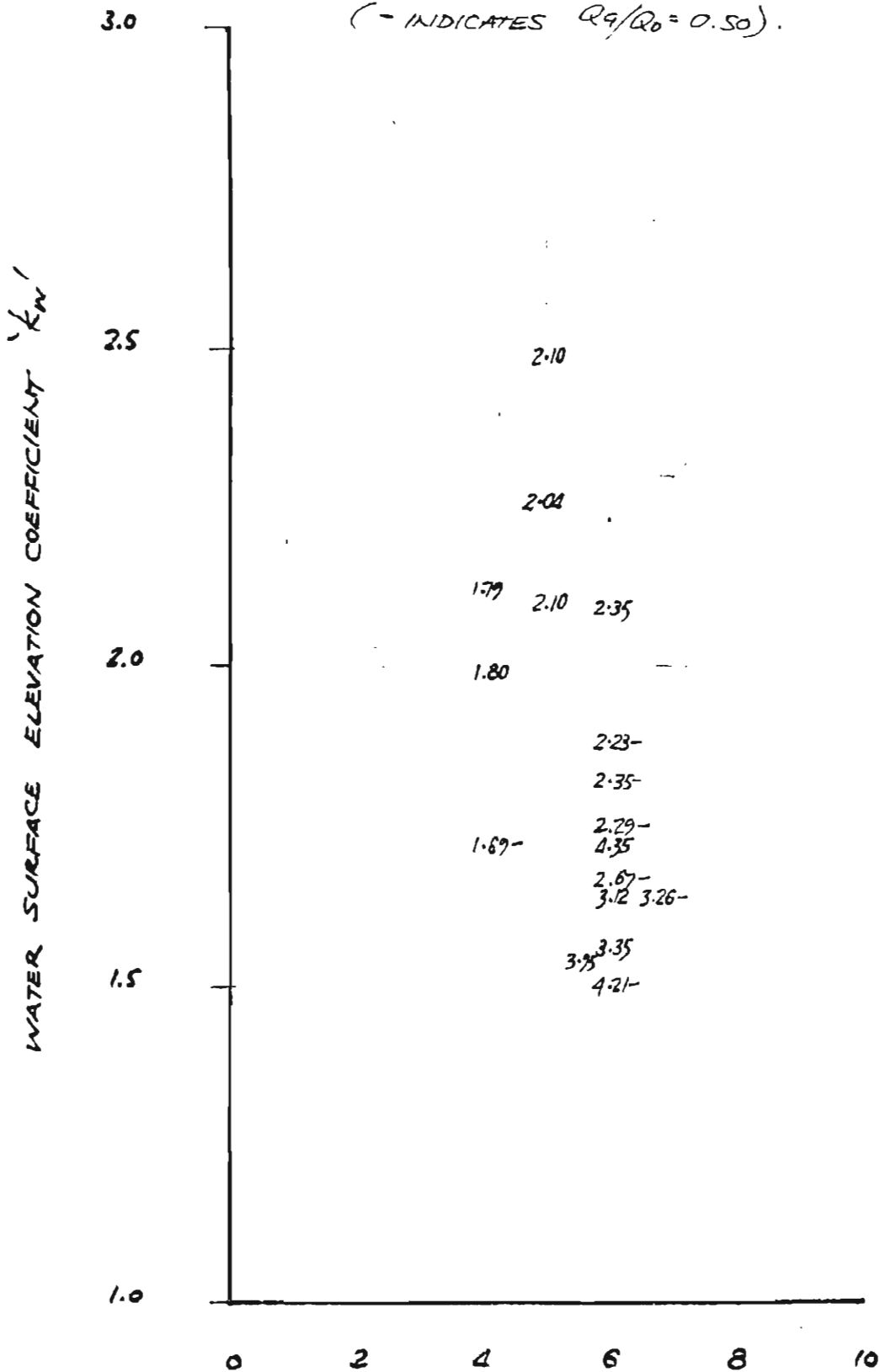


FIGURE A49 : DATA PLOT FOR MODEL NO. 25.PRESSURE HEAD CHANGE COEFFICIENT VS. DISCHARGE  $Q_0$ .

$$\Theta = 45^\circ, D_0 = 94 \text{ MM}, D_c = 70 \text{ MM}, A_0/A_{1c} = 1.00.$$

(FIGURES INDICATE SUBMERGENCE RATIOS).

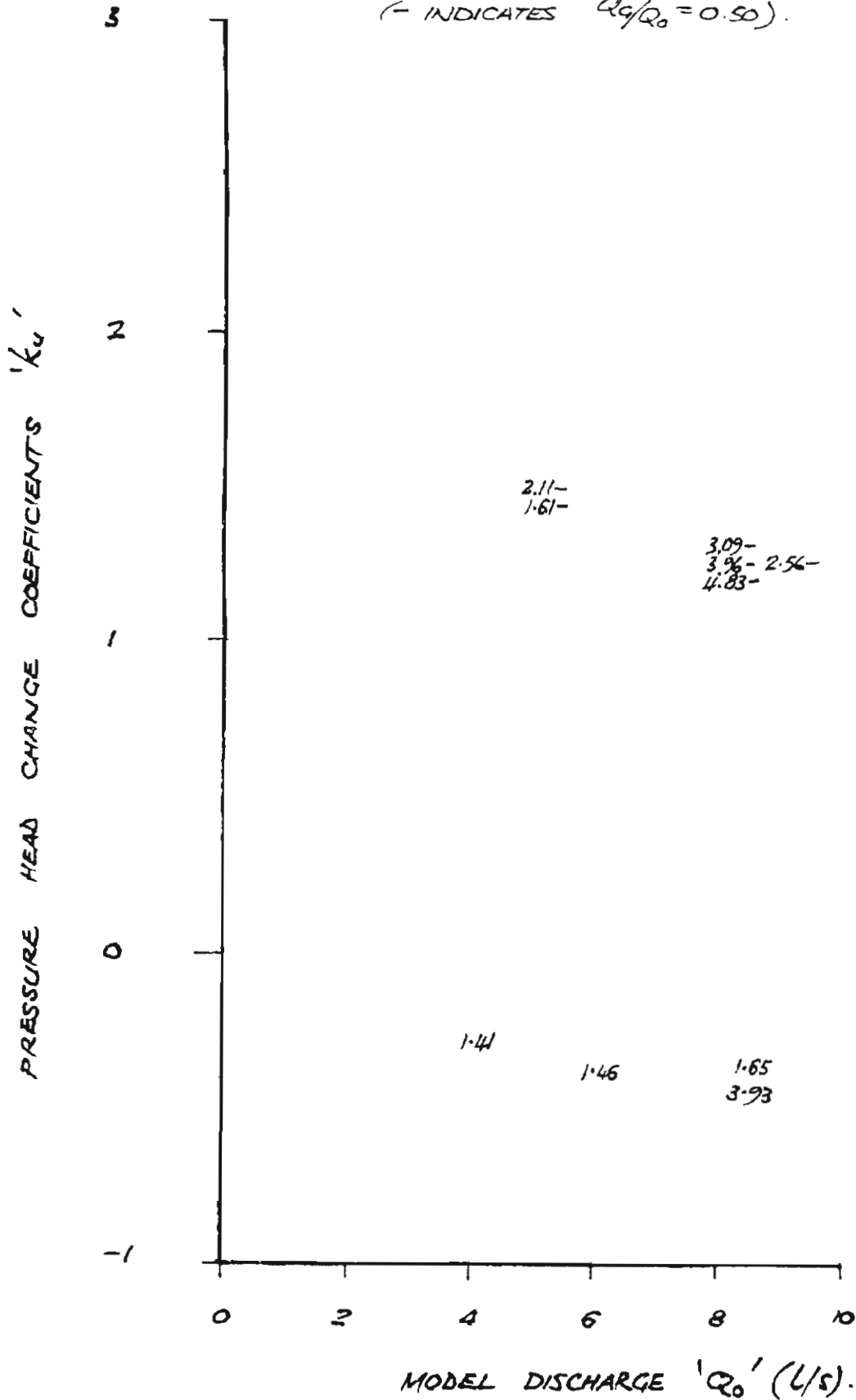
(- INDICATES  $Q_1/Q_0 = 0.50$ ).

FIGURE A50 : DATA PLOT FOR MODEL NO. 25.

WATER SURFACE ELEVATION COEFFICIENT VS. DISCHARGE  $Q_0$ .

$\theta = 45^\circ$ ,  $D_0 = 94 \text{ MM}$ ,  $D_c = 70 \text{ MM}$ ,  $A_0/A_u = 1.803$ .

(FIGURES INDICATE SUBMERGENCE RATIOS).

(- INDICATES  $Q_0/Q_0 = 0.50$ ).

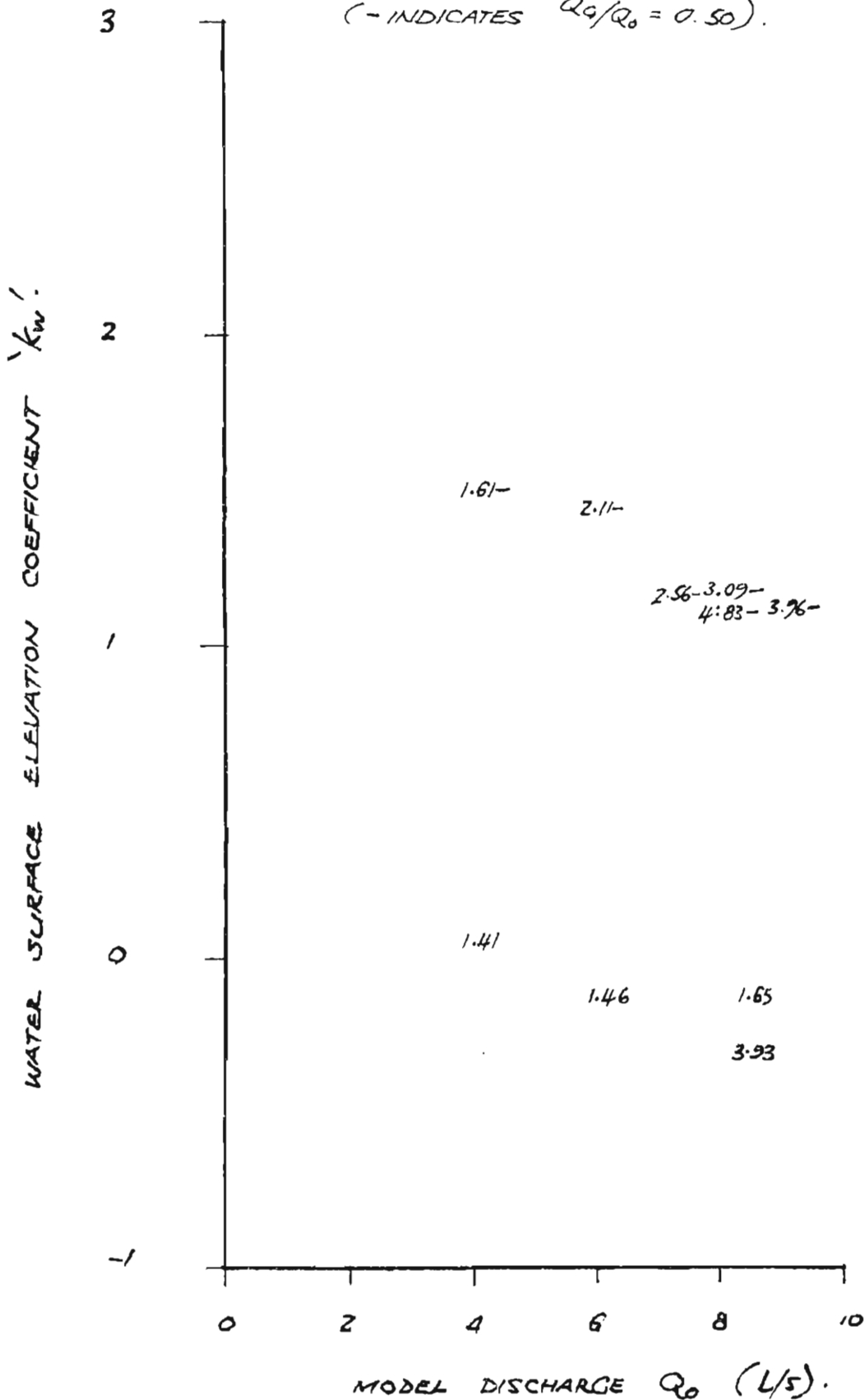




FIGURE A51 : DATA PLOT FOR MODEL NO. 26.

PRESSURE HEAD CHANGE COEFFICIENT VS. DISCHARGE  $Q_0$ .

$\Theta = 67\frac{1}{2}^\circ$ ,  $D_0 = 94 \text{ MM}$ ,  $D_1 = 70 \text{ MM}$ ,  $A_0/A_u = 1.803$ .

(FIGURES INDICATE SUBMERGENCE RATIOS)

( - INDICATES  $Q_9/Q_0 = 0.50$  ) .

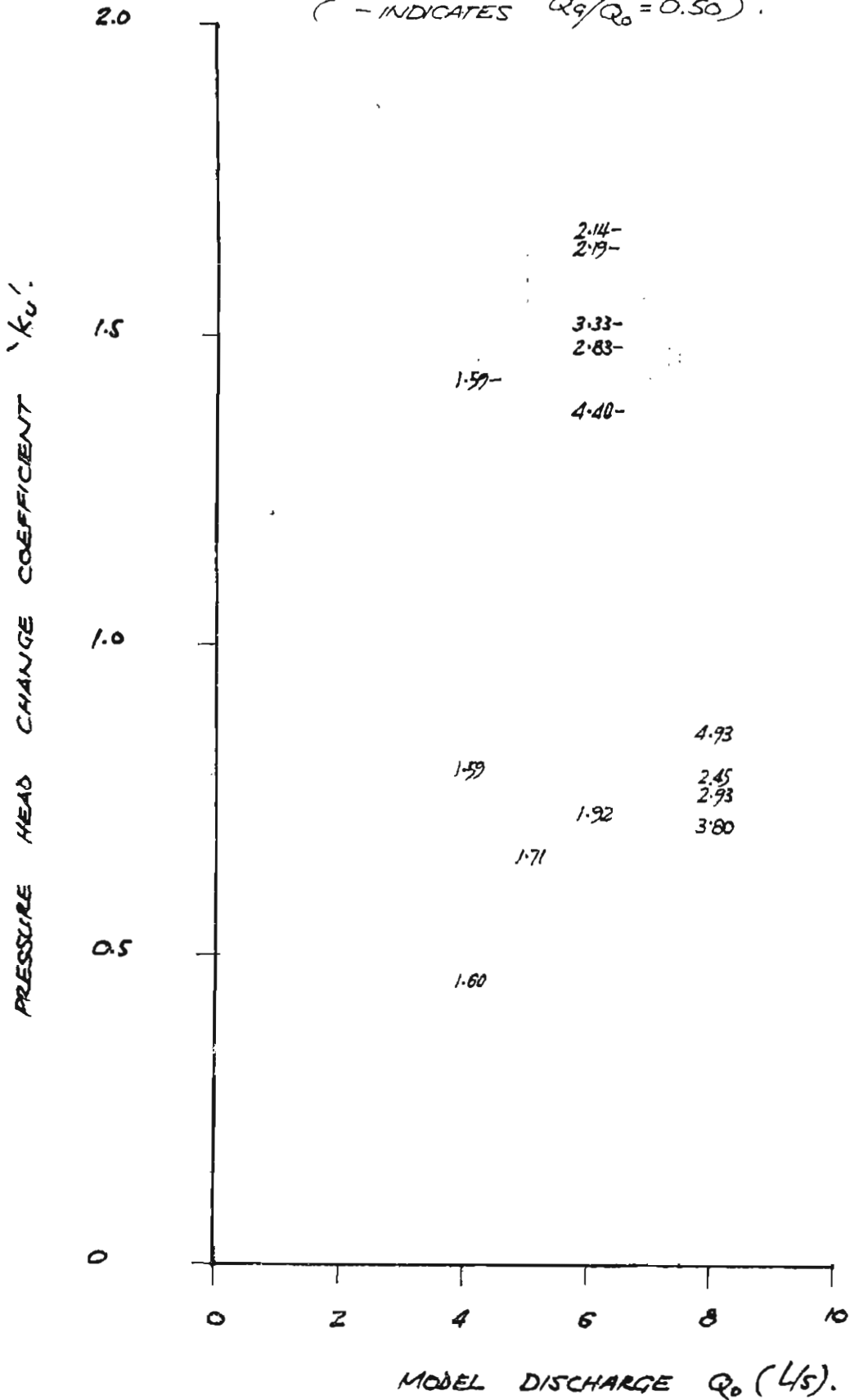


FIGURE A52 : DATA PLOT FOR MODEL NO. 26

WATER SURFACE ELEVATION COEFFICIENT VS. DISCHARGE  $Q_0$ .

$\theta = 67\frac{1}{2}^\circ$ ,  $D_0 = 94 \text{ MM}$ ,  $D_v = 70 \text{ MM}$ ,  $A_0/A_u = 1.803$ .

(FIGURES INDICATE SUBMERGENCE RATIOS) ..

(- INDICATES  $Q_9/Q_0 = 0.50$ ).

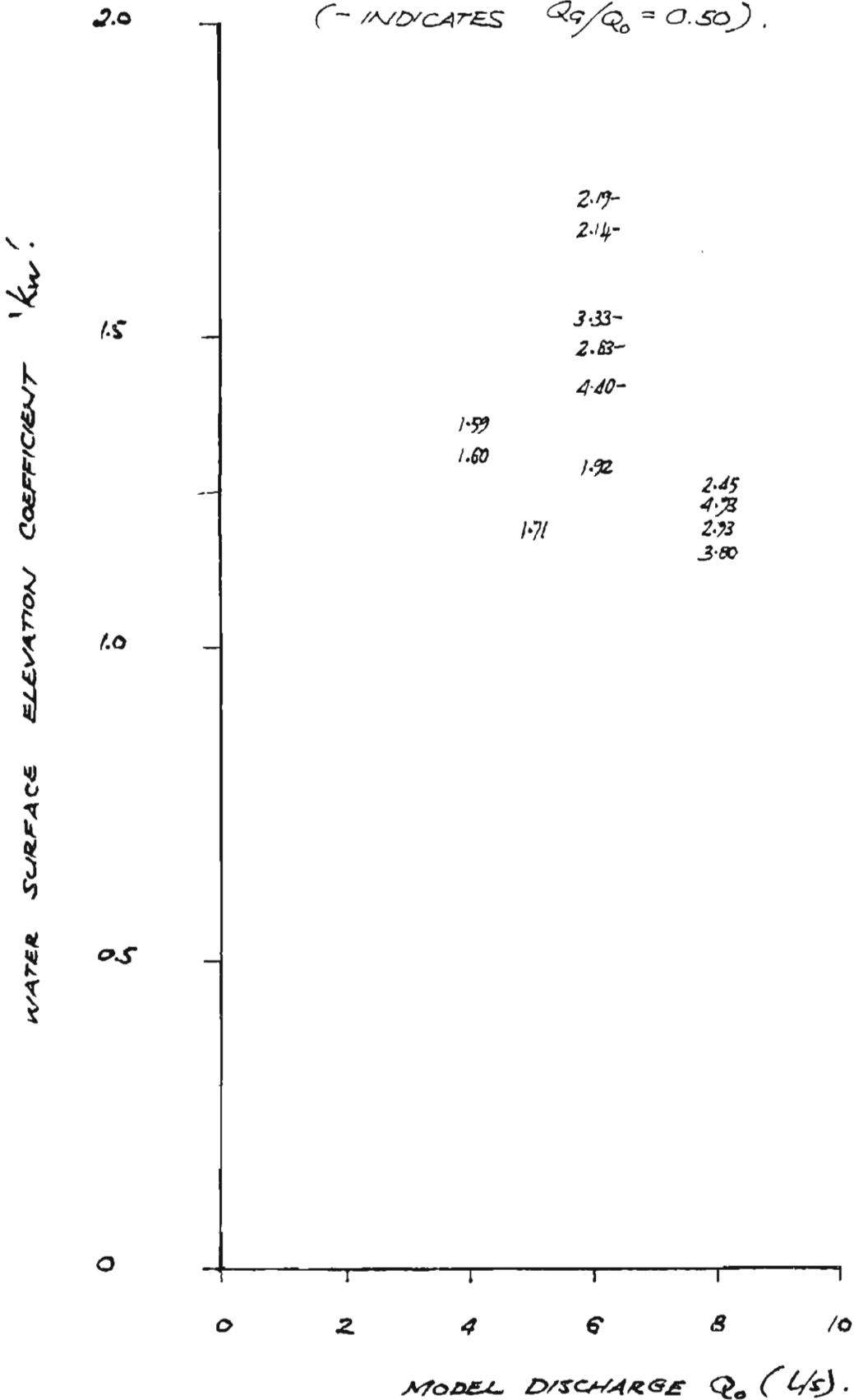


FIGURE A53 : DATA PLOT FOR MODEL NO. 27PRESSURE HEAD CHANGE COEFFICIENT VS DISCHARGE  $Q_0$ .

$$\theta = 22\frac{1}{2}^\circ, \quad D_0 = 127 \text{ MM}, \quad D_1 = 70 \text{ MM}, \quad A_0/A_1 = 3.292$$

(FIGURES INDICATE SUBMERGENCE RATIOS)..

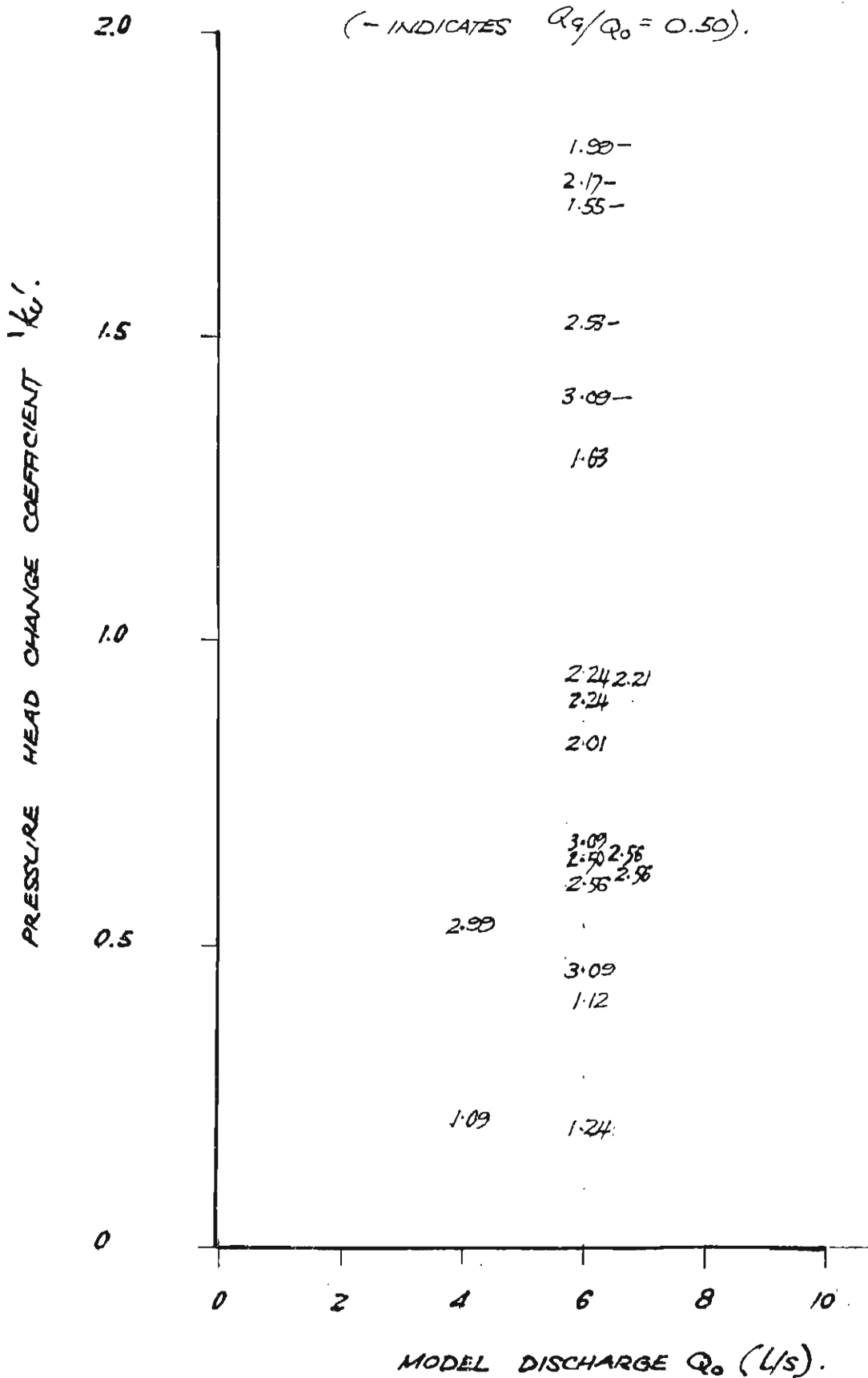


FIGURE A54 : DATA PLOT FOR MODEL NO. 27.

WATER SURFACE ELEVATION COEFFICIENT VS. DISCHARGE  $Q_0$ .

$\theta = 22\frac{1}{2}^\circ$ ,  $D_0 = 127 \text{ MM}$ ,  $D_c = 70 \text{ MM}$ ,  $A_0/A_c = 3.282$

(FIGURES INDICATE SUBMERGENCE RATIOS).

(- INDICATES  $Q_c/Q_0 = 0.50$ ).

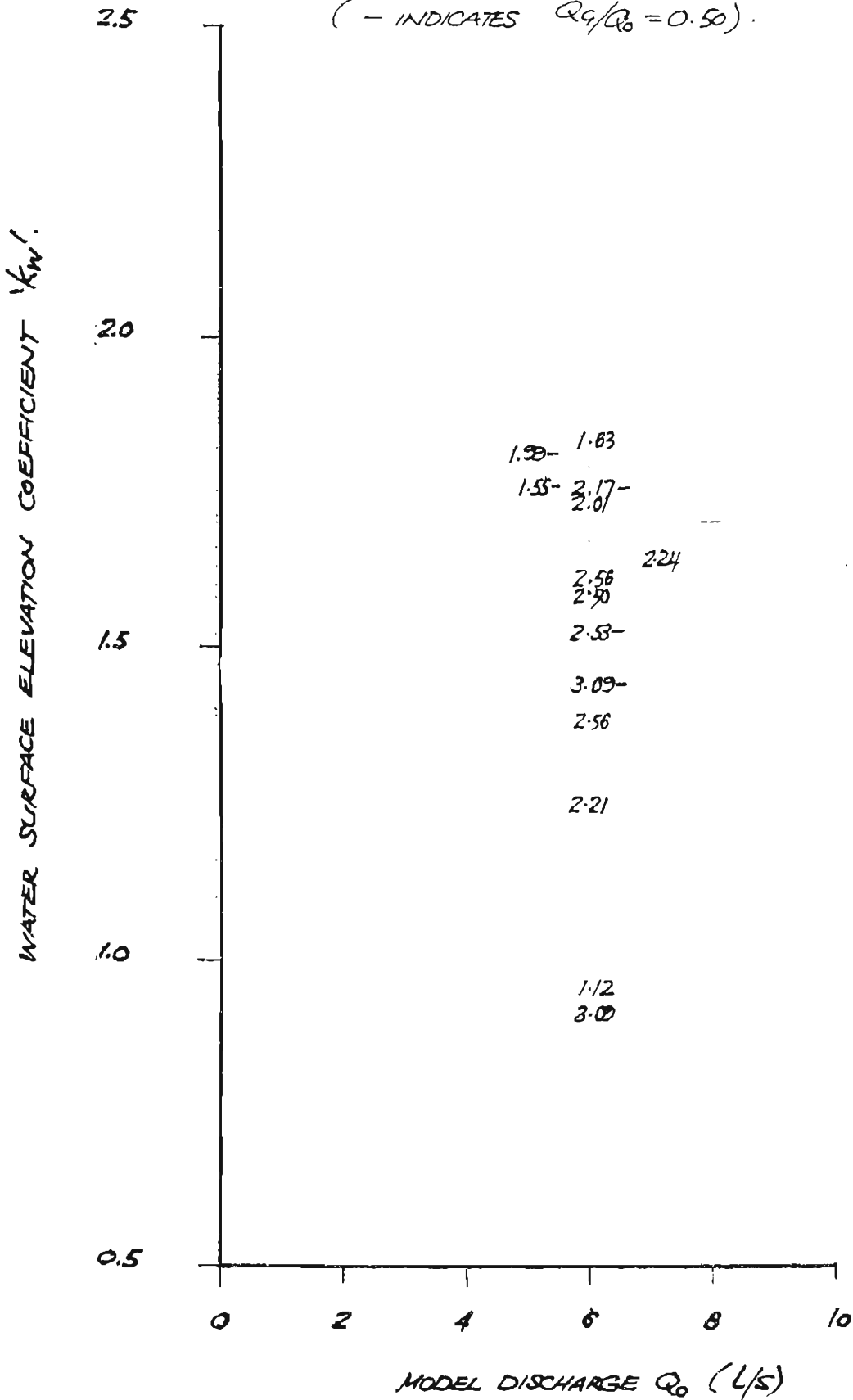


FIGURE A55 : DATA PLOT FOR MODEL NO. 20.PRESSURE HEAD CHANGE COEFFICIENT VS DISCHARGE  $Q_0$ .

$$\theta = 15^\circ, D_0 = 127 \text{ MM}, D_u = 70 \text{ MM}, A_0/A_u = 3.282.$$

(FIGURES INDICATE SUBMERGENCE RATIOS).

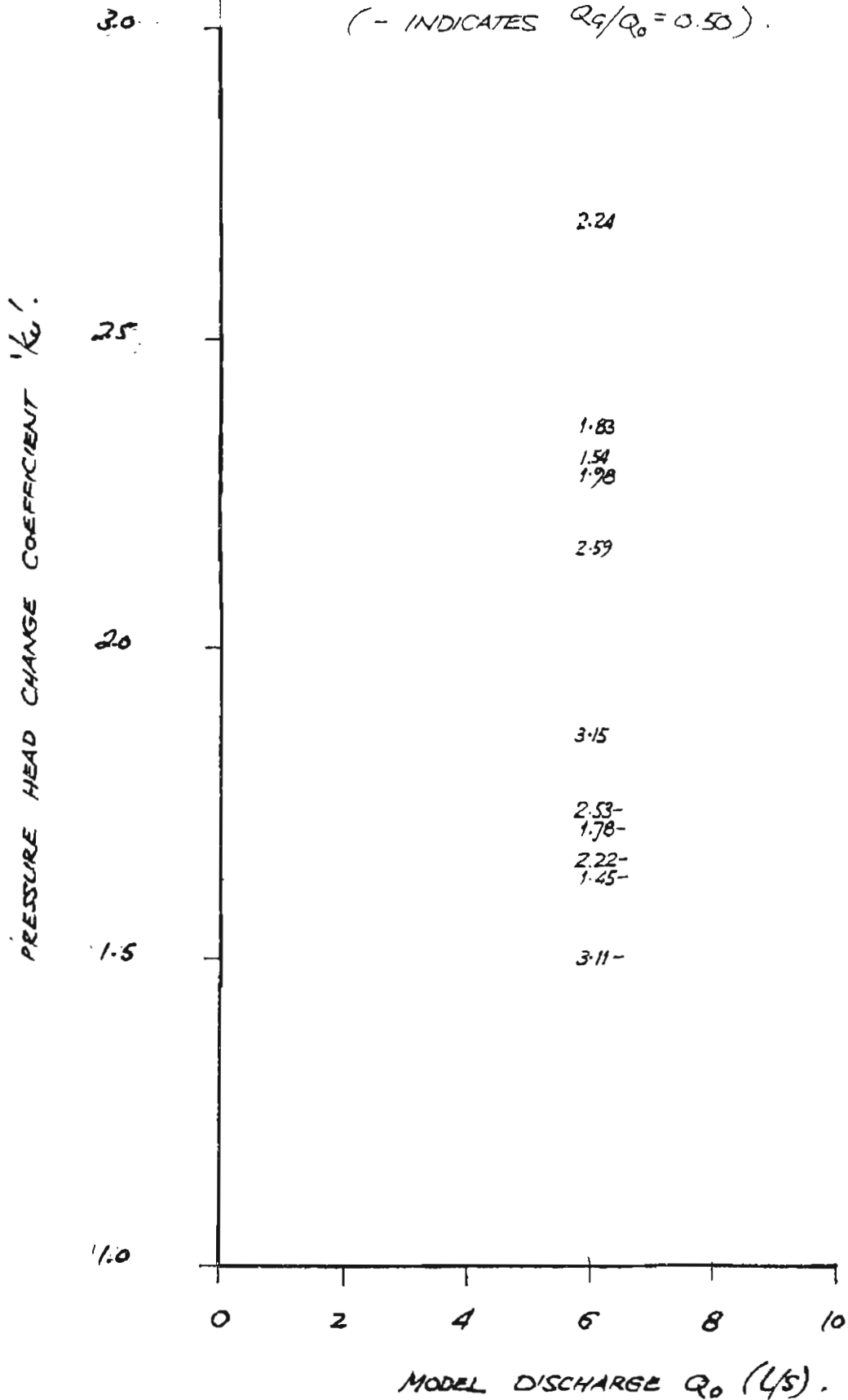
(- INDICATES  $Q_g/Q_0 = 0.50$ ).

FIGURE A56 : DATA PLOT FOR MODEL NO. 28.

WATER SURFACE ELEVATION COEFFICIENT VS DISCHARGE  $Q_0$ .

$\theta = 45^\circ$ ,  $D_0 = 127 \text{ MM}$ ,  $D_1 = 70 \text{ MM}$ ,  $A_0/A_1 = 3.282$ .

(FIGURES INDICATE SUBMERGENCE RATIOS)

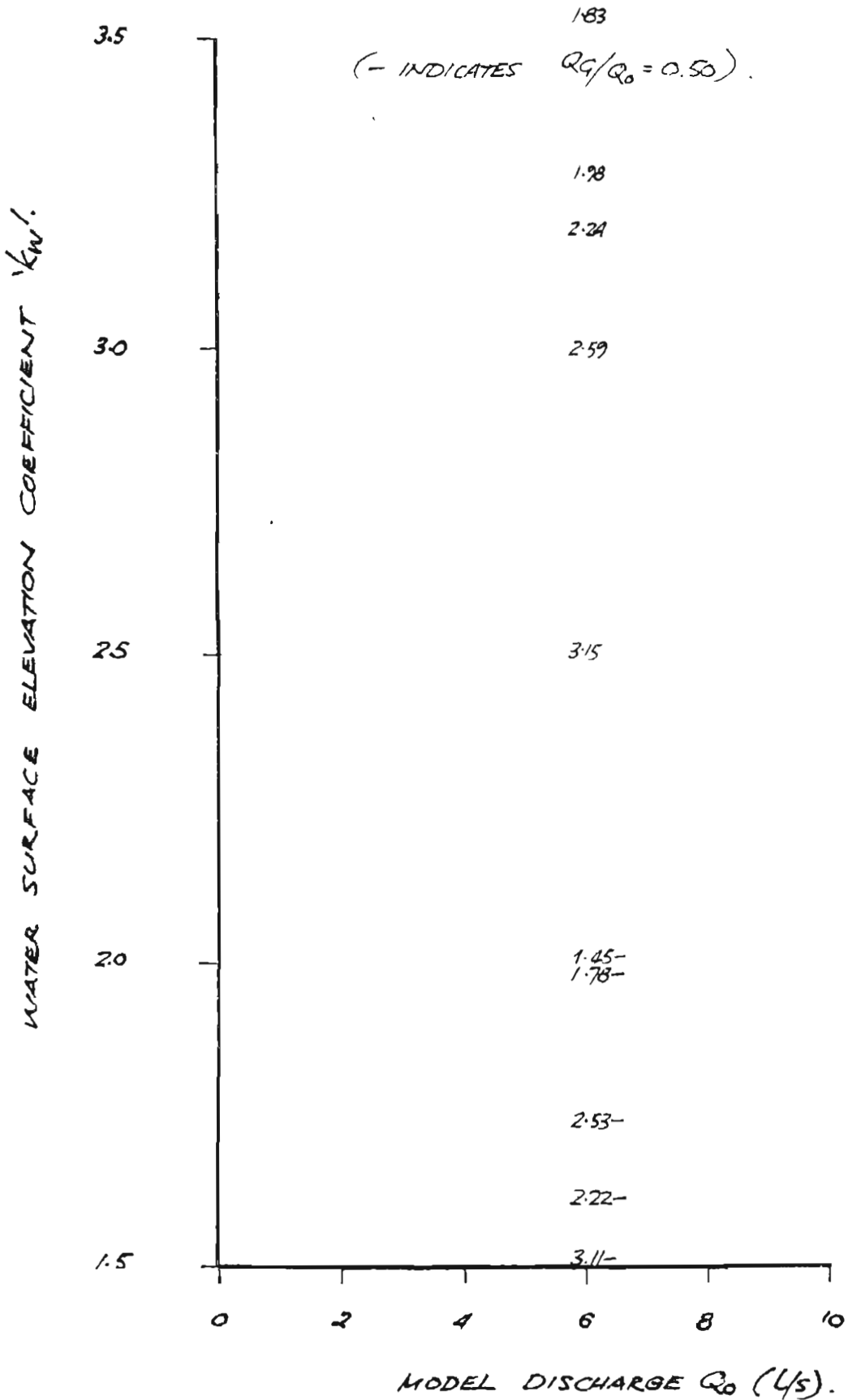


FIGURE A57 : DATA PLOT FOR MODEL NO. 29

PRESSURE HEAD CHANGE COEFFICIENT VS. DISCHARGE  $Q_0$ .

$\Theta = 45^\circ$ ,  $D_0 = 127 \text{ MM}$ ,  $D_u = 70 \text{ MM}$ ,  $A_0/A_u = 3.282$ .

(FIGURES INDICATE SUBMERGENCE RATIOS)

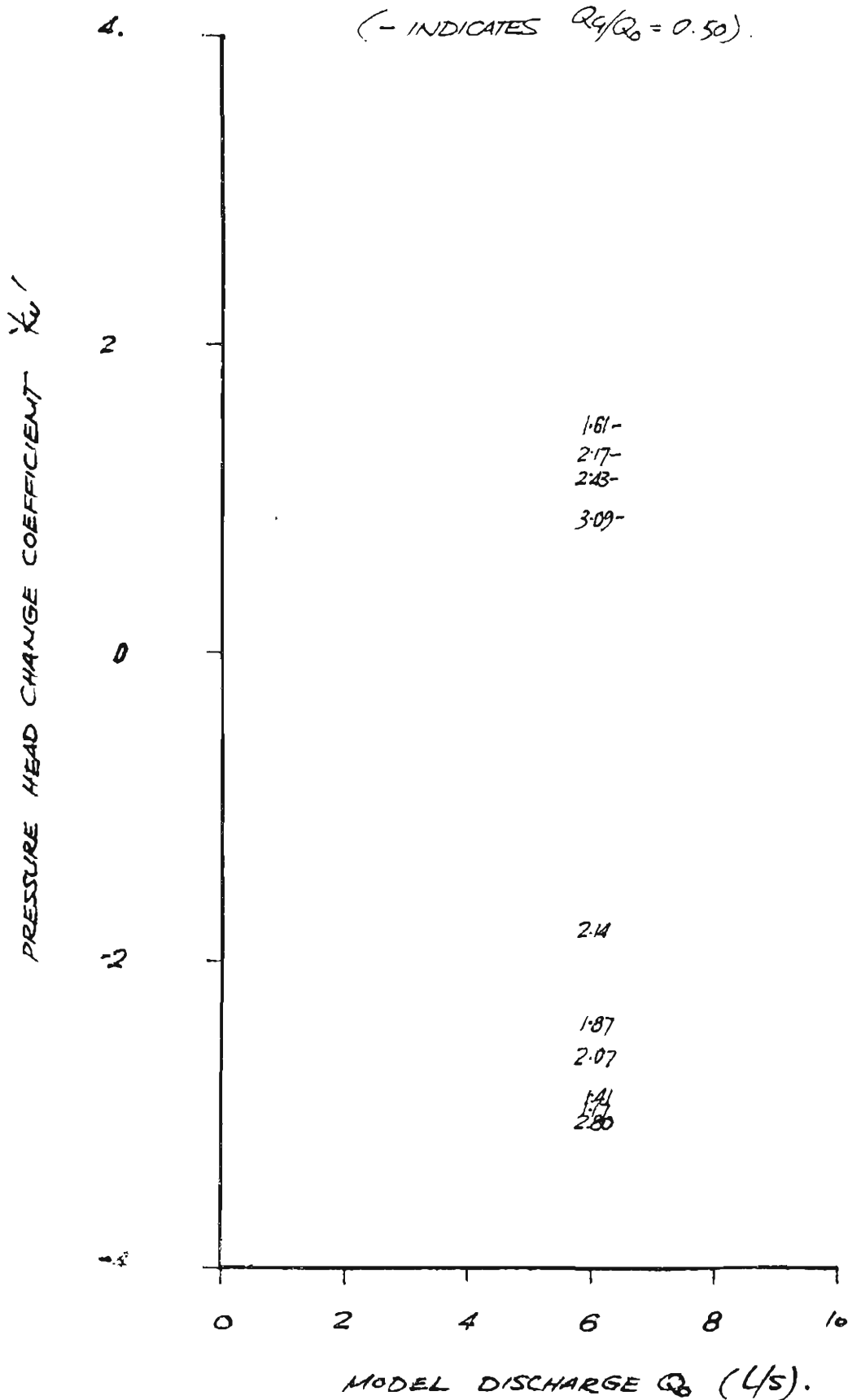


FIGURE A58 : DATA PLOT FOR MODEL NO. 29.

WATER SURFACE ELEVATION COEFFICIENT VS. DISCHARGE  $Q_0$ .

$\theta = 45^\circ$ ,  $D_0 = 127 \text{ MM}$ ,  $D_u = 70 \text{ MM}$ ,  $A_0/A_u = 3.282$ .

(FIGURES INDICATE SUBMERGENCE RATIOS)

(- INDICATES  $Q_1/Q_0 = 0.50$ ).

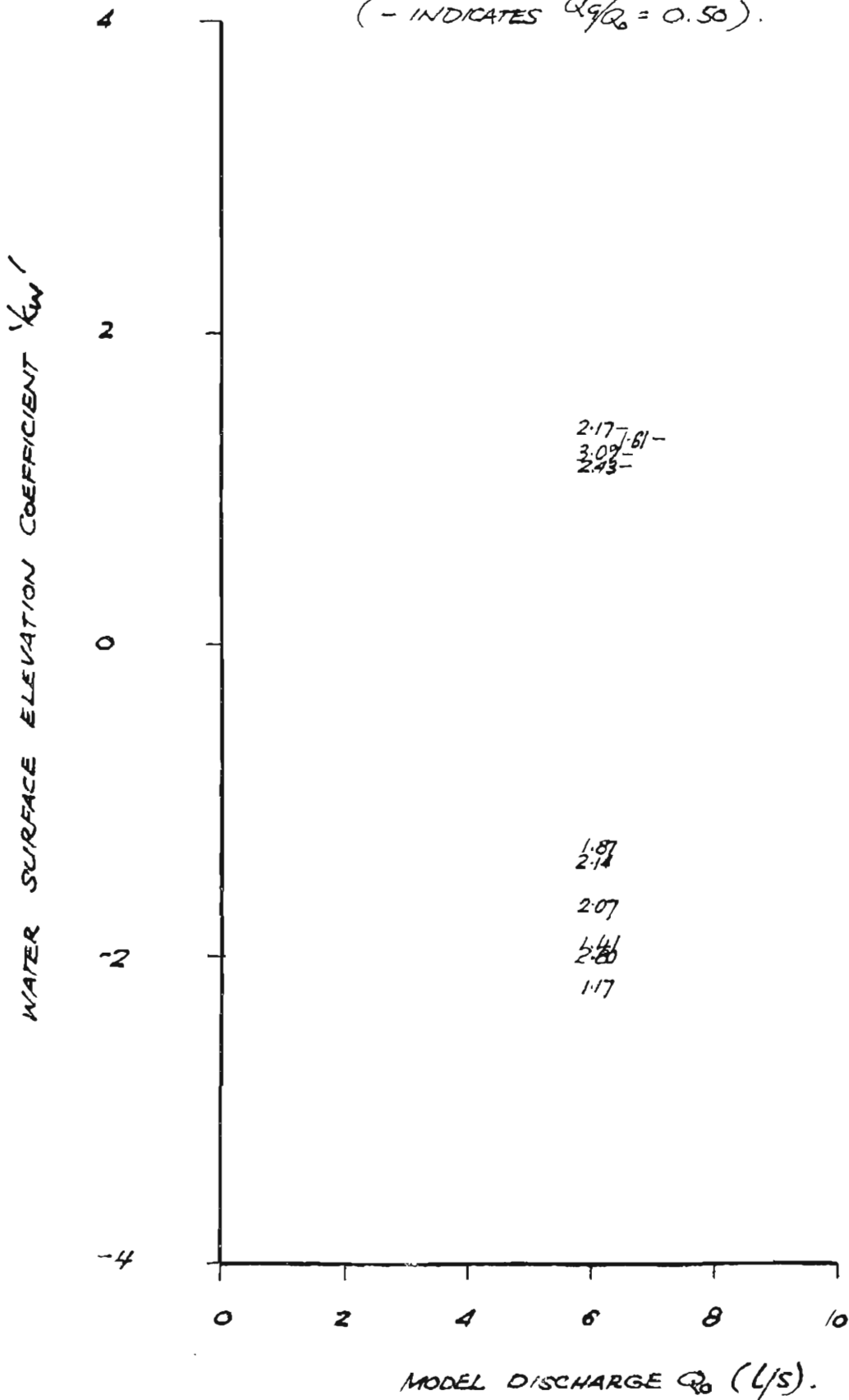




FIGURE A59 : DATA PLOT FOR MODEL NO. 30.

PRESSURE HEAD CHANGE COEFFICIENT VS. DISCHARGE  $Q_0$ .

$\theta = 67\frac{1}{2}^\circ$ ,  $D_0 = 127 \text{ MM}$ ,  $D_u = 70 \text{ MM}$ ,  $A_0/A_u = 3.282$ .

(FIGURES INDICATE SUBMERGENCE RATIOS)

(- INDICATES  $Q_g/Q_0 = 0.50$ ).

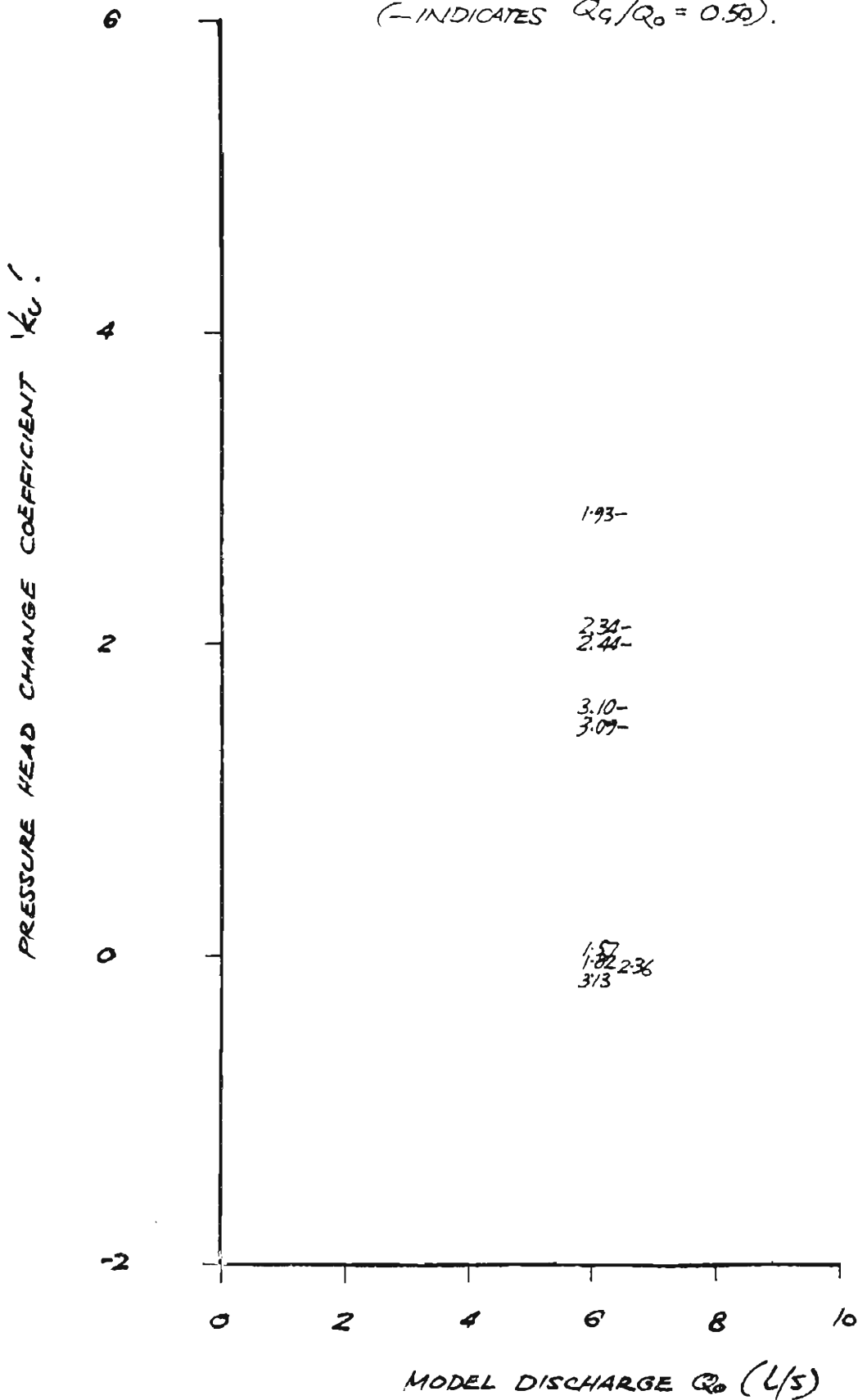


FIGURE A60 : DATA PLOT FOR MODEL NO. 30.

WATER SURFACE ELEVATION COEFFICIENT VS DISCHARGE  $Q_0$ .

$\theta = 67\frac{1}{2}^\circ$  ,  $D_0 = 127\text{MM}$  ,  $D_u = 70\text{MM}$  ,  $A_0/A_u = 3.282$ .

(FIGURES INDICATE SUBMERGENCE RATIOS).

(- INDICATES  $Q_1/Q_0 = 0.50$ ).

